An Assessment of Patient Doses from CT Scanning

Bijan Hashemi Malayeri

Ph.D.

The University of Edinburgh

1997

DECLARATION

I declare that this thesis has been composed by myself and that the work contained in it is my own.

Bijan Hashemi Malayeri

October 1997

ACKNOWLEDGEMENTS

I am sincerely and deeply grateful to Mr. J. R. Williams who has been responsible for instigating this project and for his generous and constructive guidance, criticism, and encouragement throughout.

I am very grateful to Dr. A. T. Redpath for providing part of the computing facilities used in this project. I am specially grateful to Dr. N. C. Nicolson for his continual computing support and help at the beginning of this project. I am also grateful to Mr. C. Ferrington for his computing system support and help.

I am also grateful to Mr. G. Campbell for his help in preparation and constructing some of the materials and equipment used in this project. The help and co-operation of Mrs. M. Catling, Mr. T. Kehoe, Dr. D. Williamson, Dr. P. Hoskins and the rest of the staff of the Diagnostic X-ray Physics and the Radiotherapy Physics of the Western General Hospital of Edinburgh is gratefully acknowledged.

The help and co-operation of the staff of Radiology and Clinical Neuroscinces Departments of the Western General Hospital of Edinburgh; and X-ray Departments of: Royal Infirmary of Edinburgh; St. Johns Hospital of Livingston; and Queen Margaret Hospital of Dunfermline are gratefully acknowledged.

I am also thankful to all staff in the Department of Medical Physics and Medical Engineering (including the Radiotherapy Physics staff) for their friendliness during my time here. In particular my thanks goes to Professor W. N. McDicken for his kindness and support. My thanks also goes to my fellow students, specially Dr. M. M. Aspradakis, for their support, help, and good advice.

Most of all, I am grateful and indebted to my family, specially my honourable wife, for their continuous love, trust, patience and support through the years and keeping me sane and happy during this study.

Financial support from the Ministry of Culture and Higher Education of Islamic Republic of Iran, from the Department of Medical Physics and Medical Engineering, and from the Western General Hospital of Edinburgh for purchase of the Rando phantom are also gratefully acknowledged.

ABSTRACT

Computed Tomography (CT) is an x-ray imaging technique introduced into clinical practice in the early 70's and is now considered an essential element in radiological imaging.

Notwithstanding the undoubted benefits of CT in health care, growth of the techniques has taken place without full appreciation of the relatively high patient doses involved. A national survey carried out in the UK in 1989 indicated that while CT represented about 2% of the total of all x-ray examinations, it accounted disproportionately for 20% of the resultant collective dose (Shrimpton et al. 1991). Recent studies (Shrimpton et al. 1993) suggest that CT may now represent about a third of the collective dose from diagnostic x-rays in the UK. There has been a similar proliferation of scanners throughout the world, such that the average frequency of CT examination in developed countries has been reported to be about 10 per 1000 population (Shrimpton and Wall 1992). Therefore CT practice is causing significant concern and based on the ALARA principle and other advisory bodies' recommendation (NRPB 1990), the doses to patient from this x-ray modality should periodically be monitored and kept within guideline doses.

The most common CT dosimetry approaches are standard method, Monte Carlo (MC) method and direct method. In the standard method CTDI is assessed inside a head and a body perspex phantom giving an index of the CT dose efficiency. This is used mainly for QA purposes. In the MC method the patient doses are estimated by applying this mathematical technique to simulate the interaction of CT generated radiation with matter inside a mathematical model of phantom. In the direct method, measurement of organ doses is carried out directly inside an anthropomorphic physical phantom.

We have developed the direct method by assessing CT axial and longitudinal dose distribution in an anthropomorphic phantom. Measurement of these dose distribution for any scanner allows us to quickly measure organ doses and effective dose, and hence patient doses for any examination protocol with a limited number of

TLDs. This work describes the underlying principles and assumption of the direct CT dosimetry method we have developed and implemented. In addition the review of CT dosimetry provides a comprehensive and critical analysis of the methods developed to date. All dosimetry related concepts for the developed direct technique are considered. Comprehensive dose measurements were carried out to estimate the level of error involved in the developed approach. The MC approach was also used to compare the results of our proposed direct method with this commonly used method in CT dosimetry for routine examinations of some scanners.

The proposed direct CT dosimetry method has now been used for several scanner models. The developed dosimetry method has been successfully implemented to assess the radiation doses resulted from various examination protocols using the recent modern CT modalities, that could not easily be investigated by other dosimetry approaches. We believe that the developed direct CT dosimetry approach overcomes many limitations imposed by other common approaches. It also provides a reliable and practical method for the assessment of patient doses from CT practices for a wide range of scan protocols. Another major advantage of the developed direct dosimetry method is that, it could easily and independently be adapted and implemented for any upcoming new model of CT scanner to be introduced into clinical practice.

1. Table of Contents

Title I

Declaration II

Acknowledgement III

Abstract IV

Table of Contents VI

List of Figures X

List of tables XII

1. Introduction 1

1.1 Computed Tomography 1
1.2 The Significance of the Radiation Dose Associated with the CT 2
1.3 Computed Tomography Dosimetry - General Aspects and Background 4
1.4 Common CT Dosimetry Approaches 9
1.4.1 Standard CT Dosimetry Approach (using Quality Assurance Phantom) 10
1.4.2 Monte Carlo CT dosimetry Approaches 10
1.4.2.1 Monte Carlo Approach using Total Energy Imparted Quantity 10
1.4.2.2 Monte Carlo Approach using Mathematical Phantoms 11
1.4.3 Direct CT Dosimetry Approach using Physical Phantoms 12
1.5 Current Problems in CT Dosimetry 12
1.6 Proposed CT Dosimetry Approach 16
1.7 Aims of Thesis 17
1.8 Outline of Thesis 18

2. CT Dosimetry Principles 19

2.1 Basic Dosimetric Quantities 20
2.1.1 Absorbed Dose 21
2.1.2 Equivalent dose 21
2.1.3 Effective Dose and Effective Dose Equivalent 22
2.2 CT Dosimetry Devices 24
2.2.1 CT Dosimeters 24
2.2.1.1 Film 24
2.2.1.2 Thermoluminescent Dosimeter (TLD) 25
2.2.1.3 Pencil Ionisation Chamber 26
2.2.2 CT Phantoms 27
2.2.2.1 Early Phantoms 28
2.2.2.2 Physical Humanoid Anthropomorphic Phantom 28
2.2.2.3 Standard/Quality Assurance Phantom 29
2.2.2.4 Mathematical Anthropomorphic Phantom 30
2.3 CT Dose Descriptors 32
2.3.1 Surface Dose or Skin Dose 32
2.3.2 CT Dose Profile 32
2.3.3 CTDI 33
2.3.4 Effective dose 35

3. COMMON CT SCANNER CHARACTERISTICS 37

3.1 THE INVENTION OF CT 37
3.2 BASIC OPERATIONAL PRINCIPLES AND TECHNICAL DEVELOPMENTS OF CT SCANNERS 41
3.2.1 Data Acquisition 41
3.2.2 Image Reconstruction 42
3.2.3 Image display, manipulation, storage, and recording 43
3.3 HISTORICAL DEVELOPMENT OF CT 43
3.4 TECHNICAL AND COMPUTING DEVELOPMENT OF CT 47
3.4.1 Data Acquisition Developments of CT 47
3.4.1.1 Generator 47
3.4.1.2 X-ray tube 48
3.4.1.3 Filtration 49
3.4.1.4 Collimation 49
3.4.1.5 Detector Characteristics 50
3.4.2 Image Reconstruction Developments of CT 51
3.4.2.1 Three-dimensional imaging 53
3.4.2.2 Spiral or Helical CT 54
3.4.3 Image Display Development of CT 55
3.5 BASIC PHYSICAL CHARACTERISTICS OF THE CT SCANNERS 56
3.5.1 Siemens Somatom Plus 57
3.5.2 GE HiSpeed Advantage 59
3.5.3 GE SYTEC 3000 Plus 60
3.5.4 GE 9000HP 60
3.5.5 GE 8800 61
3.5.6 Philips Tomoscan CX/S 61
3.6 ROUTINE CT EXAMINATION PROTOCOLS 62

4. PHANTOM SPECIFICATIONS 64

4.1 REFERENCE (STANDARD) MAN 64
4.2 DESCRIPTION OF THE PHYSICAL PHANTOM 65
4.3 POSITIONING OF ORGANS AND TISSUES IN THE PHANTOM 67
4.4 VOLUME DISTRIBUTION OF ORGANS IN SECTIONS OF THE PHANTOM 70
4.4.1 Brain 71
4.4.2 Parotid, Thyroid and Thymus Glands 72
4.4.3 Lung and Oesophagus 72
4.4.4 Liver, Spleen, Stomach, Pancreas, and Intestines 72
4.4.5 Kidneys and Adrenals 73
4.4.6 Ovaries, Prostate, Uterus, and Bladder 73
4.4.7 Skin, Bone, and Red Bone Marrow 73
4.5 SUMMARY AND CONCLUSION 74

5. CT DOSIMETRY USING THE PHYSICAL ANTHROPOMORPHIC PHANTOM (MATERIALS AND METHODS) 76

5.1 INTRODUCTION 76
5.2 THE DEVELOPED DIRECT CT DOSIMETRY METHOD 77
5.3 TLD STUDY 81
5.3.1 Type of TLDs 83
5.3.2 Calibration of TLDs 85
5.3.3 Uncertainties in the TLD Measurements 88
5.3.4 Other Technical Considerations with the Use of the TLDs 89
5.4 THE ABSORBED DOSE CORRECTIONS 90

5.4.1 CT X-ray Spectra 91
5.4.2 Mass Energy Absorption Coefficient 93
5.5 Dose Measurement Methods 95
5.5.1 Dose Distributions inside the Scan Volume 96
5.5.2 Dose Distribution and Fall Off of the Dose outside the Scan Volume 100
5.5.3 Central Axis Dose Measurements 102
5.5.4 Packing Factor 103
5.6 Validations of Dose Distributions 105
5.6.1 Representative Sections 105
5.6.2 Parallel Sections 110
5.6.3 Evaluation of Errors in Measurements of Effective Dose 117
5.7 Customised Computer Spreadsheet Program 120
5.7.1 Input Data 121
5.7.2 Output Data 123
5.7.3 Data Flow Chart 123
5.8 Summary of the Developed Direct Dosimetry Method 125

6. CT Dosimetry using Physical Anthropomorphic Phantom (Results) 127

6.1 GE 8800 CT Scanner 128
6.2 GE 9000HP CT Scanner 129
6.3 Philips Tomoscan CX/S CT Scanner 130
6.4 GE Sytec 3000 Plus CT Scanner 131
6.5 GE HiSpeed Advantage CT Scanner 132
6.5.1 Conventional CT Examinations 133
6.5.2 Spiral CT Examinations 134
6.6 Siemens Somatom Plus CT Scanner 135
6.6.1 Conventional CT Examinations 136
6.6.2 Spiral CT Examinations 138
6.7 Summary of the Results 140
6.7.1 Patient Doses from Head Scanning Techniques 142
6.7.2 Patient Doses from Chest Scanning Techniques 146
6.7.3 Patient Doses from Abdomen and Pelvis Scanning Techniques 148

7. CT Dosimetry using the Monte Carlo Method and the Mathematical Anthropomorphic Phantom 152

7.1 Introduction 152
7.2 Materials and Methods 154
7.2.1 CTDI Measurements 156
7.2.1.1 CTDI Measurements with the TLD 157
7.2.1.2 CTDI Measurement with the Pencil Ionisation Chamber 159
7.2.2 Organ and Tissue Doses and Effective Dose Calculations 161
7.3 CTDI Results 164
7.3.1 CTDI values 165
7.3.2 CTDI Analysis 171
7.3.2.1 Variation of CTDI by Measuring Technique 172
7.3.2.2 Variation of CTDI by Slice Width 175
7.3.2.3 Variation of CTDI by Tube Potential 180
7.3.2.4 Variation of CTDI by Scanner Model 181
7.3.2.5 Comparison of CTDI Values with the NRPB Mean Values 184
7.4 Patient Doses 185
7.4.1 Organs and Effective Doses 185
7.5 Summary and Conclusion 190

8. Comparison of Different Dosimetry Approaches and Estimated Patient Doses 192

8.1 Comparison of Patient Doses Resulting from the Direct and the MC Dosimetry Approaches 193
8.1.1 Head & Neck 193
8.1.2 Chest 196
8.1.3 Abdomen & Pelvis 197
8.1.4 Comparison of Measurements Errors in the Dosimetry Approaches 199
8.1.5 Summary of Dose Comparison 202
8.2 Variation of Effective Doses among the CT Scanners and the Normalised Effective Dose 204
8.3 Comparison of Patient Doses Resulting from Conventional and Spiral Examinations 207
8.4 Comparison of Effective Dose and Effective Dose Equivalent Values 207
8.5 Comparison of Measured Patient Doses with the NRPB Typical Doses 210
8.6 Summary 213

9. Discussion and Conclusion 214

9.1 Discussion 214
9.2 Conclusion 217
9.3 Future Work 219

References 221

Appendix A. Rando Phantom Design 234

Appendix B. CT Scanners Dose Conversion Factors 270

Appendix C. Macro programs 282

LIST OF FIGURES

Figure 1.1: Contribution of different types of manmade radiation to the collective annual dose for the UK population (Source: Hughes and O'Riordan 1993)....3
Figure 2.1: FDA Standard CT Dosimetric Phantoms....29
Figure 2.2: CT (Plexiglass) QA phantom designed by Siemens....30
Figure 2.3: NRPB Anthropomorphic Mathematical Phantom....31
Figure 2.4: A typical free in air axial CT dose profile....33
Figure 2.5: Illustration of CT system geometry and co-ordinate used for CTDI definition by Shope et al. (1981)....34
Figure 3.1: The original lathe bed scanner used in early CT experiments by Hounsfield of EMI (Webb 1990)....40
Figure 3.2: Examples of CT images of the head, chest, abdomen, and spine produced by a modern CT scanner (Seeram 1994)....42
Figure 3.3: Data collection scheme used in the first CT brain scanner: 1, object; 2, X-ray tube; 3, collimator; 4, head support containing a water bag; 5, crystal detector; 6, photomultiplier tube (Seeram 1994)....43
Figure 3.4: Four generations of CT scanners illustrating two types of beam geometry, the parallel beam and the fan beam (Seeram 1994)....45
Figure 3.5: Major components of the Ultrafast CT scanner (Imatron) (Webb 1988)....46
Figure 3.6: Examples of 3D images now available through CT technology (Seeram 1994)....54
Figure 4.1: The Alderson Rando phantom....65
Figure 4.2: The Alderson Rando phantom with breast sections....66
Figure 4.3: The breast phantoms, cut in two sections in frontal plane with the holes for holding the dosimeters....66
Figure 4.4: A CT image (topogram) of the chest, abdomen and pelvis regions of the Rando phantom showing the embedded human skeleton and two different materials used to simulate soft tissues and lungs in the phantom....67
Figure 4.5: Four typical sections from head (Section 2), chest (Section 14), abdomen (Section 26), and pelvis (section 31) regions of the Rando Alderson phantom showing demarcated positions of organs and tissues of interest....68
Figure 4.6: A CT image (topogram) of the Rando Alderson phantom showing the displacement of the skeleton in the sections (0-8) that comprise the head region of the phantom....69
Figure 4.7: A radiograph of section 24 of the Rando phantom showing the displacement of the skeleton within one of the sections that comprise the abdomen region of the phantom....70
Figure 5.1: The TLDs (white circles) positioned in some points of interest in a single section of the Rando phantom....83
Figure 5.2: A box of LiF: MgTi round TLDs containing 50 chips....85
Figure 5.3: Toledo TLD reader with automatic sample changer....86
Figure 5.4: Schematic drawing of the set up of TLDs, a traceable ionisation chamber, and the X-ray unit for a calibration measurement....87
Figure 5.5. The variation of the calculated TLD calibration factor over the period of the study. The error bars represent "2×standard deviation" of each calibration data set....88
Figure 5.6: A typical CT X-ray spectrum....93
Figure 5.7: Variation of (weighted) μ_{en}/ρ by photon energy for different body tissues and air for two different CT scanners....95
Figure 5.8: A typical section of the phantom showing the way the TLDs were put in the section for dose distribution measurements....97
Figure 5.9: A typical dose distribution in the head area of the Rando phantom (section 2, GE HiSpeed Advantage CT scanner)....98

Figure 5.10: A typical dose distribution in the chest area of the Rando phantom (section 14, GE HiSpeed Advantage CT scanner)..... 99
Figure 5.11: A typical dose distribution in the abdomen area of the Rando phantom (section 26, GE HiSpeed Advantage CT scanner)..... 100
Figure 5.12: Comparison of measured and calculated phantom central dose values outside the scan volume for seven sections (5-11) for a particular "head" examination..... 101
Figure 5.13: Comparison of measured and calculated phantom central dose values outside the scan volume for five sections (6-10) for a particular "chest" examination..... 102
Figure 5.14: Comparison of measured and calculated phantom central dose values outside the scan volume for five sections (16-20) for a particular "abdomen & pelvis" examination..... 102
Figure 5.15: Calculated dose distribution in the representative section (no. 14) of the chest area for the Siemens Somatom Plus CT scanner..... 107
Figure 5.15R: Dose distribution in section 14 with the body contour..... 107R
Figure 5.16: Calculated dose distribution in the representative section (no. 26) of the "abdomen & pelvis" area for the Siemens Somatom Plus CT scanner..... 109
Figure 5.16R: Dose distribution in section 26 with the body contour..... 109R
Figure 5.17: The Data components in the spreadsheet Computer Program..... 121
Figure 5.18: The data flow chart of the spreadsheet computer program..... 124
Figure 7.1: The design of the plastic tube that held TLDs for CTDI measurement..... 158
Figure 7.2: The design of the device used for CTDI measurements. For more explanation refer to the text 158
Figure 7.3: A photograph of the device and a box of the TLDs used for CTDI measurements..... 158
Figure 7.4: The Model 20X5-10.3CT Radcal ® pencil ionisation chamber..... 159
Figure 7.5: Physical Dimensions of the Radcal ® 20X5-10.3CT model pencil ionisation chamber. 160
Figure 7.6: Radcal ® 20X5-10.3CT model pencil ionisation chamber energy response..... 160
Figure 7.7: Lateral and anterior view of the adult mathematical phantom used in the CTDOSE program. The axis numbers are in cm from the base of the trunk. For more explanation refer to the text..... 163
Figure 7.8: Comparison of measured CTDI values (using the TLDs and the IC) with the NRPB mean values (Shrimpton et al. 1991b)..... 167
Figure 7.9: Comparison of measured CTDI values (using the TLDs sand the IC) with the NRPB mean values (Shrimpton et al. 1991b)..... 168
Figure 7.10: Comparison of measured CTDI values (using the TLDs and the IC) with the NRPB mean values (Shrimpton et al. 1991b)..... 169
Figure 7.11: Comparison of CTDI values resulting from the TLDs and the IC measurements..... 169
Figure 7.12: Comparison of CTDI values resulting from the TLDs and the IC measurements..... 170
Figure 7.13: Comparison of CTDI values resulting from the TLDs and the IC measurements..... 171
Figure 7.14: Free in air recorded dose profile for the Siemens Somatom Plus scanner (120 kV, 10 mm nominal slice width)..... 178
Figure 7.15: Free in air recorded dose profile for the Siemens Somatom Plus scanner (137 kV, 10 mm nominal slice width)..... 178
Figure 7.16: Free in air recorded dose profile for the Siemens Somatom Plus scanner (120 kV, 1 mm nominal slice width)..... 179
Figure 7.17: Free in air recorded dose profile for the Siemens Somatom Plus scanner (137 kV, 1 mm nominal slice width)..... 179
Figure 7.18: variation of estimated CTDI values (using IC) with the tube potential for the GE HiSpeed Advantage CT scanner..... 181
Figure 7.19: variation of estimated CTDI values (using IC) with the tube potential for the GE Siemens Somatom Plus CT Scanner..... 181
Figure 7.20: Variation of CTDI values by the type of CT scanner and kV (for 10 mm slice width).182
Figure 7.21: Variation of CTDI values by the type of CT scanner and kV (for 5 mm slice width).. 183

LIST OF TABLES

Table 1.1: Contributions to the annual collective dose from all medical and dental X-ray examinations in the UK (Source: Hughes and O'Riordan 1993) 3
Table 1.2: Typical lifetime risks of fatal cancer from X-ray examinations 4
Table 2.1: Radiation weighting factors (source: ICRP 1991) 22
Table 2.2: Recommended tissue weighting factors (w_T) in 1977 and 1990 (sources: ICRP 1977, ICRP 1991) 23
Table 3.1: The locations, manufacturers, and models of the CT Scanners 57
Table 4.1: Measured fractional values of the lungs for Average-Man Rando phantom 72
Table 4.2: Distribution of the oesophagus in the Rando phantom 72
Table 4.3: Relative distribution of the liver in the Rando phantom 73
Table 4.4: Relative distribution of the intestines in the Rando phantom 73
Table 4.5: Fractional values for the skin, bone, and red bone marrow (RBM) in each section of the Rando Phantom 74
Table 5.1: Different radiological factors used for determining the CT X-ray spectra 92
Table 5.2: The ratios of the μ_{en} (tissue/air) for different types of CT scanners 94
Table 5.3: The average ratio of the measured to the calculated normalised doses in the three representative sections of the Rando phantom 106
Table 5.4 : Measured TLD values* in the representative section of the "chest" (no. 14) 108
Table 5.5: Ratios of the normalised measured values to the calculated values in the representative section of the "chest" (no. 14) 108
Table 5.6: Measured TLD values* in the representative section of the "abdomen & pelvis" (no. 26) 109
Table 5.7: ratios of the normalised measured values to the calculated values in the representative section of the "abdomen & pelvis" (no. 26) 110
Table 5.8: Measured TLD values* in section 18 for the "chest" examination 111
Table 5.9: Ratios of the normalised measured values in section 18 to the calculated values in the representative section of the "chest" (no. 14) for the "chest" examination 111
Table 5.10: Measured TLD values* in section 20 for the "chest" examination 112
Table 5.11: The normalised measured values to the central value in section 20 for the "chest" examination 112
Table 5.12: The average ratio of the normalised measured values in section 20, 22, and 24 to the calculated values in the representative section of the "abdomen & pelvis" area (no. 26) 113
Table 5.13: Measured TLD values* in section 20 for the "abdomen & pelvis" examination 114
Table 5.14: Measured TLD values* in section 22 for the "abdomen & pelvis" examination 114
Table 5.15: Measured TLD values* in section 24 for the "abdomen & pelvis" examination 114
Table 5.16: The ratios of the normalised measured values in section 20 to the calculated values in the representative section of the "abdomen & pelvis" area (no. 26) 115
Table 5.17: The ratios of the normalised measured values in section 22 to the calculated values in the representative section of the "abdomen & pelvis" area (no. 26) 115
Table 5.18: The ratios of the normalised measured values in section 24 to the calculated values in the representative section of the "abdomen & pelvis" area (no. 26) 115
Table 5.19: Measured TLD values* in section 18 from the abdomen & pelvis" examination 116
Table 5.20: The normalised measured values to the central value in section 18 for the "abdomen & pelvis" examination 116
Table 5.21:Ratios of the calculated to the measured values for lungs and liver for the "chest" and "abdomen & pelvis" examinations 118
Table 5.22:The overall uncertainties in estimated patient doses for two typical CT examinations with the developed dosimetry method 120
Table 6.1: Typical clinical scanning parameters for the routine examinations with the GE 8800 CT Scanner 128

Table 6.2: Calculated organ doses and dose indices for the routine examinations with the GE 8800 CT scanner..... 129
Table 6.3: Typical clinical scanning parameters for the routine examinations with the GE 9000HP CT Scanner..... 129
Table 6.4: Calculated organ doses and dose indices for the routine examinations with the GE 9000 HP CT scanner..... 130
Table 6.5: Typical clinical scanning parameters for the routine examinations with the Philips Tomoscan CX/S CT Scanner..... 130
Table 6.6: Calculated organ doses and dose indices for the routine examinations with the Philips Tomoscan CX/S CT scanner..... 131
Table 6.7: Typical clinical scanning parameters for the routine examinations with the GE Sytec 3000 Plus CT Scanner..... 132
Table 6.8: Calculated organ doses and dose indices for the routine examinations with the GE Sytec 3000 Plus CT scanner..... 132
Table 6.9: Typical clinical scanning parameters for the conventional routine examinations with the GE HiSpeed Advantage CT Scanner..... 133
Table 6.10: Calculated organ doses and dose indices for the routine conventional examinations with the GE HiSpeed Advantage CT Scanner..... 134
Table 6.11: Typical clinical scanning parameters for the spiral examinations with the GE HiSpeed Advantage CT Scanner..... 134
Table 6.12: Calculated organ doses and dose indices for the routine spiral examinations using the GE HiSpeed Advantage CT scanner..... 135
Table 6.13: Typical clinical scanning parameters for routine conventional examinations with the Siemens Somatom Plus CT Scanner..... 136
Table 6.14: Calculated organ doses and dose indices for different routine conventional "head" examinations using the Siemens Somatom Plus CT scanner..... 134
Table 6.15: Calculated organ doses and dose indices for two routine conventional "chest" examinations using the Siemens Somatom Plus CT scanner..... 137
Table 6.16: Calculated organ doses and dose indices for three routine conventional "abdomen & pelvis" examinations using the Siemens Somatom Plus CT scanner..... 138
Table 6.17: Calculated organ doses and dose indices for two routine conventional pelvis examinations using the Siemens Somatom Plus CT scanner..... 138
Table 6.18: Typical clinical scanning parameters for the routine spiral examinations with the Siemens Somatom Plus CT Scanner..... 139
Table 6.19: Calculated organ doses and dose indices for different spiral examinations using the Siemens Somatom Plus CT scanner..... 139
Table 6.20: Summary of the effective dose and normalised effective dose values for the most common scanning techniques of the head..... 143
Table 6.21: Summary of the effective dose and normalised effective dose values for the most common scanning techniques of the chest..... 147
Table 6.22:Summary of effective dose and normalised effective dose values for the most common scanning techniques of the abdomen & pelvis..... 149
Table 7.1: Standard Planes for different types of CT Examinations referred to the NRPB mathematical phantom (Source: Poletti 1992)..... 163
Table 7.2: Extent (lower and upper limits in mm) of organs and tissues of the mathematical phantom as modified in the CTDOSE program..... 164
Table 7.3: Estimated CTDI values (mGy/mAs using IC) for all conditions and all makes and models of CT scanners..... 166
Table 7.4: Estimated CTDI values (mGy/mAs using TLDs) for all conditions and all makes and models of CT scanners..... 166
Table 7.5: The NRPB mean CTDI values (mGy/mAs) for three CT scanner models..... 167
Table 7.6: Comparison of the IC and the TLD (I) measuring techniques..... 173

Table 7.7: Comparison of the IC and the TLD (I) measuring techniques by CT scanner model..... 173
Table 7.8: Comparison of the gaussian (TLD (III)) and TLD (I) measuring techniques..... 174
Table 7.9: Comparison of the TLD (II) and TLD (I) measuring techniques..... 174
Table 7.10: Ratios of estimated CTDI values (with the IC) to that of 10 mm slice width for all the CT scanners..... 176
Table 7.11: Ratios of estimated CTDI values (with the TLDs) to that of 10 mm slice width for all the CT scanners..... 176
Table 7.12: A comparison between the nominal slice width with the FWHM and the true values derived from the dose profiles and CTDI ratios for the narrowest slice widths of all the CT scanners..... 177
Table 7.13: Variation of CTDI values (with the IC) by the kV..... 180
Table 7.14: Variation of CTDI values (with the TLDs) by the kV..... 180
Table 7.15: Variation of CTDI among the CT scanners (10 mm slice width, 120 kV)..... 183
Table 7.16: Ratios between estimated CTDI values with the TLDs for all the CT scanners and the NRPB values (from the national survey of CT practice in the UK)..... 184
Table 7.17: Typical clinical scanning parameters for the GE 8800 CT Scanner..... 186
Table 7.18: Typical clinical scanning parameters for the GE 9000HP CT Scanner..... 186
Table 7.19: Typical clinical scanning parameters for the Philips Tomoscan CX/S CT Scanner..... 187
Table 7.20: Calculated organ doses and dose indices for different examinations using the GE 8800 CT scanner..... 188
Table 7.21: Calculated organ doses and dose indices for different examinations using the GE 9000 HP CT scanner..... 189
Table 7.22: Calculated organ doses and dose indices for different examinations using the Philips Tomoscan CX/S CT scanner..... 189
Table 8.1: Contribution of organ/tissue doses to effective dose from the direct dosimetry method for the head and neck examinations..... 194
Table 8.2: Contribution of organ/tissue doses to effective dose from the MC dosimetry method for the head and neck examinations..... 194
Table 8.3: Ratios of organ/tissue, remainder, brain and effective doses between the direct and the MC dosimetry methods for the head and neck examinations..... 195
Table 8.4: Contribution of organ/tissue doses to effective dose from the direct and MC dosimetry methods for the chest examination..... 196
Table 8.5: Ratios of organ/tissue, remainder, and effective doses between the direct and the MC dosimetry methods for the chest examinations..... 197
Table 8.6: Contribution of organ/tissue doses to effective dose from the direct and MC dosimetry methods for the abdomen and pelvis examinations..... 198
Table 8.7: Ratios of organ/tissue doses and effective dose between the direct and the MC dosimetry methods for CT abdomen & pelvis examinations..... 198
Table 8.8: Percentage of the individual (the calibration and the phantom central doses) and the overall uncertainties (the CTDI and the "head" and "abdomen & pelvis" examinations) resulting from the TLD measurements..... 201
Table 8.9: Averaged normalise effective dose values to 100mAs, 10 mm scan volume, and CTDI over the measured effective dose values from all the CT scanners for three areas of the body..... 206
Table 8.10: Ratios of H_E to E for the most common CT examinations..... 208
Table 8.11: Typical effective doses to standard adult patients in the 1990s (From Wall and Hart 1997) 212

1. INTRODUCTION

1.1 Computed Tomography

Computerised Axial Tomography or more briefly Computed Tomography (CT) is an X-ray imaging technique providing excellent radiographic contrast between soft tissues and high quality clinical information for localised planes within the body. This revolutionary imaging technique was developed by Sir Godfrey Hounsfield and was introduced into clinical practice in the early 70's. The first commercially available CT machine, the EMI brain scanner, was installed in London in 1972. Over nearly a decade a large number of CT systems were introduced into the market being more than twenty models from over ten manufacturers (Speller et al. 1981a). The number and diversity of types of scanners continued to increase and about ten years later the National Radiological Protection Board (NRPB) of the UK reported that around 220 scanners, comprising 39 different models from 10 manufacturers, were operating in the National Health Services of this country (Shrimpton et al. 1991a). There has also been a similar proliferation of scanners throughout the world, such that the average frequency of CT examination in developed countries has been reported to be about 10 per 1000 population (Shrimpton and Wall 1992).The modality's explosive growth is also illustrated by the fact that approximately 2.2 million CT studies were performed in hospitals in 1980, only seven to eight years after the first commercial CT units became available (Bunge and Herman 1987). CT is now considered an essential element in radiological imaging. CT has replaced some other diagnostic techniques, often of a more invasive nature, some associated with a high morbidity or even mortality. Many of these also involved considerable patient exposures. Although this technique is proposed more in the diagnosis, it is also used in radiotherapy planning for the treatment of cancer and other pathological conditions and has allowed significant advances in good patient care. For example, about one third of scanners operating in the UK in 1989 were utilised in the planning of treatment for patients having radiotherapy (NRPB 1992).

There has therefore been a world-wide proliferation of scanners over the last 25 years, with the number in clinical operation in the UK rising steadily -and with no apparent sign of saturation- to around 200 in 1989 (NRPB 1992).

Notwithstanding the undoubted benefits of CT in health care, growth of the techniques has taken place without full appreciation of the relatively high patient doses involved.

1.2 The Significance of the Radiation Dose Associated with the CT

An assessment of diagnostic radiology in the UK for 1983 indicated a total of about 35 million medical and dental X-ray examinations with a collective dose equivalent from conventional procedures of 15500 man Sv (Shrimpton and Wall 1986). Although there have been changes in practice since 1986, it is still judged that the collective dose from conventional techniques remains unchanged at 16000 man Sv approximately (Hughes and O'Riordan 1993).

The estimate of collective dose given above does not include a contribution from CT. A survey recently carried out by the NRPB in collaboration with the Institute of Physical Sciences in Medicine (IPSM)[1] shows that in the UK 2.4% of all medical and dental X-ray examinations involve CT (Shrimpton et al. 1991b). The collective effective dose equivalent from the 200 CT scanners operating in the UK during 1989 is estimated at about 4500 man Sv.

The overall collective dose from diagnostic radiology is the sum of those from conventional and CT examinations. There is some uncertainty in combining data from different periods of time because techniques of radiology continue to evolve and usage changes. Nevertheless, a rounded value of 20000 man Sv would seem to be appropriate as a revised total annual collective effective dose equivalent from all radiological practices including conventional and CT practices. The relative contribution from various types of examination are given in Table 1.1. Therefore the available data suggest that while CT represented about 2% of the total of all X-ray

---

[1] The IPSM name has now (1997) been changed to the Institute of Physics and Engineering in Medicine abbreviated by IPEM.

examinations, yet accounted disproportionately for 20% of the resultant collective dose. Therefore it has a great impact on the total collective dose and it now represents the major source of exposure from diagnostic X-rays (Shrimpton et al. 1991b, NRPB 1992, Hughes and O'Riordan 1993, Wall and Hart 1997). Moreover, recent information (Shrimpton and Wall 1993) confirms the trend of ever increasing numbers of scanners and suggests that CT may now represent about a third of the collective dose from diagnostic X-rays in the UK.

Table 1.1: Contributions to the annual collective dose from all medical and dental X-ray examinations in the UK (Source: Hughes and O'Riordan 1993).

Examination	**% frequency**	**% collective dose**
Computed Tomography	**2.4**	**22**
Lumbar spine	3.3	15
Barium enema	0.9	14
Barium meal	1.6	12
Intravenous Urography	1.3	11
Abdomen	2.9	8
Pelvis	2.9	6
Chest	24	2
Limbs and joins	25	1.5
Skull	5.6	1.5
Thoracic spine	0.9	1
Dental	25	1
Others	4.2	5
Total	**100**	**100**
Annual collective dose from all procedures		**20000 man Sv**

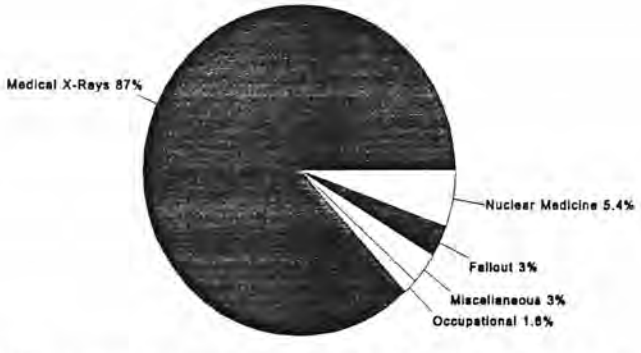

Figure 1.1: Contribution of different types of manmade radiation to the collective annual dose for the UK population (Source: Hughes and O'Riordan 1993).

The dose received by patients from diagnostic medical X-rays comprise about 87% of the total collective dose to the population of the UK from all man made sources of radiation (Figure 1.1) (Hughes and O'Riordan 1993).

Ionising radiations are associated with certain risks, the main at these levels being the induction of cancer. The risk factor for fatal cancers for a population of all ages and both sexes is believed to be a 45 in one million chance of death following irradiation of 1 mSv (for low LET radiation) (ICRP 1991). Approximate estimates for the risk of fatal cancers arising within the lifetime of patients is dependent on the age of the patient as well as the type of examination. However, the risk factors averaged over all ages and both sexes varies from 0.7 per million for a chest X-ray to 100 per million for a barium enema (Table 1.2) (NRPB 1990).

Table 1.2: Typical lifetime risks of fatal cancer from X-ray examinations

Examination	Lifetime risk of fatal cancer*	
	Lower bound	Upper bound
Skull	2	7
Chest	0.7	2
Thoracic spine	15	40
Lumbar spine	30	100
Abdomen	20	60
Pelvis	15	55
Intravenous Urography	60	200
Barium meal	50	170
Barium enema	100	350

***average for all ages and both sexes (Per million)**

1.3 Computed Tomography Dosimetry - General Aspects and Background

One of the principles of radiation protection is that doses should be kept as low as reasonably achievable which is abbreviated as ALARA principle. There is a wide range of methods for reducing doses to patients without loss of diagnostic value and the more important ones are listed in Appendix B of the NRPB documents (NRPB 1990). One of the radiological procedures for reducing doses to patients from X-ray examination is periodically measuring patient doses and taking action if they exceed "guideline doses" which has a potential of 20% dose reduction per

examination (NRPB 1990). Furthermore it is obvious that reduction of patient dose to a minimum is one of the objectives of good radiology practice. The simplest method of monitoring whether this objective is achieved is to measure dose for a sample of patients or under standard conditions. This has been recommended by a joint working party of the NRPB and the Royal College of Radiologists (RCR) (NRPB 1990).

In recent years different dosimetry methods have been used for characterising radiation doses associated with a CT scanner. Objectives of these measurements include ensuring that a CT scanner meets the manufacturer's specifications and comparing dose associated with different types of scanner, and also comparing CT doses with radiation doses resulting from other radiological examinations.

Another important reason for investigating radiation doses associated with CT scanners is to estimate radiation risks to patients undergoing CT examinations (Mossman 1982, Huda and Sandison 1985, Faulkner and Moores 1987). The most appropriate method of estimating the radiation risk associated with a CT examination is to obtain the mean absorbed dose in every irradiated organ and tissue, permitting each organ risk to be obtained (UNSCEAR 1988, NCR 1990, NCRP 1990, ICRP 1991). Knowledge of individual organ/tissue doses permits the computation of a single dose descriptor such as the effective dose equivalent (H_E) (ICRP 1977) or effective dose (E) (ICRP 1991). H_E and E data may be used for intercomparison of CT techniques and also to compare the radiation risks associated with CT examinations to other diagnostic examinations that use ionising radiation.

Since the introduction of CT in the early 1970s, dosimetric investigations have generally followed two different tracks. One track has been the specification of radiation dose to specific locations in patient and phantoms. The other track has been the evaluation of effective dose equivalent or effective dose as an indicator of total radiation risk to the patient from CT examinations.

Standard CT dosimetry techniques, generally involving the use of QA phantom, are normally based on the first track. These techniques often give rise to dose descriptors that are poorly correlated with patient risk such as maximum or average surface dose and integrated dose profiles recorded either on the surface or at the centre of the QA phantom. The second track, i.e. the assessment of the effective

dose resulting from CT examinations, requires a knowledge of the dose to all radiosensitive organs of the patient arising from the complex pattern of irradiation employed in clinical practice. The assessment of the effective dose has generally been done in one of two ways: organ-by-organ dose determination or by estimation of total energy imparted to the patient (Atherton 1993). Based on these two tracks several dosimetry approaches have been followed using various combinations of different sets of equipment and methods.

Sets of equipment used for CT dosimetry could be divided into two categories of dosimeters and phantoms. All conventional dosimeters, normally used for X-ray dosimetry, such as: thermoluminescent dosimeter (TLD) crystals (Jucius and Kambic 1977, Dixon and Ekstrand 1978, Shope et al. 1982, Cack and Hendee 1979), special ionisation chambers (Moore et al. 1979, Poletti 1984), and films have also been used for CT dosimetry. A range of solid and water filled phantoms, simulating part or whole of the human body have been used and developed over the past 25 years for CT dosimetry purposes. These phantoms could be categorised in: regular geometry phantoms (Speller et al. 1981a), physical anthropomorphic phantoms including epoxy-resin based (Speller et al. 1981a) and Rando (Nishizawa et al. 1991) phantoms, and finally mathematical anthropomorphic phantoms (Kramer et al. 1982, Drexler et al. 1984, Jones and Shrimpton 1991, Shrimpton et al. 1991b) similar to Medical Internal Radiation Dose (MIRD) phantoms. Apart from these two broad classes of physical and mathematical phantoms, another type of phantoms, called Quality Assurance (QA) phantoms, designed primarily for CT performance measurements, has also been used by some researchers to assess doses and risks to the patients resulting from CT examinations.

Regarding methods two major methods, namely **"direct"** and **"Monte Carlo"** methods, have been used either for the first or the second track of CT dosimetry. The **"direct"** method is also referred to as "**measurement"** or **"experimental"** dosimetry method by some researchers.

Over the last twenty five years since the introduction of CT into clinical practice (Hounsfield 1973), researchers have used various combinations of the above sets of equipment and methods for CT dosimetry.

Initial investigation of radiation dose in CT followed the first track, reporting dose to specific points in phantoms. When Sir Godfery Hounsfield introduced this revolutionary diagnostic technique (Hounsfield 1973), he reported the exposure at the patient's skin for an examination which provided six tomographic slices over the whole of head. He found the CT skin dose approximately equivalent to a conventional X-ray examination. Perry and Bridges (1973) used a conventional ionisation chamber (IC) mounted in a short perspex cylinder filled with water as a head phantom and reported isodose curves and gonad dose for a single scan. They concluded that the integral dose from a single complete CT scan was likely to be less than that from a single skull X-ray. Horsely and Peter (1976) used capsules of LiF powder inserted around the circumference of a Rando phantom skull in the plane of the CT scan. They produced isodose curves similar to that of Perry and Bridge (1973) for a single scan and multiple scans for an EMI scanner. They also reported on the dose to skin from multiple scans from this scanner as measured in a Rando phantom. They concluded that the dose to the cranium of patients undergoing routine skull scans on the EMI scanner was higher than previously reported by Perry and Bridge (1973). McCullough and Payne (1976) used TLDs and an Alderson phantom and measured doses at the centre and four peripheral locations of the phantom and reported the maximum surface dose for three different scanner models. Weistein et al. (1976) reported the results of surface dose measurements for some scanners using single and multiple scans. Shrivastava et al. (1977) reported measurements of gonads and other organs exposures due to scattered radiation from CT scans. Boyd et al. (1977) used a slightly flattened plexiglass cylinder to simulate the contour of a torso, with a circumference of 91 cm, filled with water. They measured and compared doses for two different types of scanners with the TLDs inserted at the centre and four peripheral locations inside and on the surface of the phantom. Bassano et al. (1977) measured doses for a series of scans using TLD-100 placed in head and abdomen sections of the Alderson phantom. They constructed isodose curves from several measurements at various positions in the head and abdomen of the phantom and reported the range of doses. They also used an IC for the testis and TLDs for the ovary and reported range of doses to gonads for different scan protocols for a particular scanner. Krauss and

Shumacher (1977) reported patient doses using similar isodose profiles for whole body CT examinations. Jucius and Kambic (1977) reviewed methods of CT dosimetry and discussed the use of TLDs, films, and IC to obtain exposure profiles. They used both the TLDs and a pencil IC and measured the exposure distributions of peak exposure for a single scan and average exposure for a series of scans. They also used film as a qualitative exposure device to study the surface dose for a single scan and a series of scans. Dixon and Eckstrand (1978) used a film dosimetry system to measure surface dose for single and multiple scans in circular and elliptical acrylic phantoms. They also measured the film response to both the entrance and exit doses relative to that of a Farmer IC using a 20 cm thick water phantom. Villafana et al. (1978) measured doses received by the surface of head and interior brain points, lens of the eye and gonads. They used a Rando phantom and TLD-100 powder capsules in a grid matrix at appropriate levels of the head placed around the exterior surface of the phantom head. Brasch et al. (1978) used two child sized (with 36 and 66 cm circumference) phantoms (composed of polystyrene at the centre and acrylic at the end) on seven models of CT and TLD capsules. They reported average surface dose and internal doses for a complete abdominal CT examination comprised of eight scans. Hobday and Parker (1978) reported the maximum exposure to the skin from an EMI scanner using Temex skull and body phantoms and LiF TLDs. They also estimated doses to the lens of the eye from skin doses near to the orbit. Agarwal et al. (1979) used a water filled (17.5 cm diameter) Lucite cylinder and ten pairs of LiF TLD-100 to measure dose distribution from a particular scanner. They concluded that the isodose curves for different combinations of slice thickness and scan speed were similar, although the absolute values of the doses were different. They also concluded that the increase in dose with slice width is linear. They also reported surface dose measured with the TLD chips taped to the outer surface of the phantom. Wall et al. (1979) used a Rando phantom and $LiBO_4$ TLDs to measure doses for some neurological thoracic and abdominal examinations for three scanners. They reported maximum skin doses and some isodose curves for these scanners based on measurements made at the centre of and four locations on the surface of the phantom sections. Souton (1980) measured peak doses and surface line integral doses by a row

of TLD-100 chips on the surface of a phantom at the point of expected maximum on either side of the centre for several scanners. White et al. (1980) proposed that dose to the patient could be assessed for either single or multiple scans at the surface and centre of the special skull and thorax phantom sections using film or TLDs. Moor et al. (1981) proposed a multisegmented IC for CT dosimetry to avoid what they described as the drawbacks of TLDs including the inherent imprecision of thermoluminescent dosimetry and the time required for calibration and the inventory of individual TLD chips. They concluded that there was a good agreement at narrower beam widths (3&6 mm) between their IC profiles and TLD measurements, although a series of ten exposures was needed to obtain the IC segment responses. Speller et al. (1981b) carried out a survey during 1978-9 on the performance characteristics of 29 EMI brain and body CT scanners in Britain. They presented dose profiles for a single slice using TLD and film and a physical anthropomorphic phantom. They reported mean doses in the form of maximum surface dose for single slice scans and compared their results with others (Hobday and Parker 1978 and Wall et al. 1979). They also reported typical dose profiles for these scanners at the centre of the phantom. Shope et al. (1982) used TLD to measure point doses for single and multiple scans in both cylindrical and anthropomorphic phantoms in scanners from ten manufacturers. They presented surface and centre doses for the cylindrical phantoms and the maximum dose measured in the anthropomorphic phantom. Fearon and Vucich (1985) measured surface doses in paediatric patients for several standard examinations and compared the results to in-phantom measured values. Storrs and Byrd (1988) and Maclennan and Hadley (1995) measured the dose to the lens of the eye for paediatric patients. There have also been studies of foetal or intrauterine dose from CT (Wagner et al. 1986, Fearon and Vucich 1987, Guidozzi et al. 1987, Femlet et al. 1990, Adams et al. 1997).

1.4 Common CT Dosimetry Approaches

Apart from the initial investigations of assessing the radiation dose associated with the CT, the most common approaches in CT dosimetry could be grouped in three distinctive categories and could be called as: **Standard**; **Monte Carlo**; and

Direct approaches.

1.4.1 Standard CT Dosimetry Approach (using Quality Assurance Phantom)

This technique involves using the QA phantoms (Perspex/Plexiglass phantoms), originally designed for evaluating CT performances, and measuring skin dose and CTDI (**C**omputed **T**omography **D**ose **I**ndex) values. These terms will be explained in more detail in the following chapter.

1.4.2 Monte Carlo CT dosimetry Approaches

Monte Carlo (MC) technique is a powerful tool in the study of radiation transport, where known probability distribution simulate physical process and the random paths of particles in materials and geometry of interest (Cashwell and Everett 1959). This calculation technique (MC) has been used in two ways in CT dosimetry. In one approach it has been used to estimate the organ doses and other radiation dose descriptors through the total energy deposited or imparted to the patients. In the other approach this computational technique has been used to yield organ doses normalised to the free-in-air dose on the axis of rotation of the scanner, known as CTDI, to calculate other radiation risk indicators (H_E and E).

1.4.2.1 Monte Carlo Approach using Total Energy Imparted Quantity

In this approach the assessment of the radiation doses to the patient is through estimation of the total energy deposited or imparted to the patient. The studies cited below claim, the energy imparted to the patient (formerly "integral dose") has been shown to be a useful estimator of stochastic risks in diagnostic radiology. The energy imparted is a physical quantity and is independent of organ weighting factors contrary to other usual approaches which will be explained in the following chapters. The use of energy imparted to a patient as a risk estimator assumes a homogeneous mix of radiosensitive and radioresistant tissues within the body (Wall et al. 1988). This approach, which was determined as "a less versatile way" a few years ago (Shrimpton

et al. 1991b), has recently been developed and used for CT dosimetry and claimed to be simpler but cruder than organ dose estimation approaches (Atherton 1993, Atherton and Huda 1995, Atherton and Huda 1996).

Bengtsson et al. (1978) used energy imparted as a basis for risk estimates for conventional radiographic examinations. They based their estimates on the risk coefficient 1.65 10^{-2} Sv^{-1} for radiation workers (ICRP 1977) and identified a risk of 2.0 10^{-4} J^{-1}, which corresponds to a ratio of 12.1 mSv/J. Southon (1981) reported values for energy imparted in comparison of six different CT scanners but did not present any explicit risk estimates corresponding to energy imparted values. Shrimpton (1985) studied the relationship between the energy imparted and the effective dose equivalent in common radiographic examinations and found a linear relationship (within a factor of two) between the two of 13.8 mSv/J. Le Heron (1992) claimed "good agreement" between the energy imparted and the effective dose in conventional radiography, although he did not present any values. He based his work on the NRPB organ dose data (Jones and Wall 1985).

Atherton and Huda (1995, 1996) indicated that these studies show that the energy imparted can either be used outright as an indicator of patient risk estimate or to estimate other risk estimators. Using this quantity (energy imparted) they have developed a computational MC method to estimate the CT doses.

1.4.2.2 Monte Carlo Approach using Mathematical Phantoms

An alternative approach of patient dosimetry employs MC computer techniques to simulate the absorption and scattering of X-ray photons within a mathematical anthropomorphic phantom, yielding organ doses normalised to the CTDI measured for a single scan, free-in-air on the axis of rotation of the scanner. This is the method used by the NRPB in the national survey of CT practice in the UK (Shrimpton et al. 1991a, Shrimpton et al. 1991b, and Jones and Shrimpton 1991).

This approach is based upon measurement of the CTDI with either a CT ionisation chamber or a stack of TLDs inside a hollow, cylindrical plastic tube -and long enough to cover the X-ray beam width -which could be positioned along the axis of rotation of the scanner. This approach known as Monte Carlo or sometimes CTDI

method has also been used by several groups of workers (Shrimpton et al. 1991a, Shrimpton et al. 1991b, Jones and Shrimpton 1991, Zankl et al. 1991, Zankl et al. 1992, Poletti 1992, Atherton 1993, Gleijns et al. 1994, Atherton and Huda 1995, Zankl et al. 1995, Poletti 1996, Caon et al. 1997).

1.4.3 Direct CT Dosimetry Approach using Physical Phantoms

In this approach a physical anthropomorphic phantom is used and direct measurements of the absorbed dose in relevant organs are performed with TLDs. This approach, sometimes called direct or experimental method, has also been employed by several researchers (Faulkner and Moores 1987, Huda et al. 1989, Nishizawa et al. 1991, Gleijns et al.1994).

1.5 Current Problems in CT Dosimetry

As noted above, since the introduction of CT into clinical practice in the early 1970s different quantities have been used to quantify patient doses resulting from CT practice. Quantities involved include a wide range of simple quantities such as tube-current exposure-time product (mAs), surface dose, single organ or tissue dose. As mentioned earlier, early attempts in CT dosimetry generally involved reporting various dose descriptors derived from the above simple quantities. These quantities often give rise to dose descriptors that are either crude or poorly correlated with the patient risk. Nowadays the CTDI quantity (Shope et al. 1981), and the more complex quantity of effective dose (ICRP 1991) are being used more often. But the problem is that the complex quantity of effective dose (formerly effective dose equivalent (ICRP 1977)) requires a knowledge of the dose to all radiosensitive organs of the patient arising from the complex pattern of radiation employed in CT practices.

The mAs of a scanner gives information on the radiation exposure proportional to dosimetric quantities such as surface dose, CTDI, and effective dose. However, this quantity can only be used as a relative measure of radiation exposure resulting from different CT scanning techniques for a specific type of scanner and anatomical region of the body (Naidich et al. 1990, Babbel et al. 1991, Marmolya et

al. 1991, Zwirewich et al. 1991), and can not be used for comparing different types of CT scanners.

Surface doses in terms of maximum skin or surface dose and maximum doses at selected locations within various types of phantom were presented in the first reports of measurements of exposure or absorbed dose from either a single scan or multiple scans for different CT systems. From the early time of the invention of the CT up until recent years many researchers have reported surface doses resulting from CT examinations for various types of scanners (Hounsfield 1973, Perry and Bridges 1973, McCullough et al. 1974, McCullough et al. 1976, Horsely and Peter 1976, Weinstein et al. 1976, Thomas et al. 1978, Brasch et al. 1978, Villafana et al. 1978, Dixon and Ekstrand 1978, Agarwal et al. 1979, Boyed et al. 1979, Wall et al. 1979, Southon 1980, White et al. 1981, Speller et al. 1981a, Shope et al. 1982, Lund and Halaburt 1982, Jones and Garett 1985, Murphy and Heaton 1985, Fearon and Vucich 1985, Evans et al. 1989, Mayo et al. 1993). There is no doubt that surface dose on a phantom or the skin of a patient may give enough information to assess patient doses for conventional X-ray examinations. This simple quantity can easily be measured and used with available data sets or software (Rosenstein 1976, Rosenstein 1989, Hart et al. 1994, Hart et al. 1996a) to assess organ doses and subsequently effective dose values for conventional X-ray examinations. But because of the variation in X-ray intensity as a function of position of the CT scan and the complexity and variety of CT scanner characteristics, the surface dose quantity is rather inhomogeneous for CT examinations. Therefore contrary to the conventional x-ray examinations this quantity can not be obtained from a single measurement on scanners and used to derive organ doses and effective dose values for CT examinations.

Doses to a single organ or tissue, such as the lenses of the eye (Villafana et al. 1978, Storrs and Byrd 1988), thyroid gland (Brasch et al. 1978), gonads (Perry and Bridges 1973, Bassano et al. 1977, Shrivastava et al. 1977, Villafana et al. 1978), and foetus (Wagner et al. 1986, Fearon and Vucich 1987, Guidozzi et al. 1987, Felmlee et al. 1990) measured inside various phantoms using TLDs at the location of the single organs of interest provide a better knowledge of the risk to these organs. Nevertheless, these quantities will not lead to the assessment of the patient risk

involved with the CT practice that requires doses to more than twenty other radiosensitive organs. Furthermore, there are remarkable significant differences in absorbed dose distributions resulting from CT practices and differences in dose distributions from different types of CT systems. These differences are due to the variety of scanning techniques, x-ray beam collimation geometries, and operating conditions. Therefore single number dose descriptors such as the maximum or average dose from a single scan are often inadequate.

Because of the inadequacy of single number dose descriptors and rapid variation in x-ray intensity as a function of position normal to the plane of the scan, as noted above profiles of the exposure or dose as a function of position along a line parallel to the axis of rotation of the CT system were used to describe the dose from CT systems. Such dose profiles were reported for a single scan (Cohen 1979) and used to estimate the doses for multiple scans as a function of the number of scans and the increments between scans (Krauss and Shumacher 1977, Hobday and Parker 1978, Brasch et al. 1978, Dixon and Ekstrand 1978, McCullough and Payne 1978, Jucius and Kambic 1977, Cack and Hendee 1979, Olson and High 1979). Such profiles, however, give no information about the dose distribution in "z" direction and few CT scanning techniques consist of only one scan. Following these efforts, the computed tomography dose index (CTDI) proposed by Shope et al. (1981) was a big step to overcome the weakness of the above reports on the CT single dose profile. CTDI is measured at a specific depth inside a phantom such as cylindrical PMMA standard head or body phantom (Mayo et al. 1987, McCrohan et al. 1987, Conway et al. 1992) or free in air at the centre of rotation of the CT scanner (Panzer et al. 1989, Shrimpton et al. 1991b, Christensen et al. 1992). Although this dose profile, CTDI, provides a better index for studying the performance of different CT systems (Shope et al. 1981, Speller et al. 1981b, Shope et al. 1982, Shrimpton et al. 1991b), it does not provide enough information, on its own, to assess the patient doses in terms of effective dose. This can be achieved by combining CTDI with a computational phantom and Monte Carlo techniques (Jones and Shrimpton 1991 and 1993, Zankl et al. 1991).

The ICRP in its 1990 recommendations (1991) has proposed that the quantity of effective dose be used as an index for the assessment of patient doses from all varieties of medical x-rays. In this regard, as noted above, two dosimetry approaches, namely the MC and the direct approaches, have commonly been employed for the assessment of patient doses from CT practices. Nonetheless, either of these common CT dosimetry approaches have their own constraints.

If the direct approach is selected, organ and tissue doses should be measured inside a physical phantom employing TLDs at the location of the selected radiosensitive organs from which the effective dose value could be calculated (Murphy and Heaton 1985, Evans et al. 1989, Brasch and Cann 1982, Wagner et al. 1986, Fearon and Vuich 1987, Sager et al. 1989, Vañó et al. 1989, Nishizawa et al. 1991, Collie et al. 1994a and 1994b). This approach requires numerous TLD measurements (>200) for just an individual CT examination making it a laborious and impractical task for routine patient dose assessment from CT practices. If the MC dosimetry approach is employed organ doses and subsequently effective dose values can be calculated rapidly and easily by measuring the CTDI free in air and using available conversion factors for a limited number of CT models (Shrimpton et al. 1991b, Jones and Shrimpton 1991, Jones and Shrimpton 1993, Panzer et al. 1989, Panzer and Zankl 1989, Zankl et al. 1991). The problem with this method is that it is applicable to a limited number of old CT scanners for which conversion factors are available. On the other hand application of this method for the new CT scanner models requires details of the scanner configuration and also implementing the Monte Carlo computational technique. This involves acquiring the scanner configuration data from the manufacturers and special computing facilities and expertise for the MC technique. Although some efforts has been made to determine a correlation between new CT models and older models for which the conversion factors are available (Edyvean et al. 1997), the above prerequisites make this approach, too, impractical for routine patient dose assessment from CT practices.

1.6 Proposed CT Dosimetry Approach

It is obviously the second track of CT dosimetry, i.e. the assessment of the radiation risk (in terms of effective dose) based on the absorbed doses in all organs and tissues of interest, that is of importance in CT practice. In addition from various approaches of the second track of CT dosimetry described above, the last two approaches are common and used frequently. Hence, in this study we aimed to determine the absorbed dose in all organs and tissues of interest and other dose indices using these two common approaches, namely the direct approach using a physical anthropomorphic (Rando) phantom and the MC approach using the mathematical anthropomorphic phantom. For brevity, the "direct" and "MC" terms will be used respectively for these CT dosimetry approaches in the rest of this thesis.

However, as mentioned above, either of these common approaches are not quite practical to be implemented for routine patient dose assessment from CT practices. There are two prerequisites in order to utilise the MC approach in CT dosimetry. Firstly, it is necessary to gain the necessary data on the scanner design from the CT manufacturers for every CT scanner model. Secondly, it is required to write an algorithm or use others' algorithms for the MC calculations. Therefore this dosimetry approach is dependent on the co-operation of two external bodies. Even if, it is preferred to write down the necessary codes for the MC calculations, a considerable amount of time must be spent to test and run the program on a suitable computer. On the other hand if the common direct CT dosimetry approach is used, it will require a large number of point dose measurements (~200) at the location of all organs and tissues of interest inside a physical phantom. This, in turn, makes the direct approach a laborious and impractical procedure for the routine assessment of patient doses from CT practices.

Therefore to avoid these constraints, the direct CT dosimetry approach was developed in this study. This was achieved by assessing CT axial and longitudinal dose distribution in an anthropomorphic physical phantom. Measurement of these dose distributions enabled us to propose a method to quickly estimate patient doses, for any CT examination protocol performed by any CT scanner, with a limited number of TLD measurements in a Rando phantom. All dosimetry related concepts were

considered for the proposed direct CT dosimetry method. A spreadsheet computer program was also designed that handles all necessary data processing and reports organ absorbed doses and other dose indices with a very user friendly interface. Comprehensive dose measurements were also carried out to estimate the level of error in the developed direct CT dosimetry approach.

In addition the MC approach was also used to estimate patient doses resulting from routine CT examinations for some of the scanners in this study for which conversion factors were available. This enabled us to compare our developed direct dosimetry method with this common CT dosimetry approach for some scanners. In this regard the patient doses were estimated by combining our measured CTDI values with calculated organ dose conversion factors provided by the NRPB (Jones and Shrimpton 1991). The CTDI values were measured with both a stack of the TLDs and the CT ionisation chamber.

1.7 Aims of Thesis

The ultimate goal of this work is to develop a simple and practical dosimetry method for the assessment of patient doses from CT practice with an acceptable degree of accuracy. The aims of this study are:

1. To provide a comprehensive and critical literature review on the dosimetry approaches used for the assessment of patient doses from CT practice.
2. To provide an overview on the CT technical developments from the early prototype invented in the early 70s to the state-of-the art CT models.
3. To propose a simple and practical method for routine CT dosimetry.
4. To implement and validate the proposed CT dosimetry method.
5. To evaluate different CTDI measuring techniques used for the MC CT dosimetry approach.
6. To assess patient doses using the developed method for routine CT practices performed by all the CT scanners operating at the NHS hospitals in the Lothian and Fife areas of Scotland.
7. To assess patient doses with the MC approach for routine CT practices performed by some of the CT scanners operating at the NHS hospitals in

the Lothian and Fife areas of Scotland.

8. To compare the developed and the MC dosimetry approaches for CT.
9. To find a quick method for the estimation of patient doses for similar protocols with a good degree of approximation.

1.8 Outline of Thesis

This thesis is organised as follows to address the aims of this study. As noted, this chapter introduces a comprehensive background on computed tomography. It includes a general description of CT and its importance in medical diagnostics, the significance of the dose associated with the CT practice, a critical review of the common dosimetry approaches used and current difficulties in the assessment of patient doses with the common approaches, and finally a general description of our proposed CT dosimetry method. Chapter 2 compiles the principles of CT dosimetry including basic dosimetric quantities, CT dosimetry devices, and finally CT dose descriptors. Chapter 3 contains an overview of common CT scanner characteristics in which the basic operational principles and technical developments of CT, its historical and technical developments, and the basic physical characteristics of the CT scanners used in this study are described. Chapter 4 presents the extra design carried out on the physical phantom required for the implementation of the proposed CT dosimetry method. Chapter 5 is the core of the thesis presenting the practical CT dosimetry method developed. Chapter 6 provides the results of the implementation of the developed dosimetry method for the assessment of patient doses resulting from routine CT practices using all the CT scanner models operating at different NHS hospitals in Lothian and Fife areas of Scotland. Chapter 7 presents the application of the MC CT dosimetry method in this study including the principles of the method, CTDI measurements, and patient doses for some of the CT scanners. Chapter 8 compares the developed direct dosimetry method with the MC dosimetry method. Chapter 9 contains a discussion on the implementation of the proposed dosimetry method and the conclusion of the thesis. In this chapter our results are also compared with the available data provided by the NRPB from a national survey of CT practice in the UK (Shrimpton et al.1991b, NRPB 1992, Wall and Hart 1997).

2. CT Dosimetry Principles

Comprehensive assessment of risk, in CT dosimetry, requires a knowledge of the dose to all radiosensitive organs of the patient arising from the complex pattern of irradiation employed in clinical practice.

As explained in the first chapter, three different approaches are followed for CT dosimetry. These are: the standard method using a quality assurance phantom, the Monte Carlo (MC) approach using either the computed tomography dose index (CTDI) or the total energy imparted value and a mathematical anthropomorphic phantom, and finally the direct or experimental approach through the direct measurements of organ or tissue doses inside a physical anthropomorphic phantom.

The standard dosimetry methods for CT have been designed primarily to monitor CT scanner performance characteristics. These methods often give rise to dose descriptors that are poorly correlated with patient risk such as maximum or average skin dose or surface dose and integrated dose profiles recorded either on the surface or at the centre of a QA phantom. On the other hand although the CT dosimetry approach that uses the Monte Carlo technique and a mathematical phantom through the estimation of the total energy imparted to the patient has recently been developed (Atherton 1993, Huda and Atherton 1994, Atherton and Huda 1995, Atherton and Huda 1996), it has already been described as a less versatile technique for CT dose assessment (Shrimpton et al. 1991b). Hence these two approaches are not quite common and practical in CT dosimetry if the assessment of the radiation risks to the patients is considered.

Therefore, there are just two more common approaches for CT dosimetry. These are the Monte Carlo approach using the CTDI value and a mathematical anthropomorphic phantom and the direct approach using a physical anthropomorphic phantom. For brevity in the rest of this thesis we will refer to these approaches as the Monte Carlo and the direct dosimetry methods.

The MC approach is a very popular CT dosimetry method, at the moment, and has been adopted by several national bodies in the UK, other European countries, and

many individual researchers world-wide. When the NRPB used this approach for the national survey of CT practice in the UK (Shrimpton et al. 1991a, Shrimpton et al. 1991b, Jones and Shrimpton 1991), it published organ doses for several models of CT scanners normalised to CTDI measured in air. These data can easily be used for calculation of effective dose, but they are limited to some older types of CT scanners. Hence, for the assessment of patient doses from some of the CT scanners in this study, we also used this approach parallel to our developed direct CT dosimetry approach and compared them with each other. The fundamentals and results of applying this dosimetry method are introduced in a separate chapter.

In the other common approach a physical anthropomorphic phantom (Rando Alderson) is used and direct measurements of the absorbed dose in relevant organs are performed. Doses are measured in the location of organs and tissues of interest usually by using TLDs from which effective dose (or effective dose equivalent) can be calculated. This approach, called the direct or experimental method, is obviously a very time consuming and laborious procedure.

Therefore, to avoid the limitations of these two approaches, a simplified direct method of dose measurement was developed to assess the radiation doses from CT scanners that can be implemented more rapidly than the full survey of dose in all organs and tissues. The details of this approach, including the extra design carried out on the physical phantom, the material used, and the developments carried out to simplify the method are explained in the following chapters.

In this chapter basic dosimetry quantities; different CT dosimetry devices including dosimeters and phantoms; and finally different CT dose descriptors will be described.

2.1 Basic Dosimetric Quantities

In this section all dosimetric quantities that are used in this study and referred to in the following chapters will be explained. For further information about these quantities the reader is referred to several references that are mentioned throughout this section.

2.1.1 Absorbed Dose

The fundamental dosimetric quantity in radiological protection is the absorbed dose, D. This is the energy absorbed per unit mass and its unit is the joule per kilogram (J kg^{-1}), which is given the special name gray (Gy) (ICRP 1991).

The International Commission on Radiological Protection (ICRP), in its 1990 recommendations, defined a new weighted-dose quantity called effective dose. This is based on another weighted dose, namely equivalent dose, for controlling the exposure to radiation of workers and members of the public. According to the ICRP recommendations, both equivalent dose and effective dose are quantities intended for use in radiological protection, including the assessment of risks in general terms. They provide a basis for estimating the probability of stochastic effects only for absorbed doses well below the threshold of deterministic effects (ICRP 1991). These concepts will be explained briefly in the following sections.

2.1.2 Equivalent dose

Since the effective dose has been defined by the ICRP as the sum of the weighted equivalent doses in all radiosensitive tissues and organs of the body, it seems to be necessary to explain first the concept of the equivalent dose.

The probability of stochastic effects is found to depend not only on the absorbed dose, but also on the type and energy of radiation causing the dose. This is taken into account by weighting the absorbed dose by a factor related to the quality of the radiation. In radiological protection, it is the absorbed dose averaged over a tissue or organ and weighted for the radiation quality that is of interest. The weighted factor for this purpose is now called radiation weighting factor, w_R, and is selected for the type and energy of the radiation incident on the body or, in the case of sources within the body, emitted by the source. The value of this factor for a specified type and energy of radiation has been selected by the ICRP to be representative of relative biological effectiveness (RBE) of that radiation in inducing stochastic effects at low doses. The RBE of one radiation compared with the other is the inverse ratio of the

absorbed dose producing the same degree of a defined biological end-point. The weighted absorbed dose is called the equivalent dose in a tissue or organ, using the symbol $\mathbf{H}_T$. The equivalent dose in tissue T is given by the following expression:

$$\mathbf{H}_T = \sum_R W_R \cdot \mathbf{D}_{T,R} \qquad \text{(Equation 2.1)}$$

where $\mathbf{D}_{T,R}$ is the absorbed dose averaged over the tissue or organ T, due to radiation R. Since W_R is dimensionless the SI unit of equivalent dose is the same as for absorbed dose, namely the J kg $^{-1}$, and its special name is sievert (Sv) (ICRP 1991).

The ICRP has chosen a value of radiation weighting factor of unity for all types of radiation of low LET (Linear energy transfer, a measure of the density of ionisation along the track of an ionisation particle), including X and gamma radiation of all energies. The choice for other radiation is based on observed values of the RBE, regardless of whether the reference radiation is X or gamma radiation. The values of W_R for different types and energy ranges of radiation are given in Table 2.1 (ICRP 1991).

Table 2.1: Radiation weighting factors (source: ICRP 1991).

Type and energy range	Radiation weighting factor (W_R)
Photons, all energies	1
Electrons and muons, all energies	1
Neutrons, energy < 10 KeV	5
10 KeV to 100 KeV	10
> 100 KeV to 2 MeV	20
> 2 MeV to 20 MeV	10
> 20 MeV	5
Photons, other than recoil protons, energy > 2 MeV	5
Alpha particles, fission fragments, heavy nuclei	20

2.1.3 Effective Dose and Effective Dose Equivalent

Effective dose is a quantity to measure overall risk of stochastic effects from ionising radiation. The effective dose, **E**, is the sum of the weighted equivalent doses in all the tissues and organs of the body. It is given by the expression:

$$\mathbf{E} = \sum_{T} W_T . H_T \qquad \text{(Equation 2.2)}$$

where $\mathbf{H}_T$ is the equivalent dose in tissue or organ T and W_T is the weighting factor for tissue T. Tissue weighting factors, W_T, have been defined by the ICRP to indicate the radiation risk to the organs and tissues in a way that is likely to correlate well with the total of the stochastic effects. The values of W_T are chosen so that a uniform equivalent dose over the whole body gives an effective dose numerically equal to that uniform equivalent dose. The sum of tissue weighting factor is then unity.

This weighted equivalent dose was previously called **effective dose equivalent** (ICRP 1977). But in its 1990 recommendations (ICRP 1991) ICRP took into account new biological information and trends for all organs and tissues and recommended different values of tissue weighting factors compared with those recommended in 1977 for effective dose equivalent. Therefore in its 1990 recommendations ICRP decided to use a simpler name of **effective dose** for this quantity.

Table 2.2: Recommended tissue weighting factors (W_T) in 1977 and 1990 (sources: ICRP 1977, ICRP 1991).

Tissue or organ	W_T **(1977)**	W_T **(1990)**
Gonads	0.25	0.20
Red Bone Marrow	0.12	0.12
Colon	-	0.12
Lung	0.12	0.12
Stomach	-	0.12
Bladder	-	0.05
Breasts	0.15	0.05
Liver	-	0.05
Oesophagus	-	0.05
Thyroid	0.03	0.05
Skin	-	0.01
Bone Surfaces	0.03	0.01
Remainder	0.30	0.05

However change in name was done to indicate the new tissue weighting factors used in the 1990 ICRP recommendations (ICRP 1991). Effective dose has weighting factors for a large number of specified organs and tissues and is likely to be

a better indicator of the risk to stochastic effects than effective dose equivalent. The unit of effective dose is J kg^{-1}, with the special name sievert (Sv) (ICRP 1991). This quantity could be used to compare the patient doses resulting from CT examination with other diagnostic procedures involving the use of ionising radiation.

The new and old recommended values for tissue weighting factors by the ICRP (ICRP 1991, ICRP 1977) are given in Table 2.2.

2.2 CT Dosimetry Devices

Devices used for CT dosimetry could be categorised into two major groups of dosimeters and phantoms. Various known dosimeters have been used to measure doses resulted from CT examinations. These include film, thermoluminescent dosimeter (TLD), and ionisation chamber, that will be discussed in the first part of this section. On the other hand, phantoms are devices simulating the human body. Different materials and techniques have been used for this purpose and several types of phantoms have been proposed for CT dosimetry. However, there are only two types of phantoms, namely physical and mathematical anthropomorphic phantoms, that are quite common in CT dosimetry. These phantoms will be described in the second part of this section.

2.2.1 CT Dosimeters

Soon after the introduction of CT into clinical practice in 1972, various types of dosimeters, normally being used for measuring doses from conventional radiography examinations, were also used for measuring CT doses. These include film, thermoluminescent dosimeters (TLD), an array of silicon detectors and a small (pencil shape, or CT) ionisation chamber (Suzuki and Suzuki 1978).

2.2.1.1 Film

Film has been used in early attempts as an exposure measuring device for CT dosimetry (Jucius and Kambic 1977). Dixon and Ekstrand (1978) used a film

dosimetry system (Kodak XV-2 film wrapped around a cylindrical water-filled phantom) to calculate the surface dose delivered by a CT scanner. Comparing with TLD measurements for a variety of CT scanners they indicated that an accuracy of +/- 15 % could be achieved using this system.

Although some advantages have been encountered for CT dosimetry by film such as: low cost, indication of exposure profile, relatively fast operation, and availability; its disadvantages in quantitative measurement, small dynamic range, densitometry requirement, and its restricted utility for surface dose measurements (Jucius and Kambic 1977) has not proved it as a good indicator in CT dosimetry. Hence, nowadays it is neither used in simple single CT dose measurements (like surface dose or dose at the central axis of the rotation) nor in comprehensive CT dosimetry to assess doses to individual organs and risk estimates associated with CT examinations.

2.2.1.2 Thermoluminescent Dosimeter (TLD)

The second dosimetry device used for CT dosimetry is TLD. The advantages of TLD are high sensitivity and dynamic range, small size, and the fact that it can be used to measure dose profile, internal doses and surface dose (Jucius and Kambic 1977). Furthermore, compared with pencil ionisation chambers the small size of TLDs permits easy quantitative measurement at the location of several organs of interest without any attachment elements. Although some disadvantages have been mentioned for TLD, such as the many dosimeters per measurement, the need for an external system to read the dosimeters, the long time preceding final result and high initial cost (Jucius and Kambic 1977), it is still the most common dosimetry device used for CT dosimetry. A stack of TLDs, from 16 to ~40 depending on the CT slice thickness, could be utilised to produce the CT dose profile (Figure 2.4) either in a phantom or free in air. TLDs with this geometry arrangement, positioning chips on their sides to provide ~1 mm spacing, could provide desirable resolution for very narrow beams profiles. TLDs could also easily be inserted in regions of interest in a physical humanoid phantom. This allows the measurement of the amount of radiation doses received by various radiosensitive organs and consequently the estimation of the

effective dose for CT examinations.

2.2.1.3 Pencil Ionisation Chamber

The third measuring device used for CT dosimetry is the ionisation chamber. The advantages of an ionisation chamber are: high sensitivity and dynamic range, quantitative measurement, the ability to measure internal and surface doses, and immediacy of readings (Jucius and Kambic 1977). The disadvantages of this device are: the lack of information required about beam profile and the requirement of a special chamber (pencil shape) due to the special CT X-ray field configuration (Jucius and Kambic 1977). Utilising a very small volume ionisation chamber to measure a cross section similar to TLD measurement has two serious disadvantages of: 1) the large number of scans required to generate a dose profile and 2) the lower sensitivity of a small volume ionisation chamber. In addition to these disadvantages it should be considered that this device is just applicable for acquiring single surface doses on phantoms or doses along an axis of interest in phantoms.

The type of ionisation chamber adopted for CT dosimetry is a long pencil chamber which measures the entire cross section of the CT X-ray beam field. This is a specially developed pencil-shaped ionisation chamber designed by Suzuki and Suzuki in 1978. It is an air-equivalent, coaxial ionisation chamber and its volume is ventilated to the environment via a small canal. The chamber measures the average "air kerma" (**K**inetic **E**nergy **R**eleased per unit **MA**ss of irradiated material) over its length.

Nowadays TLDs have almost been replaced with the pencil ionisation chamber for determining the CTDI value. This is largely because this chamber could easily be used quite straightforward compared with the relatively lengthy multiple processes required for acquiring the CTDI value from the TLD measurements. Using this type of chamber, CTDI value could be determined either inside a perspex (QA) phantom for the standard CT dosimetry technique or free in air on the axis of rotation of the scanner for the Monte Carlo CT dosimetry approach.

The measured exposure at any location utilising this chamber is equal to the total exposure, primary and scatter radiation, along the axis. The product of measured exposure and the active length of the pencil ionisation chamber (10 cm) gives a

number related to the area under the CT exposure profile.

2.2.2 CT Phantoms

Any material that simulates a body tissue in its interaction with ionising radiation is termed a tissue substitute (ICRU 1989). For example bolus is a tissue substitute placed in proximity to the irradiated subject to provide extra scattering or build up or attenuation in the beam. A structure that contains one or more tissue substitutes and is used to simulate radiation interactions in the body is termed a phantom. Phantoms are used widely in radiotherapy, radiological imaging, radiation protection, and radiobiology but their major application is in radiation dosimetry and radiotherapy. Phantoms may be broadly categorised according to their primary function as either dosimetric, calibration or imaging (ICRU 1992). Dosimetric phantoms are used for the measurement of absorbed dose in a specified geometry.

Therefore a phantom is a structure that contains or simulates one or more tissue substitutes and is used to simulate radiation interactions in the body in radiation dosimetry. Since the introduction of CT into clinical practice, various types of phantoms have been used to simulate human body in CT dosimetry. There are two categories of phantoms used in CT dosimetry. These are mathematical phantoms, and physical phantoms. Mathematical phantoms are computational phantoms normally used for the first track of CT dosimetry (the Monte Carlo approach). Apart from the early types of the physical phantoms designed for specific purposes, nowadays, mostly two types of these phantoms are used in CT dosimetry, dependent on the chosen approach. One type is the quality assurance phantom used for the standard CT dosimetry approach and QA measurements. The other physical type is the humanoid (a Rando Alderson or similar type) anthropomorphic phantom used for the second track of CT dosimetry. This type of physical phantom has been used and redesigned in this study. In the following sections the development and general characteristics of these phantoms are described.

2.2.2.1 Early Phantoms

Since the introduction of tissue substitutes at the beginning of this century (Kienböck 1906) Phantoms in one form or another have been used extensively in experimental radiation dosimetry. During the first two decades of this century water and different types of wax were established as muscle or soft-tissue substitutes. A decade later it was reported that the attenuation coefficients of wax at low photon energies differed widely from those of muscle and soft tissues (ICRU 1992). Therefore the high atomic number fillers, such as magnesium oxide and titanium dioxide were then added to correct for these deficiencies. Phantoms fabricated from these improved wax based tissue substitutes, in particular Mix D (Jones and Raine 1949) and later M3 (Markus 1956), were employed widely in radiation dosimetry. During the fifth decade of the 20th century gradually the greater awareness of the importance of realism in body phantom design led to production of a diverse selection of phantoms, but the limited tissue substitutes often resulted in phantoms of dubious relevance to the human body.

2.2.2.2 Physical Humanoid Anthropomorphic Phantom

The trend towards innovative body phantom design continued with the introduction of two elaborate adult-sized body phantoms containing real skeletons, body cavities and artificial lungs in the early 1960's. These were the Temex system (Stacy et al. 1961) and the Rando Alderson system (Alderson et al. 1962). In addition with the introduction of new plastic and resin based tissue substitutes in the 70's and 80's and associated fabrication techniques, a wider range of high quality phantoms can now be manufactured (ICRU 1992). Improved tissue substitutes and fabrication techniques has led to more reliable, realistic phantoms which inevitably has led to improved radiation dosimetry and measurement.

These phantoms were originally designed for use in radiotherapy dosimetry. From 1970 to the present day, more phantoms have been produced for other applications such as radiodiagnosis and radiation protection.

2.2.2.3 Standard/Quality Assurance Phantom

This type of phantom is known as standard CT dosimetric phantom or QA phantom. These phantoms are based on the standard phantoms developed by the Centre for Devices and Radiological Health of the US Food and Drug Administration (FDA 1980b) mainly for CT quality assurance measurements (Shope et al. 1982). FDA has recommended one position at the centre and four equally spaced positions on radii of 5.0, 10.0, and 15.0 cm for the body phantom with 32 cm diameter; and one position at the centre and four equally spaced positions on radii of 5.0, 7.0 cm for the head phantom with 16 cm diameter (FDA 1980a, ICRU 1992). But most manufacturers provide these phantom with means for the placement of a dosimeter(s) along its axis of rotation and along a line parallel to the axis of rotation 1.0 centimetre from the outer surface and within the phantom (Figure 2.1). Means for the placement of a dosimeter(s) or alignment device at other locations may be provided for convenience. The means used for placement of a dosimeter(s) (i.e., hole size) and the type of dosimeter(s) used is at the discretion of the manufacturer.

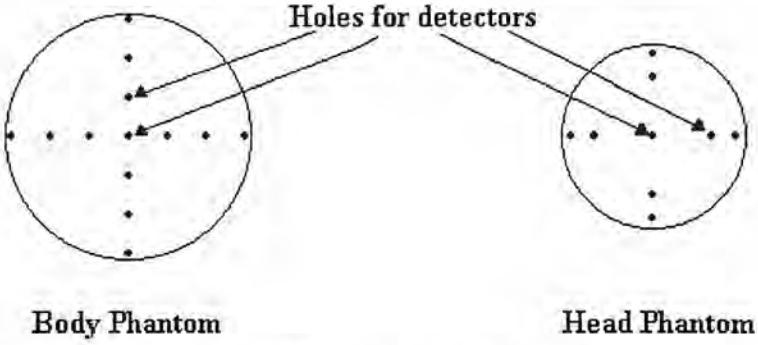

Figure 2.1: FDA Standard CT Dosimetric Phantoms.

For example the phantoms designed by Siemens, for QA measurements, are two right circular cylinders of water-filled acrylic containers or solid blocks fabricated from a suitable water substitute (polymethyl-methacrylate of density 1.19 ± 0.01 grams per cubic centimetre). These phantoms are both 14 centimetres in length. One of them with the diameter of 32.0 centimetres is for testing their CT systems designed to image any section of the body (whole body scanners) and the other one with 16.0 centimetres is for any system designed to image the head (head scanners) or for any

whole body scanner operated in the head scanning mode. As could be noticed in the Figure 2.2 seven positions have been determined in this phantom for CTDI measurements. One of these position is at the central axis (A) and anther one on the surface (O) of the phantom. But the rest are all located at equal radii (one centimetre from the edge of the phantom). Four of these peripheral positions (B, C, D, and E) are equally spaced and one of them (F) is located in the middle of two other peripheral positions.

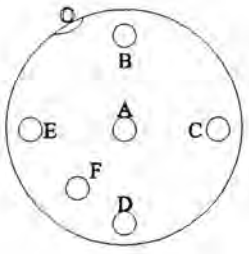

Figure 2.2: CT (Plexiglass) QA phantom designed by Siemens.

2.2.2.4 Mathematical Anthropomorphic Phantom

Since the measurement of absorbed dose to organs in a physical phantom requires a considerable experimental effort, several computational models have been defined to represent a specific body organ or a defined groups of organs or tissues, generally with associated mathematical relationships. These can range from a simple, idealised geometric form, such as a sphere, cylinder or slab, to a complex, realistic representation of a detailed anatomical feature (ICRU 1992), such as the model designed by the NRPB (Jones and Wall 1985) for organ dose measurements from medical X-ray examinations using Monte Carlo techniques (Figure 2.3). This phantom was also used later in the NRPB national survey of CT practice in the UK (Shrimpton et al. 1991a, Shrimpton et al. 1991b, Jones and Shrimpton 1991). Mathematical models use mathematical expressions to represent plane, cylindrical, elliptical or spherical surfaces. Mathematical models of these simple geometric shapes have been

widely used for absorbed dose measurements (ICRP 1987). With Regard to anthropomorphic models, such surfaces, sometimes intersecting, are combined to replicate idealised body organs. This model was introduced by Fisher and Snyder (1967 and 1968) for the adult human following the earlier work of Hayes and Brucer (1960) and has been extended and refined by numerous authors (ICRU 1992). As scaling was not appropriate for some organs, more elaborate paediatric mathematical models have been developed by Cristy (1980) and Cristy and Eckerman (1987), while male and female mathematical phantoms have been introduced by Kramer et al. (1982). These two models are the most popular ones used in CT dosimetry.

The NRPB phantom (Figure 2.3) used for CT dosimetry (Shrimpton et al. 1991b, Jones and Shrimpton 1991) is based on the adult phantom described by Cristy (1980), which in turn is derived from the MIRD-5. The MIRD-5 phantom was primarily designed for calculating organ doses from internal sources in nuclear medicine (Snyder et al., 1969). It then had several development phases (Snyder 1974, Cristy 1980, Cristy and Eckerman 1987, Jones and Wall 1986, Zankl et al. 1991) to improve it for diagnostic X-ray dosimetry purposes in conjunction with Monte Carlo techniques.

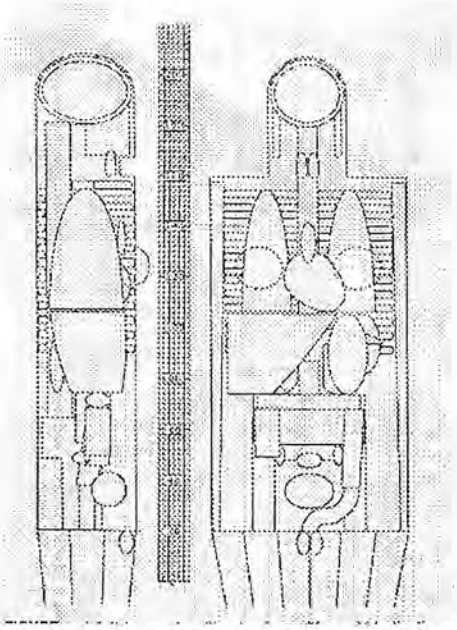

Figure 2.3: NRPB Anthropomorphic Mathematical Phantom.

2.3 CT Dose Descriptors

As mentioned earlier, apart from early attempts reporting doses received by single or multiple organs from CT examinations, several dose descriptors have been adopted and used to describe or characterise the radiation delivered by CT examinations. These include simple single point surface dose or skin dose, and more complicated ones such as CT dose profile, CTDI, and finally effective dose equivalent and effective dose. In this section these dose descriptors will be explained more in details.

2.3.1 Surface Dose or Skin Dose

These dose descriptors are based on the assumption that the personal dose to which the patient is exposed be given as the absorbed dose at the skin or surface dose. As mentioned in the first chapter most of the early works on CT dosimetry (Horsely and Peter 1976, Dixon and Eckstrand 1978, Shope et al. 1982, Fearson and Vucich 1985) used either surface or skin dose as their dose descriptor for CT dosimetry.

The skin dose is measured with two perspex (plexiglass) phantoms for the cranial region (16 cm diameter) and body region (32 cm diameter) on the surface (measured point O, Figure 2.2). Its value is given in mGy/100 mAs by most manufacturers and refers to the routine degree of the rotation of the scanner (normally 360°) single slice, with slice thickness and kVp value cited as parameters.

2.3.2 CT Dose Profile

Dose profile is determined free in air using a stack of TLDs along the central axis of rotation of the CT scanner. CT dose profile shows the dose as a function of position on the axis of rotation for the particular condition of exposure and could be used to examine the nominal slice width of the CT scanner. It determines the significance of spreading of the CT X-ray beam beyond the nominal slice width that is particularly useful for examining narrow thickness settings.

Figure 2.4 shows a typical dose profile of a two millimetre slice thickness, recorded in this study for a GE 9000 HP CT scanner, with a routine exposure setting used for head examinations. The peak of the dose profile could be used to estimate the overall level of dose for a single slice. But for a series of contiguous slices, there would be an overlap of tails of such profiles and contributions to the dose in adjacent slices. Under these circumstances, the peak dose for a single slice would be an underestimate of the overall dose over the region scanned. The quantity that takes account of this build-up in dose for multiple slices is the computed tomography dose index (CTDI) which is described in the next section.

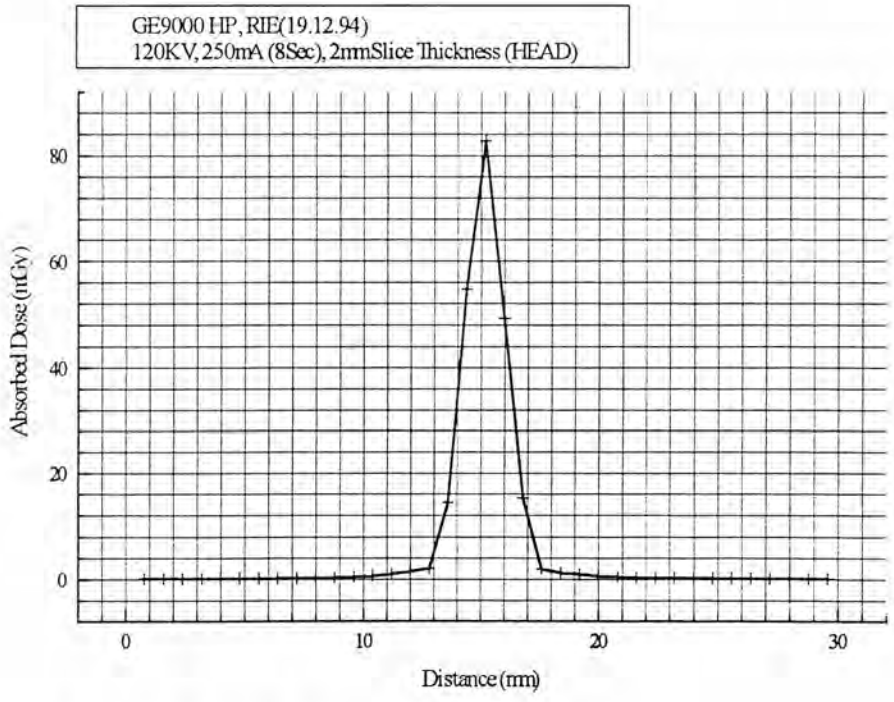

Figure 2.4: A typical free in air axial CT dose profile.

2.3.3 CTDI

CTDI is the integration of the CT dose profiles. This dose descriptor proposed, at first, by Shope et al. (1981) in an attempt for a convenient estimation for the approximate doses resulting from CT procedures consisting of a series of scans as a function of the distance between scans and the system conditions of operation. This

work was based on earlier works by Jucius and Kambic (1977) and later on by Suzuki and Suzuki (1978) who devised a special long, thin ionisation chamber for measuring the average dose resulting from a single scan. Shope et al. (1981) defined the CTDI by:

$$CTDI = (1/T)\int_{-\infty}^{+\infty} D_i(Z)dZ \qquad \text{(Equation 2.3)}$$

Where $D_i(Z)$ is the dose as a function of position along the z axis co-ordinate for a single scan dose profile at a given point (x, y) (Figure 2.5). T is the slice thickness as stated by the manufacturer or selected by the CT system operator.

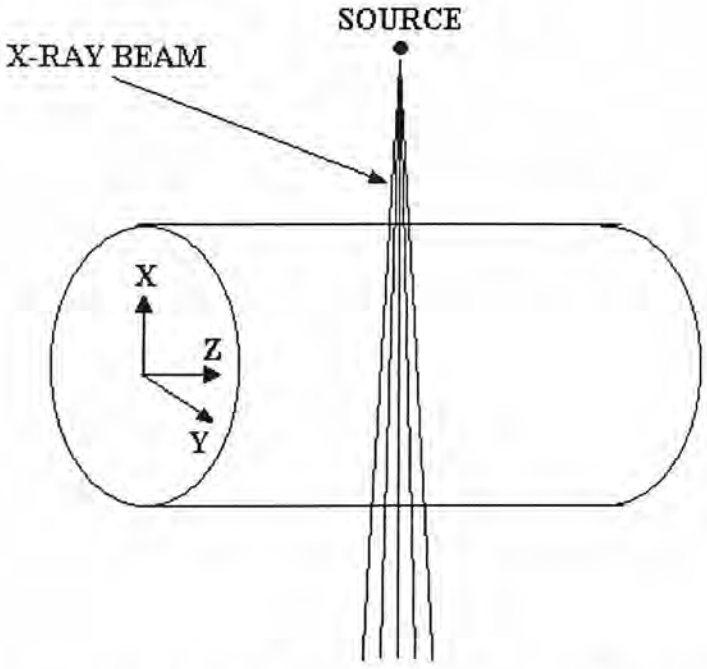

Figure 2.5: Illustration of CT system geometry and co-ordinate used for CTDI definition by Shope et al. (1981).

Later in 1985, the US Food and Drug Administration (FDA) defined the CTDI as an objective value for the measurement of dose integrated over 14 times the slice width along the system longitudinal axis (Z) (FDA 1985):

$$CTDI = (1/T)\int_{-7T}^{+7T} ZdZ \qquad \text{(Equation 2.4)}$$

For the purpose of dose comparison, the FDA recommended CTDI be measured in both a 16 cm and a 32 cm perspex (plexiglass) phantom at the centre (Measurement point A) and at a depth 1 cm from the outer surface (measurement points B-E) (Figure 2.2).

For the purpose of this definition the FDA specified that the absorbed dose should be stated in the perspex. These CTDI values are given as the absorbed doses in mGy and generally referred to a tube output of 100 mAs. Due to scattered radiation and the finite slope of the edges of the dose profiles, the CTDI value depends on the slice thickness setting and kVp values.

The FDA definition of CTDI is used just for QA purposes and examining the CT performances. There is also another different definition for CTDI, adopted by the NRPB (Shrimpton et al. 1991b) and used for the national survey of CT practice in the UK, that is also used and referred to by several other researchers in the UK and other countries (Zankl at al. 1991). Details of this definition of CTDI are mentioned in chapter 6 where the principles of CT dosimetry using the Monte Carlo technique in this study are explained.

2.3.4 Effective dose

As mentioned above ICRP introduced this new weighted dose quantity in its 1990 recommendations for controlling the exposure to radiation of workers and members of the public. Since 1977 when ICRP introduced the old version of this quantity (effective dose equivalent), it has been used widely by most of the researchers for reporting radiation doses to patients for most of the other conventional diagnostic procedures like different conventional X-rays modalities in radiology and radioisotopes in nuclear medicine. However effective dose has weighting factors for a larger number of specified organs and tissues and is likely to be a better indicator of the risk to stochastic effects than effective dose equivalent. In recent years, while the significance of patient doses from CT examinations has been notified, this quantity has also been used as a dose descriptor in CT dosimetry by most of the researchers. This makes it possible not only to compare the radiation doses received by different CT examination protocols and different CT scanners, but also to

compare the patient doses resulting from CT examinations with other diagnostic procedures involving the use of ionising radiation.

3. COMMON CT SCANNER CHARACTERISTICS

Medical Imaging has experienced significant changes in both the technical and clinical arenas and developed dramatically in recent years (Seeram 1994). Modern medical imaging makes use of a large number of tomographic techniques by which physical properties of biological tissues are displayed in three-dimensional matrices of volumes or voxels. Selected planes within the patient can be viewed by displaying the two dimensional distribution when one of the three position coordinates is kept fixed. Perhaps the most widely used of such techniques is X-ray CT in which the X-ray linear attenuation coefficient property of body cross-sections is used to reconstruct the cross sectional images of the body. Although the mathematical principles underlying the method were known early in the twentieth century, it was only when digital computers became available for implementing fast reconstruction algorithms that CT imaging became possible. The impact in medicine has become colossal and CT imaging is in widespread use (Webb 1990).

The first part of this chapter describes briefly the events leading to the invention of CT. The second part embraces the basic operational principles and technical developments of CT scanners. The last part embodies the basic features of physical characteristic parameters and common radiological factors used for routine examinations for every CT scanner in this study.

3.1 The Invention of CT

The word "tomography" is not new - it can be traced back to the early 1920s, when a number of investigators were developing methods to image a specific layer or section of the body that is oriented parallel to the film. At that time, terms such as "body section radiography" and "stratigraphy" (from *stratum*, meaning layer) were used to describe the technique. However, it was not until 1935, when Grossman, who refined the technique labelled it tomography (from the Greek *tomos*, meaning section). In 1937 Watson developed a tomographic technique in which the sections were transverse sections (cross sections). This technique was referred to as transverse axial

tomography. These images, however, lacked enough detail and clarity to be used as a clinical tool in diagnostic radiology (Seeram 1994).

CT overcomes these limitations by using a procedure known as image reconstruction from projections to produce sharp, clear images of cross-sectional anatomy. Image reconstruction from projection had its theoretic roots in 1917 when Radon an Austrian mathematician, proved that it was possible to reconstruct (build) an image of a two-dimensional or three-dimensional object from a large number of its projections from different directions (Webb 1990). This procedure has been used in a number of fields, ranging from astronomy to electron microscopy to reconstruct the images of the sun and the molecular structure of bacteria (Brooks and Di Chiro1976, Seeram 1994). But in medicine it was in the early 70s that this procedure was used for the first time by Hounsfield and he announced the revolutionary medical imaging system of X-ray CT (Hounsfield 1973).

X-ray CT has been hailed as possibly the greatest innovation in radiology since the discovery of X-rays themselves for which Wilhelm Roentgen received the first Nobel Prize for Physics in 1903. In this respect the year 1972 has been regarded as the birth of CT since it was in this year the EMI scanner, the first medically useful X-ray CT scanner, was announced (Ambrose and Hounsfield 1972, Hounsfield 1973, Ambrose 1973, New Scientists 1972). The work built on earlier experiments and theoretical work by A. M. Cormack and for their contribution to medicine they were jointly awarded the 1979 Nobel Prize for Physiology and Medicine (Hounsfield 1980, Cormack 1980). The following paragraphs outline the accounts of these two pioneering scientists whose work led to the invention of the CT.

Allan MacLeod Cormack first considered CT in 1956. Part of his time was spent on the Groot Schuar Hospital (South Africa) where he observed radiotherapy planning techniques. He concluded that these could be improved if there were a map of X-ray linear attenuation coefficient in the slice being planned - what today we would call tissue inhomogeneity corrections. Since this problem had not been thought and solved before, he formulated the mathematics of reconstruction from projections for simple attenuation objects with certain symmetry, while he was not aware that it had already been done by Radon in 1917. He applied this reconstruction technique in

1957 to experimental data with some success. In 1963 he constructed an experimental (positron tomography) scanner used to reconstruct the asymmetrical sections of phantoms and published the results (Cormack 1963, Cormack 1964) but there was no expressed interest in them for clinical use. He also foresaw the possibility of proton CT using the sensitivity of the photon range to tissue inhomogeneity and noting that the CT sections could be used for planning proton radiotherapy. It is sometimes remarked that Cormack's main contribution lay in the mathematics of CT but his was also an innovative experimental contribution to winning the joint Nobel Prize. (Webb 1990).

In 1967, Godfrey Newbold Hounsfield was investigating pattern recognition and reconstruction techniques using the computer. From this work he deduced that, if an X-ray beam were passed through an object from all directions, and if measurements were made of all the X-ray transmission, it would be possible to obtain information about the internal structure of the body. It was decided that this information be presented to the radiologist in the form of pictures that would show three-dimensional representations (Seeram 1994).

With encouragement from the British Department of Health and Social Security (DHSS) to investigate the clinical feasibility of the technique, an experimental apparatus was constructed (Figure 3.1) (Seeram 1994). This equipment used a gamma-ray source collimated to face a single detector. Between the two a phantom was rotated in 1° steps on a turntable. The scanning movement of the scanner and detector were provided by a lathe bed and 28000 measurements were recorded per slice on paper tape. The data took 9 days to collect per slice and 2.5 hours to reconstruct on a mainframe computer. A further 2 hours was required to display an image from the digitised result. By replacing the gamma-ray source with an X-ray source the data capture time was reduced to 9 hours. However only one image per day was possible. The machine, the first prototype head scanner, which eventually went into clinical trial at the Atkinson Morley Hospital took high-resolution images in just 18 minutes. The first clinical scan was made on the 1st of October 1971, that was of a 41 year old female with a suspected left frontal lobe tumour. The project was carefully kept secret until the 1972 British Institute of Radiology Conference in April

(Ambrose and Hounsfield 1972). When the news broke the scientific community were amazed at what has been achieved. Hounsfield recognised early the applicability of CT data in X-ray diagnosis (Hounsfield 1973). The designs of CT scanners were very soon optimised in terms of their photon utility and, in his lecture, Hounsfield pointed to the next logical development of essentially real-time CT scanning (Hounsfield 1972, Hounsfield 1980). The company in which Hounsfield was employed (EMI) pioneered the commercial development of transmission CT imaging (Webb 1990).

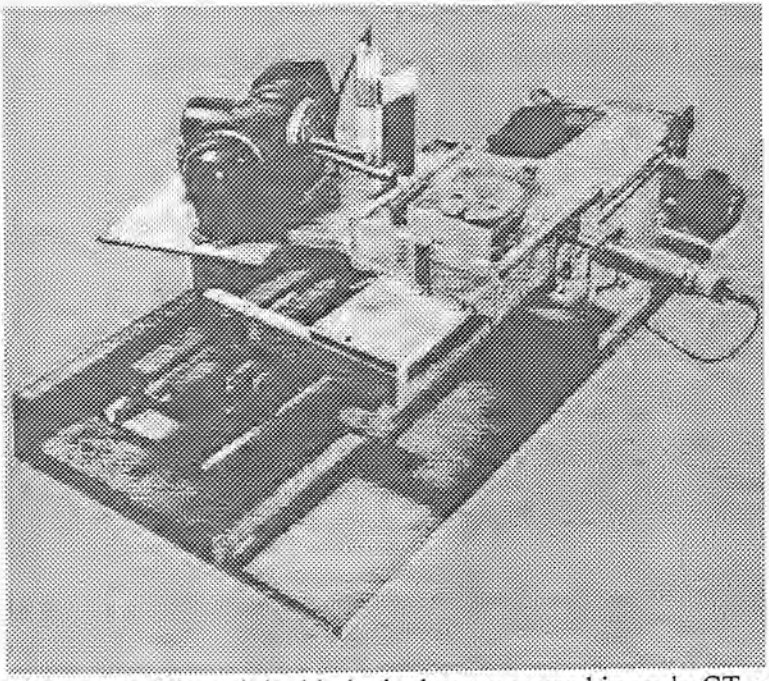

Figure 3.1: The original lathe bed scanner used in early CT experiments by Hounsfield of EMI (Webb 1990).

Dr. Hounsfield's research resulted in the development of a clinically useful CT scanner for imaging the brain. For this work, prior to the 1977 Nobel Prize for Physiology and Medicine, Hounsfield received the McRobert Award (apparently equivalent to a Nobel Prize in Engineering) in 1972 (Seeram 1994, Webb 1990).

As might be expected the development of CT has origins which stem back many years to unconnected pieces of research narrated very well by Webb (1990). But it was not until the late 1960s that what today we should recognise as modern CT came to be achieved. This was characterised by departure from the use of film as detector, by complex mechanical and electrical engineering to implement the

projection data capture and by digital numerical computer reconstruction which led to quantitative, spatially accurate sensitive mapping of the X-ray attenuation properties of body cross-sections (ibid.). Although other workers investigated the idea of CT, it was Hounsfield who developed the first practical CT scanner. He is recognised as the individual who opened a whole new domain for scientists, just as Roentgen was when he discovered X-rays (Seeram 1994).

3.2 Basic Operational Principles and Technical Developments of CT scanners

In a CT examination, the patient is exposed to a narrowly collimated beam of X-rays at a number of angular increments. The transmitted X-rays are absorbed by a series of detectors, and the data from these projections are used to create a two-dimensional map of linear attenuation coefficients, i.e., an image. Figure 3.2 shows several transverse axial images of the head and body produced by a CT scanner. The formation of CT images by a CT scanner involves a three-step process: data acquisition; image reconstruction; and image display, manipulation, storage, and recording (Seeram 94).

3.2.1 Data Acquisition

The term "data acquisition" refers to the collection of X-ray transmission measurements from the patient. Once X-rays have passed through the patient, they fall onto special detectors that measure the transmission values. Enough transmission measurements (data) must be recorded to meet the requirements of the reconstruction process. This measurement technique or data acquisition process consists of various schemes to collect data from the patient, referred to as data collection schemes (Figure 3.3) (Seeram 1994).

Figure 3.2: Examples of CT images of the head, chest, abdomen, and spine produced by a modern CT scanner (Seeram 1994).

3.2.2 Image Reconstruction

Once enough transmission measurements have been collected by the detectors, they are sent to the computer for processing. The computer uses special mathematical techniques to reconstruct the CT images in a finite number of steps called reconstruction algorithms.

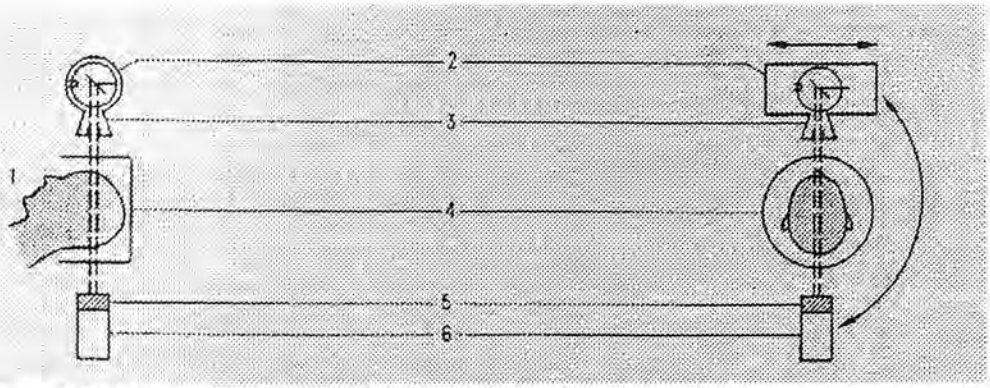

Figure 3.3: Data collection scheme used in the first CT brain scanner: 1, object; 2, X-ray tube; 3, collimator; 4, head support containing a water bag; 5, crystal detector; 6, photomultiplier tube (Seeram 1994).

3.2.3 Image display, manipulation, storage, and recording

Once the computer has performed the image reconstruction process, the reconstructed image can be displayed and recorded for subsequent viewing, as well as stored for reanalysis at some later time. The image is usually displayed on a cathode ray tube (CRT), although other display technologies have now become available; for example, touch screen technology is used for scan set-up and control in some scanners. The CRT, however, currently remains the best device for the display of grey scale imagery. Display monitors are mounted onto control consoles that allow both the technologist (operator's console) and radiologist (physician's console) to manipulate, store, and record images (Seeram 1994).

3.3 Historical Development of CT

The clinical usefulness of CT quickly became established, because the technique made possible the demonstration of a wide variety of diseases of both the head and body. Numerous developments in this technology were made 10 years after its introduction, not only in the technical arena but also in the clinical sphere (Seeram 1994).

In the first 10 years of CT, the number of units installed world-wide increased dramatically. Perhaps the first significant technical development came in 1974 when

Ledly, a physicist from Georgetown University, developed the first whole-body CT scanner (Hounsfield's scanner referred to as EMI scanner, was restricted to scanning only the head). This was followed by the introduction of three "generations" (a term used to refer to the method of scanning) of CT scanners. In 1974, a fourth generation CT system was developed. These four basic types of scanning system are illustrated in Figure 3.4 (Seeram 1994).

The first prototype CT scanner introduced by Hounsfield (1973) had a single detector and a pencil X-ray beam, which moved in a translate-rotate manner, i.e., the detector and X-ray tube translated along a line parallel to the image plane acquiring data. The tube and detector were then rotated one degree, and the process repeated. In this CT version a finely collimated source defines a pencil beam of X-rays, one sample at a time, by stepping linearly across the patient. After each projection, the gantry rotates to a new position for the next projection (Figure 3.4). This system was very slow, however, with typical acquisition time of 4 min per section, even for relatively low-resolution images (Webb 1988).

To overcome the problems of slow scan times and poor resolution, a second generation was devised with multiple detectors (a bank of detectors) and a small fan shaped X-ray beam (~ 10°) (Figure 3.4). This assembly, which was the first commercial CT scanner, traversed the patient and measured N parallel projections simultaneously (N is the number of detectors). The gantry angle incremented by an angle equal to the fan angle between consecutive traverses (Webb 1988). The second generation retained the original translate-rotate motion. Data gathering was speeded up considerably (~ 20 s).

In the third generation of CT scanners, the translate motion of the tube and the detectors was replaced with a rotate only motion. A broad fan-shaped X-ray beam is used to cover the whole field of view (Figure 3.4) with several hundred detectors, and the entire tube-detector system rotates around the machine's isocentre. Consequently, the gantry needs only to rotate, in a continuous movement, and the data gathering can be done in 4-5 s. Detector balancing is critical for this geometry if circular ring artefacts are to be avoided. Xenon gas chamber detectors are often chosen because of the stable nature of their operation (Webb 1988).

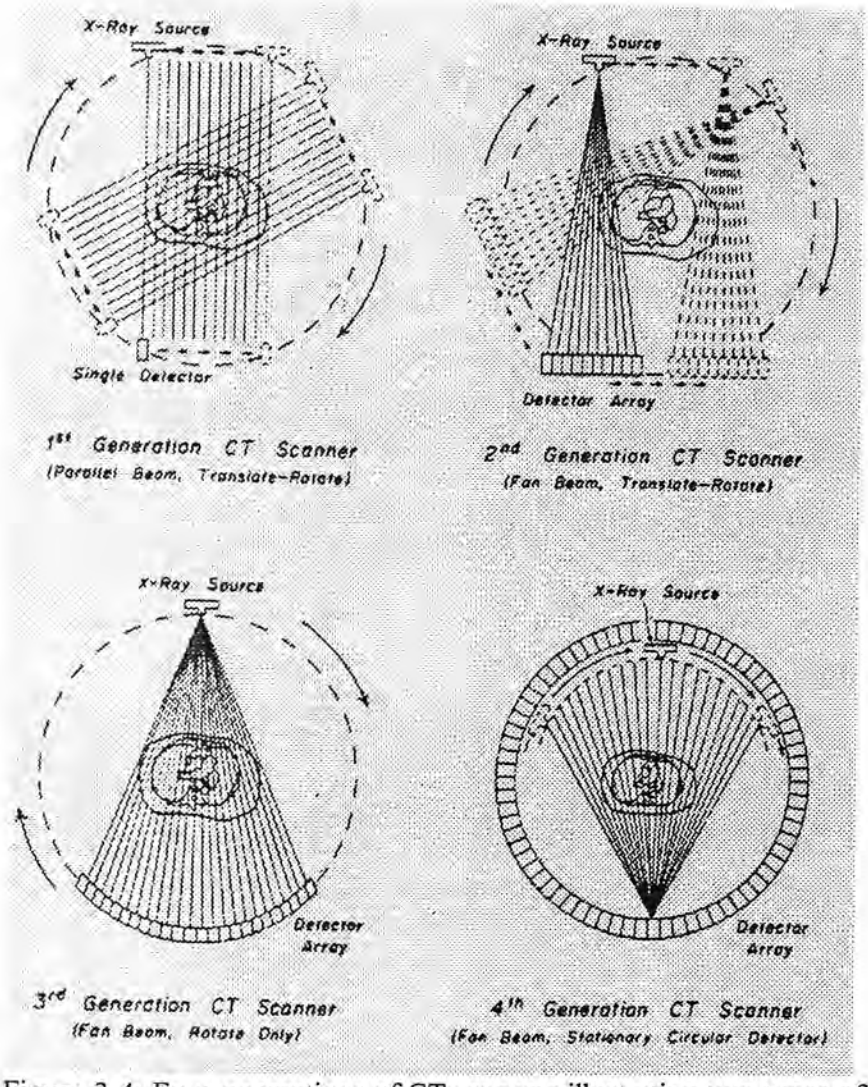

Figure 3.4: Four generations of CT scanners illustrating two types of beam geometry, the parallel beam and the fan beam (Seeram 1994).

The fourth generation CT scanner has stationary detectors (typically 1000) and only the X-ray tube rotates around the patient (Figure 3.4). Scan speed remains fast and the ring artefact is overcome and since every detector is, at some time during the scan, sampling the unattenuated X-ray beam, calibration in "real time" can be performed (Webb 1988).

A new type of CT scanner has been developed by Imatron[1]. This model has no moving parts. In these scanners, the patient lies on a large evacuated chamber. An electron beam is scanned across a series of small tungsten targets lining the interior of

the evacuated chamber. These targets act like the anode in a standard X-ray tube and produce X-rays which are collimated, traverse the patient, and are detected by an array of detectors. Both the tungsten targets and the array of detectors cover an arc of 210° (Figure 3.5).

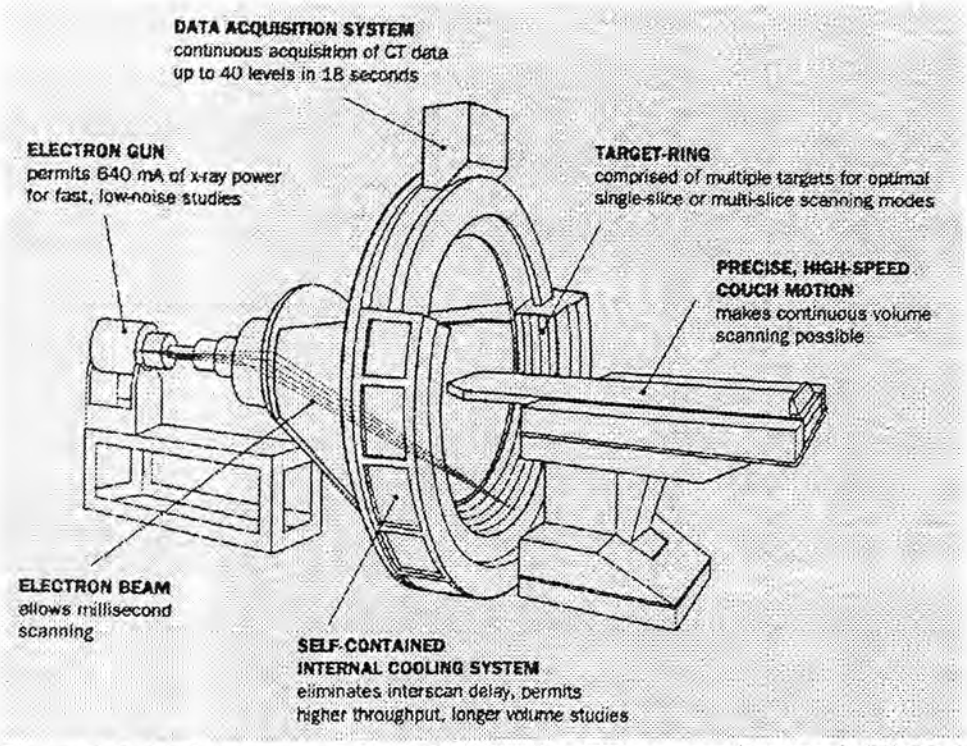

Figure 3.5: Major components of the Ultrafast CT scanner (Imatron) (Webb 1988).

These machines have the advantage of fast (50-100 ms) scan time but have slightly poorer image quality than conventional CT scanners (Atherton 1993). This high speed scan time permits cardiac motion to be frozen. This will allow clearer images not only of the heart but also of organs that are well perfused with blood, such as the liver, and which pulsate in synchrony to the heart beat. Mechanical movement is ruled out and multiple stationary sources are prohibitively cumbersome and expensive (Webb 1988).

One problem with the third generation scanners is the ring artefact caused by detector failures. Ring Artefacts with 4th generation machines are not seen and their design presents "on the fly" calibration of the detectors. However improved stability

---

[1] **Imatron Inc., San Francisco CA 94080.**

of the components has largely eliminated these problems with the 3rd generation machines and most of the modern and state-of-the-art CT scanners are this type. Therefore classifying CT scanners based on the generation does not seem to be a valid nomenclature. It would seem more relevant if CT scanners are classified based on their scanning motions. Apart from the last CT type (Imatron) mentioned above, which could be regarded as a special purpose designed type, CT scanners could be classified in three classes of: Rotate-Translate (RT), Rotate-Rotate (RR) and Rotate-Stationary (RS) (or Rotate-Fixed or Rotate-only (Webb 1990, Seeram 1994, Romans 1995)). Using these terms, for example, the first and second generations could be regarded as RT, the third generation as RR, and the fourth generation as RS CT scanners. Modern CT scanners are either RR or RS. The RT CT scanners are no longer in clinical use.

3.4 Technical and Computing Development of CT

CT has acquired visibility well beyond its role in medicine or even in radiology. No one can deny that non-invasive diagnostic approaches are an extremely important development (Moss and Goldberg 1980).

As discussed above the CT process can be broken down into three segments: data acquisition, image reconstruction, and image display. In this section developments taken place in these segments are discussed.

3.4.1 Data Acquisition Developments of CT

The components that are involved in the data acquisition phase of image creation are the generator, the gantry, and the patient table. The gantry houses the X-ray system (comprising of X-ray tube, X-ray beam filter, and collimators), and detectors.

3.4.1.1 Generator

The generator produces high voltage and transmits it to the X-ray tube. CT

scanners use three-phase power for the efficient production of X-rays. In the past, generators for the CT scanners were based on either the 50-Hertz (Hz) (Europe) or the 60-Hz (North America) voltage frequency, and the high voltage generator was a bulky piece of equipment located in a corner of the X-ray room. CT scanners now use high frequency generators, which are small, compact, and more efficient than conventional generators. As a result, these generators are located inside the CT gantry and even in some modern CT scanners it is mounted on the rotating frame of the gantry with the X-ray tube. It is necessary to mention that spiral-helical CT, a new type of CT examination which will be explained later, is made possible through the use of slip-ring technology, which allows for continuous gantry rotation. Today most CT scanners incorporate slip-ring design and, as a result, have been referred to as continuous rotation, volume CT, or slip-ring scanners. Such rotation results in very fast data collection. Slip-rings are "electromechanical devices consisting of circular electrical conductive rings and brushes that transmit electrical energy across a rotating interface" (Brunnett et al. 1990).

3.4.1.2 X-ray tube

Formerly RT CT scanners (1st and 2nd generations) used fixed anode, oil-cooled X-ray tubes, but because of the demand for increasing output resulting from faster scan times typical of modern CT scanners, rotating anode X-ray tubes have become standard in CT. These tubes produce a beam of radiation from a large diameter anode disk with focal spot sizes to facilitate the spatial resolution requirements of the scanner. The introduction of spiral CT, made possible with continuous rotation scanners, has placed new demands on X-ray tubes. Because of the continuous rotation of the tube for a long period of time (compared with conventional scanners), it must be capable of sustaining higher power levels. One significant change for slip-ring scanners is that they are designed to increase not only the heat storage capacity but also the cooling rate (dissipation).

3.4.1.3 Filtration

Ideally the photon beam for CT scanners should be monochromatic, but this is not achievable in practice. It is essential, therefore, that the polychromatic beam be shaped so that it appears to be a monochromatic beam to satisfy the requirements of the reconstruction process.

Without filtration the X-ray polychromatic beam will result in the beam hardening artefact. One purpose of using filters is to reduce this effect. Two types of filters are used in CT scanners. One is a substance such as aluminium and copper which reduces the range of X-ray energies that reach the patient. This removes soft, or low energy, X-ray beams which do not play a role in CT image formation and minimises patient doses. On the other hand because of the circular shape of the cross section of the body the radiation path through the body varies. Hence certain filters are used to reduce the beam intensity at the periphery of the beam, corresponding to the thinner areas of patient's anatomy, and shape the profile of the radiation beam to make it more uniform. In this respect specially shaped filters have been designed for CT scanners. The shape of these filters should conform to the shape of the object being scanned. Because of their shape these types of filters are often referred to as "bow tie filters". These filters are positioned between the X-ray tube and the patient, and shape the beam to produce a more uniform beam at the detectors.

3.4.1.4 Collimation

The main purpose of collimation is to produce a beam of the required width for the slice thickness of interest being scanned. On the other hand it also protects the patient by restricting the beam only to the anatomy of interest. In CT collimation is important, because it not only protects the patient by restricting the beam only to the anatomy of interest but also improves image quality by reducing the effects of scattered radiation.

In CT two collimators are used: pre-patient or proximal collimators and post-patient or pre-detector or distal collimators. In general a set of collimator sections is carefully arranged to shape the beam. The collimators, both proximal and distal are

arranged to ensure constant beam width at the detector and therefore define the thickness of the slice to be imaged. Slice thickness is generally variable and can range from 1.0 to 12 mm, depending on the type of the scanner. Pre-detector collimators also help remove scattered radiation and therefore improve contrast resolution and consequently image quality.

3.4.1.5 Detector Characteristics

To be useful in CT, a detector must exhibit several characteristics that are essential for CT image production. These include efficiency, response time, dynamic range, high reproducibility, and stability. It should be noted that the total detector efficiency, referred to as the dose efficiency, is the product of capture efficiency, absorption efficiency, and conversion efficiency that is often listed in the product specification literature by CT manufacturers.

Two types of detectors are used in CT scanners: scintillation detectors and ionisation detectors.

Scintillation detectors

In the past scintillation detectors consisted of a scintillation crystal coupled to a photomultiplier (PM) tube. Early scanners used sodium iodide (NaI) crystals. Later, because of afterglow problems and the limited dynamic range of NaI, other crystals such as calcium fluoride (CaF_2) and bismuth germinate ($Bi_4Ge_3O_{12}$, BGO) were used. Today, scintillation detectors with PM tubes have been superseded by scintillation crystal detectors with solid-state photodiodes. Photodiodes are normally used with amplifiers because the output from the diode is very low. In addition the response time of a photodiode is extremely fast, about 0.5 to 250 nanoseconds, depending on its design. Solid state crystal detectors are made from a variety of materials. Two scintillation materials that are currently used with photodiodes are cadmium tungstate ($CdWO_4$) and a ceramic material made of high-purity, rare earth oxides. These crystals are optically bound to the photodiodes. The advantages and disadvantages of these two scintillation materials can be discussed in terms of the detector characteristics mentioned earlier. Specifications literature should be consulted for

details of the performance of these detectors (Villafana 1987, CT manufacturers product specifications catalogues).

Gas Ionisation Detectors

The gas ionisation detectors were introduced with the development of third-generation scanners. These consist of a series of individual gas chambers usually separated by tungsten plates to prevent cross over of scattered radiation. The gas chambers are filled with high pressure xenon and are up to 50 mm deep to increase the detector efficiency which is within the range of 35%-50%. The signal current, resulting from the ionisation of the gas is proportional to the number of photons absorbed by the chamber. Xenon detectors offer good stability with fast response times, and do not have afterglow problems. Modern CT scanners use an arrangement referred to as detector modules, in which the entire array of detectors consists of groupings of detectors. Each grouping is known as a detector module, and each detector module plugs into a mother board unit of the detection system.

3.4.2 Image Reconstruction Developments of CT

Image reconstruction techniques were first developed for use in radioastronomy by Bracewell (1956) for the purpose of identifying regions of the sun which emitted microwave radiation (Brooks and Di Chiro 1976). The introduction of the first X-ray CT scanner in 1972 by EMI Ltd (Hounsfield 1973) was preceded by a number of less sophisticated experiments and demonstrations very well explained in the Brooks and Di Chiro's review article (1976). In these experiments the back projection mathematical approach was used for image reconstruction. This is a crude method of reconstruction easily implemented without need of a computer or sophisticated mathematics but produces reconstruction with substantial artefacts.

The "back projection technique", also referred to as the "summation method" or "linear superposition" method, was first used by Oldendorf in 1961 and Kuhl and Edwards in 1963 (Seeram 1994). Since this technique does not produce a sharp image of the object it is not used in clinical CT (ibid.).

Another approach to image reconstruction is based on "iterative techniques". An iterative reconstruction starts with an assumption and compares this assumption

with measured values, makes corrections to bring the two into agreement. This process is repeated until the assumed and measured values are the same or within acceptable limits (Curry et al. 1990). The algebraic reconstruction technique was one of several different iterative techniques which was used by Hounsfield in the first EMI brain scanner (Hounsfield 1972). Because of the limitations of these techniques they are not used in commercial scanners nowadays (Seeram 1994).

The third category of reconstruction algorithms used in CT is the "analytical reconstruction method" based on exact mathematical solutions to the image equations and is faster. These algorithms have been developed to overcome the limitations of the back-projection and iterative algorithms. These algorithms are used in modern CT scanners and have sound mathematical bases (ibid.). The two analytical reconstruction algorithms are "filtered back-projection" and the "Fourier" reconstruction algorithms. The filtered back-projection, used in most commercial CT scanners, is also referred to as the "convolution method". This is similar to the back-projection technique, but its striking difference is that the projection profile (data) is filtered or convolved (using mathematical filters) to remove the problem of image blurring characteristics of simple back-projection (ibid.). The Fourier reconstruction technique is a practical algorithm used by some CT scanners, based on the Fourier theorem. Essentially, Fourier reconstruction transforms the object from the spatial domain to the frequency domain using Fourier transform. All the projection data collected from the object are Fourier-transformed into spatial frequencies, which are subsequently interpolated onto a rectangular grid. Finally by using inverse Fourier transform, the interpolated image is converted into a spatial domain image.

Another most recent reconstruction algorithm is the "3D algorithm". Three-dimensional CT imaging uses 3D surface and volumetric reconstruction. The algorithms for 3D imaging are based on those used in such fields as computer graphics and visual perception science. Essentially these algorithms are based on at least two processes, pre-processing and display, and consist of the following four operations: interpolation, segmentation, surface formation, and projection. A comprehensive report on 3D algorithms has been published by Udupa and Odhner (1991).

For more detailed description of image reconstruction techniques the reader is referred to several reviews in this regard (Brooks and Di Chiro 1975, Brooks and Di Chiro 1976, Edholm 1975, Peters 1975, Gordon et al. 1975, Budinger and Gullberg 1974, and Gordon and Herman 1974, Strong et al. 1990, Udupa and Odhner 1991, Seeram 1994).

3.4.2.1 Three-dimensional imaging

Three-dimensional (3D) imaging has become a popular technique in CT because of the availability of large amounts of digital data. 3D imaging is now possible on CT scanners and the results have been promising. 3D-CT is already being used in radiation treatment planning, craniofacial imaging, surgical planning, and orthopaedics (Seeram 1994).

3D images can be obtained by using a hardware-based or software-based approach. The hardware approach uses specialised equipment such as electronic computer display units to execute algorithms (sets of instruction to carry out a particular task) for 3D imaging, and the software approach uses computer programmes (software-coded algorithms). These algorithms have been referred to as rendering techniques. These techniques transform the transaxial CT data into simulated 3D images (Figure 3.6). 3D CT has opened up a whole new area of interest for scientists (ibid.).

One area of computer science that has played a role in the evolution and refinement of 3D imaging is computer graphics. Computer graphics involves the creation, manipulation, and display of pictures or images using the computer. It allows the user to express ideas and information in a visual format. It includes various ways to represent data to create and display images using graphics programming languages and image processing techniques.

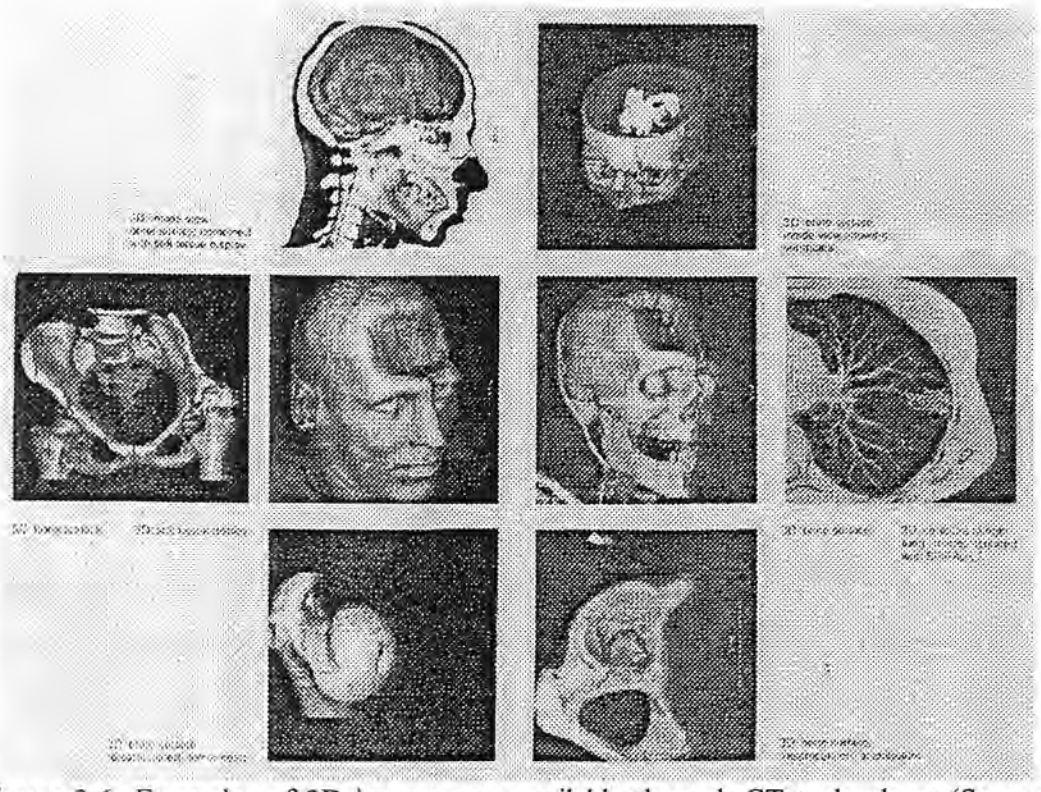

Figure 3.6: Examples of 3D images now available through CT technology (Seeram 1994).

3.4.2.2 Spiral or Helical CT

The need for shorter scan times to sub-second levels and for improvements in three-dimensional imaging, as well as the limitations imposed by conventional start-stop CT systems in which the data is acquired slice-by-slice, has been met and overcome by the development of continuous rotation scanners. These scanners are based on the use of slip-ring technology, which makes it possible to acquire the data in volumes- that is, complete organ volumes or sub-volumes, rather than slice by slice.

Continuous rotation CT scanners have led to the introduction of a new scanning technique that may be considered as one of the most significant recent developments in CT, and that has become common in CT applications. This technique is referred to as spiral, helical or volume CT. In the rest of this section this technique will be referred to as spiral CT.

The spiral method uses a continually rotating X-ray gantry with constant X-ray outputs and uninterrupted table movements. Required data for each

reconstruction slice is interpolated at each projection angle from the data measured on either side of the slice. The pitch of a spiral scan is defined as the ratio of distance made by the patient per revolution of the tube and the slice width. Increase of pitch reduces dose and scan time but increases the uncertainties in the interpolated values. Spiral scanning has the advantage in reducing scan times and eliminating slice misregistration. This is of particular importance in examinations of the chest in which detail can be lost in conventional scanners due to inconsistent breath holds from slice to slice. It is also of great benefit to remove movement artefacts when undertaking 3-D reconstruction method. The data volume may be viewed as conventional transaxial images or with multiplanar and three-dimensional methods. Spiral scanning is already of proved efficacy for vascular and airway imaging as well as for identifying and characterising pulmonary nodules. It may be anticipated that the indications for the use of spiral imaging will continue to expand. Of particular interest is the ongoing development of reconstruction algorithms that allow high-quality images to be obtained with rapid table incrementation while simultaneously reducing radiation exposure (Naidich 1994).

3.4.3 Image Display Development of CT

From another angle, CT is classified as a digital imaging system because it uses computers to process images. In CT scanning computers are used to control the operation of the scanner, to reconstruct the transaxial or spiral image, display and manipulate the image and also for further 3-D reconstruction.

Developments in computer hardware including processing speed, memory size, storage capacity, display system and data transmission have had major influence on CT capability. On the other hand software developments in the recent years and the recent achievement of image processing techniques have brought significant benefits to CT. These benefits are made possible through the use of special image processing algorithms. For example, CT images can be enhanced, restored and analysed.

3.5 Basic Physical Characteristics of the CT scanners

This section outlines the basic physical characteristic parameters of various models of CT scanners used in this study. These are routine radiological technique factors including kV, mA, scan time and mAs; tube characteristics, geometry; and filtration characteristics. It must be considered that the peak electrical potential across the X-ray tube is abbreviated as "kV", the current through the X-ray tube is represented by "mA", and the product of the exposure time and the tube current is abbreviated as "mAs". The reported CTDI values by manufacturers mentioned in this section are based on the FDA definition of CTDI and CT dosimetry phantoms (US Office of Federal Register 1984). However for some of the CT models in this study, manufactured before the above regulations became made effective, the CTDI values were presented for different values of mAs. Therefore to make all the CTDI values concordant and in accordance with the ImPACT[2] reports, they are expressed in mGy/100mAs for all different models of CT scanners in this section.

Information regarding the physical characteristics of the CT scanners in this study derived from the technical and user manuals provided by the relevant manufacturer and also from the ImPACT reports (MDD 1991, MDA 1994, MDA 1995) if they were available.

Several types of CT scanner are used at different hospitals in the Lothian and Fife areas of Scotland. When this study started there were several models from three different CT manufacturers, namely: Siemens [3]; GE Medical System [4]; and Philips [5]. Different models of CT scanners were operational at different hospitals. The operational CT scanners at the Western General Hospital (WGH) of Edinburgh were a model of Siemens and a model of GE Medical System. However the older type of GE scanner at this hospital was replaced with a GE HiSpeed Advantage scanner in 1996. In the Royal Infirmary of Edinburgh (RIE) all operational scanners were made

---

[2] ImPACT (Imaging Performance Assessment of Computerised Tomography) is the MDA's (Medical Device Agency, formerly Medical Devices Directorate(MDD)) CT evaluation facility of the UK Department of Health (London WC1B 5EP)

[3] Siemens Aktiengesellschaft, Medical Engineering Group HenkestraBe 127, D-8520 Erlangen, Germany.

[4] GE Medical Systems, Milwaukee, W1 53201.

[5] Philips Medical Systems.

by GE Medical System. When this study started the GE HiSpeed Advantage CT model was not in use at the RIE. After installing this new model of CT scanner at RIE in late 1995, the other relatively older scanners were taken out of clinical use. The two older types of GE CT scanners at the RIE and the WGH (GE 8800 and GE 9000 HP) were included in the national dosimetry survey on CT scanners in the UK (Shrimpton et al. 1991a and 1991b, Jones and Shrimpton 1991). Therefore performed measurements on these scanners were quite necessary to be able to compare different dosimetry methods used in this study with each other. The CT scanner of St. Johns Hospital in Livingston was a Tomoscan model of Philips. Finally the CT scanner of Queen Margaret Hospital in Dunfermline district (QMH) was a GE Sytec 3000 Plus model. The locations, manufacturers and models of all the CT scanners used in this study are summarised in Table 3.1. Since there were two identical models of GE scanners (8800 & HiSpeed Advantage) operating at the RIE and the WGH, the dose measurement was carried out only on one of these CT scanners.

Table 3.1: The locations, manufacturers, and models of the CT Scanners.

CT Scanner Locations		CT Scanner Type	
Hospital	**Department**	**Manufacturer**	**Model**
WGH (Edinburgh)	**Radiology** **Clinical Neuroscinces**	**Siemens** **GE**	**Somatom Plus** **8800 *** **HiSpeed Advantage**
RIE (Edinburgh)	**Radiology**	**GE**	**HiSpeed Advantage** **8800 *** **9000HP ***
QMH (Dunfermline)	**X-Ray**	**GE**	**Sytec 3000 Plus**
St. Johns (Livingston)	**Radiology**	**Philips**	**Tomoscan CX/S**

* These models are no longer in clinical use.

3.5.1 Siemens Somatom Plus

This scanner is a high-voltage slip-ring RR scanner. It features a continuously rotating tube-detector system and functions according to the fan beam principle with spiral capability. Spiral scanning of a volume of up to 30 cm long is achieved with continuous table feed and continuous data acquisition.

Three peak tube potentials available are 80, 120, 137 kV. However, Siemens

recommends that 120 kV be used for optimised standard operation, 80 kV for special application, and 137 kV for contrast enhancement in strongly absorbing regions, e.g. spine or shoulder. The tube current range available is from 70 to 320 mA, and the scan times available are: 0.7 (for 240° rotation); 1; and 2 sec (for 360° rotation). The generator has a high-frequency waveform with continuously supplied voltage.

The X-ray tube has a flying focal spot with two nominal focal spot sizes of 1.3×1.2 mm and 0.8×0.9 mm. The inherent filtration is equivalent to 2.7 mm Al equivalent at 120 kV.

The available slice thickness settings (1, 2, 3, 5, and10 mm) are specified at the isocentre. The source-to-isocentre distance is 70 cm, and the source-to-detector distance is 113.5 cm. There are two scan angles (240°, and 360°) available with this scanner. The gantry tilt range is ±25° with respect to vertical.

The CTDI values are reported by the manufacturer for this scanner for both standard and spiral techniques and for different slice thickness settings. But we just mention the values for 10 mm slice thickness here.

For conventional CT, using the standard head phantom and the recommended techniques (10 mm, 360°), reported CTDI values (in mGy/100mAs) are: 2.2 (80 kV), 8.5 (120 kV), and 11.0 (137 kV) in the centre; and 2.5 (80 kV), 9.2 (120 kV), and 11.7 (137 kV) in the maximum value position (1 cm from the edge of the phantom). But for the standard body phantom the reported CTDI values are: 0.7, 3.4, and 4.5 in the centre; and 1.7, 6.4, and 8.3 in the maximum value position for 80, 120 and 137 kVs respectively.

For spiral CT, using the same standard technique, the CTDI values (in mGy/100mAs) are reported just for 120 kV. These values are: 8.5 and 3.4 in the centre; and 9.2 and 6.4 in the maximum value for the standard head and body phantoms respectively. This indicates that based on the manufacturer data the CTDI values are the same for both of the conventional and the spiral examinations for this CT scanner.

3.5.2 GE HiSpeed Advantage

This model is the GE top-of-the-range CT scanner. It is also a RR slip-ring CT scanner with helical (spiral) capability.

Four peak tube potentials are available (80, 100, 120, 140 kV), with 140 kV recommended by GE for standard head scans in America, whereas in Europe 120 kV is more commonly used. The tube current range available is from 40 to 400 mA, with 10 mA increments. The scan times available are: 1, 2, 3, and 4 (for 360° acquisition, full scan), and 0.6 sec (for 225° acquisition or partial scan). The generator is a high-frequency on-board or gantry mounted with continuous operation, and low voltage generator with 48 kW output power .

There are two focal spot sizes: 0.7×0.9 mm and 1.2×1.2 mm. The smaller one being automatically employed for tube currents of 200 mA or less.

The inherent tube filtration is equivalent to 2.7 mm Al equivalent at 140 kV and the anode angle is 7 degrees.

All slice widths: 1,3,5,7, and 10 mm, specified at the isocentre, are collimated on the tube side of the patient. A routine scan time of 1 sec, with 1 sec inter-scan delay, is available as standard on this model. With the continuous scan option, scans can be acquired continuously for up to 60 sec with no inter-scan delay, and may be carried out either with helical with or without (cine) table incrementation. The helical scan pitch is variable between 1:1 and 2:1. The focus to isocentre distance is 63 cm, and the focus to detector distance is 109.9 cm. There are two scan angles (360°, and 225°) available with this model, although 360° is routinely used. The gantry tilt range is ±30°, in 0.5° increments.

The manufacturer has reported the CTDI values, using the standard scan techniques, regardless of the scan being conventional or helical. The reported CTDI values (in mGy/100mAs) for the standard head phantom are: 11.8 (120 kV), in both the centre and the maximum value position; Whereas for the standard body phantom these values are: 3.2 (120 kV) and 5.9 (120 kV) in the centre and the maximum value position respectively.

3.5.3 GE SYTEC 3000 Plus

This CT scanner is also a GE RR model and employs a continuous rotation fan-beam design, with rotation of both the X-ray tube and detectors.

The peak tube potential is 120 kV. The tube currents available with this scanner are: 40, 60, 80, 100, 130, and 160 mA; and the scan times available are 1.8, 2.7, and 4.5 sec.

The scanner X-ray tube has just one focal spot size with the nominal size of 0.7 mm × 0.9 mm.

The four slice widths available with this scanner (1, 3, 5, 10 mm) are specified at the isocentre. The tube-to-isocentre distance is 52.5 cm. There are two scan angles available with this model; partial scan for the lowest scan time and full 360° rotation scan for the other scan times. The gantry tilt range is ± 25°.

The inherent filtration is equivalent to 2.7 mm Al equivalent at 140 kV and the anode angle is 9 degrees.

The reported CTDI values (in mGy/100mAs), using the standard head technique, are: 62 in the centre and 62-65 in the locations 1 cm under the edge of the standard head phantom. For the standard body phantom, using the same standard technique, the reported CTDI values are: 19 in the centre and 32-36 in other locations 1 cm from the edge of the phantom.

3.5.4 GE 9000HP

This CT scanner is an early GE RR model that employs a continuous rotation fan-beam design, with rotation of both the X-ray tube and detectors.

The X-ray tube peak potential is 120 kV. The tube currents available are 50-250 mA; and the scan times available are 3, 5 and 8 sec. The generator is a pulsed constant potential. The pulse length time is 3.7 millisecond. and the number of pulses are 344, 460, and 576 for scan times of 3, 5 and 8 sec respectively.

The inherent tube filtration is equivalent to 2.7 mm Al equivalent. The unit has two shaped filters of PMMA type; one for head examinations and the other one for body examinations.

The three available slice widths (2, 5, 10 mm) are specified at the isocentre. The focus-to-isocentre distance is 78 cm. There are two scan angles of 212°, and 360° available with this model, although 360° is routinely used.

The CTDI values, using the recommended head technique, are: 6.2 in the centre and 5.4-6.0 in the locations 1 cm under the edge of the standard head phantom. For the body phantom, using the same technique, the CTDI values are: 1.2 in the centre and 1.9-2.5 in other locations 1 cm from the edge of the phantom. These values are in mGy/100mAs unit; converted from the values reported by the manufacturer in another unit.

3.5.5 GE 8800

This is another early RR model of GE CT scanners that employs a continuous rotation fan-beam design, with rotation of both the X-ray tube and detectors.

The X-ray tube peak potential is 120 kV. The tube currents available are 20-600 mA, and the scan times available are 6, 7, and 12 sec, although the 12 sec is routinely used. The generator is a pulsed constant potential. The pulse length time is 4 msec and the number of pulses are 288, 342, and 576 for the respective scan times of 6, 7 and 12 sec.

The three available slice thickness settings (1.5, 5, 10 mm) are specified at the isocentre. The source-to-isocentre distance is 78 cm. There are two scan angles of 212°, and 360° available with this model, although 360 is routinely used.

The inherent filtration is equivalent to 2.7 mm Al equivalent at 120 kV. The unit has two shaped filters of PMMA type; one for head examinations and the other one for body examinations.

No CTDI values have been reported for this CT model by the manufacturer.

3.5.6 Philips Tomoscan CX/S

Like the previous models this model is also a RR CT scanner that employs a continuous rotation fan-beam design, with rotation of both the X-ray tube and detector.

Only one peak tube potential is available (120 kV) with this scanner. The tube current range available is from 120 to 370 mA (120, 170, 220, 270, 320, 370), and the scan times available are 2.8 (for 224° rotation), 4.5, and 9 sec. The generator is a pulsed constant potential with a 3.0 (msec)/8.3 (msec) ratio of pulse width to pulse period.

The three slice widths available with this scanner (2, 5, and 10 mm) are specified at the isocentre. The source-to-isocentre distance is 60 cm. Two scan angles of 224 °, and 360 ° are available. The partial rotation is used with 2.8 sec scan time and the full rotation with the other scan times. The gantry tilt range is ± 20 °.

The inherent filtration is 1.0 mm Al plus 0.1 mm Cu and the anode angle is 9 degrees. Information on the collimator adapter was provided by the manufacturer for this CT model.

Neither the manufacturer nor the MDA has reported the CTDI values for this model of Philips CT scanner.

3.6 Routine CT Examination Protocols

Several different protocols were in use for routine examinations performed by the CT scanners in this study. However, not all of these protocols were commonly used. Therefore, through consulting with the CT users, radiologists and radiographers, the most common examination protocols as used for the head, chest, abdomen and pelvis areas of the body were chosen. The routine radiological factors were determined for all the routine protocols. These factors include: kV; mA and scan time (or mAs); slice width (thickness); couch increment (table feed) for conventional or pitch value for spiral or helical examinations; number of slices (or scan volume); and the starting position of scans. The radiological factors for all the common CT examinations performed by all the CT scanners are mentioned in chapter five and six where the dosimetry results are presented. It must be noted that all examinations were assumed to be performed with the patient in supine position and from the head towards the toe, except for the head region examinations where the scans are normally performed from the toe towards the head.

Based on the determined locations of organs or regions of the body in an anthropomorphic physical phantom (Rando Alderson), the patient related data (scan starting position and scan volume) were adopted for the phantom. This was carried out in a way to simulate an average size patient for every specific routine CT examination. Details of the modifications to the phantom made for this purpose are mentioned in the next chapter. In addition, the patient related data (scan starting position and scan volume) were also adopted for the mathematical phantom (Shrimpton et al. 1991a, Shrimpton et al. 1991b, Jones and Shrimpton 1991) in a way to simulate every common CT examination being performed for an average size patient. The reader is referred to chapter six for the details of the work carried out in this regard.

4. PHANTOM SPECIFICATIONS

The dosimetric phantom used in this study was a complex-realistic body (anthropomorphic) Rando phantom. The phantom is composed of various tissue substitutes and real human skeleton simulating the human body with respect to size, shape, spatial distribution, mass density and radiation interaction. Although this type of phantom has originally been designed for use in radiotherapy dosimetry, its physical properties, namely its tissue-equivalence (density and elemental composition), and the suitability of its tissue substitute has also been investigated for X-rays of diagnostic qualities by Shrimpton et al. (1981). From their reported results it has been concluded by several authors (Huda and Sandison 1985, NRPB 1990) that the Rando phantom is suitable for dose determinations at the relatively high photon energies that are typical for CT examinations.

4.1 Reference (Standard) Man

In estimation of radiation doses to the human body from external sources like CT, apart from the spatial distribution of dose over the body, it is necessary to take into account the interaction coefficient of X-rays for different types of materials composing each organ or tissue of interest. This requires a certain amount of data about the mass and elemental composition of the organs and tissues concerned. Hence to achieve this, reference was made to the ICRP report of the Task Group on Reference Man (ICRP 1975). The elemental compositions recommended by the ICRP for all organs and tissues of interest were used for calculating the relevant interaction coefficients of X-rays produced by the CT scanners in this study. Details of the work carried out in this regard are explained in the following chapter, where our developed direct CT dosimetry method has been described.

4.2 Description of the Physical Phantom

The dosimetric phantom used for CT dosimetry in this study was an anthropomorphic Rando Alderson type (RT-HUMANOID PHANTOM) produced by Humanoid Systems, Incorporated, USA (Alderson et al. 1962). This is an Average-Man Rando phantom (Figure 4.1). Two Rando Breast phantoms were also obtained that can be attached to the Average-Man to simulate a female phantom (Figure 4.2).

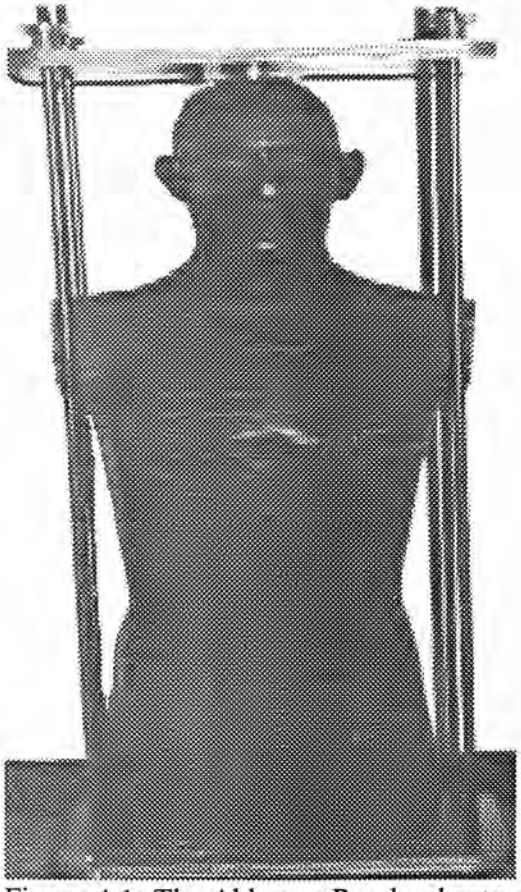

Figure 4.1: The Alderson Rando phantom.

The Average-Man Rando phantom has no limbs and consists of 36 sequentially numbered sections (0 to 35) each 2.5 cm thick with section 0 located at the top of the head and section 35 located at the upper most region of the thighs that is about four times thicker than other sections (Figure 4.1). The breast phantoms are cut into 2-cm-wide sections in the frontal plane (Figure 4.3). The phantom is modelled about a 50th percentile human skeleton, 175 cm (5' 9") tall and 77 kg (162 lbs) in weight. The phantom is comprised of a human skeleton embedded in tissue equivalent

material and the lungs are simulated by lung equivalent material. The lung equivalent material is made of a plastic foam material providing normal radiographic appearance (Figure 4.4).

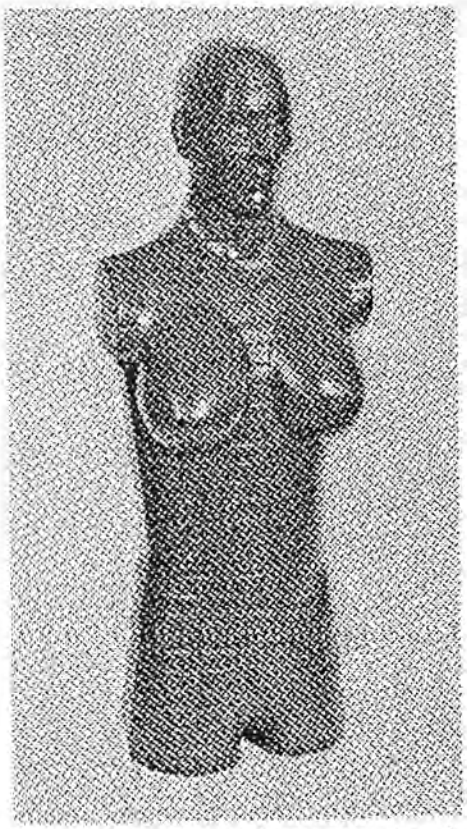

Figure 4.2: The Alderson Rando phantom with breast sections.

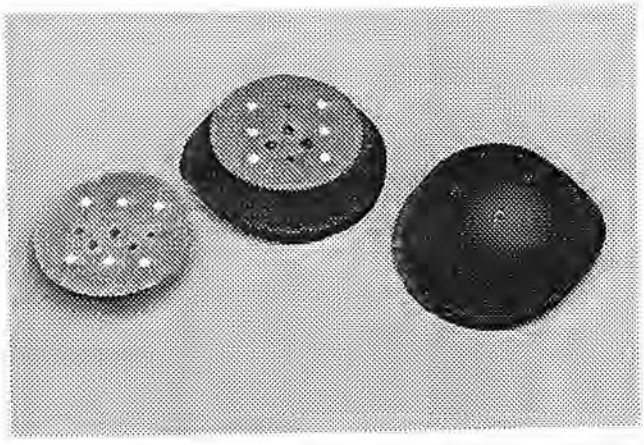

Figure 4.3: The breast phantoms, cut in two sections in frontal plane with the holes for holding the dosimeters.

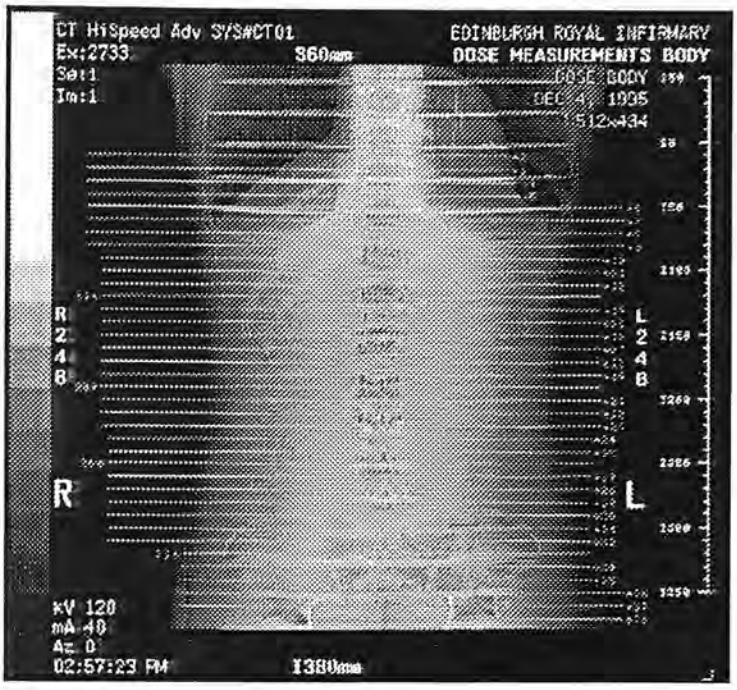

Figure 4.4: A CT image (topogram) of the chest, abdomen and pelvis regions of the Rando phantom showing the embedded human skeleton and two different materials used to simulate soft tissues and lungs in the phantom.

4.3 Positioning of Organs and Tissues in the Phantom

For calculating effective dose equivalent (ICRP 1977) and effective dose (ICRP 1991) resulting from CT practices it was necessary to determine the doses received by all those organs and tissues recommended by the ICRP. These organs and tissues are gonads, red bone marrow, colon (lower large intestine), lung, stomach, bladder, breast, liver, oesophagus, thyroid, skin, and bone surface, which all have a significant and quantified risk of induced cancer. A group of tissue or organs has also been regarded as "Remainder", that is composed of the following additional tissues and organs: adrenals, brain, upper large intestine, small intestine, kidney, muscle, pancreas, spleen, thymus, and uterus. These are the organs that are likely to be selectively irradiated and some of them are known to be susceptible to cancer

induction but for which the risk has not been accurately estimated yet. Therefore it was required to determine the location and proportion of these organs and tissues in the phantom.

The location of organs and tissues of interest, in each section of the phantom, were demarcated using an atlas of human cross-sectional anatomy (Ellis et al. 1991). In this regard, based on the position of the skeleton, embedded in the phantom, the position of every organ and tissue of interest was determined and its approximate boundary was demarcated in each section of the phantom. Figure 4.5 shows four typical sections from the head (Section 2), chest (Section 14), abdomen (Section 26), and pelvis (section 31) regions of the Rando phantom illustrating demarcated positions of the organs and tissues of interest. The estimated location of all organs and tissues of interest in every individual section of the Rando Alderson phantom are collected in Appendix A.

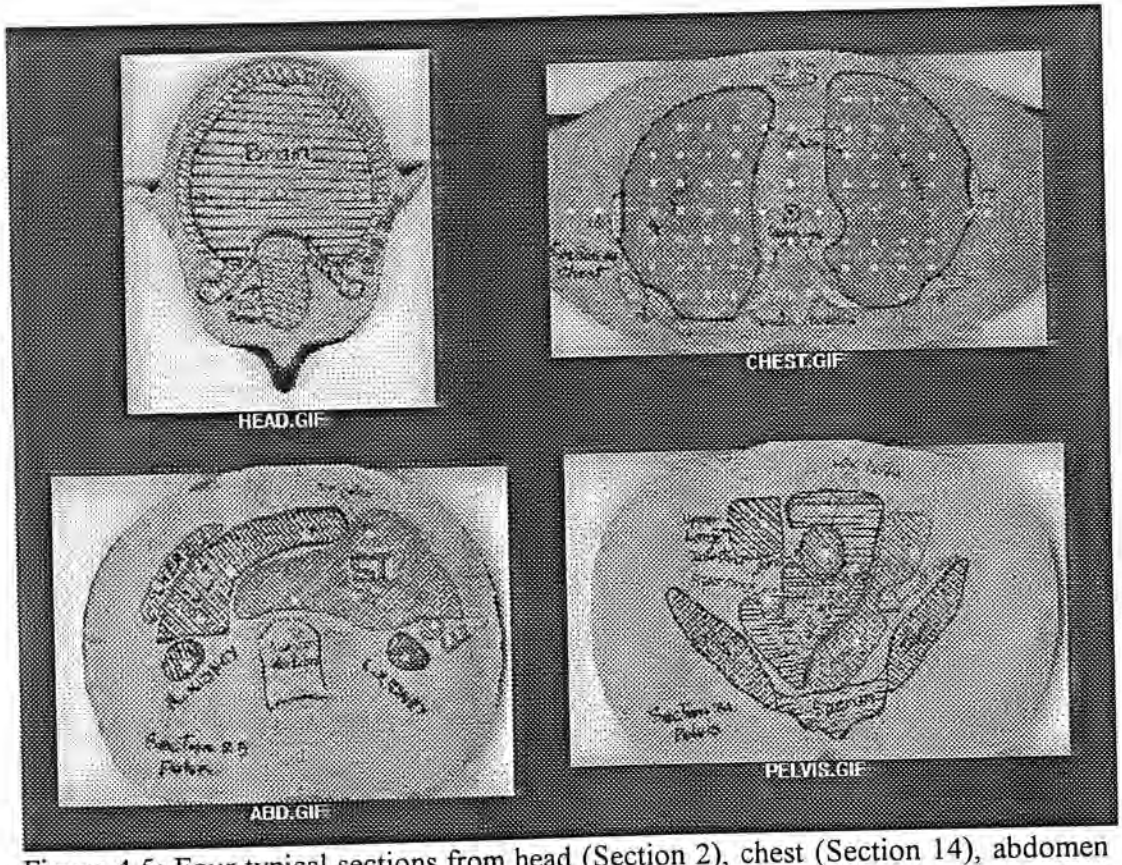

Figure 4.5: Four typical sections from head (Section 2), chest (Section 14), abdomen (Section 26), and pelvis (section 31) regions of the Rando Alderson phantom showing demarcated positions of organs and tissues of interest.

The skeleton was not embedded very well in the phantom and its location within the sections of the Rando phantom was not anatomically correct at all levels. Comparing with the normal position of the skeleton within the body it seems that it has been slightly moved towards the posterior within those sections comprising the head part (Figure 4.6), but moved towards the anterior within other sections comprising the abdomen part (Figure 4.7) of the phantom. In other words the skeleton was displaced in the anterior/posterior direction in many sections. This required certain compromises in determining the location of organs in the Rando phantom. Therefore although the position of skeleton was taken as a reference point, necessary corrections were made for the above displacements. Generally the position of the organs were determined in respect of their position with respect to bony structures. This position was adjusted in the anterior/posterior direction based on the displacement of the bone structures in particular the spine.

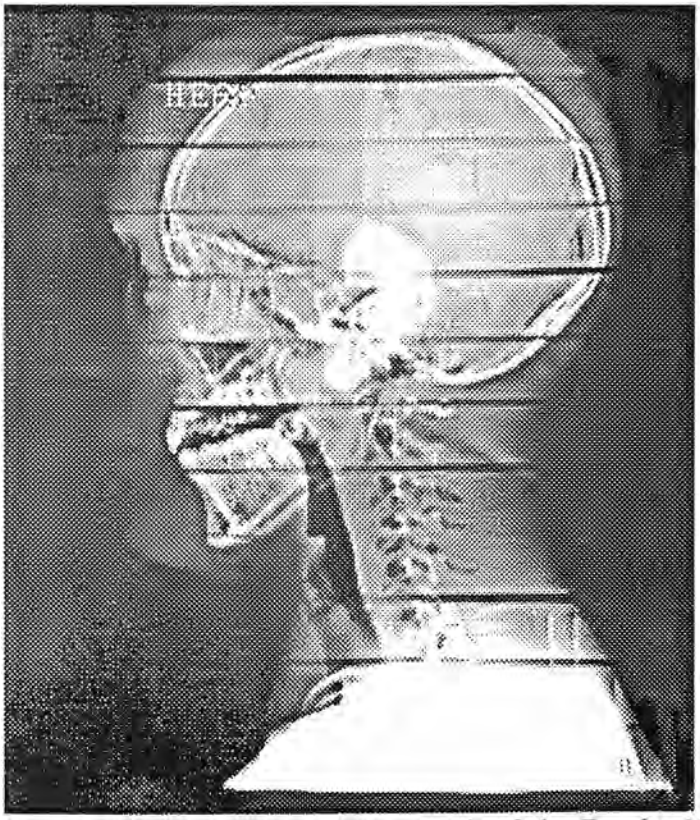

Figure 4.6: A CT image (topogram) of the Rando Alderson phantom showing the displacement of the skeleton in the sections (0-8) that comprise the head region of the phantom.

For organs with complex distribution over a large region of the body, for

example the intestines, areas encompassing the complete structure of the organ were drawn rather than trying to reflect the structures given for an individual patient in the atlas of Ellis et al. (1991). The reader is referred to appendix A for approximate locations and boundaries of all organs and tissues of interest within each section of the Rando phantom. Regarding the chest region, it must be considered that the lung tissue has been simulated in this region of the phantom by applying a different material by the manufacturer. Therefore there was no need for determining the location of this organ in the phantom. The demarcation of this organ was carried out based on the simulated area of this organ in the relevant sections of the Rando phantom.

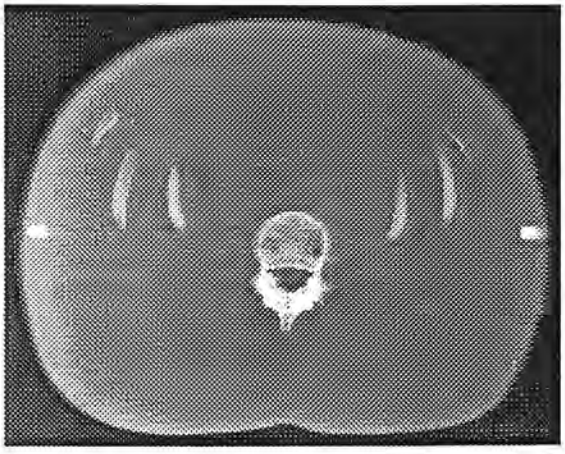

Figure 4.7: A radiograph of section 24 of the Rando phantom showing the displacement of the skeleton within one of the sections that comprise the abdomen region of the phantom.

4.4 Volume Distribution of Organs in Sections of the Phantom

Software developed as a part of a radiotherapy treatment planning system (Redpath 1991) was used to determine the area of each organ within each section of the phantom. This was achieved by tracing the outline of the organ on the surface of each section of the phantom using a light pen. From this the volume of the organ in each section was determined, from which its percentage to the total volume of the organ in the phantom was calculated. Using this method the distribution of every organ and tissue of interest, except skin, red bone marrow (RBM), bone, and muscle

in all sections of the phantom was determined. Then the fractional value of each organ and tissue of interest in every section of the Rando phantom was derived and rounded off to 3 significant figures in a way to sum to unity over the phantom.

The distribution of skin, RBM and bone were derived from a study by Huda and Sandison (1984). They obtained the values of skin by taking the measured surface area for every one of the 36 sections of the Rando phantom and expressing it as a fraction of the total surface area (180000 cm^2) given for the Adult Reference Man (ICRP 1975). They also obtained the values of bone by estimating the volume of skeleton in X-ray radiographs for every one of the 36 sections of the Rando phantom and multiplying it by 0.667, that is the fraction of the total skeleton within the skull and trunk for the ICRP Reference Man (ICRP 1975). They also derived the RBM distribution from documents provided by others (Cristy 1981, Ellis 1961). On the basis of their data, 15% of the RBM was taken to be located within sections 0-9, 43% within sections 10-26 and the remaining 42% within sections 27-35. For each section within these regions, it has been assumed that the RBM content is proportional to the skeletal mass in that section. It has also been assumed that there is no RBM in the limbs. The fractional values for these tissues in every section of the phantom have also been rounded off to 3 significant figures in a way to sum to unity over the phantom.

Based on the ICRP report (ICRP 1975) the major proportion (75%) of the muscle is located in limbs. In addition, normally in all routine CT examinations, the limbs are kept outside the scan volume and are not practically exposed to the X-ray radiation. Therefore, the distribution of this tissue in the phantom was not determined and it was not taken into account for CT dose measurements in our study.

The experimentally determined fractional values for all the organs and tissues of interest in the Rando phantom are presented in the following sections.

4.4.1 Brain

The brain is located within sections 1-4 of the Rando phantom inclusive, with the proportional fractions of 0.214, 0.318, 0.294 and 0.174.

4.4.2 Parotid, Thyroid and Thymus Glands

The parotid gland is located in sections 5-7 inclusive with relative fractional values of 0.373, 0373, and 0.254. The thyroid is positioned in section 9 (0.739) and section 10 (0.261) and the thymus is equally divided between section 12 and 13.

4.4.3 Lung and Oesophagus

The lungs are located within sections 10-19 inclusive and the result of their experimentally determined values in each section of the phantom is summarised in Table 4.1. The oesophagus is located within sections 9 to 19 of the phantom as shown in Table 4.2.

Table 4.1: Measured fractional values of the lungs for Average-Man Rando phantom.

Section No.	10	11	12	13	14	15	16	17	18	19
Fraction	0.008	0.039	0.080	0.112	0.135	0.145	0.146	0.141	0.118	0.076

Table 4.2: Distribution of the oesophagus in the Rando phantom.

Section No.	9	10	11	12	13	14	15	16	17	18	19
Fraction	0.069	0.120	0.101	0.101	0.101	0.101	0.101	0.101	0.101	0.101	0.101

4.4.4 Liver, Spleen, Stomach, Pancreas, and Intestines

The liver in located within sections 18 to 25 of the phantom by the fractional values mentioned in Table 4.3 . The spleen is located within sections 19 to 22 of the phantom by the relevant fractional values of 0.127, 0.352, 0.361, and 0.160. The stomach extends to one more section and is located within sections 19-23, with the relevant fractional values of 0.170, 0.331, 0.235, 0.147, and 0.117. The pancreas is divided among section 21 (0.244), section 22 (0.396), section 23 (0.204), and section 24 (0.156) of the Rando phantom. The small intestine (SI), upper large intestine (ULI), and lower large intestine (LLI) spread over a large proportion of the body (over 12 sections), and their measured values all over the individual sections of the phantom are summarised in Table 4.4.

Table 4.3: Relative distribution of the liver in the Rando phantom

Section No.	18	19	20	21	22	23	24	25
SI	0.067	0.177	0.233	0.216	0.147	0.087	0.050	0.024

Table 4.4: Relative distribution of the intestines in the Rando phantom

Section No.	21	22	23	24	25	26	27	28	29	30	31	32	33	34
SI	0.006	0.018	0.039	0.062	0.077	0.090	0.120	0.136	0.135	0.147	0.115	0.054	-	-
ULI	0.018	0.032	0.022	0.025	0.123	0.213	0.174	0.113	0.083	0.061	0.063	0.075	-	-
LLI	-	0.011	0.020	0.017	0.011	0.011	0.011	0.008	0.007	0.061	0.295	0.323	0.152	0.073

4.4.5 Kidneys and Adrenals

The Kidneys are located within sections 22-25 of the Rando inclusive, with the respective values of 0.062, 0.227, 0.297, 0.245, 0.169. One third of the adrenals is located in section 20 and their remainder is located in section 21.

4.4.6 Ovaries, Prostate, Uterus, and Bladder

Since the sizes of these organs are quite small their locations can be readily determined by consulting the above CT atlas (Ellis et al. 1991) which indicates that the ovaries are located in section 31, the prostate in section 33, one third of the uterus in section 31 and the rest of it in section 32, and finally the bladder is divided among three sections (32,33, and 34) with the respective values of 0.348, 0.492, and 0.160.

4.4.7 Skin, Bone, and Red Bone Marrow

As mentioned above the fractional values for these tissues were derived from a study by Huda and Sandison (1984). The resultant fractional values of these tissues in each section of the Rando phantom are summarised in Table 4.5.

Table 4.5: Fractional values for the skin, bone, and red bone marrow (RBM) in each section of the Rando Phantom.

Section No.	Skin	Bone	RBM
0	0.011	0.010	0.010
1	0.008	0.030	0.030
2	0.008	0.010	0.010
3	0.008	0.010	0.010
4	0.008	0.030	0.030
5	0.008	0.030	0.030
6	0.007	0.005	0.005
7	0.006	0.010	0.010
8	0.006	0.005	0.005
9	0.007	0.010	0.010
10	0.010	0.030	0.048
11	0.014	0.040	0.062
12	0.014	0.030	0.048
13	0.015	0.020	0.032
14	0.014	0.020	0.032
15	0.014	0.010	0.016
16	0.013	0.020	0.032
17	0.013	0.010	0.016
18	0.013	0.010	0.016
19	0.012	0.010	0.016
20	0.012	0.010	0.016
21	0.012	0.010	0.016
22	0.012	0.010	0.016
23	0.011	0.010	0.016
24	0.011	0.010	0.016
25	0.011	0.010	0.016
26	0.011	0.010	0.016
27	0.012	0.010	0.034
28	0.012	0.030	0.053
29	0.012	0.030	0.053
30	0.012	0.030	0.053
31	0.013	0.020	0.034
32	0.013	0.030	0.053
33	0.013	0.030	0.053
34	0.014	0.020	0.034
35	0.044	0.030	0.053

4.5 Summary and Conclusion

The anthropomorphic physical phantom chosen was the Rando Alderson phantom produced by Humanoid Systems, Incorporated, USA (Alderson et al. 1962) being proved to be suitable for CT dosimetry purposes (Huda and Sandison 1985,

NRPB 1990). This was an average-man phantom. Two breast phantoms could be added to form a female phantom if required. The phantom had no limbs. It was cut into 36 sections (0 to 35) each 2.5 cm thick with the last section being located at the upper most region of the thighs with a thickness four times thicker than other sections.

The position of the organs required for the calculation of effective dose determined with reference to a standard atlas of human cross-sectional anatomy (Ellis et al. 1991). The proportion of each organ and tissue of interest in every section of the phantom was derived. The distributions of bone, red bone marrow and skin in the body were chosen with reference to a report by Huda and Sandison (1984). The fractional values of these tissues were also normalised to 1.000 for the whole body.

5. CT Dosimetry using the Physical Anthropomorphic Phantom (Materials and Methods)

5.1 Introduction

As explained in the first chapter two dosimetry approaches, namely the Monte Carlo approach using a mathematical phantom and the CTDI and the direct approach using a physical phantom, are used commonly for the assessment of patient doses from CT examinations. The application of the Monte Carlo dosimetry approach in CT dosimetry and the way it was used in our study will be discussed in detail in chapter seven. In this chapter the only alternative common CT dosimetry method, that is the direct approach, and the way it was developed and used in this study will be explained.

The direct dosimetry approach has been followed by several researchers for the assessment of patient doses from CT practices (Hashemi-Malayeri and Williams 1996a, 1996b, and 1996c; Wright et al. 1996; Collie et al. 1994a and 1994b; Kron 1995; Geleijns et al. 1994; Ekestubbe et al. 1993; Nishizawa et al. 1991; Wall et al. 1979; Horsely and Peters 1976). As mentioned earlier, this dosimetry approach is based on the direct measurement of organ doses at their approximate locations in a physical phantom simulating an average human body. There are 23 organs and tissues of interest for which the average absorbed doses need to be determined. Therefore, considering the distribution of organs inside the physical phantom used (Rando Alderson), if this dosimetry approach is employed, at least 200 TLD measurements will be required to estimate organ doses and other dose indices for every CT examination. Due to this fact, this approach has been described as a laborious and impractical procedure for routine CT dosimetry studies and has not attracted the attention of many researchers in this field of study.

On the other hand, although the Monte Carlo dosimetry approach, as used in this study, is quite easy and practical for routine patient dose assessments from CT examinations, it is limited to those models of CT scanners that were included in the national survey of CT practice in the UK (Shrimpton et al. 1991b). This survey

included the CT scanners that were operational in the UK before 1989. As our study indicates, most of these scanners have either been taken out of service or replaced with the new CT models. Unfortunately, neither any data file nor the required manufacturer data on the scanner design appears to be easily available, that are required for implementing this dosimetry approach for new CT models.

Hence a preliminary study was first undertaken to establish an easier practical direct approach for CT dosimetry, with an acceptable degree of accuracy and confidence. It was aimed to develop this approach in a way that not only, it will be independent of the type of the scanner but also, it will be quite simple and practical to be carried out routinely for the assessment of patient doses from CT examinations.

This chapter covers the underlying principles and the steps followed to improve and simplify the direct dosimetry approach, that eventually led to our proposed developed direct CT dosimetry approach. This includes the description of the method, the materials used, the dosimetry aspects considerations, and other processes employed for the simplification of the method.

The description of the developed dosimetry method will be presented in the following sections. This includes the assumptions made and the phases followed for the development of the direct CT dosimetry approach.

The results of applying our developed dosimetry method for the assessment of patient doses from several models of CT scanners will be presented in chapter six.

5.2 The Developed Direct CT Dosimetry Method

The common direct CT dosimetry approach requires a physical humanoid phantom, to simulate a standard average human body, as recommended by the ICRP (1975). It also requires a suitable radiation dosimeter to measure the radiation doses received at the approximate locations of the organs of interest throughout the phantom.

From available physical humanoid phantoms, the Rando Alderson anthropomorphic phantom was chosen being concluded to be suitable for dose determinations at the photon energies typical for CT examinations (Shripmton et al. 1981, Huda and Sandison 1985, NRPB 1990). As explained earlier except for some

organs or tissues, the position and distribution of other organs and tissues of interest were not defined in this phantom by either the manufacturer or other researchers. Hence, an additional design was carried out on the Rando phantom to determine the position and distribution of all the organs and tissues of interest recommended for the calculation of effective dose by the ICRP (1991). This stage of the work has been described in the previous chapter and appendix A. Therefore the reader is referred to chapter four and appendix A for the details of the work carried out on the phantom to make it suitable for our developed direct CT dosimetry.

Having the approximate locations of all organs determined in every section of the phantom, a suitable dosimeter must be used to measure the radiation doses received at the locations of all organs and tissue of interest throughout the phantom. Then the average absorbed dose delivered to every individual organ or tissue of interest can be calculated, from which other dose indices can be estimated. The radiation dosimeter must have such a physical shape and size, that could offer enough spatial resolution and could be easily accommodated in various locations in the phantom. On the other hand, the dosimeter must posses suitable dosimetry characteristics required for the typical X-ray spectra of CT scanners. The dosimeter must also meet minimum requirements as regards for accuracy and precision. From the available X-ray dosimeters, the lithium fluoride (LiF) thermoluminescent dosimeter (TLD) was chosen, providing both the physical and the dosimetric characteristics required for this CT dosimetry approach.

The common direct dosimetry approach is the only alternative approach that does not have the limitations of the MC approach and could provide an indication of the patient risk involved with CT examinations. On the other hand, if this approach is employed for the assessment of patient doses from CT practices, it will require a knowledge of the dose to all radiosensitive organs and tissues of the body. This could be achieved, as noted before, by numerous point dose measurements at the location of all organs and tissue of interest throughout the phantom. Therefore it is brought to the attention that, although this dosimetry approach does not have the limitations of the MC approach, it imposes other restrictions. Not only, this approach is limited to a particular CT examination for a particular scanner, but also it requires a considerable

number of point dose measurements for every examination. These constraints have made this dosimetry approach rather a laborious and impractical procedure for monitoring patient doses from CT practices.

Hence the primary objective of the developed direct dosimetry method was to overcome the limitations imposed by the common direct dosimetry method and to establish a practical and reliable method for estimating the levels of patient doses resulting from CT practices with an acceptable degree of accuracy.

In this regard a study was designed and implemented in the following four phases:

(I) The basis for the assessment of patient dose from CT practice was the use of a common physical phantom to simulate the human body. Extra design needed to be carried out on the phantom to locate the position and determine the distribution of all radiosensitive organs and tissues of interest.

(II) A suitable dosimetry device was chosen and a calibration procedure was established for it, with an acceptable degree of confidence. In addition necessary calculations was carried out for determining all factors required for the assessment of the risk from CT procedures in terms of the absorbed dose to all radiosensitive organs and other dose indices. This required a knowledge of the CT X-ray spectra and the concept of the organs' mass energy absorption coefficient for converting the measured quantity of exposure to absorbed dose in organs and tissues.

(III) Calculations were performed to provide a basis for simplifying and reducing the number of measurements required for the common direct CT dosimetry approach. In this regard three assumptions were made:

1. Dose distribution, inside the scan volume, in parallel sections of three relatively homogenous regions of the phantom; namely the head, the Chest, and the abdomen and pelvis; can be represented by a single dose distribution to a representative section, chosen from these regions and normalised to the central axis dose value in the section. This assumption was based on earlier studies reporting similar isodose dose distributions for single scans using a particular CT scanner as mentioned in chapter one.

2. Dose distribution in sections of the phantom outside the scan volume can be represented by a simple function characteristic to the scanner central axis dose and the region of the body. This assumption was based on earlier studies reporting small amount of the scattered dose outside the CT scan volume as mentioned in chapter one. Another base for this assumption was the new configurations of filters available with modern CT scanners providing a very well collimation beam as mentioned in chapter three.
3. The proportion of the muscle tissue being irradiated during CT practices is not significant. Therefore the contribution of the absorbed dose to this tissue can be ignored for the calculation of the dose indices. This assumption was based on the fact that, the major portion of the muscle tissue is located in the limbs that are normally kept outside the scan volume as a convention in CT practices.

These assumptions were made in order to be able to determine the organs absorbed doses and the other dose indices with a limited number of measurements on the central axis of the phantom. This made us able to overcome the limitation of the direct dosimetry method and simplify it in away that it could be implemented for the routine patient dose assessment from many diverse and fast growing CT practices.

(IV) Further to simplify the developed direct dosimetry approach, a spreadsheet was customised using a common computer program (Microsoft Excel ®). This spreadsheet was designed to store the calculated data regarding the phantom, the CT scanners, and the calibration of the dosimeters. It also handles the input of the required data, and reports the resultant patient doses in terms of the organs absorbed doses and the other dose indices recommended by the ICRP (1977, 1991) as its output. The spreadsheet was designed in a way to perform the data processing in a very user friendly manner.

Regarding the phase one, as was already noted, a comprehensive work was carried out for the extra designs required on the physical Rando phantom. Chapter four and appendix A were resulted from the implementation of this phase of the study.

The other phases were resulted in the following sections of this chapter.

Section 5.2 describes the dosimetry device used for the dose measurement. This includes our rationale for choosing this type of dosimeter (LiF TLDs), the procedure established for its calibration factor calculation, and the estimated level of uncertainty in the measurements.

The absorbed dose corrections will be explained in section 5.4. This includes one part of our preliminary study carried out to determine and take into account the CT X-ray spectra and the organs and tissues mass energy absorption coefficients.

Dose distribution studies are introduced and discussed in section 5.5. In this regard dose distributions inside and outside the CT scan volume are presented, discussed and analysed. This was done in an attempt to simplify the common CT dosimetry approach by overcoming the cumbersome of the numerous point dose measurements required for the implementation of this dosimetry approach.

Section 5.6 contains the results of the measurements carried out for the validation of the assumptions made for the dose distributions. In this regard the accuracy of the method sued for calculating dose distributions from orthogonal measurements in the representative sections of the "head", "chest", and "abdomen & pelvis" areas of the phantom are validated. In addition the assumption made about the similarity of the dose distributions in parallel sections to that of the representative sections in the overlap region between chest and abdomen has been validated.

Section 5.7 describes the computer program customised for the automation of data processing for the developed dosimetry method. In this section the computer spreadsheet program used and customised for further simplification of the direct dosimetry approach is provided. This includes data storage handling, data processing, and reporting the resultant organ and tissue doses and other dose indices of interest for a particular CT examination.

Finally the summary of the developed direct CT dosimetry method will be presented in the last section of this chapter.

5.3 TLD Study

To achieve the minimum exposure to patients from CT examinations consistent with good diagnosis, the accurate measurement of radiation doses is

important in the assessment of patient doses exposed to ionising radiation resulting from this diagnostic procedure. The dose measurements for conventional X-ray examinations have traditionally been carried out using devices such as air ionisation chambers and film badges, although nowadays TLDs are increasingly being used (McKinlay 1981). Thermoluminescent dosimeters have been available for dosimetry of ionising radiation for nearly 100 years (Kron 1995). The variety of these materials and their different physical forms allow the determination of different radiation qualities over a wide range of absorbed dose. This makes TLDs useful in radiation protection where dose levels of about 10 μGy are monitored as well as in radiotherapy where doses up to several Gy are to be measured.

TLD has proved to be a useful dosimeter in the assessment of patient doses from diagnostic X-rays and has been used successfully in CT dose measurements (Hashemi-Malayeri and Williams 1996a, 1996b, 1996c; Wright et al. 1996; Collie et al. 1994a and 1994b; Kron 1995; Geleijns et al. 1994; Ekestubbe et al. 1993; Nishizawa et al. 1991; Wall et al. 1979; Horsely and Peters 1976). TLDs offer obvious advantages over ionisation chambers for CT dosimetry. The major advantages of these radiation detectors are their small physical size and that no cable or auxiliary equipment is required during the dose assessment. Therefore thermoluminescent (TL) detectors allow point dose measurements, in the approximate position of organs in phantoms, as required for the direct CT dosimetry approach. Furthermore, if in vivo measurements are required they are radio-transparent and less obstructive to most X-rays. Figure 5.1 is a CT image showing the TLDs positioned in some points of interest in a single section of the Rando phantom.

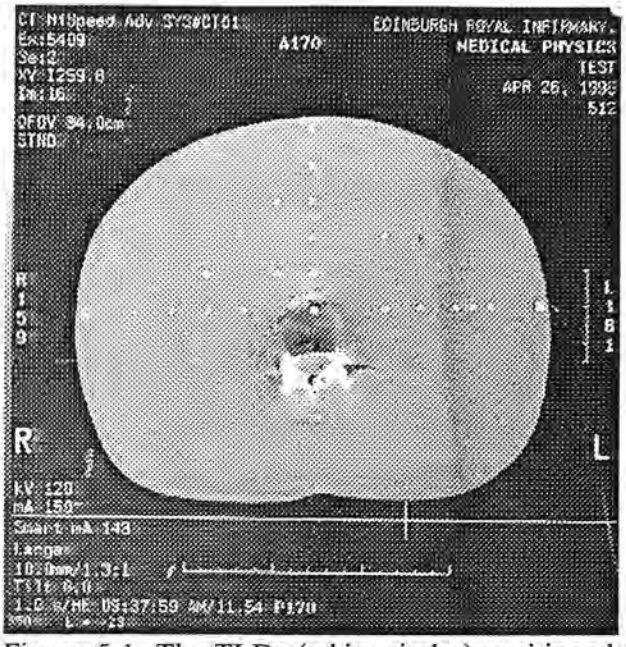

Figure 5.1: The TLDs (white circles) positioned in some points of interest in a single section of the Rando phantom.

5.3.1 Type of TLDs

Various types of TL materials are used for radiation dosimetry. The material chosen for radiation dose monitoring is based on the popularity of use, commercial availability and specific applications, including personal, clinical and environmental dosimetry. The most important families of TL materials used in clinical dosimetry are lithium fluoride (LiF), lithium borate ($Li_2B_4O_7$), calcium sulphate ($CaSO_4$) and calcium fluoride (CaF_2) phosphors. From these families, LiF based TLDs demonstrate a linear dose response from between 50 and 100 mGy threshold to between 3 and 10 Gy depending on the form of the dosimeter (McKinlay 1981). In addition, LiF has a photon effective atomic number of Z_{eff}=8.2, that if compared with the average value of 7.4 for body tissues, it can be considered to be approximately tissue-equivalent for most applications (ibid.). Considering the particular peak of the LiF glow curve, normally used in practical dosimetry, the fading of this type of TLD is negligible over a long time (~ 80 years half-life) (ibid.). Hence, the dosimetric characteristics of LiF based TLDs make it particularly well suited for use in X-ray dosimetric studies of diagnostic qualities, such as CT, in view of its ease of use (loading in the Rando

phantom), linear dose response, and its negligible fading. The reader is referred to McKinlay's (1981) book on the thermoluminescence dosimetry for a full theoretical background, description and application of all types of TL materials.

For all CT examinations, dose measurements were achieved using LiF doped with magnesium and titanium (LiF: MgTi). This is one of the most commonly used family of thermoluminescence phosphors, first investigated in 1953 and abandoned due to its variable TL properties. But, later interest in this material was renewed in 1961 (ibid.) and this type of TLD has been the first choice for TLD users for over the last 30 years and is still being used widely. Its chemical stability, close "tissue equivalence" and well-defined response to ionising radiation make it ideal for diagnostic X-ray dosimetry.

Harshaw Chemicals produces a commercial LiF phosphor known as TLD 100 and its isotopic variants TLD 600 and TLD 700. By comparing the TLD 700 (comprising of 0.01% ^{6}Li and 99.99% ^{7}Li phosphor type) with some other LiF based phosphors, it has been concluded that TLD 700 is the most sensitive TLD (ibid.). From this family of TLDs, LiF-7 round chips (Figure 5.2) manufactured by Vinten Instrument Limited[1] were used. Based on the manufacturer's data sheets, this type of TLD has been designed for general purpose dosimetry for penetrating photons and electrons. This TLD has a diameter of 4.5 mm and a thickness of 0.8 mm. 99.95% of this TLD is LiF-7 and is claimed to offer high sensitivity with a performance compares favourably with the well-known Harshaw TLD-100 chips, being approximately 25% more sensitive and ideal for accurate, low dose (0.01 to 1000 mGy) measurements. The measuring range is claimed to be linear from 20 μGy to 2 Gy with better than ± 2% reproducibility and repeatability. It is also stated that its fading is less than 2% in 30 days, dependent on read anneal cycle, and its reusability is more than 200 cycles (Vinten Instruments Limited).

---

[1] **Vinten Instruments Limited, Jessamy Road, Weybridge, Surrey KT13 8LE, England.**

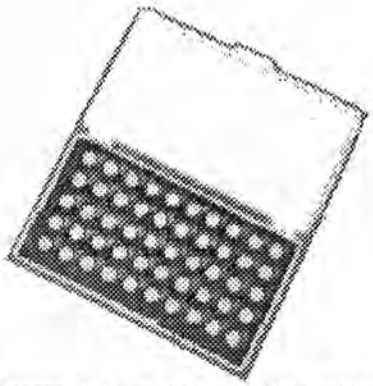

Figure 5.2: A box of LiF: MgTi round TLDs containing 50 chips.

5.3.2 Calibration of TLDs

A batch comprising of 250 round TLD chips was used in this study. Dosimeters were read out on a Toledo TLD reader with an automatic sample changer (Vinten Instruments Ltd, Weybridge, UK) (Figure 5.3). First, all 250 TLDs were read out to eliminate any possible background history. Then all TLDs were given a known dose (about 20 mGy at 100 kV) generated from a conventional X-ray machine and were read out on the TLD reader. This process was repeated three times and the average (AVG) value and the standard deviation (STD) for the batch of TLD were calculated. Those TLDs which consistently showed a value out of the "AVG ± (2×STD)" range were excluded and the rest were used for our dosimetry measurements. In this way TLD chips whose sensitivity was significantly different from the remainder of the batch were excluded.

TLDs, irradiated during each CT examination, were processed using a single calibration factor determined from twenty TLDs. These TLDs were comprised of ten non-dosed controls (subjected only to the background radiation) and ten dosed controls. The dosed controls were exposed at 100kV constant potential to a dose of approximately 20mGy generated from a conventional X-ray machine, along with an ionisation chamber (Radcal[2] Model 20X5-3 chamber with Model 2025 electrometer). The ionisation chamber had a traceable calibration in terms of exposure. The ten

---

[2] **NE Technology Limited, Bath Road, Berkshire RG7 5PR England.**

dosed TLDs and the traceable ionisation chamber (IC) were positioned on the surface of a bloc of perspex perpendicular to the central axis of the beam as shown in Figure 5.4. The bloc of perspex was used to produce a uniform and consistent backscatter radiation. In addition, in order to avoid the heel effect, the IC was positioned along that central axis of the radiation field that was perpendicular to the anode-cathode direction of the X-ray tube. The dosed TLDs were put on two parallel lines at an equal distance along both sides of the active length of the IC. Figure 5.4 shows schematic drawing of the set up of the dosed TLDs, the ionisation chamber, and the X-ray unit as set for the calibration measurement.

Figure 5.3: Toledo TLD reader with automatic sample changer.

The following equation was used to determine TLDs calibration factor (CF_{TLD}):

$$CF_{TLD} = 1/(R - R_{bgd}) \cdot M \cdot \left(\frac{P_0}{P} \cdot \frac{T}{T_0}\right) \cdot CF_{IC} \cdot f \qquad \text{(Equation 5.1)}$$

where CF_{IC} is the calibration factor for the ionisation chamber, R is the average of dosed TLD readings, R_{bgd} is the average of control TLDs readings, M is the IC reading (in roentgen), P_0 and T_0 are the standard pressure (760 mmHg) and temperature (293 °K) values, P and T are the ambient pressure and temperature values, and f is the exposure to absorbed dose conversion factor. The value of f was

assumed to be 8.73 mGy/R based on the definition (ICRU 1980) of the roentgen (2.58×10-4 C/Kg), and the reported value (ICRU 1979) of the average energy (33.85 J/C) required to create an ion pair in air.

As could be noted in Figure 5.4, the dosed TLDs were exposed with their major planar surfaces perpendicular to the X-ray beam while they were not oriented in this way during CT scan. Earlier reports (Shope et al. 1982) assumed that no correction is required for variation in TLD response as a function of orientation. Nevertheless measurements were carried out to compare the TLD response as a function of orientation with respect to the direction of the incident X-ray beams during a CT scan. Our measurements indicated that an approximate correction (1.08) must be applied to the response of the TLDs, to account for variation in TLD response resulting from its different orientation to the direction of the X-ray beam during our calibration procedure and the CT scanning.

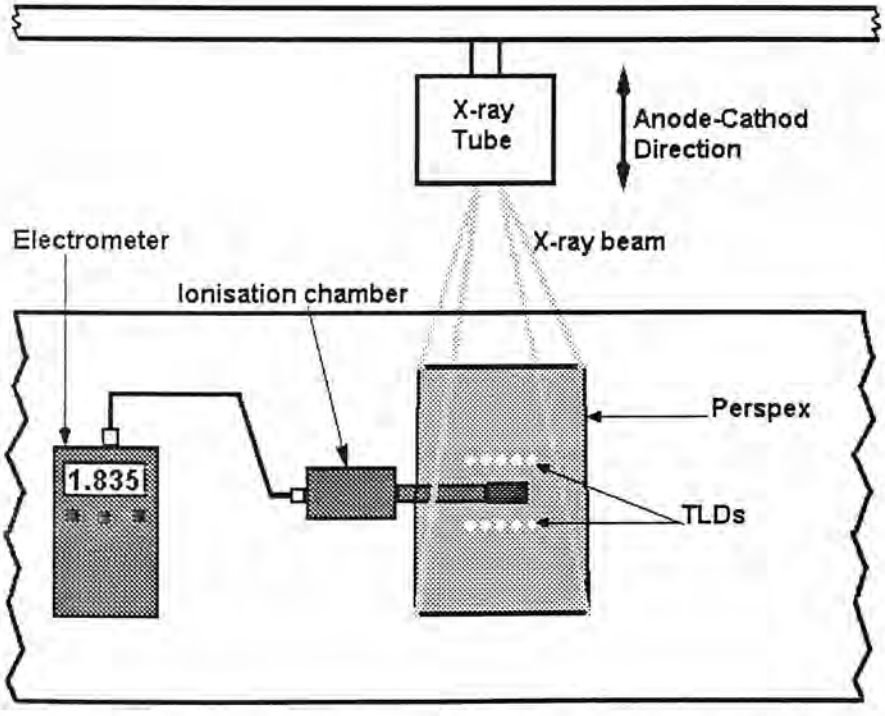

Figure 5.4: Schematic drawing of the set up of TLDs, a traceable ionisation chamber, and the X-ray unit for a calibration measurement.

5.3.3 Uncertainties in the TLD Measurements

Over the whole period of the study 35 sets of calibration measurement were carried out. This provided 35 data sets each one comprising ten dosed and ten control TLD measurements. These data sets were used to determine the uncertainties involved with the use of TLDs for CT dose measurement in our study.

The level of uncertainties for every data set was calculated for the 95% level of confidence in terms of the standard error resulting from both the dosed and the control TLD measurements. Figure 5.5 shows the variation of the calculated TLD calibration factor (CF_{TLD}) over the whole period of the study, with the level of uncertainties for every data set.

This variation in calculated CF_{TLD} is due to some systematic errors involved in the process of the TLD calibration measurement. There were some factors over which we had neither control nor information on their level of uncertainties. These could be taken to be responsible for the observed variation in CF_{TLD} values. For example, there were uncertainties in the consistency and accuracy of the calibration factor of the traceable ionisation chamber and the TLD reader readout.

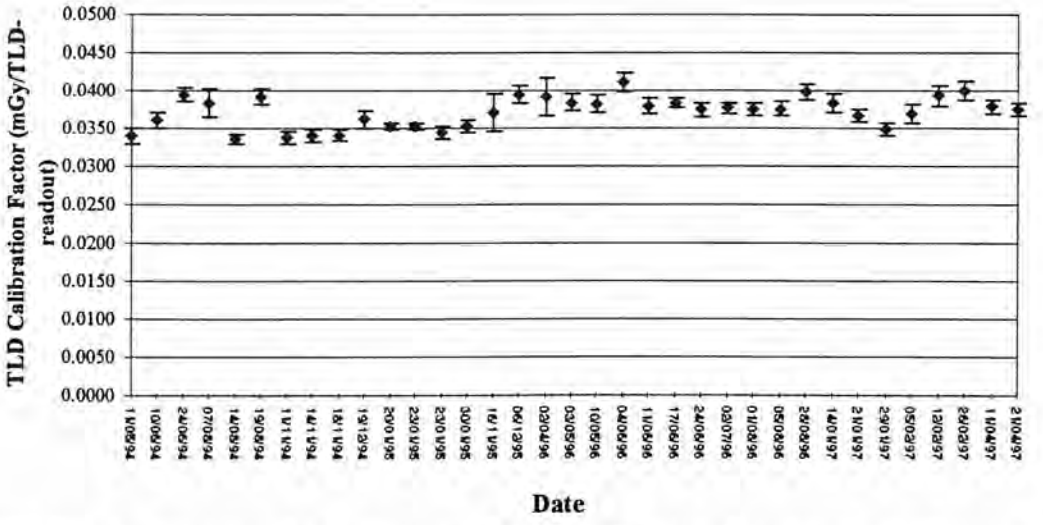

Figure 5.5. The variation of the calculated TLD calibration factor over the period of the study. The error bars represent "2×standard deviation" of each calibration data set.

A systematic uncertainty raised from the processing procedure of the TLDs in the TLD reader was detected and avoided in this study. For about 1-2% of all

readings, unexpectedly low values were observed. It was concluded that this systematic uncertainty is caused by the poor contact between either the TLDs and the trays or the trays and the heater compartment of the TLD reader.

The bigger error bars may have been noted for three calibration data sets in the above figure. These are due to the above systematic error. The highest observed level of uncertainties is estimated to be about 10.8% at the 95% confidence level for an individual TLD calibration measurement if the identified systematic error is ignored. But, if this systematic error is excluded, the highest observed uncertainty is estimated to be about 5.4% for an individual calibration measurement.

The overall uncertainties in the TLD measurements could be estimated by further analysis of the calibration data sets. For every calibration data set a weighted coefficient variation (CV) could be calculated from the CV values of the dosed and control TLDs. Then, if the root mean square of all the weighted CVs is taken, it will indicate that there is an overall 4.8% uncertainty in the TLD processing procedure.

The point doses could have been determined using only one TLD measurement at every location of interest in the phantom. But, in order to exclude the above identified systematic uncertainty, a pair of TLDs was used for every single point dose measurement in the phantom. The average value of the pair of TLDs was taken to represent the single point dose at every location of interest in the phantom. However, if one TLD read more than 10% of the second, then it was concluded that the systematic error had occurred and the higher reading was chosen to represent the point dose value.

Based on the overall estimated uncertainty in the TLD measurements, the level of uncertainties in the measurements of point doses in the phantom is estimated to be about 6.8% at the 95% confidence level.

5.3.4 Other Technical Considerations with the Use of the TLDs

To measure the central axis dose values, a hole was drilled at the centre of each section of the Rando phantom to host the pair of TLDs. It was necessary to accommodate the TLD round chips in the middle of these holes. This was made possible by using a pair of plastic rods with 5 mm diameter. The TLDs were kept

between the pair of rods in every hole. The length of the pair of rods, including the pair of TLDs, was long enough to encompass the whole thickness of an individual section of the phantom (25mm). In addition, plastic rods with 25 mm length were used in the phantom to fill any hole not used for dosimetry to maintain a nearly homogenous phantom.

The type of TLDs used in this study were quite fragile. To avoid the TLDs from being cracked during the loading and unloading process, the holes were drilled with a few tenths of millimetres larger diameter than that of the TLDs and plastic rods.

5.4 The Absorbed Dose Corrections

As mentioned in the second section a preliminary study was carried out to investigate other dosimetric aspects specific to CT. Other dosimetric aspects, specific to CT, which needed to be examined were the X-ray spectra of the CT scanners and the ratios of mass energy absorption coefficients for different organs and tissues of the body to that of air.

As mentioned in the previous section, the calibration factor of the TLDs was determined in exposure (roentgen) and converted to absorbed dose in air (mGy) using the conversion factor determined from the ICRP (1977, 1980) reports. But, it was needed to determine absorbed doses in different organs or tissues of the body composed of materials other than air. The quantity that could be used for this purpose is the mass energy absorption coefficient (μ_{en}/ρ). μ_{en}/ρ is a measure of the average fractional amount of incident photon energy transferred to kinetic energy of charged particles as a result of interactions between these photons and matter that occur in a given mass-per-unit area thickness of material concerned. The energy absorbed per unit mass of various materials subjected to the same energy fluence is proportional to the mass energy absorption coefficients of those materials. So having the absorbed dose in air (D_{air}), the absorbed dose in other materials (D_m) could be derived from the following equation.

$$D_m = D_{air} \times \frac{(\mu_{en}/\rho)_m}{(\mu_{en}/\rho)_{air}} \qquad \text{(Equation 5.2)}$$

Therefore, to estimate absorbed doses in the organs and tissues of interest, it was necessary to determine the ratios of mass energy absorption coefficient of organs and tissues of interest to that of air.

For materials with atomic number close to that of air the factor $(\mu_{en}/\rho)_m/(\mu_{en}/\rho)_{air}$ varies only slowly with photon energy. But, for materials of higher atomic number, such as bone or those with a high hydrogen content, this rule does not apply and the ratio of the mass energy absorption coefficients should be calculated based on the photon energy distribution of the X-ray. Therefore, it was required to take into account the CT scanners' output photon energy distribution that, like any other X-ray generator, is a spectrum. Hence, in order to calculate the ratios of $(\mu_{en}/\rho)_m/(\mu_{en}/\rho)_{air}$ for different models of CT scanners, we had to determine the CT scanners' X-ray spectra first.

In addition, as mentioned earlier, to determine organ or tissue doses, using the common direct CT dosimetry approach, numerous point dose measurements are required. To overcome this cumbersome task and make this dosimetry approach simpler and more practical, it was necessary to decrease the number of these measurements. Hence, we also studied dose distributions inside and outside the scan volume for different CT scanners in this study.

In this section the above concepts will be explained in detail and our proposals will be introduced. First the CT X-ray spectra will be discussed. Then the calculated ratios of mass energy absorption coefficients will be introduced.

5.4.1 CT X-ray Spectra

As mentioned above to take into account the ratios of μ_{en}/ρ for different organs and tissues of the body to that of air, it was required to determine the X-ray spectra for all CT scanners in this study. CT X-ray spectrum comprises X-rays varying in photon energy from lower energies near to zero of up to the maximum energy attained by electrons from the applied voltage across the tube. The unwanted

lower energy X-rays are normally removed by added filters. The shape of the CT X-ray spectrum, or the CT photon energy distribution, is dependent on the tube target material, the anode angle, the filtration, and finally the applied potential (kV) across the tube.

Lately, an electronic version of the IPEM Report 78 prepared by D. Sutton (Cranley et al. 1997), that is a spectrum processor software, became available to us. This software could be used to generate the X-ray spectrum if the required input data is provided. The required input data includes the applied potential (kV), the target material, the anode angle and the tube filtration. Table 5.1 shows these data for all the CT scanners in this study. These data were obtained by referring to the available CT scanners' manuals provided by the manufacturers.

Table 5.1: Different radiological factors used for determining the CT X-ray spectra.

CT Scanner Model	Tube voltage (kV)	Target material	Anode angle (degree)	Filtration (mm)
Siemens Somatom Plus	120 & 137 *	Tungsten	10	2.7 Al
Philips Tomoscan CX/S	120	Tungsten	9	1.0 Al & 0.1 Cu
GE HiSpeed Advantage	120*	Tungsten	7	2.7 Al
GE Sytec 3000 Plus	120	Tungsten	9	2.7 Al
GE 9000HP	120	Tungsten	9	2.7 Al
GE 8800	120	Tungsten	9	2.7 Al

*Other kVs were also available with these scanners but only the mentioned settings were routinely used.

Using data mentioned in Table 5.1, as the input data for the above software, the X-ray photon spectra for all the CT scanners were determined at 0.5 Kev intervals. Figure 5.6 shows a typical X-ray spectrum determined for one of the CT scanners in this study. The CT X-ray spectral data were then used to determine the ratios of mass energy absorption coefficients of body tissues to that of air for every CT scanner as explained in the following section.

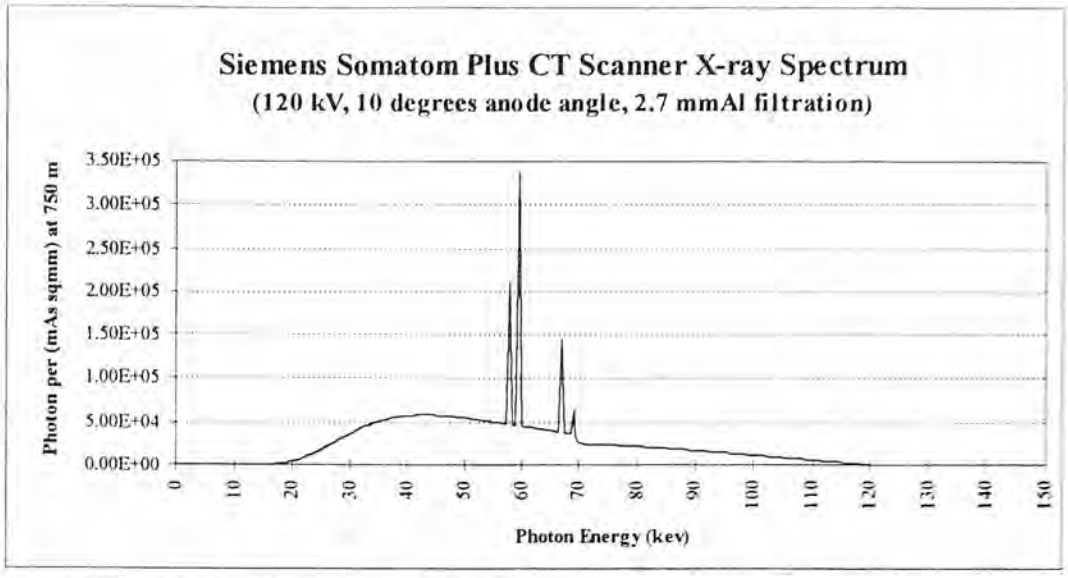

Figure 5.6: A typical CT X-ray spectrum.

5.4.2 Mass Energy Absorption Coefficient

In order to calculate μ_{en}/ρ values it was first required to determine the compositions of all organs and tissues of interest. For this purpose reference was made to the ICRP publication 23 (1975). It was noted that the contribution of major elements in various organs or tissues compositions, except bone and red bone marrow, were very close to each other. Therefore, the μ_{en}/ρ values were determined for dry air and three tissue categories of bone, red bone marrow and muscle. The latter represented all various organs and tissues of interest of the body except bone and red bone marrow.

The μ_{en}/ρ values for these categories were taken from the ICRU (1992) tables of photon mass energy absorption coefficients for all the photon energy ranges existed in the CT X-ray spectra. Having determined the X-ray spectrum for every CT scanner as explained in the previous section, the sum of the amount of photons at each energy interval was calculated from the X-ray spectrum of that scanner. Then for each category the μ_{en}/ρ value at each energy range interval was weighted by the relevant sum of the amount of photons at that energy interval for every CT scanner. Then for each category the integral of the weighted μ_{en}/ρ values was taken over the entire energy range of every CT X-ray spectrum, to represent the μ_{en}/ρ value of that

category for that particular scanner. Figure 5.7 shows the variation of weighted μ_{en}/ρ for the three tissue categories and dry air for two different CT models by photon energy.

The following equation shows the way the μ_{en}/ρ values were calculated:

$$\left(\frac{\mu en}{\rho}\right)_{(\text{tissue, air})} = \int_{e\,\min}^{e\,\max} \left(\frac{\mu en}{\rho}\right)_E . \frac{d\varphi}{\varphi} \qquad \text{(Equation 5.3)}$$

where $(\mu_{en}/\rho)_E$ is the mass energy absorption coefficient at E energy level of the tissue or air, $d\varphi$ is the amount of photons at E energy level, φ is the sum of photons over the entire energy range, and e_{min} and e_{max} are the integral lower and upper limits determined from the relevant CT X-ray spectrum for every CT scanner.

The μ_{en}/ρ calculations were carried out for the above three tissue categories representing all organs and tissues of interest of the body and dry air. This was done for every CT scanner model, based on its calculated X-ray spectrum derived from its relevant setting of parameters as was already mentioned in Table 5.1.

The ratios of the mass energy absorption coefficient (μ_{en}/ρ) to dry air for bone, red bone marrow and muscle (representing all other body organs and tissues) were calculated for each CT model (Table 5.2). Then these data were incorporated in a spreadsheet designed for CT dose assessment, using the Microsoft® Excel program as explained in section 5.7.

Table 5.2: The ratios of the μ_{en} (tissue/air) for different types of CT scanners.

Tissue categories	**CT Scanner**				
	GE HiSpeed Advantage	GE Sytec, GE 8800, & GE 9000HP	Philips Tomoscan (CX/S)	Siemens Somatom Plus (120 kV)	Siemens Somatom Plus (137 kV)
Muscle	1.06	1.06	1.06	1.06	1.06
Cortical bone	5.96	5.95	5.65	6.01	5.78
Red bone marrow	0.91	0.91	0.92	0.90	0.92

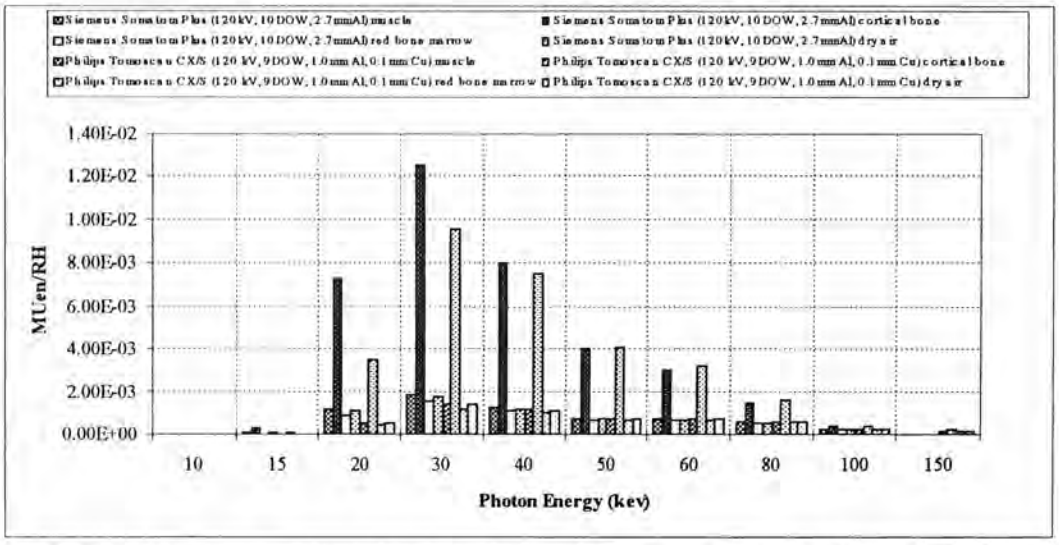

Figure 5.7: Variation of (weighted) μ_{en}/ρ by photon energy for different body tissues and air for two different CT scanners.

5.5 Dose Measurement Methods

Based on the assumptions described section 5.2, dose distributions had to be determined and analysed in the representative sections of the head, chest and abdomen & pelvis areas of the phantom for all the CT scanners. This was necessary to cut down numerous point dose measurements required for the common direct CT dosimetry approach and to simplify the developed dosimetry approach in a way that it could be carried out easily for routine patient dose assessments. Extra dose measurements were also required to validate the accuracy of the method adopted for the dose distribution calculations in the representative sections. Measurements were also required in some of the parallel sections in the overlap region between the chest and abdomen areas of the phantom to validate the assumption made above for dose distributions in these sections.

In this section the results of our study on dose distributions inside and outside the scan volume for all the CT scanners are presented. In this regard the method adopted for determining the dose distributions inside and outside the scan volume are explained and typical dose distributions calculated for one of the CT scanners is presented. In addition, the concept of "central axis doses" from which the organs

doses and the other dose indices are derived by the developed direct CT dosimetry approach will be introduced and explained. The concept of packing factor used for some special CT examination techniques will also be presented. The results of the measurements carried out to validate the accuracy of the calculated dose distributions and the assumptions made above with regards to the dose distributions in parallel sections will be presented in section 5.6.

5.5.1 Dose Distributions inside the Scan Volume

For each scanner in the study an axial dose distribution was determined in representative sections of the phantom at three levels of the body: the "head", the "chest", and the "abdomen" for a full CT scan which included that section. these regions comprised sections 0-9. 10-19, and 20-34 of the phantom respectively. Dose distributions in section 2, 14, and 26 were chosen to be representative of these regions. It was assumed that the dose distribution in the other sections of each of the regions were represented by these sections. This was done based on one of the assumptions made above that, "inside the scan volume, the dose distribution normalised to the scanners' isocentre are identical in parallel sections in these three relatively homogenous regions of the body".

To determine the dose distributions in the three representative sections of the phantom, TLDs were put at 2 cm intervals along two perpendicular axes, crossing each other at the centre of the section as shown in Figure 5.8 for a typical one.

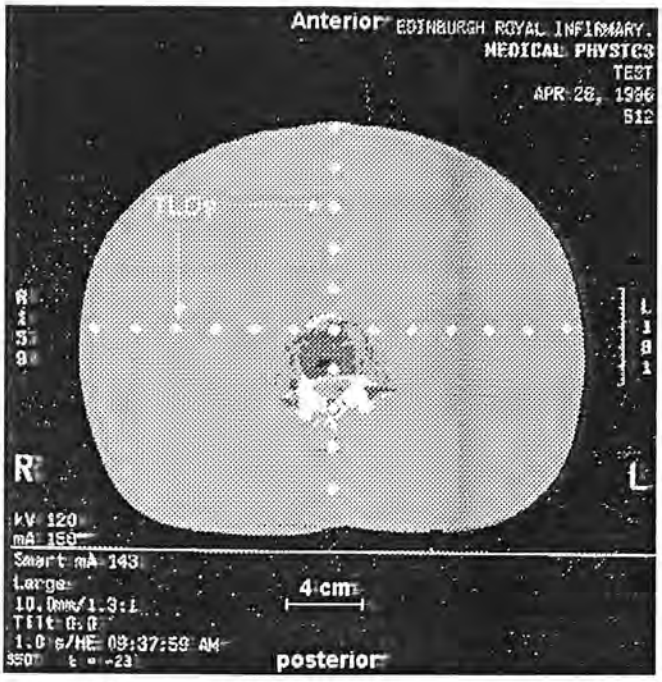

Figure 5.8: A typical section of the phantom showing the way the TLDs were put in the section for dose distribution measurements.

The measured TLD values along these orthogonal axes were normalised to the central values of the section. Using the result of these measurements and an available computer graphic program (UNIMAP[3]), the dose values were interpolated for a 2cm×2cm grid covering the extreme limits of these three regions of the body.

Figure 5.9, Figure 5.10, and Figure 5.11 show three typical dose distributions in the three representative sections of the phantom for one of the CT scanners.

Based on these dose distributions, a parameter, named dose factor, was determined for all organs and tissues of interest in every section of the phantom for each scanner. The dose factor represents the average dose to the organ within the specific section normalised to the central dose. Whenever an organ or tissue had a considerable large size in a section, enough locations were selected, to reflect the variation of dose distribution over the entire portion of the organ or tissue in the dose factor.

Details of all the organ dose factors are presented in a long table in Appendix B. The table includes all organs and tissues of interest, the location of point doses

---

[3] **UNIMAP, Interactive Mapping System, Copyright © 1985 by European Software Contractors A/S. 7, Nørregade, DK-28000 Lyngby, Denmark.**

being considered for each organ in every section of the phantom, and their calculated point and average dose factors for all the CT scanners.

These dose factors were then incorporated in the customised spreadsheet designed for the CT dose assessment, using the Microsoft Excel® computer program as explained in section 5.7.

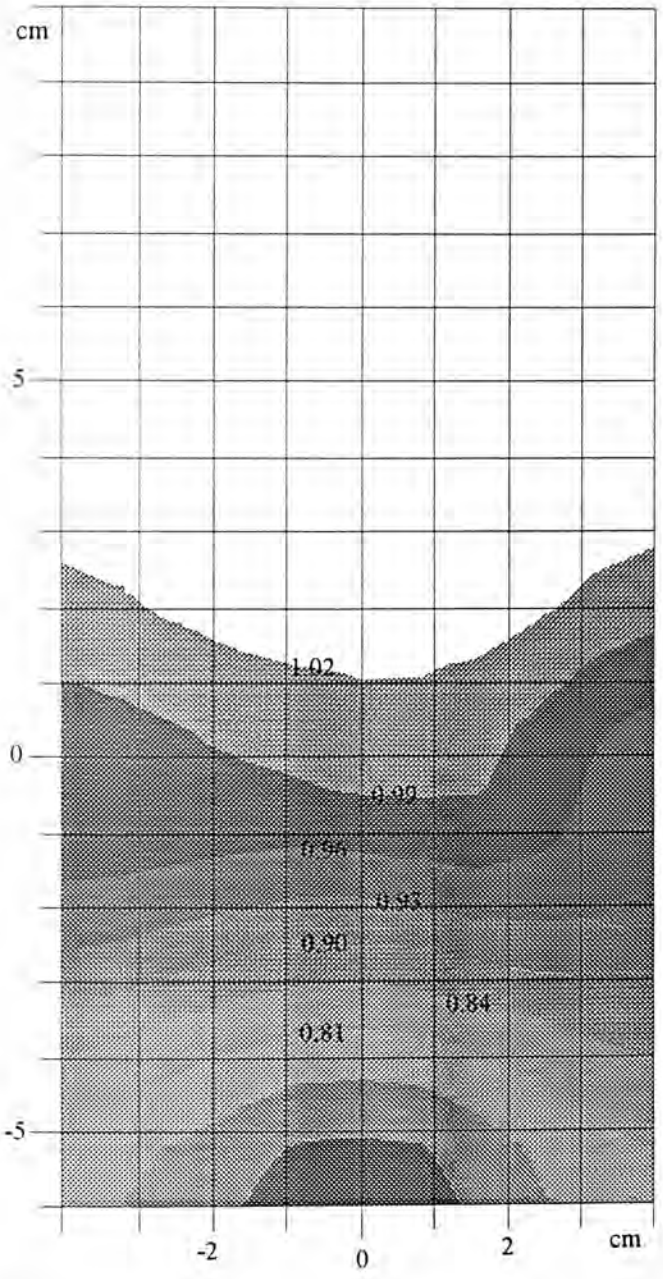

Figure 5.9: A typical dose distribution in the head area of the Rando phantom (section 2, GE HiSpeed Advantage CT scanner).

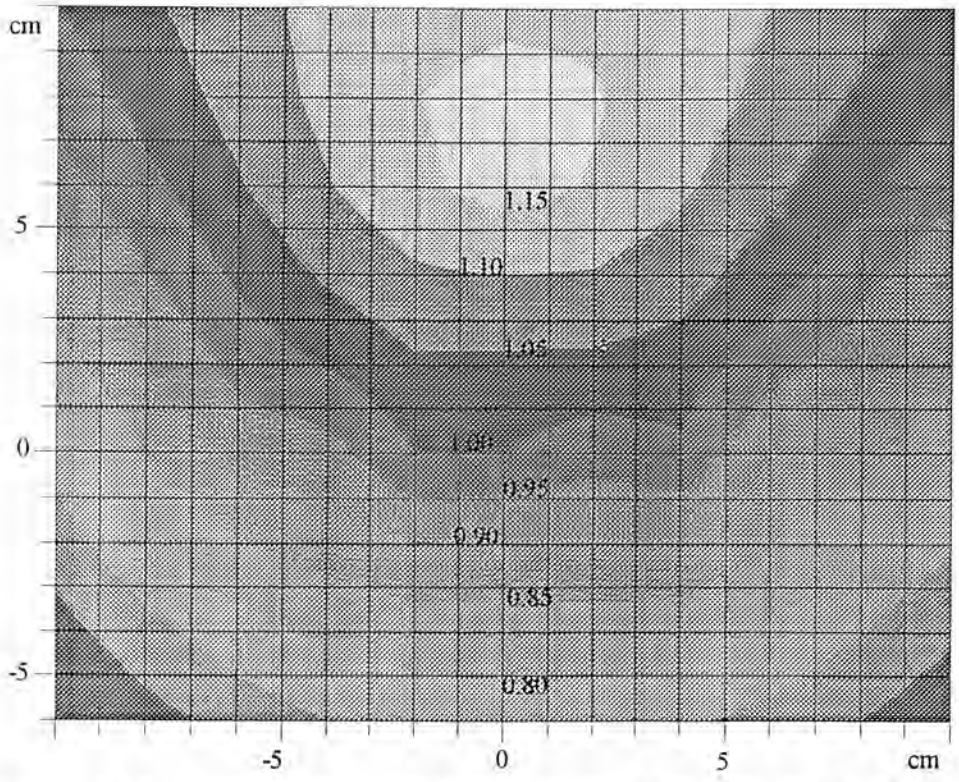

Figure 5.10: A typical dose distribution in the chest area of the Rando phantom (section 14, GE HiSpeed Advantage CT scanner).

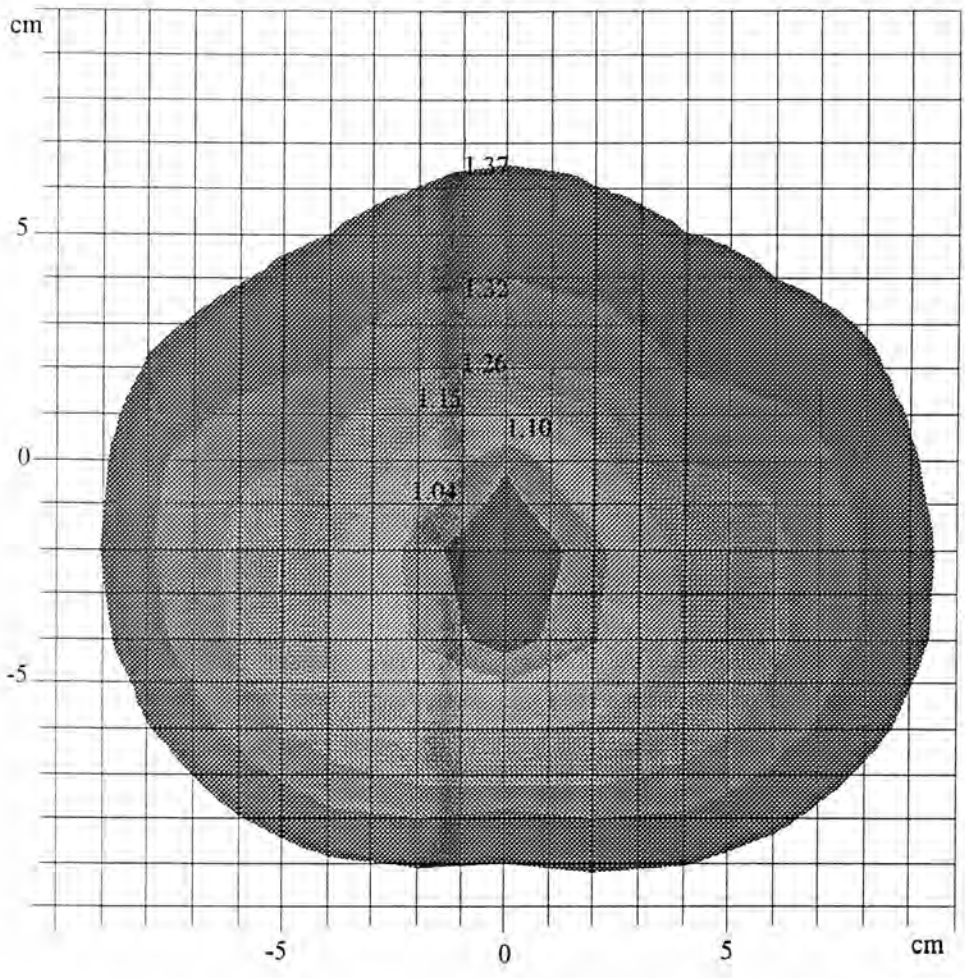

Figure 5.11: A typical dose distribution in the abdomen area of the Rando phantom (section 26, GE HiSpeed Advantage CT scanner).

5.5.2 Dose Distribution and Fall Off of the Dose outside the Scan Volume

Besides the dose distribution inside the scan volume, dose distribution and fall off of the dose outside the scan volume were studied. These studies showed a negligible variation in dose distribution within these sections and an exponential reduction in the dose with the distance from the edge of the scan volume. This provided a sufficiently accurate method for dose estimation outside the scan volume requiring just a few TLD measurements. Based on the experimental results the following formula was used to estimate the radiation dose in those sections of the phantom that fall outside the scan volume.

$D_n = D_r e^{-kx}$ (Equation 5.4)

where D_n is the central axis dose in section "n", D_r is the central axis dose in the reference (r) section located at that edge of the scan volume, x is the distance (in cm) between section "n" and section "r", and finally "k" is a constant derived from a measurement made at 10 cm distance (four sections away) from the edge of the scan volume as presented in the following equation:

$$k = \ln\left(\frac{D_r}{D_{r+10}}\right)/10 \qquad \text{(Equation 5.5)}$$

Equation 5.4 was employed for various examination protocols using all the various CT models. It provided a good approximation for estimating the fall off of the dose outside the scan volume, requiring just one extra central axis dose measurement. Figure 5.13, Figure 5.13, and Figure 5.14 show typical comparisons between the measured values of the central axis doses in sections outside the scan volume and our calculated values using the above equations for three particular "head", "chest" and "abdomen & pelvis" examinations using the Siemens Somatom Plus CT scanner.

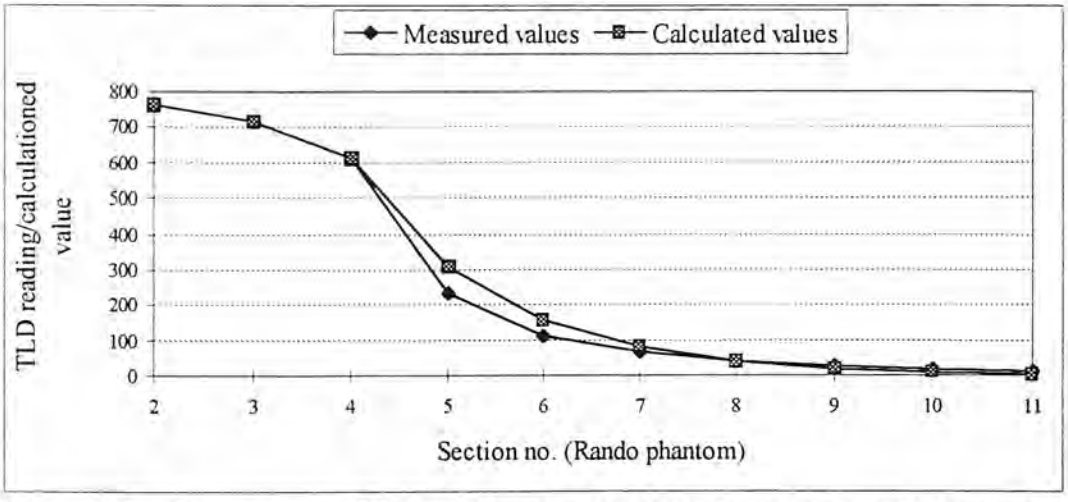

Figure 5.12: Comparison of measured and calculated phantom central dose values outside the scan volume for seven sections (5-11) for a particular "head" examination.

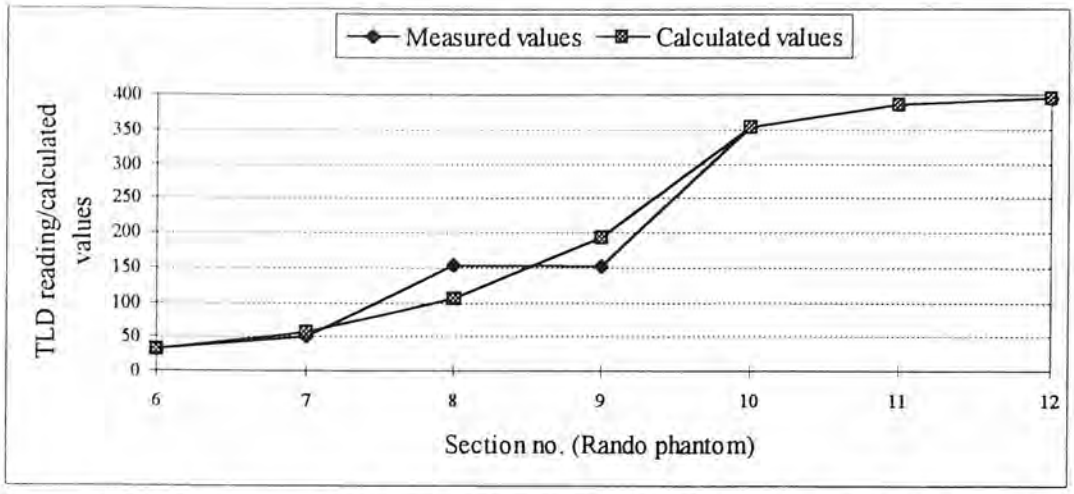

Figure 5.13: Comparison of measured and calculated phantom central dose values outside the scan volume for five sections (6-10) for a particular "chest" examination.

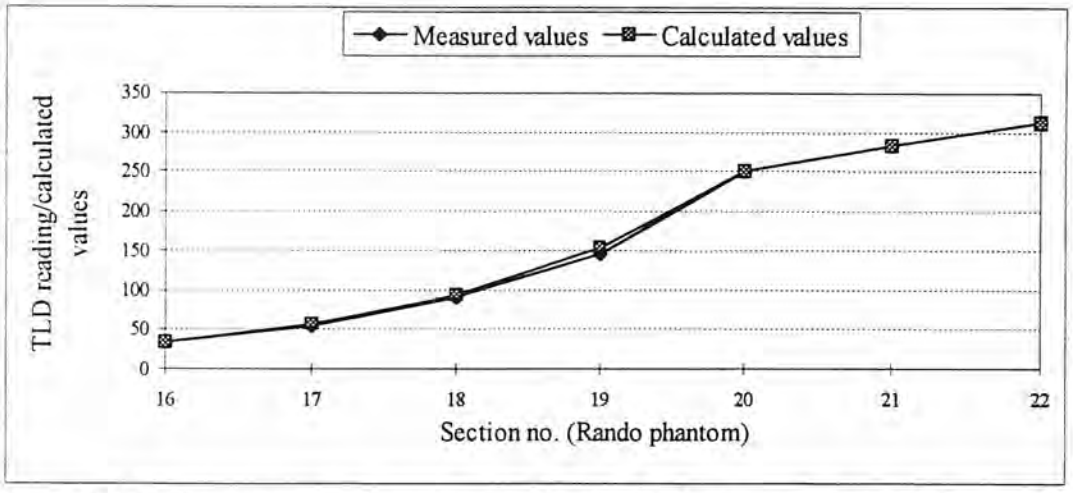

Figure 5.14: Comparison of measured and calculated phantom central dose values outside the scan volume for five sections (16-20) for a particular "abdomen & pelvis" examination.

5.5.3 Central Axis Dose Measurements

Knowledge of the pattern of dose distributions inside and outside the scan volume of the phantom facilitates the direct CT dosimetry approach by limiting the required measurements to only several central axis dose measurements. The exact number of the required measurements depends on the length of the scan volume. At least one central axis dose measurement is required in every section of the phantom

located inside the scan volume. In addition, two extra central axis dose measurements are required outside the scan volume to estimate the fall off of the dose if there are two tails for a particular CT examination. Otherwise, if there is only one tail outside the scan volume, like most routine head and pelvis CT examinations, one extra measurement outside the scan volume will be sufficient.

Based on the justification made in section 5.3.3, to eliminate the identified systematic uncertainties from the point dose measurements, a pair of TLDs was used to determine the central axis dose values for each section of the phantom inside the scan volume. The pair of TLDs were put in the centre of each section of the Rando phantom. The TLDs' average value was taken to represent the central axis dose value in the section if the difference between their readouts was not greater than 10%. Otherwise, the TLD which showed the highest value was chosen to represent the central axis dose value in that section of the phantom.

As mentioned in section 5.5, when the dose distributions were determined inside the scan volume, they were normalised to the central axis dose values for every representative section. Therefore, the measured central axis dose values in every section of the Rando phantom inside the scan volume can be used as an index to estimate the value of doses at any desired location in these sections. We called this index the **phantom central dose** for our developed direct CT dosimetry method. Hence, if the phantom central dose is combined with the relevant normalised dose distribution inside the scan volume, the radiation doses received at the location of all organs and tissues of interest from CT examinations could easily be estimated. The way this is carried out has been explained in section 5.7 where the designed computer spreadsheet program for our developed direct dosimetry method has been described.

5.5.4 Packing Factor

The developed direct dosimetry method was designed for contiguous conventional CT examinations, or in the case of spiral CT examinations for the pitch value of one. However, other scan protocols are quite common in CT practice in which the conventional scans are not performed contiguously or the pitch value of the spiral scans is not equal to one. For these types of examinations a packing factor

should be applied to the measured values of the phantom central doses (TLD readings) with contiguous condition (or with the pitch value of one if a spiral scan is performed). Then the resultant values should be regarded as the phantom central dose values to be entered in the computer spreadsheet program.

The packing factor, p, is given by the following expression:

$$p = \frac{w}{c} \qquad \text{(Equation 5.6)}$$

where w is the slice width (in mm) and c is equal to the couch increment (in mm) if a conventional scan is performed. For spiral scans p is the inverse of pitch. It is obvious that we will have:

- $p=1$: for contiguous conventional examinations (when the slice width is equal to the couch increment), or for spiral examinations with the pitch value of 1.
- $p>1$: for overlapping conventional examinations (when the couch increment is less than slice width) or for spiral examinations with the pitch value of less than 1.
- $p<1$: for the conditions where there is a gap between slices in a conventional scan (i.e. couch increment is more than slice width) or for spiral examinations with the pitch value of more than 1.

This constraint is due to the fact that the TLDs used in this study did not have such a size to encompass the entire thickness (25 mm) of the sections of the Rando phantom. Therefore, if scans with a couch increment bigger than the slice width or spiral scans with a pitch value more than one were carried out, the TLDs in some sections would fall in the gaps between consecutive scans and lead to an underestimation of the central dose values. In addition, if scans with a couch increment less than the slice width or spiral scans with a pitch value less than one were considered, the TLDs in some sections may fall in the overlaps between consecutive scans and lead to an overestimation of the central dose values. Applying the above packing factor to the contiguous conventional scans (or spiral scans with the pitch of one) provides a good approximation of the average central dose values for these scanning techniques.

5.6 Validations of Dose Distributions

The methods described in section 5.5 were used to determine patient doses from six CT scanners and the results are presented in chapter 6. Following these studies some further investigations were made to validate some of the assumptions in the assessment of effective dose.

Three assumptions were made in this study with regard to dose distributions. Firstly that the dose distribution in a section of the phantom can be adequately derived from measurements of the dose profile on two orthogonal axes using a contour mapping system. Secondly that the dose distributions in representative sections of the phantom can be used with sufficient accuracy to represent the dose distribution in parallel sections in the same anatomical region. Thirdly that the dose distributions in sections outside the scan volume are uniform.

5.6.1 Representative Sections

To validate the method employed in this study for determining the dose distributions in the three representative sections of the Rando phantom, these sections were drilled on a 2 cm by 2 cm rectangular grid. Locations within 1 cm of the surface or within bone were omitted. Points were also omitted from the regions near the edge of the phantom, particularly in the chest sections, where no organs of interest were located. A total of 34, 69, and 89 locations were used in the representative sections of the "head" (no. 2), "chest" (no. 14), and "abdomen & pelvis" (no. 26) respectively.

To estimate the relative dose received at every position, a pair of TLDs was used. It was noted previously that intermittent low readings were experienced with the TLD reader. When the readings from one TLD in a pair was 10% less than the other, then the higher value was used. Otherwise an average was taken.

Three complete routine "head", "chest" and "abdomen & pelvis" examinations were carried out separately using the Siemens Somatom Plus CT scanner covering the three representative sections in these areas of the phantom. For every examination the average value of 10 unirradiated TLDs was taken as the background reading. The background was subtracted from the average measured reading at each position. Then

for each representative section all the values were normalised to the central position of the section.

The ratios of the measured to the calculated normalised values were calculated for all the positions in the three representative sections of the Rando phantom. The calculated values were derived from the original three sets of orthogonal dose measurements in the representative sections which were made with the UNIMAP program to obtain the dose distributions from which the doses in chapter 6 were derived. It may be noted that the dose contour maps showed values bigger than one for the isocentre locations to which data were normalised. This may be due to the limitation of the interpolation approach used by the UNIMAP program. When calculations were made in these distributions, the central doses were set to the TLD readings.

The following scan protocols were used: "head" (sections 1-4), 120 kV, 420 mAs, 10 mm slice width, 10 mm slice increment, 10 slices; "chest" (sections 10-19), 137 kV, 210 mAs, 10 mm slice width, 10 mm slice increment, 27 slices; "abdomen & pelvis" (sections 20-34), 120 kV, 210 mAs, 10 mm slice width, 10 mm slice increment, 38 slices.

Table 5.3 shows the average ratios of the measured to calculated normalised doses in the three representative sections along with the standard deviation (s.d.), minimum and maximum values resulting from the above scan protocols.

Table 5.3: The average ratio of the measured to the calculated normalised doses in the three representative sections of the Rando phantom.

CT examination	head	chest	abdomen & pelvis
no. of positions	34	69	89
average	1.03	1.05	1.02
standard deviation	0.04	0.05	0.07
minimum	0.94	0.93	0.87
maximum	1.09	1.16	1.22

As mentioned earlier there is an overall 5% uncertainty (s.d.) in the TLD measurement. Therefore the expected uncertainty in the paired TLD measurements will be $\pm$ 7% at the 95% confidence level. When the ratios of the dose at each position were calculated, the TLD values were normalised to the central values. Hence the

expected uncertainty in the calculation of the ratios will be ± 10% (equivalent to 5% s.d.).

The measured variance in the results can be mainly attributed to the uncertainties inherent in the TLD readings. However, closer inspection of the result for the "chest" and "abdomen & pelvis", shows that there are positions for which the discrepancy between the measured dose distribution and the calculated distributions differ by more than 10%.

Figure 5.15 shows the calculated dose distributions in the representative section of the "chest" area (section 14). Table 5.4 shows the results of TLD measurements in section 14. The ratios between the measured and calculated values for all the selected positions are shown in Table 5.5. As can be seen in this table the most significant discrepancies are towards the edge of the phantom.

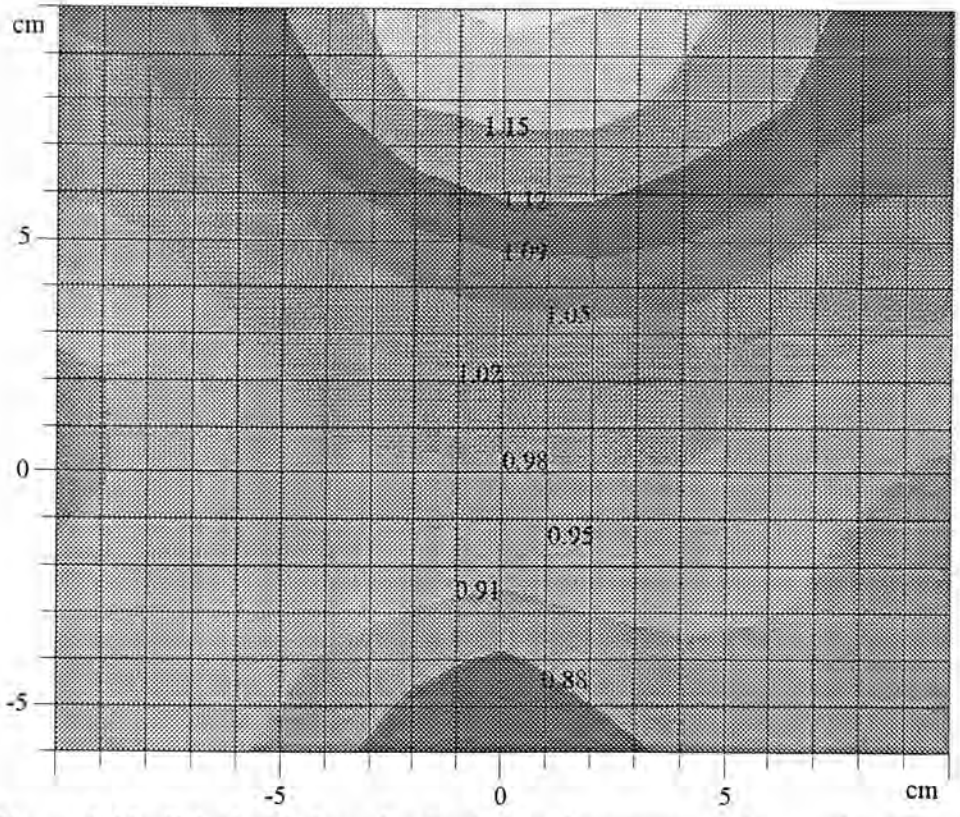

Figure 5.15: Calculated dose distribution in the representative section (no. 14) of the chest area for the Siemens Somatom Plus CT scanner.

Figure 5.15R: Dose distribution in section 14 with the body contour

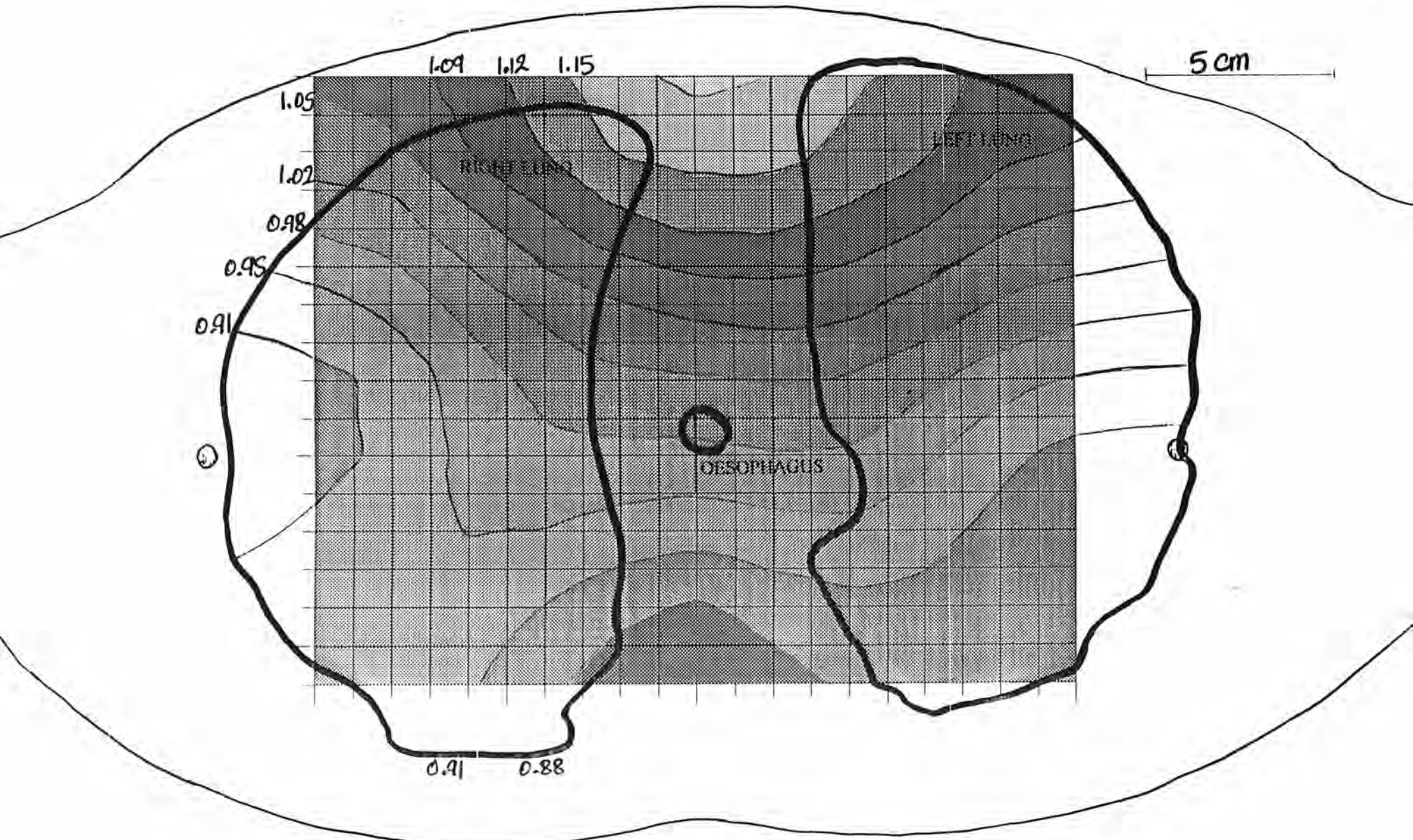

Table 5.4 : Measured TLD values* in the representative section of the "chest" (no. 14).

Vertical position	Horizontal position (cm)																
(cm)	-18	-16	-14	-10	-8	-6	-4	-2	0	2	4	6	8	10	14	16	18
10	-	-	-	-	-	-	-	-	456.08	-	-	-	-	-	-	-	-
8	-	-	-	-	-	-	-	-	-	-	458.44	448.53	414.63	-	-	-	-
6	-	-	-	-	411.32	436.29	419.28	434.59	399.62	-	413.10	450.97	429.95	389.33	-	-	-
4	-	-	-	376.80	375.40	397.52	418.51	-	424.16	-	406.24	428.40	407.61	392.52	-	-	-
2	-	-	-	377.54	376.98	389.31	381.66	-	396.28	-	403.77	421.37	392.62	381.06	-	-	-
0	374.24	366.14	354.05	362.78	388.54	375.42	386.86	387.04	374.66	409.35	373.02	420.85	376.72	385.97	362.23	327.36	369.27
-2	-	-	-	357.94	363.31	391.78	363.62	-	357.28	-	380.39	387.27	395.79	364.25	-	-	-
-4	-	-	-	363.00	375.30	381.13	378.01	-	-	-	394.70	374.62	382.11	370.53	-	-	-
-6	-	-	-	-	359.37	379.59	395.34	-	389.35	-	-	-	359.54	-	-	-	-

* Approximate TLD calibration factor was 0.0370 (mGy).

Table 5.5: Ratios of the normalised measured values to the calculated values in the representative section of the "chest" (no. 14).

Vertical	Horizontal position (cm)																
Position (cm)	-18	-16	-14	-10	-8	-6	-4	-2	0	2	4	6	8	10	14	16	18
10	-	-	-	-	-	-	-	-	1.02	-	-	-	-	-	-	-	-
8	-	-	-	-	-	-	-	-	-	-	1.06	1.04	0.99	-	-	-	-
6	-	-	-		1.08	1.11	1.00	1.04	0.93	-	0.98	1.07	1.05	0.95	-	-	-
4	-	-	-	1.06	1.02	1.04	1.06	-	1.04	-	0.99	1.09	1.04	1.00	-	-	-
2	-	-	-	1.06	1.06	1.06	1.00	-	1.04	-	1.03	1.10	1.03	1.04	-	-	-
0	1.05	1.03	0.99	1.02	1.09	1.02	1.05	1.05	1.00	1.11	1.02	1.15	1.06	1.13	1.06	0.96	1.08
-2	-	-	-	1.01	1.02	1.10	1.02	-	1.00	-	1.07	1.10	1.16	1.07	-	-	-
-4	-	-	-	1.02	1.05	1.07	1.11	-	-	-	1.16	1.10	1.12	1.09	-	-	-
-6	-	-	-		1.01	1.07	1.16	-	1.14	-	-	-	1.05		-	-	-

Figure 5.16 shows the calculated dose distributions in the representative section of the "abdomen & pelvis" area (section 26). Table 5.6 shows the results of TLD measurements in section 26. The ratios between the measured and calculated values for all the selected positions in this section are shown in Table 5.7. In common with the chest section, this table indicates that the largest discrepancies are towards the periphery of the phantom, particularly in the posterior region in which the calculations appear to underestimate the dose.

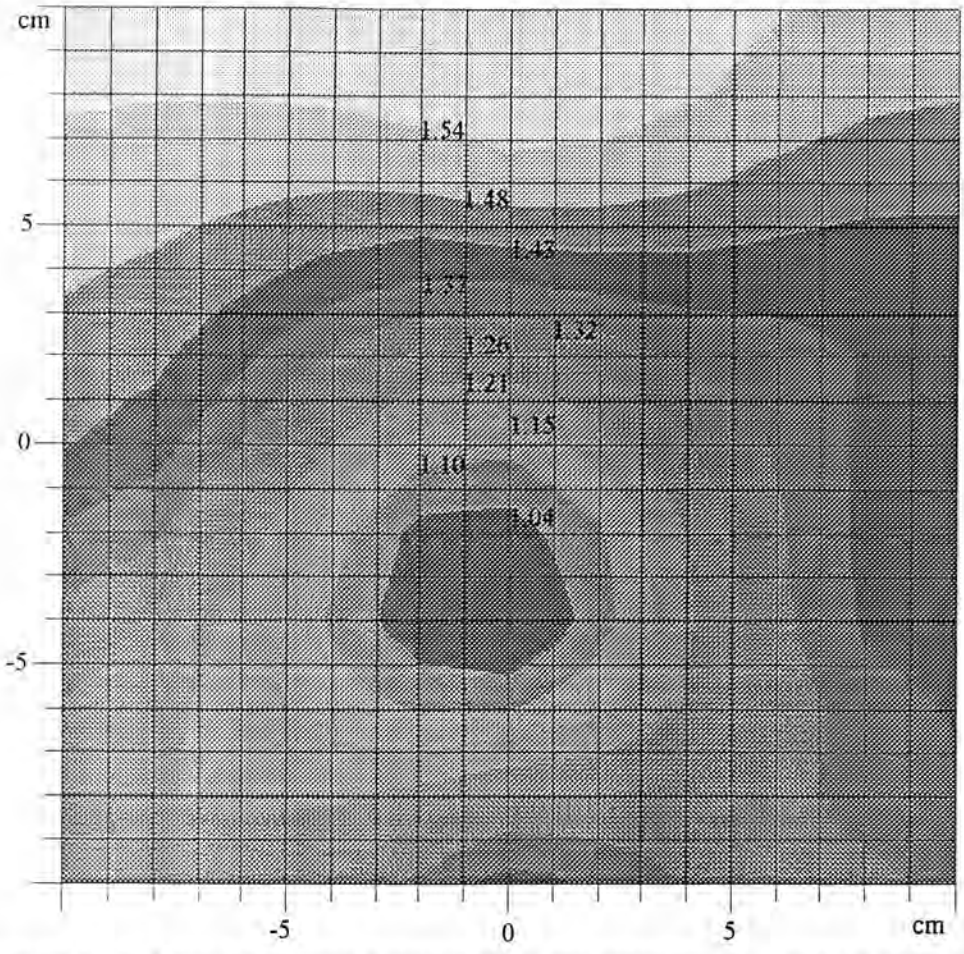

Figure 5.16: Calculated dose distribution in the representative section (no. 26) of the "abdomen & pelvis" area for the Siemens Somatom Plus CT scanner.

Table 5.6: Measured TLD values* in the representative section of the "abdomen & pelvis" (no. 26).

Vertical Position	Horizontal position (cm)												
(cm)	-12	-10	-8	-6	-4	-2	0	2	4	6	8	10	12
10	-	-	-	-	-	-	512.25	-	-	-	-	-	-
8	-	-	-	-	496.79	505.66	517.57	541.23	521.27	504.05	-	-	-
6	-	-	518.80	524.53	496.79	488.22	490.55	484.43	506.74	521.61	549.89	-	-
4	-	533.66	508.91	499.88	466.53	423.94	440.91	442.32	458.64	475.69	475.47	518.62	-
2	-	517.33	473.45	457.82	430.84	413.62	415.65	406.73	428.03	451.22	485.65	499.88	-
0	-	528.01	467.76	431.29	415.49	380.55	333.26	362.38	400.74	448.55	445.82	491.76	-
-2	558.04	496.71	477.88	405.33	411.47	-	-	-	386.04	428.18	450.53	493.66	497.41
-4	-	489.11	434.34	428.29	403.04	-	300.34	-	407.81	439.04	460.42	468.87	-
-6	-	510.64	447.58	451.35	451.64	400.27	-	414.98	434.74	446.94	453.95	472.50	-
-8	-	445.47	428.21	449.44	488.67	435.82	475.13	441.00	475.43	464.76	453.33	436.27	-
-10	-	-	-	-	447.21	-	398.43	-	414.42	-	-	-	-

* Approximate TLD calibration factor was 0.0370 (mGy).

Figure 5.16R: Dose distribution in section 26 with the body contour.

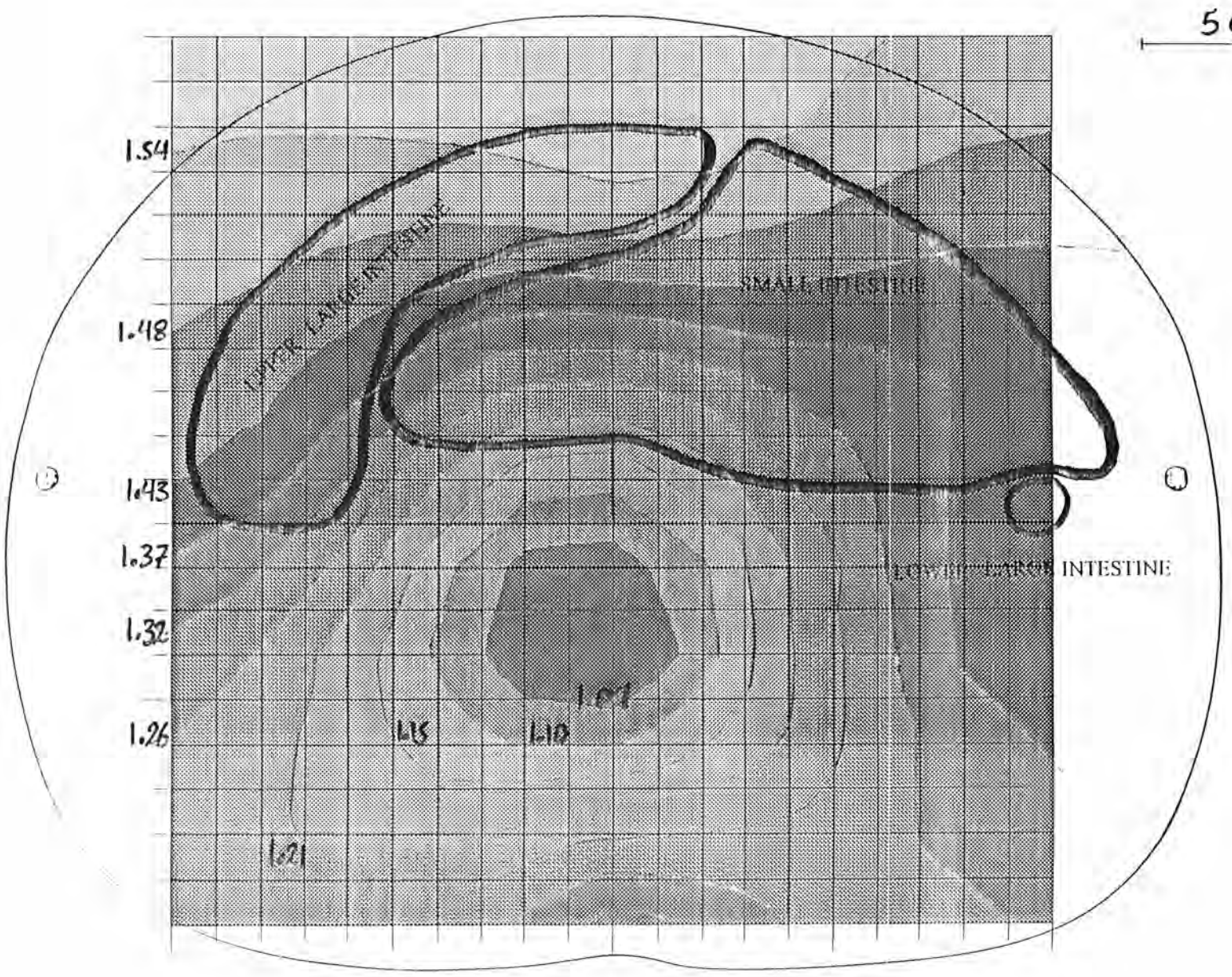

Table 5.7: ratios of the normalised measured values to the calculated values in the representative section of the "abdomen & pelvis" (no. 26).

Vertical position	Horizontal position (cm)												
(cm)	-12	-10	-8	-6	-4	-2	0	2	4	6	8	10	12
10	-	-	-	-	-	-	1.00	-	-	-	-	-	-
8	-	-	-	-	0.97	0.99	1.01	1.05	1.02	0.98	-	-	-
6	-	-	1.01	1.02	0.97	0.95	0.96	0.94	0.99	1.06	1.11	-	-
4	-	1.04	1.03	1.01	0.98	0.89	0.93	0.90	0.96	1.00	1.00	1.09	-
2	-	1.05	0.96	0.96	0.98	0.99	0.99	0.89	0.94	0.99	1.02	1.05	-
0	-	1.11	0.98	0.94	1.03	0.99	1.00	0.90	0.95	1.02	0.94	1.03	-
-2	1.17	1.09	1.05	0.97	1.07	-	-	-	0.96	0.97	0.95	1.04	1.04
-4	-	1.11	1.03	1.06	1.10	-	0.87	-	1.01	1.00	0.97	0.98	-
-6	-	1.22	1.07	1.12	1.18	1.09	-	1.08	1.04	1.02	0.99	1.03	-
-8	-	1.06	1.02	1.11	1.21	1.04	1.13	1.05	1.08	1.06	0.99	0.96	-
-10	-	-	-	-	1.07	-	0.91	-	0.94	-	-	-	-

5.6.2 Parallel Sections

We assumed that the dose distributions are similar in parallel sections to the three representative sections chosen for the "head", "chest" and "abdomen and pelvis" areas of the phantom. To test this assumption in the overlap region between the chest and the abdomen areas, measurements were performed on sections 18, 20, 22, and 24. In this regard around 30 positions were selected in each of these sections arranged in a 4 cm by 4 cm grid. The measuring technique described above was also employed to calculate the normalised dose values at each position for these sections.

"Chest" area

To estimate the level of error caused by the assumption made for dose distributions in parallel sections for "chest" examinations, the ratios between the normalised measured values in section 18 and the calculated values in the representative section of the "chest" were calculated and analysed.

It was assumed that the dose distribution in section 18 was identical to that for section 14. Table 5.8 shows measured TLD results in section 18. The ratios of the normalised measured dose values in section 18 to the calculated dose values in the representative section of the chest (no. 14) are shown in Table 5.9. Overall, the average ratio of the measured values in section 18 to the calculated values in section 14 for the 30 positions was 1.25 with an s.d. of 13% s.d. and a range of 1.00-1.68.

Table 5.8: Measured TLD values* in section 18 for the "chest" examination.

Vertical Position	Horizontal position (cm)						
(cm)	-12	-8	-4	0	4	8	12
12	-	-	-	450.17	-	-	-
8	-	439.41	444.71	425.84	423.47	595.38	-
4	361.97	424.44	371.71	359.92	370.69	400.31	408.65
0	381.55	379.86	350.92	317.46	361.32	394.00	393.28
-4	366.17	373.26	354.53	-	347.30	371.01	365.70
-8	402.21	-	386.30	386.52	394.77	-	401.02

* Approximate TLD calibration factor was 0.0370 (mGy).

Table 5.9: Ratios of the normalised measured values in section 18 to the calculated values in the representative section of the "chest" (no. 14) for the "chest" examination.

Vertical position	Horizontal position (cm)						
(cm)	-12	-8	-4	0	4	8	12
12	-	-	-	1.19	-	-	-
8	-	1.32	1.25	1.13	1.16	1.67	-
4	1.20	1.36	1.12	1.04	1.07	1.20	1.31
0	1.27	1.26	1.13	1.00	1.16	1.31	1.36
-4	1.21	1.24	1.23	-	1.20	1.28	1.27
-8	1.33	-	1.34	1.38	1.37	-	1.39

The likely reason for the increased heterogeneity in dose for this section is that in the lower region of the chest, the cross sectional area of the lungs is reduced. This is liable to result in a greater dose heterogeneity in this section than is represented by the dose distribution in section 14 (Figure 5.15).

The main organs of interests which contribute significantly to effective dose and are located in the scan volume for a routine chest examination are lungs, oesophagus, breasts, bone, and red bone marrow (RBM). Lungs are located totally in the scan volume. The underestimation of the dose to this organ will be most significant in those section for which the lung area is small. This implies that the error in calculation of the integrated dose to the lung is much less than 25%, probably no greater than 10%. There will be an underestimate of the dose to the liver and stomach. However, only 25% and 17% of these organs respectively are included within the scanned region, so that the calculated error is correspondingly small. For oesophagus there is no error since it is located at the centre of each section of the

phantom, where there is a direct measurement of the dose. Breasts are located close to the representative section of the chest. Therefore the degree of underestimation in their dose is likely to be comparable to the differences represented for section 14 (Table 5.5). For bone and RBM the average values for the whole sections were used based on the method described by Huda and Sandison (1984). Hence the doses to these tissues will be affected in the same way as dose to the lungs.

Section 20 is outside the scan volume for the chest examination. The dosimetry method assumes that the dose distributed outside the scanned region is uniform. Table 5.10 shows the results of TLD measurements in section 20. These values were normalised to the central dose to demonstrate the distribution of the dose in this section (Table 5.11).

Table 5.10: Measured TLD values* in section 20 for the "chest" examination.

Vertical position	Horizontal position (cm)						
(cm)	-12	-8	-4	0	4	8	12
8	-	107.42	120.66	129.68	129.11	112.04	-
4	94.96	128.37	133.32	140.81	139.55	130.81	105.43
0	102.82	126.20	133.03	128.44	135.21	135.34	106.86
-4	90.64	120.81	123.05	-	119.49	129.43	104.35
-8	-	101.12	108.87	110.42	116.18	-	-

* Approximate TLD calibration factor was 0.0370 (mGy).

Table 5.11: The normalised measured values to the central value in section 20 for the "chest" examination.

Vertical position	Horizontal position (cm)						
(cm)	-12	-8	-4	0	4	8	12
8	-	0.84	0.94	1.01	1.01	0.87	-
4	0.74	1.00	1.04	1.10	1.09	1.02	0.82
0	0.80	0.98	1.04	1.00	1.05	1.05	0.83
-4	0.71	0.94	0.96	-	0.93	1.01	0.81
-8	-	0.79	0.85	0.86	0.90	-	-

Overall the average ratio of the measured values normalised to the central values in section 20 for 29 positions was 0.93 with an s.d. of 11% and a range of 0.73-1.10.

There are clearly errors in the assumption of uniform dose in this section with the dose towards the periphery of the section being significantly reduced. However

the overall effect is relatively small since the central doses of the sections outside the scan volume exponentially decreases when we move away from the scanned region on either side of the region. Integrating the scattered central doses outside the scan volume for the two ends of the phantom shows that it represents approximately 19% of the total integrated dose over the scan volume (sections 10-19). The overall overestimate of the estimated dose in these sections due to the assumption of uniform dose is therefore negligible, since it is only at the lower end of the scan volume that the dose contributes significantly to effective dose.

"Abdomen & Pelvis" area

To estimate the level of error caused by the assumption made for dose distributions in parallel sections for "abdomen & pelvis" examinations, the ratios between the normalised measured values in sections 20, 22, and 24 and the calculated values in the representative section of the "abdomen & pelvis" were calculated and analysed.

It was assumed that the dose distribution in all the parallel sections in "abdomen & pelvis" area are identical to that for section 26 (Figure 5.16). The ratios of the normalised measured dose values in sections 20, 22, and 24 to the calculated values in section 26 are summarised in Table 5.12.

Table 5.12: The average ratio of the normalised measured values in section 20, 22, and 24 to the calculated values in the representative section of the "abdomen & pelvis" area (no. 26).

Section no.	20	22	24
no. of positions	30	30	26
average	0.98	0.92	0.85
standard deviation	0.13	0.09	0.08
minimum	0.72	0.71	0.67
maximum	1.27	1.11	1.00

Table 5.13, Table 5.14, and Table 5.15 show the results of TLD measurements in section 20, 22, and 24 from the "abdomen & pelvis" examination. The ratios of the normalised measured values in section 20, 22, and 24 to the calculated values in the representative section of the abdomen & pelvis are shown in Table 5.16, Table 5.17, and Table 5.18 respectively. As can be noted in the tables, the ratios are significantly higher in the posterior regions of the sections indicating that

the degree of anterior posterior asymmetry in the dose distribution in figure 2 does not properly represents the dose distribution in these parallel sections.

Table 5.13: Measured TLD values* in section 20 for the "abdomen & pelvis" examination.

Vertical position (cm)	Horizontal position (cm)						
	-12	-8	-4	0	4	8	12
8	-	421.07	375.83	359.95	370.52	354.60	-
4	269.23	308.85	307.66	288.16	302.11	328.79	259.11
0	353.06	307.33	273.19	243.04	281.38	291.80	322.47
-4	350.40	306.58	278.82	-	270.09	310.03	382.84
-8	-	383.32	373.54	355.16	364.67	380.82	-

* Approximate TLD calibration factor was 0.0370 (mGy).

Table 5.14: Measured TLD values* in section 22 for the "abdomen & pelvis" examination.

Vertical position (cm)	Horizontal position (cm)						
	-12	-8	-4	0	4	8	12
8	-	463.32	468.61	470.68	491.84	453.11	-
4	386.76	452.29	409.88	389.08	421.91	385.51	357.84
0	342.52	385.34	359.33	324.16	353.57	376.21	448.24
-4	394.76	381.16	366.16	-	361.58	404.98	458.42
-8	-	445.67	436.03	394.21	424.33	435.74	-

* Approximate TLD calibration factor was 0.0370 (mGy).

Table 5.15: Measured TLD values* in section 24 for the "abdomen & pelvis" examination.

Vertical position (cm)	Horizontal position (cm)						
	-12	-8	-4	0	4	8	12
8	-	-	512.13	521.24	516.60	-	-
4	-	460.38	435.35	422.30	451.15	455.37	-
0	415.49	425.73	402.85	385.19	386.59	448.92	477.01
-4	466.81	433.25	401.99	-	391.96	424.00	370.05
-8	-	485.01	461.69	465.35	395.06	467.99	-

* Approximate TLD calibration factor was 0.0370 (mGy).

Table 5.16: The ratios of the normalised measured values in section 20 to the calculated values in the representative section of the "abdomen & pelvis" area (no. 26).

Vertical position (cm)	Horizontal position (cm)						
	-12	-8	-4	0	4	8	12
8	-	1.13	1.00	0.96	0.99	0.95	-
4	0.72	0.86	0.89	0.83	0.87	0.95	0.75
0	0.98	0.88	0.93	1.00	0.92	0.84	0.93
-4	1.09	1.00	1.04	-	0.92	0.89	1.10
-8	-	1.25	1.27	1.16	1.14	1.14	-

Table 5.17: The ratios of the normalised measured values in section 22 to the calculated values in the representative section of the "abdomen & pelvis" area (no. 26).

Vertical position (cm)	Horizontal position (cm)						
	-12	-8	-4	0	4	8	12
8	-	0.93	0.94	0.94	0.99	0.91	-
4	0.77	0.94	0.88	0.84	0.91	0.83	0.77
0	0.71	0.83	0.92	1.00	0.87	0.81	0.97
-4	0.92	0.93	1.03	-	0.92	0.87	0.99
-8	-	1.09	1.11	0.97	0.99	0.98	-

Table 5.18: The ratios of the normalised measured values in section 24 to the calculated values in the representative section of the "abdomen & pelvis" area (no. 26).

Vertical position (cm)	Horizontal position (cm)						
	-12	-8	-4	0	4	8	12
8	-	-	0.86	0.88	0.87	-	-
4	-	0.81	0.79	0.77	0.82	0.83	-
0	0.73	0.77	0.86	1.00	0.80	0.82	0.87
-4	0.92	0.89	0.95	-	0.84	0.77	0.67
-8	-	1.00	0.99	0.96	0.78	0.89	-

The results of the measurements on section 24 indicates an over estimation of 15% in the calculated doses due to the assumption of the similarity of the dose distribution in parallel sections to the representative section of the "abdomen & pelvis" area for the examinations performed over this area of the body. From the other sections (20 and 22) the discrepancy is smaller. However, it should be noted that the

significant organs and tissues used for the calculation of effective dose are in the anterior part of the phantom. Inspection of the data in Table 5.16, Table 5.16, and Table 5.18 indicates that the calculation method may give rise to an overestimate in dose of between 10 and 20%.

Section 18 is outside the scanned volume for the "abdomen & pelvis" examination. The dosimetry method assumes that the dose distributed outside the scanned region is uniform. Table 5.19 shows the results of TLD measurements in section 18. These values were then normalised to the central dose to demonstrate the distribution of the dose in this section (Table 5.20). Overall the average ratio of the normalised measured values to the central value in section 18 for 30 positions was 0.87 with an s.d. of 12% and a range of 0.63-1.08.

Table 5.19: Measured TLD values* in section 18 from the abdomen & pelvis" examination.

Vertical position	Horizontal position (cm)						
(cm)	-12	-8	-4	0	4	8	12
12	-	-	-	43.86	-	-	-
8	-	65.31	72.84	83.18	74.99	64.04	-
4	76.92	81.96	90.32	95.70	100.24	82.84	69.68
0	78.02	90.69	89.99	94.76	94.69	90.55	76.81
-4	73.81	88.27	89.90	-	88.88	102.26	76.32
-8	60.88	-	81.21	76.38	87.75	-	59.87

* Approximate TLD calibration factor was 0.0370 (mGy).

Table 5.20: The normalised measured values to the central value in section 18 for the "abdomen & pelvis" examination.

Vertical position	Horizontal position (cm)						
(cm)	-12	-8	-4	0	4	8	12
12	-	-	-	0.46	-	-	-
8	-	0.69	0.77	0.88	0.79	0.68	-
4	0.81	0.86	0.95	1.01	1.06	0.87	0.74
0	0.82	0.96	0.95	1.00	1.00	0.96	0.81
-4	0.78	0.93	0.95	-	0.94	1.08	0.81
-8	0.64	-	0.86	0.81	0.93	-	0.63

As for "the" chest examination, the dose distribution on this section indicates that there are errors in the assumption of uniform dose in the sections outside the scan volume, with the dose towards the periphery of the section being significantly

reduced. These measurements were carried out by positioning only one TLD in every location due to limited number of available TLDs. Therefore some of the extremely low values in the table could have been due to the intermittent low readings experienced with the TLD reader as explained earlier. However, these results show that the errors in the assumption of uniform dose outside the scan volume for the "abdomen & pelvis" examination, are very similar to what noted earlier for the "chest" examination. If similar analysis is carried out in the same way accomplished for the "chest", it can be shown that the overall overestimate of the dose due to the assumption of uniform dose is small, considering that there is only one tail outside the scan volume (top end) over which this error occurs for the "abdomen and pelvis" examination.

5.6.3 Evaluation of Errors in Measurements of Effective Dose

To provide an overall assessment of the accuracy of the dosimetry method, the errors causing by various parts of the calculations of effective dose were assessed. Three sources of error were considered: (1) the use of discrete points to represent the average dose to each organ, as listed in appendix B, rather than a full integration of the dose distribution over the organ; (2) the use of a single representative section of the phantom to describe the dose distributions rather than additional distributions for each section, measurement to validate this aspect of the technique were presented in section 5.6.2; (3) the random errors associated with TLD measurements as explained in section 5.3.3.

Errors in organ doses due to the use of discrete points were assessed for the lungs in section 14 and the colon in section 26. These are the organs in these sections which give the highest contribution to effective dose due to the high weighting factor, W_T=0.12, in each case. The distribution of doses in these sections overlaid in Figure 5.15R and 5.16R for a "chest" and an "abdomen & pelvis" scan respectively. Integration of the dose distribution over the organ was derived by estimating the area between contours and weighting the dose in respect of the area, summing and dividing by the total area. The ratios of doses obtained from the discrete points given in

appendix B to the dose obtained by full integration of the distribution were 1.01 and 1.02 respectively for the lungs and colon.

It has been shown in Table 5.3, Table 5.5, and Table 5.7 that there were differences between the distribution calculated from the orthogonal data set and from a full series of measurements in the representative section for the "chest" (14) and "abdomen & pelvis" (26) and further errors are introduced when considering the intermediate sections (18 (Table 5.9 and Table 5.20); 20 (Table 5.11, Table 5.16); 22 (Table 5.17); and 24 (Table 5.18)). This assessment of errors in organ doses was made for the organs principally contributing to effective dose in these sections: lungs; liver; stomach; and colon.

The errors in organ doses were assessed by taking the ratios of the organ doses at the representative location normalised to the central value derived from the calculated dose distributions (Figure 5.15R and 5.16R) to the actual dose ratio derived from the measurements in the validation study. Whenever a required single point value was not available in the measured data set, the average of surrounding points was taken to represent it. The ratios between the calculated and the measured average normalised values are summarised in Table 5.21 for the "chest" and "abdomen & pelvis" examinations.

Table 5.21:Ratios of the calculated to the measured values for lungs and liver for the "chest" and "abdomen & pelvis" examinations.

examination	organ	section no.	normalised value (average)		
			calculated	measured	ratio *
chest	lungs	14	1.00	1.09	0.92
		18	0.96	1.22	0.79
	liver	18	1.05	1.16	0.91
abdomen & pelvis	liver	20	1.41	1.31	1.08
		22	1.49	1.34	1.11
		24	1.51	1.19	1.27
	stomach	20	1.46	1.39	1.05
		22	1.54	1.37	1.12
	colon	22	1.32	1.13	1.17
		24	1.43	1.17	1.22
		26	1.43	1.40	1.01

* calculated to measured values.

The results of estimated patient doses using the developed direct dosimetry method for all the scanners are presented in the following chapter. The tables of results presented for a typical "chest" examination by the Siemens scanner (Table 6.15) shows that lungs and liver contribute 60% and 10% respectively to the effective dose when their absorbed dose values and their relevant weighting factors are used for effective dose calculation. Similarly, for a typical "abdomen & pelvis" examination by the Siemens scanner (Table 6.16) liver, stomach, and colon contribute to the resultant effective dose by 6%, 16%, and 16% respectively. The average of errors noted above for these organs can be weighted by these values and by the proportion of the organs in the parallel slices to assess the level of error introduced in the effective dose caused by assuming the same dose distributions in parallel sections in this dosimetry method.

In addition, as noted before there was 4.8% statistical uncertainties in TLD measurement. This in turn causes a 3.4% error in the central axis dose measurements in the Rando phantom sections being measured with a pair of the TLDs in the developed dosimetry method. Ten and fifteen central axis dose measurements are carried out for a typical "chest" and "abdomen & pelvis" examination respectively. Therefore for a typical "chest" and "abdomen & pelvis" examination an error of 2.2% and 1.8% is introduced in the value of effective dose by this statistical uncertainty respectively.

If the uncertainty introduced in the dosimetry method by the discrete point doses (to the average of contour values) and the average of errors introduced by assuming the same dose distribution in parallel sections are combined with the statistical uncertainties resulting from the central dose measurements with the TLDs, an estimate of the error in effective dose can be estimated for a typical "chest" and "abdomen & pelvis" examination with the developed CT dosimetry method. This is shown in Table 5.22.

Since the errors in methodology are not random, the dose ratios have been multiplied and the resultant error added to that for the TLD measurements.

Table 5.22:The overall uncertainties in estimated patient doses for two typical CT examinations with the developed dosimetry method.

examination	organ	error/uncertainty (%)			
		dose distributions contribution	discrete points	central doses (TLD)	overal (total)
chest	lungs liver	9 % 1 %	1 %	2 %	12 %
abdomen & pelvis	liver stomac colon	9 % 1 % 2 %	2 %	2 %	16 %

5.7 Customised Computer Spreadsheet Program

As mentioned in section two, to further facilitate our proposed direct CT dosimetry method, a computer spreadsheet program was designed. A very basic spreadsheet program was primarily used and designed to handle the data management required for the developed CT dosimetry method. But, during the course of this study a new and more powerful version of the Microsoft Excel™ computer program became available. Therefore, further developments were carried out using this program in an attempt to simplify the data input and data output and to automate the data processing required for the developed dosimetry method.

Figure 5.17 shows the data components of the spreadsheet. The spreadsheet has been designed in a way that could be used routinely for regular assessment of patient doses resulting from all routine CT examinations with all the CT scanners used in our study. It could also easily be adapted for any upcoming CT scanner model if the necessary modifications are made in its stored input data.

The input data components of the spreadsheet are either stored or entered by the user. Two macros are provided to make the input data process quite simple and user friendly. The output data is also generated automatically by other macros provided with the spreadsheet. The input and output macros could be run either by using simple shortcut keys or by pushing the macro buttons provided for this purpose.

In this section all the components of the spreadsheet computer program will be described and its data flow chart will be explained. The reader is referred to appendix C, where details of all the macros used in the spreadsheet could be found.

5.7.1 Input Data

The spreadsheet input data could be divided into two categories of stored input data and the input data required to be entered by the user.

Input Data		
I.	**Phantom**	
	A.	**Organs and tissues distribution (Mass Factor)**
II.	**CT Scanner**	
	A.	**Axial dose distribution (Dose Conversion Factor)**
	B.	**Ratios of μ_{en}/ρ of organs and tissues to that of air**
III.	**Calibration**	
	A.	**Dosed and control TLDs readouts**
	B.	**Traceable ionisation chamber CF and readout**
	C.	**Ambient pressure and temperature values**
IV.	**CT Protocol**	
	A.	**Examination parameters**
	B.	**Phantom central dose values (TLD readings)**
Output Data		
I.	**Organ and tissue absorbed doses**	
II.	**Effective dose equivalent**	
III.	**Effective dose**	

Figure 5.17: The Data components in the spreadsheet Computer Program.

The stored input data includes the input data for the phantom and the input data for the CT scanners. As basic stored input data for the phantom, the spreadsheet stores the location and proportion by weight of all organs or tissues for each section. This category of data has been called the "mass factor" in the spreadsheet. As stored input data for the CT scanner, the spreadsheet stores another category of data called the "tissue dose factor", for all organs and tissues of interest in every section and for all the CT scanners. These are based on the dose distributions for the three representative sections of the Rando phantom for each scanner and the location of

organs. The other CT scanner related data, stored in the spreadsheet, are the ratios of mass energy absorption coefficients to that of the air. These ratios have been calculated for the three categories of tissues, mentioned above, representing all organs and tissue of interest for all the CT scanners (Table 5.2).

The input data required to be entered by the user in the spreadsheet are the calibration data, the CT examination parameters, and the phantom central dose values (TLDs readings). The required calibration data includes: the readouts of ten dosed and ten control TLDs, the calibration factor and readout of the traceable ionisation chamber, and the values of the ambient pressure and temperature. The CT examination parameters required to be entered by the user are: the scan volume area (head or chest or body) and the sections of the phantom located inside the scan volume, the scanner model, the settings of the kV, mAs, slice width (thickness), table/couch increment/feed (conventional CT) or scan pitch (spiral/helical CT), and the number of slices scanned for the particular CT examination. The phantom central dose values required to be provided include: the readings of the pair of TLDs put in every section located inside the scan volume and one or two extra sections located outside the scan volume. As mentioned in section 5.5.2, the number of the required extra phantom central dose measurements depends on the scan volume. If the scan volume extends to either the top end (head) or the bottom end (pelvis) of the phantom, only one extra central dose measurement is required outside the scan volume. Otherwise two extra central dose measurements must be carried out outside the scan volume along the two tails on either side of the scan volume. Two macros have been provided to simplify the data input and make the spreadsheet interface more user friendly. The first macro asks the user to enter the required calibration data consequently. The second macro asks the user to enter the CT examination parameters and the phantom central doses (the pair of TLDs readings) depending on the examination parameters. Details of these macros could be found in appendix C.

Therefore, to assess patient doses for each CT examination protocol, TLD measurements need to be made at no more than 15 locations, on the central axis of the phantom, using no more than 30 TLD chips. These are besides the TLD chips used for calibration measurements. The exact number of TLD measurements depends

on the scan volume. For example in a complete "head" examination, the scan volume normally begins at the base of the skull and concludes at the top end of the head. This CT examination will only cover the five top end sections of the Rando phantom. Therefore, input of only twelve TLD measurements are required at five locations inside and one location outside the scan volume to estimate the patient doses resulting from this CT examination. On the other hand, if an "abdomen & pelvis" examination is considered, it normally covers a larger volume of the body of the phantom beginning from section 20 and finishing at the bottom end of the phantom (section 34). To estimate the patient doses resulting from this CT examination, input of 30 TLD measurements at fourteen locations inside and one location outside the scan volume will be required.

5.7.2 Output Data

From the above mentioned stored input data and other input data entered by the user, the spreadsheet automatically calculates and reports organs and tissues absorbed doses. Two macros have also been provided allowing the user to estimate both the effective dose and effective dose equivalent values based on the ICRP recommendations (1977, 1991). Clearly effective dose equivalent (ICRP 1977) has been replaced with effective dose in 1990 ICRP recommendations (ICRP 1991). This option was included in the spreadsheet computer program to make it possible to compare the results with others reporting patient doses from CT or other related practices in terms of effective dose equivalent.

Two types of user interface have been provided to run these macros. The macros could be run by either the short cut keys or two macro buttons, provided for this purpose with the spreadsheet computer program. Details of these macros could also be found in appendix C.

5.7.3 Data Flow Chart

Figure 5.18 shows the data flow chart of the spreadsheet computer program. When the master copy of the spreadsheet is opened, a macro button named "Data

Input 1" will become available to the user. When the user pushes this button, he will be asked to enter consequently, the data required for the TLD calibration factor calculation, as mentioned earlier in section 5.7.1. This input data includes the values for: the ten dosed TLDs, the ten control TLDs, the ionisation chamber calibration factor and its readout, and finally the ambient pressure and temperature. This enables the spreadsheet to calculate the TLD calibration factor. Then another macro button, named "Data Input 2" becomes available to the user. When this button is pushed, the user will be asked to enter consequently: all the required CT examination parameters, as mentioned earlier (section 5.7.1) and the readings of the pair of TLDs located at the central axis of the sections inside and one or two sections outside the scan volume of the phantom. At this stage, spreadsheet calculates the organ and tissue absorbed doses. Then two more macro buttons, one named "Effective Dose" and the other one named "Effective Dose Equivalent" become available to the user. Whichever of these buttons is pushed, enables the spreadsheet to calculate and report the relevant dose index for the CT examination.

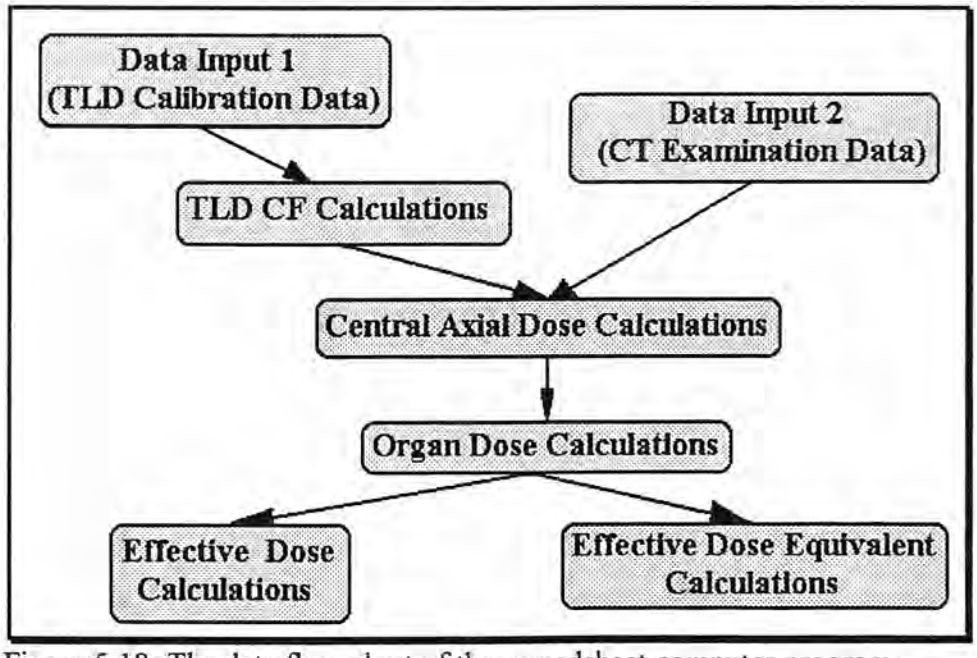

Figure 5.18: The data flow chart of the spreadsheet computer program.

5.8 Summary of the Developed Direct Dosimetry Method

The direct dosimetry approach was developed in this study to make it a more simple and practical approach for the assessment of patient doses resulting from the diverse and fast growing CT practices. The approach was chosen to avoid the complexity and extensive work involved in the common MC and direct CT dosimetry approaches respectively. The reduction of the extensive measurements was achieved by three assumptions made for the dose distributions resulting from the CT scanners. The measurements carried out for the validation of the accuracy of these assumption confirmed that overall these assumptions do not cause an error more than the degree of uncertainties (~20%) reported by the NRPB for the Monte Carlo dosimetry approach (Shrimpton et al. 1991b). However it is possible to decrease more the degree of this error caused mainly by the assumption made regarding the dose distribution in parallel sections of the phantom. More improvements could be achieved for the developed CT dosimetry method by choosing extra representative sections in the phantom to decrease the degree of error caused by the significant inhomogeneity existed specially in the overlap region between the "chest" and "abdomen" areas of the phantom.

The dosimeter chosen for the dose measurement (LiF TLDs) showed a good degree of consistency and low degree of uncertainty (4.8%). However a systematic uncertainty (low readings) was detected with dosimetry system used in this study. This error is caused by the poor contact between the TLD trays and the heater compartment of the TLD reader. This systematic error was avoided by using a pair of TLDs for the point dose measurements. Necessary corrections were also made to take into account differences in the mass energy absorption coefficients of body tissues for different CT X-ray spectra used by various CT scanners, although the differences observed among the different CT models were not significant (Table 5.2).

The customised computer spreadsheet developed in this study using the Microsoft Excel ® program provides a very simple and user friendly tool for further simplification of the developed CT dosimetry method. This spreadsheet does all the calculations required to estimate the organs absorbed doses and effective dose as recommended by the ICRP (1991) from a very limited number of TLD readouts for

all the different CT scanner models in this study. In addition this program could be used for upcoming new models of the CT scanners in the market if the initial measurements are carried out to determine the stored data required.

6. CT Dosimetry using Physical Anthropomorphic Phantom (Results)

The developed direct CT dosimetry approach was implemented and enabled us to assess the patient doses resulting from all the CT scanners used at different hospitals in the Lothian and Fife areas of Scotland. The CT scanners' characteristics were described earlier in chapter three.

Details of the routine CT examination protocols were determined through consulting with the radiologists and radiographers who used the scanners. The parameters considered for CT scan protocols were: applied potential (kV), exposure setting (mAs), number of slices (or scans), nominal slice width (or slice thickness) (mm), couch increment or table feed (mm) (for conventional CT scans), pitch value (for spiral CT scans), physical filter setting (if variable), and the first and last section of the phantom located in the scan volume. These were the same parameters applied for the dose assessment using the Monte Carlo dosimetry approach that will be described in the next chapter.

In this chapter the results of the patient dose assessment using our proposed direct CT dosimetry method will be presented for all routine CT examination protocols, performed by every CT scanner in this study. The results will be presented in terms of organ or tissue absorbed dose, effective dose (E), and effective dose equivalent (H_E) values. As mentioned earlier two models of the scanners (GE 8800 and GE 9000HP) were taken out of service or replaced with a newer model of GE HiSpeed Advantage in 1996. However, the measured values resulting from the developed direct CT dosimetry method on these model are presented here to make it possible to compare our proposed dosimetry approach with the Monte Carlo dosimetry approach. The calculated values resulting from the MC approach are presented in the following chapter. The differences between the results from the dose the developed direct dosimetry approach with that from the MC dosimetry methods are presented and discussed in chapter eight.

6.1 GE 8800 CT Scanner

As was already noted in chapter three, this scanner was rather an old GE model. Two scanners of this type were in use at two hospitals in the area. One of these scanners was not frequently in use and was mostly used as a backup for another GE 9000HP model. The measurements were carried out on the other one that was actively used. This scanner could have been used for whole body CT examinations including head, chest and abdomen and pelvis regions of the body. But, since it was installed in a clinical neuroscience department, it was mostly used for head and neck area CT examinations. The relevant parameters are listed in Table 6.1, for all the routine CT examinations used to be carried out with this scanner.

Table 6.1: Typical clinical scanning parameters for the routine examinations with the GE 8800 CT Scanner.

Examination	Physical filter	kV	mA	mAs	Slice width (mm)	Couch increment (mm)	No. of slices	Scan volume *
Head	Head	120	320	737	10	10	4	4 - 1
			250	576	10	10	4	
			160	369	10	10	2	
Orbit	Head	120	320	737	5	3	9	4 - 3
			250	576	10	10	1	
Posterior fossa	Head	120	400	922	5	5	7	4 - 1
			320	737	10	10	3	
			250	576	10	10	3	
			200	461	10	10	1	

* First and last sections of the Rando phantom included in the scan volume.

Organ and Tissue Doses and other Dose Indices:

Table 6.2 shows the calculated organ doses, effective dose equivalent, and effective dose values for the above three routine CT examinations performed by this scanner.

Table 6.2: Calculated organ doses and dose indices for the routine examinations with the GE 8800 CT scanner.

Organ/tissue	Calculated dose (mGy)		
	Head	Orbit	Posterior fossa
Gonads	0.00	0.00	0.00
Red bone marrow	1.50	1.21	1.98
Colon	0.00	0.00	0.00
Lungs	0.01	0.01	0.02
Stomach	0.00	0.00	0.00
Bladder	0.00	0.00	0.00
Breasts	0.00	0.00	0.00
Liver	0.00	0.00	0.00
Oesophagus	0.06	0.04	0.10
Thyroid	0.30	0.22	0.52
Skin	0.75	0.55	0.97
Bone surface	9.85	7.96	12.95
Remainder (mSv, ICRP 26)	1.38	1.01	1.73
H_E (mSv)	1.86	1.40	2.38
Remainder (mSv, ICRP 60)	0.47	0.31	0.57
E (mSv)	0.77	0.56	0.98

6.2 GE 9000HP CT Scanner

This was another old GE CT scanner. This scanner was used for whole body CT examinations including head, chest, abdomen and pelvis areas of the body in an X-ray department. The relevant parameters are listed in Table 6.3 for all the routine CT examinations used to be carried out with this scanner.

Table 6.3: Typical clinical scanning parameters for the routine examinations with the GE 9000HP CT Scanner.

Examination	Physical filter	kV	mA	mAs	Slice width (mm)	Couch increment (mm)	No. of slice	Scan volume*
Head	Head	120	250	888	10	10	5	4 - 3
			200	710	10	10	6	3 - 0
Chest	Body	120	250	533	10	15	18	10 - 19
Abdomen & pelvis	Body	120	250	533	10	15	28	20 - 34

* First and last sections of the Rando phantom included in the scan volume.

Organ and Tissue Doses and other Dose Indices:

Table 6.4 shows the calculated organ doses, effective dose equivalent, and effective dose values for the above three routine CT examinations performed by this scanner.

Table 6.4: Calculated organ doses and dose indices for the routine examinations with the GE 9000 HP CT scanner.

Organ/tissue	Calculated dose (mGy)		
	Head	Chest	Abdomen & pelvis
Gonads	0.00	0.04	11.57
Red bone marrow	3.28	4.56	5.89
Colon	0.00	0.19	13.19
Lungs	0.02	17.08	2.03
Stomach	0.00	7.55	17.54
Bladder	0.00	0.04	13.09
Breasts	0.00	20.03	3.11
Liver	0.00	7.73	10.139
Oesophagus	0.13	14.83	1.19
Thyroid	0.67	5.14	0.08
Skin	1.66	2.46	4.32
Bone surface	21.51	19.00	22.73
Remainder (mSv, ICRP 26)	2.97	3.52	5.68
H_E (mSv)	4.03	9.90	10.68
Remainder (mSv, ICRP 60)	1.01	0.58	0.65
E (mSv)	1.68	6.73	9.54

6.3 Philips Tomoscan CX/S CT Scanner

This was a modern model of Philips CT scanners, but had a rather poor and slow scan and reconstruction time compared with the other modern CT models in this study. The scanner was used for whole body CT examinations including head, chest, and abdomen and pelvis areas of the body in an X-ray department. The relevant parameters are listed in

Table 6.5, for all the routine CT examinations being carried out with this scanner.

Table 6.5: Typical clinical scanning parameters for the routine examinations with the Philips Tomoscan CX/S CT Scanner.

Examination	kV	mA	mAs	Slice width (mm)	Couch increment (mm)	No. of slices	Scan volume*
Head	120	220	356	10	10	11	4 - 1
Neck	120	220	356	10	10	10	6 - 10
Posterior fossa	120	270	437	5	5	6	4 - 0
		220	356	10	10	9	
Chest	120	220	356	10	15	18	10 - 19
Abdomen & pelvis	120	270	437	10	15	28	20 - 34
Lumbar spine	120	270	437	5	5	10	26 - 29

* First and last sections of the Rando phantom included in the scan volume

Organ and Tissue Doses and other Dose Indices:

Table 6.6 shows the calculated organ doses, effective dose equivalent, and effective dose values for all the routine examinations performed by this CT scanner.

Table 6.6: Calculated organ doses and dose indices for the routine examinations with the Philips Tomoscan CX/S CT scanner.

Organ/tissue	Calculated dose (mGy)					
	Head	Neck	Posterior fossa	Chest	Abdomen & pelvis	Lumbar spine
Gonads	0.00	0.00	0.00	0.06	20.51	3.69
Red bone marrow	3.33	3.88	3.33	6.85	12.12	5.01
Colon	0.00	0.00	0.00	0.26	25.45	5.84
Lungs	0.03	1.98	0.04	25.71	2.87	0.10
Stomach	0.00	0.03	0.00	10.89	27.93	1.29
Bladder	0.00	0.00	0.00	0.04	24.22	2.73
Breasts	0.00	0.37	0.00	27.82	4.49	0.16
Liver	0.00	0.04	0.00	11.51	26.17	1.66
Oesophagus	0.14	9.23	0.19	20.35	1.57	0.06
Thyroid	0.72	50.95	0.91	8.70	0.05	0.00
Skin	1.66	1.89	1.73	3.61	6.66	1.84
Bone surface	20.30	18.25	20.26	26.55	43.41	17.70
Remainder (mSv, ICRP 26)	2.97	2.17	2.85	4.89	10.02	3.32
H_E (mSv)	4.00	5.01	3.89	14.05	18.93	5.41
Remainder (mSv, ICRP 60)	1.01	0.04	1.02	0.77	1.17	0.65
E (mSv)	1.68	3.98	1.70	9.75	16.80	3.28

6.4 GE Sytec 3000 Plus CT Scanner

This was a lower range RR model GE CT scanner. The scanner was used for whole body CT examinations including head, chest, and abdomen and pelvis areas of the body in an X-ray department. The relevant parameters are listed in Table 6.7 for all the routine CT examinations being performed by this scanner.

Table 6.7: Typical clinical scanning parameters for the routine examinations with the GE Sytec 3000 Plus CT Scanner.

Examination	kV	mA	mAs	Slice width (mm)	Couch increment (mm)	No. of slices	Scan volume
Posterior fossa	120	100	450	5	5	8	4 - 1
		80	360	10	10	5	
		60	270	10	10	2	
Chest	120	130	234	10	10	25	10 - 19
Abdomen & pelvis	120	130	351	10	10	38	20 - 34

* First and last sections of the Rando phantom included in the scan volume

Organ and Tissue Doses and other Dose Indices:

Table 6.8 shows the calculated organ doses, effective dose equivalent, and effective dose values for the above three routine CT examinations performed by this scanner.

Table 6.8: Calculated organ doses and dose indices for the routine examinations with the GE Sytec 3000 Plus CT scanner.

Organ/tissue	Calculated dose (mGy)		
	Posterior fossa	Chest	Abdomen & pelvis
Gonads	0.00	0.02	42.08
Red bone marrow	5.27	10.58	26.32
Colon	0.00	0.17	50.69
Lungs	0.05	35.58	4.67
Stomach	0.00	12.27	53.06
Bladder	0.00	0.01	40.48
Breasts	0.01	40.08	7.27
Liver	0.00	13.25	47.47
Oesophagus	0.26	35.80	2.60
Thyroid	1.30	22.62	0.10
Skin	2.75	5.43	12.27
Bone surface	34.53	44.43	101.16
Remainder (mSv, ICRP 26)	4.66	6.87	18.95
H_E (mSv)	6.37	20.43	37.31
Remainder (mSv, ICRP 60)	1.53	0.38	2.20
E (mSv)	2.62	13.50	32.81

6.5 GE HiSpeed Advantage CT Scanner

This was a modern and top of the range GE CT scanner substituted for the GE 9000HP model in 1996. The scanner was used for whole body CT examinations including head, chest, and abdomen and pelvis areas of the body in an X-ray department. This scanner had capabilities to perform a variety of different

conventional and spiral (called helical by the GE manufacturer) CT examination protocols. The results of our dose measurement carried out for some of the routine and spiral CT examinations performed with this scanner will be mentioned separately.

6.5.1 Conventional CT Examinations

The relevant CT parameters are listed in Table 6.9, for all the routine conventional CT examinations being made with this model of GE scanner.

Table 6.9: Typical clinical scanning parameters for the conventional routine examinations with the GE HiSpeed Advantage CT Scanner.

Examination	kV	mA	mAs	Slice width (mm)	Couch increment (mm)	No. of slices	Scan volume*
Head (1)	120	280	280	10	10	10	4 - 1
Head (2)	120	340	340	10	10	6	4 - 0
		280	280	10	10	6	
Head (3)	120	340	340	10	10	12	4 - 0
Posterior fossa	120	340	340	5	5	5	4 - 0
		340	340	10	10	5	
		280	280	10	10	5	
Chest	120	120	120	10	10	27	10 - 19
Abdomen & pelvis (1)	120	280	280	10	10	38	20 - 34
Abdomen & pelvis (2)	120	150	150	10	10	38	20 - 34

* First and last sections of the Rando phantom included in the scan volume

Organ and Tissue Doses and other Dose Indices:

Table 6.10 shows the calculated organ doses, effective dose equivalent, and effective dose values for all the routine conventional CT examinations being performed with this scanner.

Table 6.10: Calculated organ doses and dose indices for the routine conventional examinations with the GE HiSpeed Advantage CT Scanner.

Organ/tissue	Calculated dose (mGy)						
	Head (1)	Head (2)	Head (3)	Posterior fossa	Chest	Abdomen & pelvis (1)	Abdomen & pelvis (2)
Gonads	0.00	0.00	0.00	0.00	0.01	18.10	8.43
Red bone marrow	2.08	2.85	2.70	3.26	2.62	12.07	5.62
Colon	0.00	0.00	0.00	0.00	0.08	21.60	10.93
Lungs	0.01	0.04	0.02	0.02	8.56	5.63	1.18
Stomach	0.00	0.00	0.00	0.00	3.96	26.15	10.23
Bladder	0.00	0.00	0.00	0.00	0.01	18.20	9.47
Breasts	0.00	0.00	0.00	0.00	10.41	8.06	1.82
Liver	0.00	0.00	0.00	0.00	4.16	24.50	9.65
Oesophagus	0.07	0.17	0.12	0.13	9.03	3.73	0.68
Thyroid	0.38	0.83	0.60	0.70	6.01	0.64	0.03
Skin	1.05	1.49	1.44	1.63	1.36	5.90	2.60
Bone surface	13.38	18.27	17.28	20.89	10.76	45.69	21.14
Remainder (mSv, ICRP 26)	1.88	2.52	2.31	2.77	1.90	8.34	3.84
H_E (mSv)	2.54	3.44	3.18	3.81	5.31	17.59	7.67
Remainder (mSv, ICRP 60)	0.64	0.83	0.78	0.90	0.11	0.99	0.45
E (mSv)	1.06	1.42	1.33	1.56	3.54	15.73	6.81

6.5.2 Spiral CT Examinations

The relevant CT parameters are listed in Table 6.11, for all the routine spiral CT examinations being made with this model of GE scanner.

Table 6.11: Typical clinical scanning parameters for the spiral examinations with the GE HiSpeed Advantage CT Scanner.

Examination	kV	mA	mAs	Slice width (mm)	Scan pitch	Total scan time (sec.)	Scan volume*
Chest	120	150	150	7	1.5	24.4	10 - 19
Liver (1)	120	200	200	10	1.0	18	20 - 26
Liver (2)	120	220	220	7	1.0	32	18 - 26
Liver (3)	120	200	200	10	1.0	23	18 - 26
Liver (4)	120	220	220	5	1.0	21	21 - 24
		200	200	7	1.0	12	18 - 20
		220	220	7	1.0	33	26 - 18
Abdomen & pelvis	120	150	150	10	1.3	26.4	20 - 34
Lumbar spine	120	250	250	3	1.0	51	23 - 28

* First and last sections of the Rando phantom included in the scan volume

Organ and Tissue Doses and other Dose Indices:

Table 6.12 shows the calculated organ doses, effective dose equivalent, and effective dose values for all the routine spiral CT examinations being performed with this model of GE scanner.

Table 6.12: Calculated organ doses and dose indices for the routine spiral examinations using the GE HiSpeed Advantage CT scanner.

Organ/tissue	Calculated dose (mGy)						
	Chest	Liver (1)	Liver (2)	Liver (3)	Liver (4)	Abdomen & pelvis	Lumbar spine
Gonads	0.01	0.38	0.38	0.41	0.62	5.30	1.57
Red bone marrow	2.69	2.50	3.44	3.12	5.73	4.00	3.71
Colon	0.05	1.82	2.06	1.94	3.31	7.69	3.67
Lungs	8.12	1.82	5.02	4.41	9.15	0.96	0.40
Stomach	3.16	16.91	20.74	18.46	38.03	8.61	5.85
Bladder	0.00	0.28	0.27	0.30	0.47	5.79	1.14
Breasts	9.43	3.18	9.24	8.05	16.75	1.48	0.62
Liver	3.38	15.67	20.00	17.72	36.03	8.16	6.67
Oesophagus	9.10	1.13	3.41	2.96	6.09	0.55	0.22
Thyroid	6.80	0.05	0.11	0.10	0.20	0.03	0.01
Skin	1.32	1.82	2.55	2.29	4.32	1.87	1.89
Bone surface	11.11	9.89	13.66	12.37	22.80	15.12	14.17
Remainder (mSv, ICRP 26)	1.76	5.21	6.23	5.54	11.05	3.11	3.87
H_E (mSv)	5.01	6.59	9.14	8.12	16.19	5.71	5.28
Remainder (mSv, ICRP 60)	0.10	0.66	0.76	0.68	1.31	0.36	0.58
E (mSv)	3.34	4.64	6.40	5.72	11.43	4.95	3.12

6.6 Siemens Somatom Plus CT Scanner

This was also a modern and top of the range RR model of Siemens CT scanners. The scanner was used for whole body CT examinations including head, chest, and abdomen and pelvis areas of the body in a radiology department. This scanner had also had capabilities to perform a variety of conventional and spiral CT examination. The results of our dose measurement for some of the routine and spiral CT examination with this model will be mentioned separately.

6.6.1 Conventional CT Examinations

The relevant CT parameters are listed in Table 6.13, for all routine conventional CT examinations being made with this model of Siemens scanner.

Table 6.13: Typical clinical scanning parameters for routine conventional examinations with the Siemens Somatom Plus CT Scanner

Examination	kV	mA	mAs	Slice width (mm)	Couch increment (mm)	No. of slices	Scan volume*
Head (1)	120	210	420	10	10	10	4 - 1
Head (2)	120	210	420	10	10	11	4 - 0
Posterior fossa	120	210	420	5	5	6	4 - 1
				10	10	7	
Orbit	120	165	165	5	5	8	4 - 3
Chest (1)	137	100	100	10	10	25	11 - 19
Chest (2)	137	145	145	10	10	26	10 - 19
Abdomen & pelvis (1)	120	210	210	10	10	36	20 - 34
Abdomen & pelvis (2)	120	210	210	10	15	26	20 - 34
Abdomen & pelvis (3)	120	210	210	10	10	38	20 - 34
Pelvis (1)	120	210	210	10	10	17	29 - 34
Pelvis (2)	120	315	315	10	10	17	29 - 34

*First and last sections of the Rando phantom included in the scan volume

Organ and Tissue Doses and other Dose Indices:

Table 6.14 shows the calculated organ doses, effective dose equivalent, and effective dose values for the routine conventional "head" examinations performed by this CT scanner. Table 6.15, Table 6.16, and Table 6.17 show similar dose values for the routine conventional "chest", "abdomen & pelvis", and "pelvis" examinations performed by this CT scanner.

Table 6.14: Calculated organ doses and dose indices for different routine conventional "head" examinations using the Siemens Somatom Plus CT scanner.

Organ/tissue	Calculated dose (mGy)			
	Head (1)	Head (2)	Posterior fossa	Orbit
Gonads	0.00	0.00	0.00	0.00
Red bone marrow	2.09	2.12	2.43	0.37
Colon	0.00	0.00	0.00	0.00
Lungs	0.03	0.03	0.05	0.02
Stomach	0.00	0.00	0.00	0.00
Bladder	0.00	0.00	0.00	0.00
Breasts	0.00	0.00	0.01	0.00
Liver	0.00	0.00	0.00	0.00
Oesophagus	0.12	0.13	0.21	0.06
Thyroid	0.59	0.62	0.96	0.24
Skin	1.05	1.07	1.22	0.21
Bone surface	13.80	14.00	16.03	2.42
Remainder (mSv, ICRP 26)	1.91	1.89	2.25	0.39
H_E (mSv)	2.60	2.59	3.06	0.52
Remainder (mSv, ICRP 60)	0.64	0.63	0.73	0.13
E (mSv)	1.08	1.08	1.26	0.21

Table 6.15: Calculated organ doses and dose indices for two routine conventional "chest" examinations using the Siemens Somatom Plus CT scanner.

Organ/tissue	Calculated dose (mGy)	
	Chest (1)	Chest (2)
Gonads	0.01	0.01
Red bone marrow	3.31	5.16
Colon	0.06	0.11
Lungs	10.35	16.57
Stomach	3.63	6.09
Bladder	0.01	0.01
Breasts	10.99	18.44
Liver	3.79	6.51
Oesophagus	10.31	16.27
Thyroid	7.17	11.14
Skin	1.64	2.61
Bone surface	13.36	20.82
Remainder (mSv, ICRP 26)	2.08	3.26
H_E (mSv)	5.99	9.60
Remainder (mSv, ICRP 60)	0.12	0.19
E (mSv)	3.97	6.39

Table 6.16: Calculated organ doses and dose indices for three routine conventional "abdomen & pelvis" examinations using the Siemens Somatom Plus CT scanner.

Organ/tissue	Calculated dose (mGy)		
	Abdomen & pelvis (1)	Abdomen & pelvis (2)	Abdomen & pelvis (3)
Gonads	12.34	7.85	13.99
Red bone marrow	7.87	4.81	8.18
Colon	15.66	9.35	16.88
Lungs	1.73	1.16	1.18
Stomach	15.31	9.41	13.13
Bladder	13.75	7.76	14.40
Breasts	2.65	1.75	1.81
Liver	14.45	8.89	12.82
Oesophagus	1.01	0.70	0.70
Thyroid	0.06	0.06	0.05
Skin	3.69	2.29	3.76
Bone surface	30.60	18.70	31.75
Remainder (mSv, ICRP 26)	5.67	3.45	5.93
H_E (mSv)	11.23	6.96	11.78
Remainder (mSv, ICRP 60)	0.67	0.41	0.68
E (mSv)	9.94	6.12	10.05

Table 6.17: Calculated organ doses and dose indices for two routine conventional pelvis examinations using the Siemens Somatom Plus CT scanner.

Organ/Tissue	Calculated dose (mGy)	
	Pelvis (1)	Pelvis (2)
Gonads	11.71	18.71
Red bone marrow	4.12	6.59
Colon	12.57	20.24
Lungs	0.01	0.01
Stomach	0.10	0.13
Bladder	13.09	21.73
Breasts	0.01	0.01
Liver	0.14	0.18
Oesophagus	0.00	0.00
Thyroid	0.00	0.00
Skin	1.56	2.51
Bone surface	15.67	25.02
Remainder (mSv, ICRP 26)	3.48	5.63
H_E (mSv)	7.37	11.85
Remainder (mSv, ICRP 60)	0.17	0.27
E (mSv)	5.37	8.62

6.6.2 Spiral CT Examinations

The relevant CT parameters are listed in Table 6.18, for all the routine spiral

CT examinations being performed with this model of Siemens scanner.

Table 6.18: Typical clinical scanning parameters for the routine spiral examinations with the Siemens Somatom Plus CT Scanner.

Examination	kV	mA	mAs	Slice width (mm)	Scan pitch	Total scan time (sec.)	Scan volume*
Neck (1)	120	340	340	3	1.0	24	8 - 10
Neck (2) Larynx	120	340	340	10	1.0	16	5 - 10
Neck (3) Larynx	120	230	230	3	1.0	20	8 - 10
Chest	137	145	145	10	1.0	24	11 - 20
Abdomen	120	210	210	3	1.0	24	20 - 22
Abdomen & pelvis	120	210	210	3	1.0	24	20 - 32
				10	1.0	24	

* First and last sections of the Rando phantom included in the scan volume

Organ and Tissue Doses and other Dose Indices:

Table 6.19 shows the calculated organ doses, effective dose equivalent, and effective dose values for all the routine spiral CT examinations performed by this model of Siemens scanner. It includes three "neck", one "chest", one "abdomen", and finally one "abdomen & pelvis" spiral CT examination.

Table 6.19: Calculated organ doses and dose indices for different spiral examinations using the Siemens Somatom Plus CT scanner.

Organ/Tissue	Calculated dose (mGy)					
	Neck (1)	Neck (2)	Neck (3)	Chest	Abdomen	Abdomen & pelvis
Gonads	0.00	0.00	0.00	0.02	0.10	7.12
Red bone marrow	1.27	2.71	1.00	4.09	1.19	5.91
Colon	0.00	0.00	0.00	0.12	0.57	9.46
Lungs	0.89	1.13	0.69	14.12	1.78	1.78
Stomach	0.02	0.02	0.02	5.67	13.05	14.87
Bladder	0.00	0.00	0.00	0.02	0.08	4.84
Breasts	0.18	0.16	0.18	16.14	2.70	2.70
Liver	0.02	0.02	0.03	5.96	11.41	14.09
Oesophagus	3.56	4.84	2.90	12.89	1.06	1.06
Thyroid	16.13	22.62	17.02	5.51	0.08	0.08
Skin	0.55	1.27	0.53	2.14	0.94	2.88
Bone surface	6.09	14.88	5.16	16.41	4.91	23.16
Remainder (mSv, ICRP 26)	0.49	2.02	0.45	2.87	3.84	5.31
H_E (mSv)	1.44	3.63	1.34	8.05	4.78	9.11
Remainder (mSv, ICRP 60)	0.02	0.05	0.01	0.16	0.43	0.59
E (mSv)	1.34	2.05	1.28	5.26	3.26	7.25

6.7 Summary of the Results

In CT dosimetry several variable factors affect the patient doses estimated from CT practices. These factors must be considered if the patient doses resulting from CT practices are going to be summarised or compared between different CT scanner models. The factors affecting, directly or indirectly, patient doses resulting from CT practices are: scanner rotation angle, clinical protocol, filtration, collimation, detector efficiency, scan field diameter, slice thickness and spacing or scan pitch, scan volume, patient size, repeat scans, image matrix size, and reconstruction filters if they require change of the clinical protocol. Some of these factors are either fixed or pre-set with every CT scanner model, others may be selected. The factors like inherent filtration, collimation, detector efficiency, scan field diameter (source to isocentre distance) image matrix size, and reconstruction filters are either fixed or pre-set by the CT manufacturers. For some other factors such as rotation angle and added filtration, there may be a limited number of options. The other factors that can be selected include the tube potential (kV) and current time product (mAs), the slice width and spacing or the pitch setting, and the scan volume.

In CT dosimetry, even if we ignore the pre-set and fixed factors affecting estimated patient doses, the latter group of factors mentioned above could not entirely be altered. For example regarding the tube potential, even though some modern CT scanners allow the users to choose a desirable kV from a very limited number of kV settings, typically CT scanners operate at 120 to 140 kV. Concerning the mAs setting, even though there is more flexibility, normally there are several pre-set mAs values for every particular routine CT examination recommended by the manufacturers based on the other specific characteristics of CT scanners. Regarding the slice width and table increment or the pitch and the scan volume normally the user has more control and options, although the available options are not necessarily similar among different CT scanner makes and models.

In this study, like any other CT dosimetry study, we did not have any control on the factors that are either fixed or pre-set within the CT scanners. Regarding the other category of factors, that could virtually be altered, we tried to control them in a way that the same protocols were used for similar routine CT examinations for all the

CT scanners. Nevertheless, this was not completely achievable, due to the constraints imposed by differences in the scanners' characteristics.

Regarding the tube potential, except for the Siemens CT scanner having its kV pre-set at 137 kV for the routine chest examinations, the tube potential of all the other CT scanners were either pre-set or set to operate at 120 kV.

Generally, we used the standard clinical protocols used by the radiographers and radiologists for every routine CT examination. But, we tried to carry out CT examinations with the same kV, mAs, slice width, and over the same area and length of the phantom for similar common examinations with all the CT scanners. In spite of our efforts, achieving this was not possible for all the similar scanning techniques for all the CT scanners, because of different practices adopted by their operators. For example, the "head" and "posterior fossa" examinations were commonly carried out by most of the scanners over the head area. As can be seen in Table 6.20, there was a significant variation in the mAs (280-791) and the scan length (100-120 mm) used for these examinations among the CT scanners. Similar comparison for the "chest" examinations (Table 6.21) shows that, not only there was a significant variation in the mAs (120-533) and the scan length (240-270 mm), but also, as mentioned before, two different kVs (120-137) were used by the CT scanners. Similar comparison for the "abdomen & pelvis" examinations (Table 6.22) indicates similar variation in the scan length (312-420 mm) and the mAs (150-533) among the CT scanners.

Regarding the patient size, we used a Rando phantom for all the measurements and this factor influencing patient dose was not investigated.

For a particular scanner, the patient dose should be related to the total effective scan volume and the mAs. The effective scan volume is the total scan length multiplied by the packing factor (that is the slice width divided by the couch increment for conventional scans or the inverse of the pitch for spiral scans). The relationship between the patient dose and the scan volume will depend on the region of the body scanned, e.g. head, chest, abdomen or pelvis. For scanners operating at the same kV, the effective dose normalised to the effective scan volume and mAs would be expected to have a relationship to CTDI normalised to mAs. This can also be investigated for these data.

To summarise the results and compare different models of the CT scanners for a similar condition of settings, calculated effective dose values, for the most common routine scanning techniques, were normalised to 100 mAs. They were then normalised to 10 mm scan volume and the packing factor of one for every common CT examination.

The most common routine scanning techniques carried out by the CT scanners were "head", "posterior fossa", "chest" and "abdomen & pelvis" examinations, although other special scanning protocols such as "orbit", "neck" or "larynx", "liver", and "lumbar spine" were also routinely practised by some of the scanners. As was noted in chapter three and earlier in this chapter, two CT scanners could also perform spiral scanning techniques.

In the following parts of this section the estimated patient doses assessed from all the CT scanners have been summarised for the most common scanning techniques. The dose measurement results for all the scanners have been summarised and grouped under the patient doses from "head", "chest" and "abdomen & pelvis" scanning techniques. These groups include the most common CT examination(s) carried out over the head, chest and abdomen & pelvis areas of the body respectively.

6.7.1 Patient Doses from Head Scanning Techniques

The common routine examinations performed by the CT scanners over the head area of the body were "head", "posterior fossa", "orbit", and "neck" or "larynx". The "orbit" and "neck" or "larynx" examinations were only performed by two CT scanners using quite different protocols for special purposes. Therefore the summary of patient doses for these examinations will not be mentioned here.

The routine "head" and "posterior fossa" examinations were commonly performed by most of the CT scanners. The routine "head" examination was not performed by the GE Sytec scanner. The routine "posterior fossa" examination was not carried out by the GE 9000HP scanner.

The results of dose measurements for the "head" and "posterior fossa" examinations on all the CT scanners are summarised in Table 6.20. If the absolute values of measured effective doses resulting from these examinations are compared, it

will be noted that the GE Sytec scanner gives the highest and the GE 8800 scanner the lowest values.

As can be seen in Table 6.20 there has been a variation by a factor of 3.40 between the effective dose absolute values among the CT scanners. On the other hand the effective dose values normalised to 100 mAs and 10 mm scan volume indicate a variation of 4.80 among the scanners. But apart from the GE 8800, if the effective dose values normalised to the measured CTDI values are compared, it will be noted that there has been a variation factor of 1.58 among all the CT scanners for these examinations performed on the head region of the body. There have been some uncertainties with the measured CTDI values for the GE 8800 scanner that will be explained in the next chapter.

Table 6.20: Summary of the effective dose and normalised effective dose values for the most common scanning techniques of the head.

CT scanner	Examination	E (mSv)	kV	mAs	scan length (mm)	Packing factor	E normal 1	CTDI	E normal 2
GE 8800	Head	0.77	120	599	100	1.000	0.013	0.191	0.067
GE 8800	Posterior fossa	0.98	120	726	105	1.000	0.013	0.191	0.067
GE 9000HP	Head	1.68	120	791	110	1.000	0.019	0.123	0.157
GE Sytec 3000 Plus	Posterior fossa	2.62	120	376	110	1.000	0.063	0.352	0.180
GE HiSpeed Advantage	Head (1)	1.06	120	280	100	1.000	0.032	0.191	0.198
GE HiSpeed Advantage	Head (2)	1.42	120	310	120	1.000	0.038	0.191	0.200
GE HiSpeed Advantage	Head (3)	1.33	120	340	120	1.000	0.033	0.191	0.171
GE HiSpeed Advantage	Posterior fossa	1.56	120	316	125	1.000	0.039	0.191	0.207
Philips Tomoscan CX/S	Head	1.68	120	356	110	1.000	0.043	0.190	0.226
Philips Tomoscan CX/S	Posterior fossa	1.70	120	376	120	1.000	0.038	0.190	0.198
Siemens Somatom Plus	Head (1)	1.08	120	420	100	1.000	0.026	0.135	0.190
Siemens Somatom Plus	Head (2)	1.08	120	420	110	1.000	0.023	0.135	0.173
Siemens Somatom Plus	Posterior fossa	1.26	120	420	100	1.000	0.030	0.135	0.222

E (normal 1): Effective dose normalised to 100 mAs, 10mm scan volume, and packing factor of 1.
E (normal 2): E (normal 1) normalised to the CTDI (mGy/mAs) measured with TLDs for 10 mm slice width.

As may be noted in Table 6.20, effective dose values for two routine "head" examinations have been measured for the Siemens CT scanner. The only difference in scanning technique was in the scan volume of these examinations. However no significant change in the absolute effective dose value was observed for these examinations. But about 10% difference was observed between their normalised effective dose values. This difference is somewhat greater than the total uncertainties of 7.4% (~6.8% from central dose and 3.0% from calibration factor) estimated for the developed dosimetry method. Approximately 65% of the effective dose resulting from a scan of the head arises from the dose to the brain. Increasing scan length beyond the limits of this organ has, however, a relatively small effect on effective dose. In addition, except for a small proportion of the bone, red bone marrow, and skin none of the radiosensitive organs or tissues of the body is affected by the extra scans. Therefore, we would expect a reduction in effective dose when normalised to the scan length as happened for the second "head" examination here. Hence, while the additional scan length of the second head examination has not led to any significant increase in the absolute effective dose value, the normalisation to the scan volume has caused a 10% reduction in the normalised effective dose value.

As can be seen in Table 6.20, doses for three "head" examinations were measured for the GE HiSpeed Advantage CT scanner. The first one, indicating a lower absolute effective dose value, was performed with a lower mAs and over a shorter (20 mm) scan length compare with the others. On the other hand, although the third "head" examination was carried out with a slightly higher mAs value and over the same scan length as the second one, it indicated a lower absolute effective dose value. The normalised effective dose value to CTDI indicated no significant difference between the first two "head" examinations. But, for the third examination this value was about 13% less, that is higher than the total estimated level of uncertainties (7.4%). Changes in the scanner characteristics over the time interval (~ 6 months) between the dose measurements for these head examinations might have contributed to this significant difference.

There will be an interesting point if the scanning technique of the routine "posterior fossa" examination is compared with that of the first routine "head" examination for the Siemens scanner (Table 6.13). The "posterior fossa" examination has been composed of six contiguous scans with 5 mm and a further seven scans with 10 mm slice width, instead of ten contiguous scans with 10 mm being normally used for head examinations. Therefore, although the scan volumes in both of these scanning techniques have been the same, choosing a thinner slice width at the beginning for the "posterior fossa" examination has led to a significant increase (17%) in both the absolute and normalised effective dose values. Changes in the scanner characteristics over the time interval (~2 months) between the dose measurements for these examinations may have caused this significant difference.

The relation between the scanning techniques (slice width) of the second "head" examination and the "posterior fossa" examination with the GE HiSpeed scanner (Table 6.9) has been similar to that of the Siemens scanner. If a similar comparison is made between these examinations, it will be noted that the "posterior fossa" examination has led to a 10% higher absolute effective dose value than that of the "head" examination. However, there has been no significant difference (< 4%) between the normalised effective dose values to the CTDI for these examinations.

There has been no significant difference between the absolute values of effective dose of the "head" and "posterior fossa" examinations for the Philips CT scanner. However, there has been about 14% difference between the normalised effective dose values to CTDI for these examinations, which is higher than the total estimated level of uncertainties (7.6%). But, a proportion (~9%) of this difference is caused by the longer scan volume of the "posterior fossa" examination than that of the "head" examination. This can also be explained in the same way made above for the differences between the two head examinations by the Siemens scanner. While the additional scan length of the "posterior fossa" has not caused a significant increase in the absolute effective dose value, the normalisation to the scan volume has led to about 5% reduction in the normalised effective dose value. Therefore, if this proportion of the difference is ignored, the differences between the normalised values

of these examinations with the Philips scanner will not be significant. The dose measurements for both of these examinations were carried out on the same date.

6.7.2 Patient Doses from Chest Scanning Techniques

Routine "chest" examinations were measured on all the CT scanners except the GE 8800. Besides conventional "chest" examination, spiral "chest" examination was also performed by two modern CT scanners included in this study.

The calculated effective dose values for the routine (conventional and spiral) "chest" examinations on the CT scanners are summarised in Table 6.21. The results presented in the table indicate that the GE Sytec 3000 Plus gives the highest and the GE HiSpeed Advantage the lowest patient dose (in terms of absolute effective dose) for the routine "chest" examination. If the normalised effective dose values (normal1) are compared, the old GE 9000HP scanner shows the lowest value, while the GE Sytec still shows the highest value.

Overall as can be noted from Table 6.21 there has been a variation by a factor of 4 in the absolute values of effective dose for this examination among the CT scanners. On the other hand the effective dose values normalised to 100 mAs and 10 mm slice width show a variation factor of 3.00 among the scanners. But if the effective dose values normalised to CTDI are compared in the table, it will be noted that there has been a variation factor of 1.88 among the CT scanners for this examination.

For those scanners operating at 120 kV, normalisation of effective dose to CTDI shows a variation (maximum/minimum) of 1.46. For the Siemens scanner, the doses normalised to CTDI are higher because of the greater penetration of the X-ray beam at its higher tube potential (137 kV).

There is an interesting point if the absolute effective dose values resulting from conventional and spiral "chest" examinations by the GE HiSpeed Advantage scanner are compared in the above table. Although the mAs setting of the spiral examination has been higher than the conventional one (Table 6.11), it has led to a lower effective dose value because of using a pitch setting greater than one (1.5). However, the differences between the normalised effective dose values to CTDI for these

examinations (19%) have been significantly higher than the estimated level of uncertainty (7.6%) in the dosimetry method. It must be noted that there was a considerable time interval between these dose measurements.

Table 6.21: Summary of the effective dose and normalised effective dose values for the most common scanning techniques of the chest.

CT scanner	Examination	E (mSv)	kV	mAs	scan length (mm)	Packing Factor	E normal 1	CTDI	E normal 2
GE 9000HP	Chest	6.73	120	533	270	0.667	0.070	0.128	0.548
GE Sytec 3000 Plus	Chest	13.50	120	234	250	1.000	0.231	0.352	0.656
GE HiSpeed Advantage	Chest (1)	3.54	120	120	270	1.000	0.109	0.191	0.572
GE HiSpeed Advantage	Chest (2)*	3.34	120	150	256	0.667	0.130	0.191	0.683
Philips Tomoscan CX/S	Chest	9.75	120	356	270	0.667	0.152	0.190	0.801
Siemens Somatom Plus	Chest (1)	3.97	137	100	250	1.000	0.159	0.165	0.962
Siemens Somatom Plus	Chest (2)	6.39	137	145	260	1.000	0.169	0.165	1.027
Siemens Somatom Plus	Chest (3)*	5.26	137	145	240	1.000	0.151	0.165	0.916

E (normal 1): Effective dose normalised to 100 mAs, 10mm scan volume, and packing factor of 1.
E (normal 2): E (normal 1) normalised to the CTDI (mGy/mAs) measured with TLDs for 10 mm slice width.
* Spiral mode.

There have also been two conventional and one spiral "chest" examinations performed by the Siemens CT scanner. For this scanner the second conventional "chest" examination has been performed with a higher mAs setting. As expected this has led to a higher effective dose value for this examination, although its scan length has been 10 mm shorter than the first one (Table 6.13`). There was no significant difference (< 7.6%) between the normalised effective dose values to CTDI for these examinations. The spiral "chest" examination, performed almost with the same scanning technique as the second conventional "chest" examination (Table 6.13), had a significantly lower (> 20%) absolute effective dose value than that of the conventional one for this scanner. The only factor that can be taken into account for this reduction in the dose is the shorter scan volume length (two scans or 20 mm) used for the spiral mode examination with this scanner. However, the difference

between the normalised effective dose values to CTDI for these spiral and conventional examinations was significant (12%). It must be noted that there was a considerable time interval between these dose measurements.

Overall significant differences observed between normalised effective dose values to CTDI for chest examinations using an identical model of CT scanner. A proportion of this difference can be contributed to the extra scan length of some "chest" examinations performed over a longer length. But it must be noted that for the chest examination, unlike the head examinations, increasing the scan length causes a significant increase in effective dose, because more radiosensitive organs will then be included and irradiated. However, even if the values were normalised to an equal scan volume, the difference observed between them will have still been significant. However, the differences observed between normalised values to CTDI for chest examinations (19%, and 12% for the GE HiSpeed Advantage and the Siemens scanners respectively) could have partly been due to the measurement uncertainties (7.6%). But, it should be noted that there has been a considerable time interval between the measurements over which the CT scanner characteristics may have been changed.

6.7.3 Patient Doses from Abdomen and Pelvis Scanning Techniques

The common examinations performed over the abdomen and pelvis areas of the body were routine "abdomen & pelvis", "abdomen", "liver", and "lumbar spine". We will only summarise the results for the routine "abdomen & pelvis" examination performed by all the CT scanners except the GE 8800 scanner. As may have been noted before, the other scanning techniques were either used by a few of the scanners or performed with very different scanning techniques.

The absolute effective dose values for all the routine "abdomen & pelvis" examinations performed by all the CT scanners are summarised in Table 6.22. The results presented in the table indicate that the GE Sytec 3000 Plus gives the highest and the GE HiSpeed Advantage CT scanner the lowest patient dose for the routine "abdomen & pelvis" examination. If the normalised effective dose values (normal 1) are compared, the old GE 9000HP scanner shows the lowest value, while the GE

Sytec still shows the highest value.

Table 6.22:Summary of effective dose and normalised effective dose values for the most common scanning techniques of the abdomen & pelvis.

CT scanner	Examination	E (mSv)	kV	mAs	scan volume (mm)	Packing Factor	E normal 1	CTDI	E normal 2
GE 9000HP	Abdomen & pelvis	9.54	120	533	420	0.667	0.064	0.128	0.499
GE Sytec 3000 Plus	Abdomen & pelvis	32.81	120	351	380	1.000	0.246	0.352	0.699
GE HiSpeed Advantage	Abdomen & pelvis (1)	15.73	120	280	380	1.000	0.148	0.191	0.774
GE HiSpeed Advantage	Abdomen & pelvis (2)	6.81	120	150	380	1.000	0.119	0.191	0.626
GE HiSpeed Advantage	Abdomen & pelvis (3)*	4.95	120	150	343	0.769	0.125	0.191	0.654
Philips Tomoscan CX/S	Abdomen & pelvis	16.80	120	437	420	0.667	0.137	0.190	0.723
Siemens Somatom Plus	Abdomen & pelvis (1)	9.94	120	210	360	1.000	0.131	0.165	0.797
Siemens Somatom Plus	Abdomen & pelvis (2)	6.12	120	210	390	0.667	0.112	0.165	0.679
Siemens Somatom Plus	Abdomen & pelvis (3)	11.05	120	210	380	1.000	0.138	0.165	0.839
Siemens Somatom Plus	Abdomen & pelvis (4)*	7.25	120	210	312	1.000	0.111	0.165	0.671

E (normal1): Effective dose normalised to 100 mAs, 10mm scan volume, and packing factor of 1.
E (normal2): E (normal 1) normalised to the CTDI (mGy/mAs) measured with TLDs for 10 mm slice width.
* Spiral mode.

As can be seen in Table 6.22 there has been a variation by a factor of 5.3 between the absolute effective dose values for this examination among the CT scanners. If the variation factor of absolute effective dose value for the "abdomen and pelvis" examination is compared with that of the "head" and "chest" examinations, it will be noticed that the variation factor for this examination has been significantly high among the scanners. This reflects the wide range of scanning techniques used by different scanners for the routine "abdomen and pelvis" examination. On the other hand the effective dose value normalised to 100 mAs and 10 mm slice width shows a variation of 3.8 among the scanners. But if the effective dose values normalised to CTDI are compared, it will be noted that the there has been a variation factor of 1.68 among the scanners used for this examination.

As can be seen in Table 6.22, there have been two conventional and one spiral "abdomen & pelvis" examinations performed by the GE HiSpeed Advantage CT scanner. In the first conventional "abdomen & pelvis" examination a higher mAs setting has been used (Table 6.11) that has consequently resulted in a higher effective dose value than that of the first one. But there is also a significant difference (19%) between the normalised effective dose values to CTDI for these two conventional examinations. This difference may be due to changes in the scanner characteristics over the considerable time interval (six months) between the dose measurements. The spiral examination has been performed with the same mAs setting as the second conventional one, except that its pitch has been greater than one (1.3) and its scan volume length has been 40 mm (four scans) shorter (Table 6.11). Therefore the resultant absolute value of effective dose from the spiral examination has been significantly (~38%) lower. But, there has been no significant difference (< 7.6%) between the normalised effective dose values to CTDI for these examinations.

Three conventional and one spiral "abdomen & pelvis" examinations were measured on the Siemens CT scanner. Since the second conventional examination was performed with a couch increment (15 mm) bigger than the slice width (10 mm), it led to a significantly lower effective dose value, although its scan length was 30 mm (three slices) longer (Table 6.13). The third conventional "abdomen & pelvis" examination was only extended over 20 mm more scan length than that of the first one (Table 6.13). This consequently led to a higher effective dose value for this examination. The spiral "abdomen & pelvis" examination was performed over a shorter scan volume (~70 mm) but with a narrower slice width (3 mm) at the beginning followed by the most common slice width of 10 mm and the pitch value of one. As a result, as may be noted in Table 6.22, this special scanning technique led to a significantly lower effective dose value. The range of differences between normalised effective dose values to CTDI for "abdomen and pelvis" examinations on this scanner was 1.1-1.25. This may be attributed to the experimental uncertainties (7.6%) and possible variation in the CT scanner characteristics. For this scanner it may be noted that the two lowest values of normalised doses to CTDI were for the second and the fourth examinations, which had the longest and smallest scan lengths

respectively. This tends to discount any significant influence of this parameter (scan length) on the overall results for the abdomen and pelvis examinations.

7. CT Dosimetry using the Monte Carlo Method and the Mathematical Anthropomorphic Phantom

7.1 Introduction

Generally, Monte Carlo (MC) is a mathematical technique employed to achieve random sampling of a known probability distribution with the aid of randomly generated numbers. One of the applications of this method is for studying photon and electron transport in matter that is used extensively in different fields of medical radiation physics such as, diagnostic X-ray physics, radiotherapy physics, nuclear medicine, microdosimetry, electron microscopy, and radiation dosimetry. Because of the extensive usage of this technique, many review articles have been published on the principles and applications of this technique. The reader is referred to the review published by Andreo (1991) on the application of the MC technique in medical radiation physics. This review is currently an update to the early works and almost a complete source of information.

For dosimetry purposes this mathematical technique has been applied by several workers to model exposure conditions during a range of routine, conventional X-ray examinations (Rosenstein 1976, Drexler et al. 1984, Shrimpton et al. 1991a). But, so far, there has only been two major efforts to apply this technique for CT dosimetry, one in Germany and the other one in the UK.

Following a field study (Panzer et al. 1989) conducted in 1989 by the GSF in the Federal Republic of Germany, Zankl and his colleagues (1991) implemented the MC technique for CT dosimetry. They compiled a catalogue of mean organ dose conversion factors (normalised to air kerma free in air on the axis of rotation) resulting from CT examinations. In this catalogue the doses are calculated for single axial transverse slices of 1 cm width throughout the body. This is used as a database from which organ doses resulting from a particular CT examination can be estimated by summing up the contribution to organ dose from each relevant slice. The calculations have been performed using a MC code simulating the photon transport in different materials in two different mathematical phantoms. Mean organ dose

conversion factors are given per organ and per single CT slice of 1 cm width in the sex specific mathematical phantoms of Adam (male) and Eva (female). The organ doses have been calculated for the type of CT scanners most commonly used in Germany and for three different radiation qualities (Zankl et al. 1992).

Likewise, in 1990 the NRPB carried out a survey of CT practice in the UK and used this method for estimation of CT doses (Shrimpton et al. 1991a, 1991b; Jones and Shrimpton 1991). They used a different mathematical phantom, in shape and size, and provided another data set for different types and models of most of the operating CT scanners in the UK before 1989. This also enables researchers to calculate organ doses and effective dose by measuring the CTDI free in air on the isocentre of these scanners. Many researchers (Shrimpton and Wall 1992, Felmlee et al. 1990, Geleijns et al. 1994) have used these data sets for estimating the patient doses for similar CT scanners.

However, it must be born in mind that the problem or limitation of this dosimetry approach is that data on other CT scanner models, in particular the newer ones, may not always be available. Although there have been some attempts for estimating organ doses and effective dose values for some modern CT scanner models, acquiring data for these models requires expertise in the MC technique as well as detailed information regarding the scanner design which may not be readily available.

Unfortunately, the data published by the NRPB is for those models of CT scanners which were in operation in the UK before 1989 (Shrimpton et al. 1991a, 1991b). This data does not include some of the more advanced and newer models surveyed in this study. Therefore, we were only able to implement this method for those rather older types and models of CT scanners. From all six CT scanners in this study, data were available for three rather older models. Two of these scanners were replaced with newer models in 1996 for which there was no data set available. Therefore we were not able to measure organ doses and effective dose values for three modern CT scanner models using the Monte Carlo dosimetry approach. For these scanners just the result of our CTDI measurements are presented in this chapter.

We used an existing computer programme (Le Heron 1993) that incorporates all data sets provided by the NRPB software report (Jones and Shrimpton 1993) combined with our own CTDI measurement to assess patient doses resulting from all routine CT examinations. The principles and results of applying this dosimetry approach will be presented in this chapter. In the following chapter these results will be analysed and compared with those from our developed direct CT dosimetry approach.

7.2 Materials and Methods

In CT dosimetry MC computer techniques are used to simulate the absorption and scattering of X-ray photons within a mathematical anthropomorphic phantom, yielding organ doses normalised to the free-in-air dose on the axis of rotation of the CT scanner, from which effective dose could be derived.

This has been carried out by the NRPB (Jones and Shrimpton 1991) through extending its existing computer programs for conventional X-ray examinations (Jones and Wall 1985) to model the complex rotational beam geometric characteristics of CT scanners.

Different factors affect the predicted dose distribution within the mathematical phantom. These include (but are not limited to): the radiation quality of the X-ray beam, the distance between the X-ray focus and the axis of rotation of the CT scanner, the use of pre-patient beam shaping filters, and CT scanner rotation degree. These factors vary, extensively, not only from one manufacturer to the other one, but also among different models of CT scanners from one manufacturer. Therefore, the NRPB carried out a series of MC calculations for 23 different sets of exposure conditions relating to 27 models of CT scanners. These scanners accounted for about 85% of all UK CT scanners up until 1989. In each set, 360° CT scans of every 5 mm transverse slab of the phantom have been simulated for a perfectly collimated beam of X-rays. These have provided, for all 208 such slabs of the phantom, estimates of normalised doses to 27 organs or regions of the interest in the phantom. The normalised doses are expressed in this catalogue as absorbed dose in the organs relative to the scanner central axis dose free in air

The radiation transport in the phantom has been calculated using a MC code following individual photon histories. The radiation interaction processes considered by the NRPB have been photoelectric absorption and Compton scattering. They have taken the cross section data for the photon interactions from several sources (Hubbell 1977, Knight and Roussin 1983, Hubbell 1982) and regarded energy as being deposited at the point of photon interaction (kerma approximation).

They have claimed that calculation for each slice has involved enough photon histories in order that the statistical uncertainty (standard error) in the normalised doses falls below 5% for all important organs receiving significant levels of radiation.

The absorbed doses are obtained by dividing the total amount of energy deposited in an organ by its mass. All doses presented in this catalogue are mean doses averaged over the whole organ or tissue, not doses only to that part of the organ included in the CT slice and irradiated directly.

All dose values in this catalogue are given as organ dose conversion factors, i.e., organ absorbed doses normalised to a measurable quantity. In the present catalogue this quantity is CT Dose Index (CTDI), expressed in air kerma free in air at the axis of rotation. These normalised organ dose data are published by the NRPB as NRPB-SR250 software report (Jones and Shrimpton 1993) that comprises 23 data files. These data files allow the calculation of organ doses and effective dose (or effective dose equivalent) from the CT scan parameters and central axis CTDI value in air for several different makes and models of CT scanners.

The existing computer program (CTDOSE by Le Heron 1993) used, is written to run on MSDOS computers. This program enables the calculation of organ doses and dose indices (effective dose and effective dose equivalent) for CT examinations performed on the NRPB selection (Shrimpton et al. 1991b) of common CT scanners. It uses 23 data files containing the results of MC calculations performed by the NRPB in the UK national survey (Jones and Shrimpton 1993). It requires entering the measured CTDI value, the CT radiological factors, and the phantom starting position of the proposed CT examination, to report the resultant organ or tissue doses, effective dose, and effective dose equivalent.

7.2.1 CTDI Measurements

As mentioned above in order to calculate the organ or tissue doses the measurement of the central axis CTDI value in air is required. This CTDI is different from the FDA (1985) definition of the CTDI, as mentioned in chapter two, that is normally used for QA measurements of CT scanners.

The definition of the CTDI as used by the NRPB (Shrimpton et al. 1991b) is:

$$\text{CTDI} = 1/w \int_{-\infty}^{+\infty} D(z)dz \qquad \text{(Equation 7.1)}$$

where w is the nominal slice width (thickness) and $\int_{-\infty}^{+\infty} D(z)dz$ is the line integral in the Z direction of the dose profile in air (the total area of the dose profile).

This index (CTDI) is measured using either a pencil (CT) ionisation chamber (IC) or a stack of TLDs positioned along the central axis of rotation of the CT scanner. TLDs are normally put inside a hollow and cylindrical plastic tube, long enough to cover the X-ray beam width. The sum of the TLD doses devided by the nominal slice width is equivalent to the CTDI value. But, for the pencil IC the product of the average dose by the chamber length is equivalent to the area under the CT dose profile (CTDI).

We used both of these measurement techniques and our estimates of CTDI values were obtained using both TLDs and pencil ICs. These measurements were carried out to determine the CTDI value in air for both the older scanner models for which MC data files were available from the NRPB national survey (Jones and Shrimpton 1993) and also for those rather modern models that were not included in the survey. The TLDs were used in order to be consistent with the NRPB method of CTDI measurement. The IC was also used firstly, because of its compatibility and ease of use. On the other hand this approach enabled us to compare these two dosimetry devices with each other to reach a conclusion about their performance and future use for the CTDI measurement.

7.2.1.1 CTDI Measurements with the TLD

The same type of TLD (LiF) that was used in our developed direct dosimetry approach (chapter 5) was also used for the CTDI measurements.

Calibration measurements were carried out on the TLDs for every CTDI measurement. The calibration procedure was carried out in the same way that was done for our developed direct CT dosimetry method. For this purpose a set of twenty TLDs were used from the same batch of the TLDs used for the CTDI measurement. These TLDs comprised ten non-dosed controls (exposed only to the background radiation) and ten dosed controls. The dosed controls were exposed at 100kV to a dose of approximately 20 mGy generated from a conventional X-ray machine. The reader is referred to chapter five for the details of the TLD calibration procedure.

Figure 7.1 and Figure 7.2 show the design of the plastic tube and the device used in this study for CTDI measurements with the TLDs. Figure 7.3 shows a photograph of the device and a box of the TLDs used for CTDI measurements.

The TLDs were put in the specially designed plastic tube as shown in Figure 7.2. Then the tube was engaged into a hole in the end of the horizontal arm of the jig as shown in Figure 7.2. The position of the horizontal arm of the jig was adjusted in a way that it will always stay on the central axis of the rotation of CT scanners. In order to achieve the best CT dose profile, for each slice width, sufficient TLDs were used to encompass completely the whole CT dose profile.

Then for a contiguous stack of TLDs of sufficient length to encompass completely the CT dose profile, the approximation of Equation 6.1 was used as follows:

$$\text{CTDI} = \sum_{n} (Di.t) \Big/ w \qquad \text{(Equation 7.2)}$$

where D_i is the dose to ith TLD and t is the (effective) thickness of each TLD. The CTDI values were estimated for different CT protocols for all the CT scanners in this study.

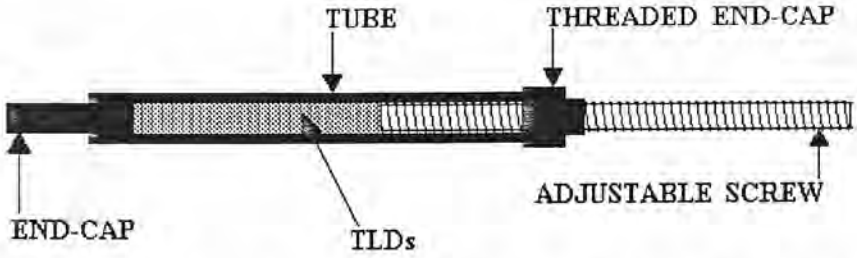

Figure 7.1: The design of the plastic tube that held TLDs for CTDI measurement.

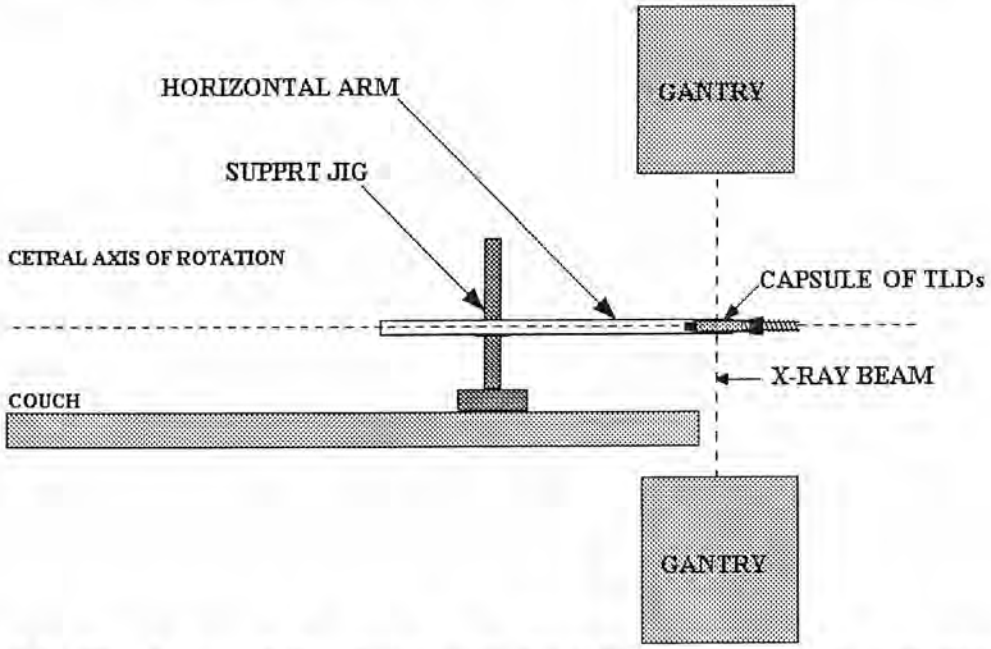

Figure 7.2: The design of the device used for CTDI measurements. For more explanation refer to the text.

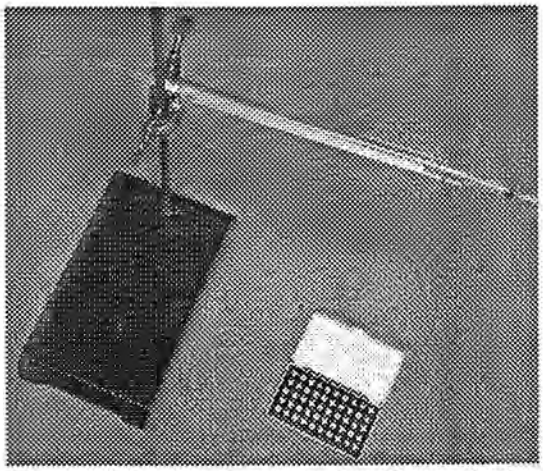

Figure 7.3: A photograph of the device and a box of the TLDs used for CTDI measurements.

7.2.1.2 CTDI Measurement with the Pencil Ionisation Chamber

If the only purpose of the CTDI measurements would be to derive the integral dose value, and not the dose profile, it is easier and more versatile to use a pencil IC. A "Radcal® 20X5-10.3CT" model pencil IC was also used for the CTDI measurements. Figure 7.4 illustrates this chamber and Figure 7.5 shows its physical dimensions.

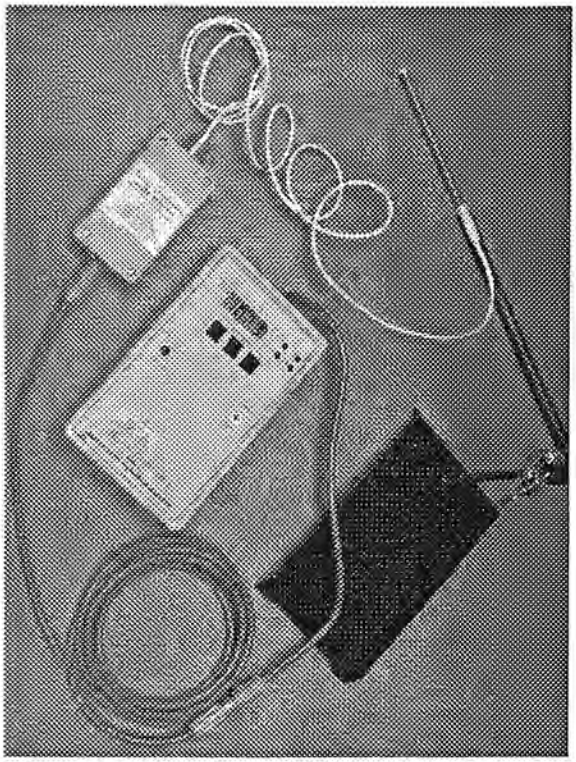

Figure 7.4: The Model 20X5-10.3CT Radcal ® pencil ionisation chamber.

The Radcal pencil IC is mounted at the end of a two meter cable, and an adapter is also included for use with QA (head or body) phantoms. Three red circle marks on the chamber body indicate the active volume and centre line of the chamber for set-up convenience. It has a Polycetal exterior cap, air equivalent walls and electrode, nominally 10 cm active length, and 3 cm^3 active volume. Its energy dependence is claimed to be within ±5% (for 3-20 mm Al HVL[1]).

---

[1] **Half Value Layer**

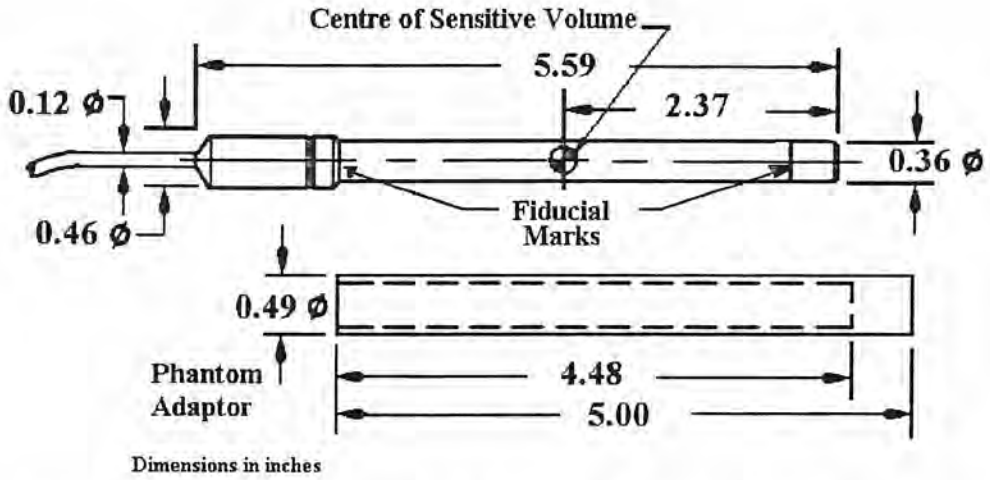

Figure 7.5: Physical Dimensions of the Radcal ® 20X5-10.3CT model pencil ionisation chamber.

Figure 7.6 shows the chamber energy dependence provided by the manufacturer. It is also claimed that it could measure integrated exposures from 0.1 mR to 199.9 R.

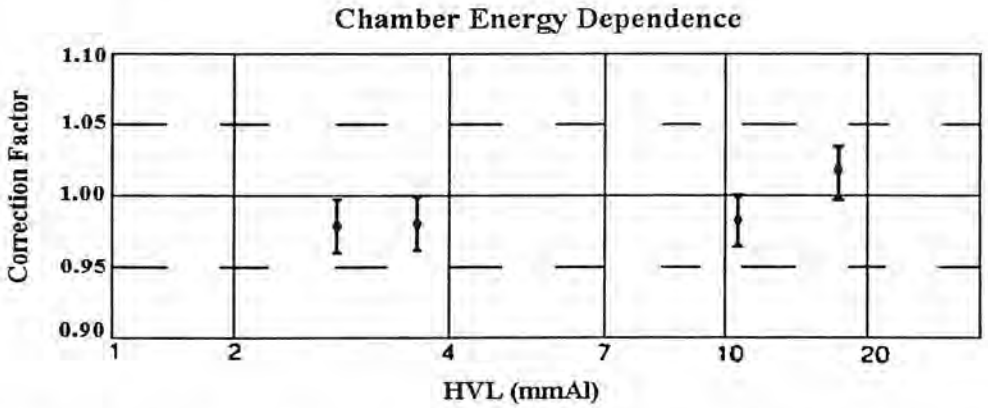

Figure 7.6: Radcal ® 20X5-10.3CT model pencil ionisation chamber energy response.

It has been indicated by the manufacturer that this chamber has been calibrated with a moderately-filtered X-ray at 150 kV and 10.2 mm Al HVL after temperature and pressure correction and its calibration accuracy is claimed to be ±4%. However some uncertainties were raised when the measured CTDI values with this chamber were compared with the TLD results. Therefore the chamber was first calibrated locally against a 3 cm^3 Radcal® 2025 model ionisation chamber which had a traceable calibration. The same radiological parameters used for TLD calibration were also used

for the calibration of this chamber and the temperature and pressure correction factors were also taken into account. Later on another pencil IC (Keithley) became available which had been calibrated at the John Perry Lab. We calibrated the Radcal chamber against this chamber. The cross calibration carried out in a radiographic output of 120 kV and 20 mAs. This led to a calibration factor of 0.995 for the Radcal pencil IC.

Using the pencil IC, the CTDI value could be approximated by the following equation:

$$CTDI = (D \times L) / w \qquad \text{(Equation 7.3)}$$

where D is the absorbed dose value calculated by multiplying the chamber reading in roentgen and the roentgen to absorbed dose conversion factor, L is the active length of the chamber (100 mm) and w is the nominal slice width. The value for the roentgen to absorbed dose conversion factor was assumed to be 8.73 mGy/R based on the definition (ICRU 1980) of the roentgen (2.58×10-4 C/Kg), and the reported value (ICRU 1979) of the average energy (33.85 J/C) required to create an ion pair in air.

7.2.2 Organ and Tissue Doses and Effective Dose Calculations

Having measured the in air CTDI data for a particular scanner under the condition of exposure used for a CT examination, estimates of organ doses and patient dose could be determined using the NRPB data set for the scanner. The NRPB data sets have been published in the format of data files on a floppy disk as the NRPB-SR250 software report (Jones and Shrimpton 1993). The data files are provided in look-up tables in the form of organ dose per 5 mm slabs of the mathematical anthropomorphic phantom, normalised in unit CTDI at the centre of rotation of the CT scanner in air. However, several steps are required to be carried out in order to be able to use these normalised organ dose data to estimate patient dose. These include specifying scan volume and calculating: total normalised organ doses, packing factor, CTDI, organ doses, and finally total patient dose. The reader is referred to the NRPB-SR250 report for a full explanation and the required approach

for carrying out these steps to estimate patient doses from CT examinations using these CT scanners.

As explained earlier we used an available computer programme called CTDOSE (Le Heron 1993) enabling the calculation of organ doses and dose indices for CT examinations performed on NRPB selection of common CT scanners. This program has incorporated all NRPB data files (Jones and Shrimpton 1993) in the NRPB look-up tables. In this computer program, the organ doses for a CT examination, using a particular scanner, are obtained by summing dose contributions over the extent of the examination. In addition the ICRP dose indices are calculated. It just requires to determine which 5 mm slabs are included in the scan volume for a particular examination protocol. To do this the program requires input data including: the scanner make and model, exposure setting (mAs), slice width, couch increment (or table feed), number of slices, normalised CTDI value per mAs (free in air), and finally the start position of the scan series. The output data of the program are: the dose to the individual organs or tissues, and estimates of the effective dose (ICRP 1991) and effective dose equivalent (ICRP 1977).

Except for the start position of the scan series, all other required input data are standard for each CT examination and quite straightforward to define for any particular CT examination. In order to determine the start position, data from the NRPB Mathematical phantom must be used. This phantom, illustrated in Figure 7.7, has already been described in chapter two. The NRPB gives a reference plane for each examination, the upper, and lower extremes. These are given in Table 7.1. For each examination, the total scan length is determined from the couch increment, slice width, and number of slices. The scan start position is then placed so that the scans are equidistant each side of the reference plane (Poletti 1992).

In the CTDOSE program the base of the trunk of the mathematical phantom is assigned a value of 0 mm and the top of the head 940 mm (Figure 7.7), while in the original NRPB phantom the base of the trunk is set at 100 mm and the top of the head as 1040 mm. Therefore for entering the start position in this program for each CT examination these changes were taken into account. Furthermore some guidance was

also taken from anatomical landmarks such as the diaphragm, lung apices, and other organs' location for this purpose (Table 7.2).

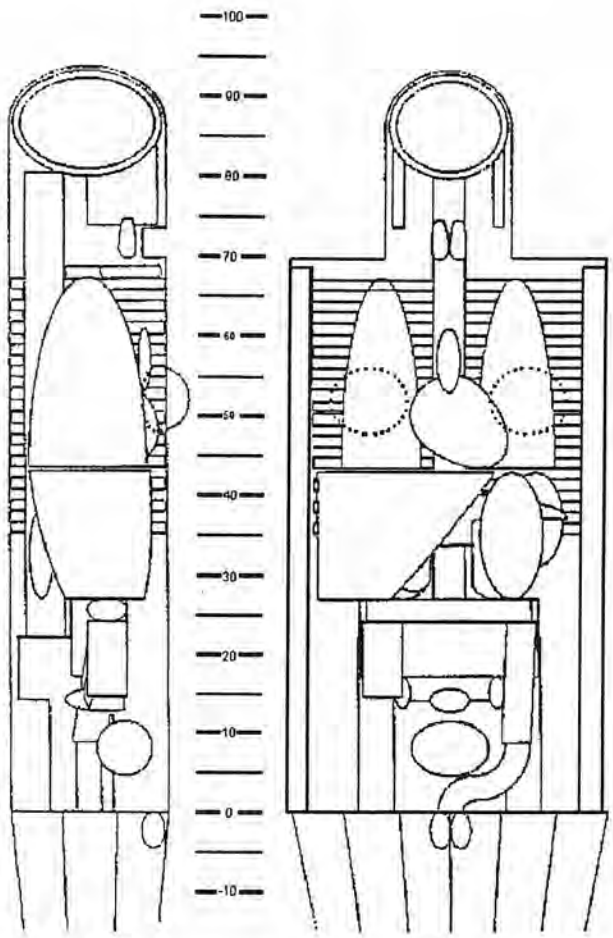

Figure 7.7: Lateral and anterior view of the adult mathematical phantom used in the CTDOSE program. The axis numbers are in cm from the base of the trunk. For more explanation refer to the text.

Table 7.1: Standard Planes for different types of CT Examinations referred to the NRPB mathematical phantom (Source: Poletti 1992).

Examination	Distance from Base of Trunk (cm)		
	Reference Plane	Lower Plane	Upper Plane
Routine head	86.5	76.0	92.5
Posterior fossa	82.5	79.5	86.0
Orbit	83.5	81.5	86.0
Routine chest	55.0	26.5	67.0
Routine abdomen	34.5	0.0	43.5
Routine pelvis	13.5	0.0	43.5
Liver	35.0	21.0	43.5
Lumbar spine	27.0	21.0	35.5

Table 7.2: Extent (lower and upper limits in mm) of organs and tissues of the mathematical phantom as modified in the CTDOSE program.

ORGAN / TISSUE	LOWER LIMIT	UPPER LIMIT
LEG BONES - UPPER	-100	0
ARM BONES - UPPER	508	680
ARM BONES - MIDDLE	335	508
ARM BONES - LOWER	0	440
PELVIS	0	510
SPINE - UPPER	700	805
SPINE - MIDLLE	341	690
SPINE - LOWER	220	341
SCALL - CRANIUM	810	925
SCALL - FACIAL	730	857
RIBS	341	663
CLAVILES	665	670
SCLAPULAE	449	663
ADRENALS	380	420
BRAIN	801	916
BREASTS	469	551
GALL BLADDER	269	366
STOMACH	270	420
SMALL INTESTINE	170	260
ASCENDING COLON	135	230
TRANSVERSE COLON	240	260
DESCENDING COLON	87	230
SIGMOID COLON	0	87
HEART	426	541
KIDNEYS	270	370
LIVER	270	420
LUNGS	425	665
OVARIES	130	160
PANCREAS	327	403
SPLEEN	310	420
TESTICLES	-44	-90
THYMUS	530	600
THYROID	700	740
UTERUS	115	135
URINARY BLADDER	25	105
LEG REGION	-100	-90
TRUNK REGION	0	690
HEAD REGION	700	930

7.3 CTDI Results

The CTDI measurements were carried out for all the slice width settings for all the CT scanners models. Both types of common dosimeters, TLDs and pencil IC, were used for these measurements.

As will be noted in section 7.4, to implement the MC dosimetry approach in accordance with the technique adopted by the NRPB, the CTDI values estimated by

the TLD measuring technique were used for the calculation of organs and effective dose values. In addition the pencil IC was not available to us at the beginning of this study. However, when the IC became available, it was used in parallel with the TLDs as much as possible.

As will be noted below, there was a time delay between the TLD and the IC measurements for some of the GE scanners. This was because the IC was not available when the CTDI measurements were started. Furthermore, just after carrying out the CTDI measurements with the IC, these scanners were either taken out of service or replaced with the newer models and were not accessible anymore. Consequently, we were not able to use both of the dosimeters, TLDs and pencil IC, for the CTDI estimation on these scanners at the same time.

An advantage of using TLDs is that in addition to the measurement of CTDI, it enables us to measure the CT dose profile and beam width. However, because the thickness of the TLD chip is a significant proportion of the slice width, the method of integration of dose profile can affect the accuracy with which CTDI is calculated. The NRPB method is simply to sum the readings of the TLDs as explained earlier in this chapter. Recently other researchers (Schofield et al. 1996) have integrated CTDI using a gaussian curve fitted to the data. We also applied this CTDI measuring technique to our measured TLD data. For simplicity the three CTDI measuring techniques employed in this study will be referred to as the TLD, the gaussian, and the IC measuring technique in the rest of this chapter.

In this section our measured CTDI values using both types of the dosimeters will be presented and compared with each other for every model of the CT scanners in this study. For those rather older models, included in the NRPB national survey of CT practice in the UK (Shrimpton et al. 1991b), our measured CTDI values will also be compared with the NRPB mean values for the same model.

7.3.1 CTDI values

Table 7.3 and Table 7.4 show all individual CTDI values estimated with the IC and TLDs respectively, for all the CT scanners, for different conditions of exposures and slice widths. In addition the mean, minimum, maximum, and maximum to

minimum ratios of the calculated CTDI values are presented in these table for every CT scanner.

Table 7.5 shows the NRPB reported CTDI mean values from the survey of CT practice in the UK (Shrimpton et al. 1991b) for three CT scanners included in this study.

Table 7.3: Estimated CTDI values (mGy/mAs using IC) for all conditions and all makes and models of CT scanners.

Slice width (mm)	GE 8800 (120 kV)		GE 9000HP (120 kV)		GE SYTEC	GE HiSpeed Advantage				Philips CX/S	Siemens Somatom Plus	
	HEAD	BODY	HEAD	BODY	(120 kV)	80 kV	100kV	120kV	140kV	(120 kV)	120kV	137kV
10	0.218	0.230	0.136	0.128	0.377	0.083	0.135	0.203	0.275	0.186	0.117	0.157
7	-	-	-	-	-	0.084	0.135	0.204	0.277	-	0.125	0.165
5	0.217	0.229	0.135	0.128	0.376	0.083	0.135	0.204	0.277	0.185	0.123	0.163
3	-	-	-	-	0.399	0.087	0.141	0.213	0.291	-	0.128	0.171
2	-	-	-	0.125	-	-	-	-	-	0.201	-	-
1.5	0.241	0.254	0.132	-	-	-	-	-	-	-	-	-
1	-	-	-	-	0.501	0.087	0.145	0.221	0.309	-	0.168	0.274
MEAN	0.225	0.238	0.134	0.127	0.413	0.085	0.138	0.209	0.286	0.191	0.132	0.186
MIN	0.217	0.229	0.132	0.125	0.376	0.083	0.135	0.203	0.275	0.185	0.117	0.157
MAX	0.241	0.254	0.136	0.128	0.501	0.087	0.145	0.221	0.309	0.201	0.168	0.274
MAX/MIN	1.1	1.1	1.0	1.0	1.3	1.0	1.1	1.1	1.1	1.1	1.4	1.7

Table 7.4: Estimated CTDI values (mGy/mAs using TLDs) for all conditions and all makes and models of CT scanners.

Slice width (mm)	GE 8800 (120 kV)		GE 9000HP (120 kV)		GE SYTEC	GE HiSpeed Advantage				Philips CX/S	Siemens Somatom Plus	
	HEAD	BODY	HEAD	BODY	(120 kV)	80 kV	100kV	120kV	140kV	(120 kV)	120kV	137kV
10	0.191	0.192	0.123	0.128	0.352	0.077	0.139	0.191	0.259	0.190	0.123	0.162
7	-	-	-	-	-	0.079	0.131	0.194	0.264	-	0.130	0.165
5	0.187	0.196	0.122	0.129	0.370	0.081	0.140	0.191	0.266	0.184	0.129	0.170
3	-	-	-	-	0.386	0.082	0.143	0.199	0.278	-	0.137	0.175
2	-	-	0.119	0.120	-	-	-	-	-	0.203	-	-
1.5	0.209	0.218	-	-	-	-	-	-	-	-	-	-
1	-	-	-	-	0.520	0.083	0.148	0.213	0.305	-	0.182	0.282
MEAN	0.196	0.202	0.121	0.126	0.407	0.080	0.138	0.194	0.267	0.192	0.140	0.191
MIN	0.187	0.192	0.119	0.120	0.352	0.077	0.131	0.191	0.259	0.184	0.123	0.162
MAX	0.209	0.218	0.123	0.129	0.520	0.082	0.143	0.199	0.278	0.203	0.187	0.282
MAX/MIN	1.1	1.1	1.0	1.1	1.5	1.1	1.1	1.0	1.1	1.1	1.5	1.7

Table 7.5: The NRPB mean CTDI values (mGy/mAs) for three CT scanner models.

Slice width (mm)	GE 8800 (120 kV)		GE 9000HP (120 kV)		Philips CX/S (120 kV)
	HEAD	BODY	HEAD	BODY	
10	0.117	0.121	0.108	0.113	0.191
5	0.136	0.144	0.107	0.122	0.187
2	-	-	0.111	0.096	0.220
1.5	0.135	0.176	-	-	-

Figure 7.8 demonstrates the differences between our estimated CTDI values with the TLDs and the IC and the NRPB mean CTDI values for the GE 8800 scanner. The results show that, our TLD measurements indicate a lower CTDI value (between 13%-17%) compare with that obtained with the pencil IC for this scanner. In addition, our CTDI values resulting from the TLDs were 24%-63% more than the reported mean values and even more than the maximum values reported by the NRPB for this CT scanner (Shrimpton et al. 1991b). It must be noted that there was a time period of three weeks due to the constraints explained above between our TLD and IC measurements.

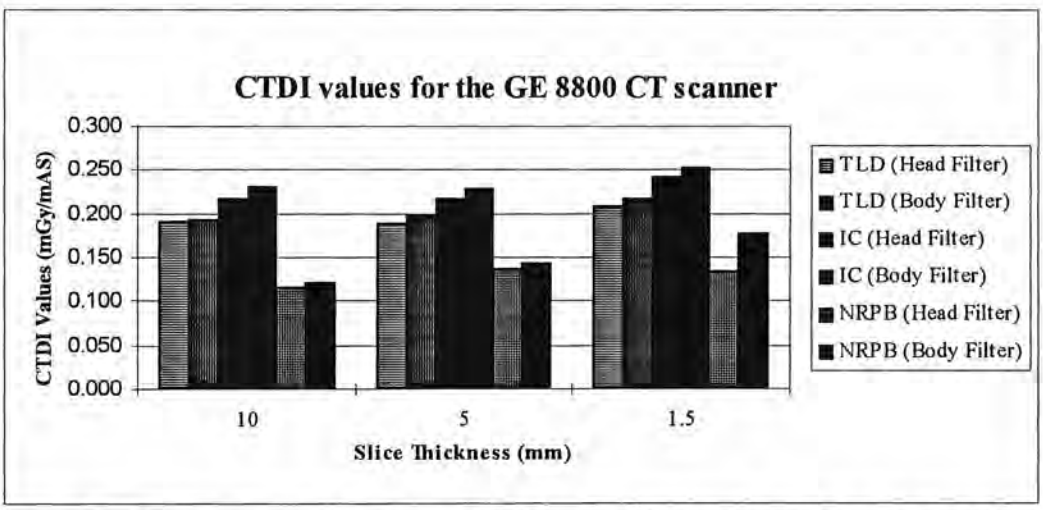

Figure 7.8: Comparison of measured CTDI values (using the TLDs and the IC) with the NRPB mean values (Shrimpton et al. 1991b).

Figure 7.9 illustrates the differences between our estimated CTDI values with the TLDs and the IC and the NRPB mean CTDI values for the GE 9000HP scanner. These results indicate that the TLD measurements showed a lower CTDI value (between 4%-9%) compared with the pencil IC. However, the CTDI values resulting from the TLDs were up to 25% higher than the CTDI mean values and most of them

were around the maximum CTDI values reported by the NRPB for this model (Shrimpton et al. 1991b). The maximum discrepancy was for the 2 mm slice width. This measurement was repeated and confirmed the above gap between our CTDI values and the NRPB reported value being derived from the measurement on only two similar CT scanners in the UK national survey of CT practice (Shrimpton et al. 1991b). It must be noted that there was a considerable time gap (four months) between the TLDs and the IC measurements due to the constraints mentioned earlier. However, we were able to repeat the CTDI measurements for 10 mm (HEAD filter) and 5 mm slice widths (BODY filter) using both dosimeters, the TLDs and the IC, at the same time on this scanner. Nevertheless, the TLDs gave about 10% lower CTDI values than that of the IC.

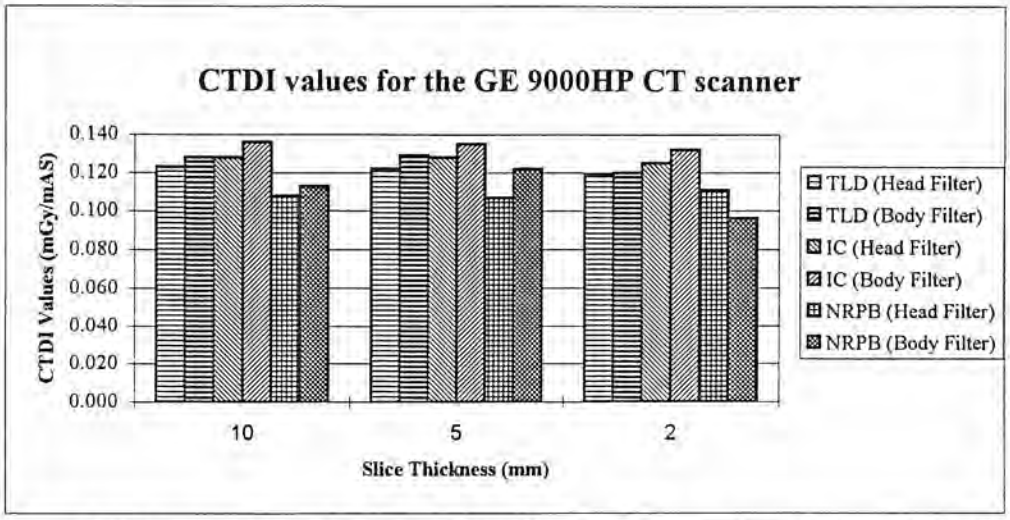

Figure 7.9: Comparison of measured CTDI values (using the TLDs sand the IC) with the NRPB mean values (Shrimpton et al. 1991b).

Our estimated CTDI values with the TLDs and the IC and the NRPB CTDI mean values are illustrated in Figure 7.10 for the Philips Tomoscan CX/S scanner. These results indicate that there was no significant difference between the CTDI values resulting from the TLDs with those derived from the IC. It must be born in mind that we were able to carry out both of the CTDI measurement techniques (the TLDs and the IC) at the same time on this scanner. The differences between our measured CTDI values using the TLDs and the NRPB mean values are not significant in view of the reported range of minimum and maximum values for this model. The

maximum discrepancy was for the 2 mm slice width for which, the NRPB mean CTD value was about 10% higher than our CTDI estimates for this scanner.

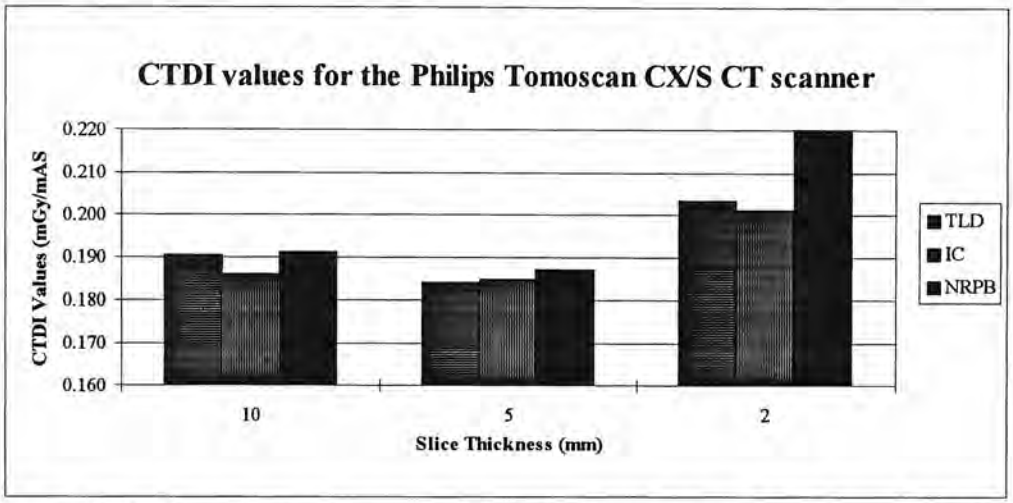

Figure 7.10: Comparison of measured CTDI values (using the TLDs and the IC) with the NRPB mean values (Shrimpton et al. 1991b).

Figure 7.11 shows our estimated CTDI values with the TLDs and the IC for the Siemens Somatom Plus scanner. Since this scanner was not included in the NRPB survey of CT practice, we were not able to compare our measured CTDI values with the NRPB mean values. Although the results indicated that the TLDs gave a CTDI value of up to 8% higher than that resulting from the IC, the differences were not statistically significant. There was no time gap between the TLDs and the IC measurements for this scanner.

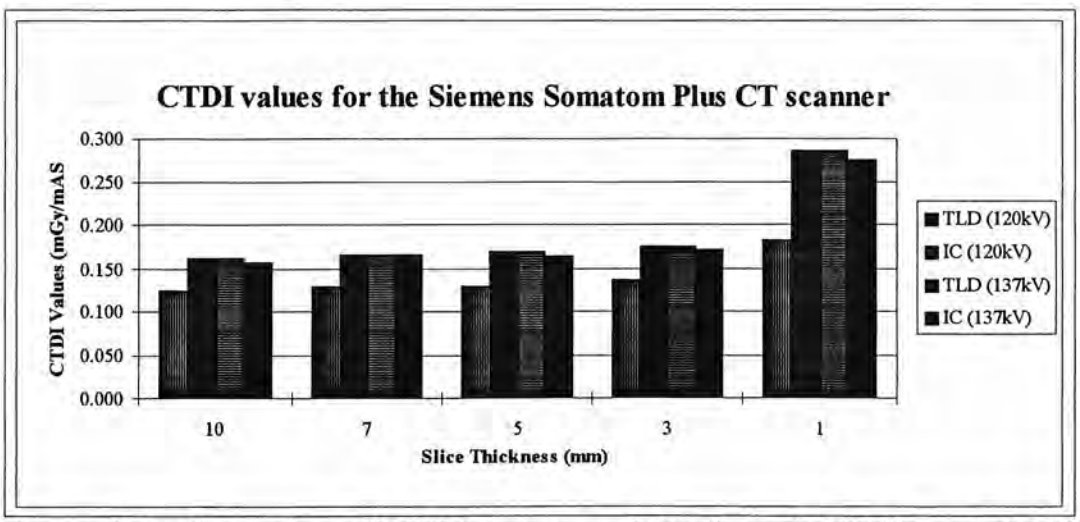

Figure 7.11: Comparison of CTDI values resulting from the TLDs and the IC measurements.

Our estimated CTDI values with the TLDs and the IC are shown in Figure 7.12 for the GE Sytec 3000 Plus Scanner. This scanner, installed in 1993, was not included in the NRPB survey of CT practice. Therefore there was no reported mean value by the NRPB for this scanner to enable us to compare our results with. Our results indicate that there was no significant difference between the CTDI values resulting from the TLDs and those derived from the IC measurements. It must be considered that both of the CTDI measurement techniques (the TLDs and the IC) were carried out at the same time on this scanner.

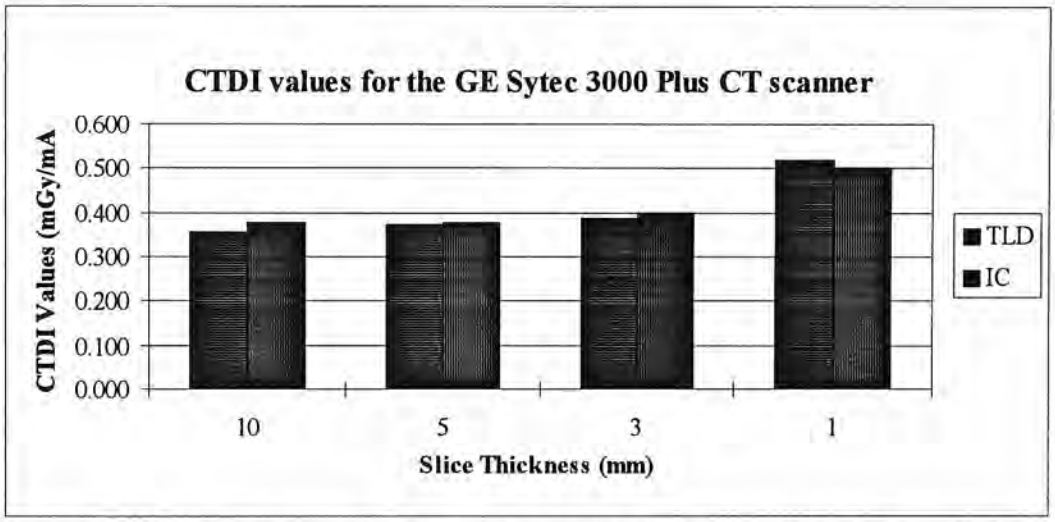

Figure 7.12: Comparison of CTDI values resulting from the TLDs and the IC measurements.

Figure 7.13 demonstrates the differences among our measured CTDI values, due to choosing different slice width and kV values for the GE HiSpeed Advantage scanner. Although only the 120 kV setting was used for most of the routine CT examination protocols with this scanner, CTDI measurements were carried out for all possible combinations of kV and slice width settings available with this scanner. As could be noted our results indicate no significant difference between the CTDI values resulting from the TLDs with that of the IC. This was another modern CT model, installed in 1995, for which there was no mean CTDI value reported by the NRPB to enable us to compare our measured CTDI values with.

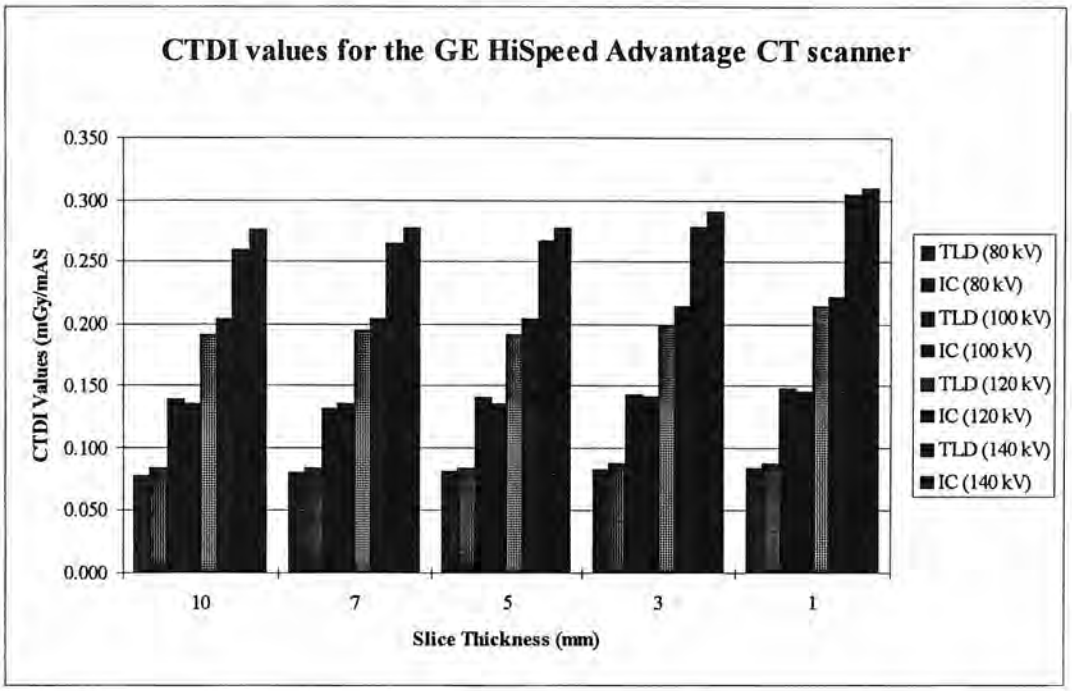

Figure 7.13: Comparison of CTDI values resulting from the TLDs and the IC measurements.

7.3.2 CTDI Analysis

In this section, first the variation of estimated CTDI values by different measuring techniques, used in this study, will be analysed and discussed. In this regard different measuring techniques used for estimating the CTDI values will be explained and the CTDI values resulting from the implementation of these measuring techniques will be analysed and their differences will be highlighted and explained. Then, the variation of estimated CTDI values by slice width will be analysed and discussed. Then, the effect of kV setting on the variation of estimated CTDI values will be explained. Then, the variation of the estimated CTDI values by scanner model will be described. Finally, the differences between our estimated CTDI values with the NRPB reported mean values for the scanners included in the national survey of CT practice in the UK (Shrimpton et al. 1991a, 1991b; Jones and Shrimpton 1991) will be discussed and summarised.

7.3.2.1 Variation of CTDI by Measuring Technique

As mentioned above, there are one IC and two TLD based measuring techniques used for the CTDI estimation. As may also be noted above, the length of the pencil IC used was 10 cm long. Therefore, the estimated CTDI values using the IC measuring technique was practically the average dose length product of the IC over 10 cm length, regardless of the slice width settings. On the other hand, as explained earlier in this chapter, for the TLD measuring technique just sufficient TLD chips were used in a way that the length of the stack of TLDs would be long enough to encompass at least three times the slice width settings. The widest slice width setting available with the CT scanners was 10 mm. Therefore, the estimated CTDI values using the TLD measuring technique was practically measured over 3 cm length. Hence, it was required to investigate the effect of different lengths used for the TLD and IC measuring techniques on the resultant estimated CTDI values. This was achieved by extending the resulting dose profiles from the TLD measurements over 10 cm length by using a suitable extrapolation process for all slice width settings and all the CT scanners. Hence, we had four sets of CTDI values for every condition of exposure and every slice width setting. These data sets were:

I. CTDI values resulting from the TLD measuring technique over 3 cm length (TLD I measuring technique),
II. CTDI values resulting from the TLD measuring technique extrapolated to 10 cm length (TLD II measuring technique),
III. CTDI values resulting from the gaussian measuring technique, and
IV. CTDI values resulting from the IC measuring technique.

Overall there were 53 data sets of CTDI measurements for different conditions of settings on all the CT scanners. As mentioned earlier at the beginning of this study the pencil IC was not available. When the IC became available we did not have enough access to two scanners (GE 8800 and GE 9000HP) that were shortly taken out service. Hence, we were not able to use both of the IC and TLD measuring techniques at the same time for CTDI estimation on these scanners. Consequently, there was a considerable time gap between the CTDI measurements with the TLDs with that of IC for 14 data sets. Therefore, there were 39 sets of measurements in

which the IC results could be compared directly with the TLDs for measuring CTDI values (Table 7.6). The average ratio of IC to TLD was 1.015 (range of 0.923 to 1.116) with a standard deviation of 4.9%. There was no significant difference in the ratios between different slice widths. The uncertainty in this ratio reflects the overall uncertainty in TLD reading, uncertainties in the measurements in the penumbra due to the profiles of the TLDs, and error with the integral method. The overall uncertainties in the estimation of the ratio (two times standard error of the mean; 2 × sem) was ± 0.015 which indicates that the difference is not significant. However the ratio appears to depend on the scanner (Table 7.7) . This may reflect uncertainties in the calibration factors on each of the measurement dates. The random uncertainties in the TLD calibration factor was approximately ± 3% (2 × sem).

Table 7.6: Comparison of the IC and the TLD (I) measuring techniques.

Slice width (mm)	10	3-7	< 3	All
No. of data sets	9	22	8	39
Average ratio	1.028	1.019	0.991	1.015
Standard deviation	0.056	0.046	0.038	0.049
2 × sem	0.038	0.020	0.027	0.016
Maximum	1.111	1.116	1.048	1.116
Minimum	0.951	0.934	0.923	0.923

Table 7.7: Comparison of the IC and the TLD (I) measuring techniques by CT scanner model.

CT scanner	GE 9000 HP	GE Sytec 3000	GE HiSpeed Advantage	Philips Tomoscan CX/S	Siemens Somatom Plus	All
No. of data sets	2	4	20	3	10	39
Average ratio	1.114	1.021	1.035	0.992	0.960	1.015
Standard deviation	0.002	0.039	0.035	0.011	0.021	0.049
2 × sem	0.004	0.039	0.015	0.013	0.013	0.016
Maximum	1.116	1.071	1.078	1.005	1.005	1.116
Minimum	1.111	0.963	0.964	0.979	0.979	0.923

As mentioned above, other writers have analysed the CTDI results by fitting a gaussian curve to the TLD data. The results of this analysis for 53 measurements gave a ratio between the methods of 1.016 ± 0.020, i.e. indicating no significant difference (Table 7.8). However, further analysis showed that this ratio depends on slice width.

The values for 10 mm slice widths, slice widths between 3 and 7 mm, and for slice widths of less than 3 mm were 1.109 ± 0.004, 1.018 ± 0.010 and 0.918 ± 0.023 respectively. The use of a gaussian curve is therefore incorrect.

Table 7.8: Comparison of the gaussian (TLD (III)) and TLD (I) measuring techniques.

Slice width (mm)	10	3-7	< 3	All
No. of data sets	13	27	13	53
Average ratio	1.109	1.018	0.918	1.016
Standard deviation	0.008	0.027	0.041	0.073
2 × sem	0.004	0.010	0.023	0.020
Maximum	1.122	1.063	0.948	1.122
Minimum	1.088	0.966	0.783	0.783

One reason for the relatively low CTDI value for the TLD measurements may have been the use of a more limited integration range. The IC integrates over the length of the chamber (100 mm), where the TLDs were used in a stack which was no more than three times the nominal slice width, i.e., a maximum length of 30 mm.

The TLD profiles were therefore extrapolated by fitting a curve to the measured TLD data over a 100 mm length. The average ratio of the results obtained by extrapolation, to those measured directly from the TLDs over 30 mm length, was 1.020 ± 0.005 (range 0.967-1.074) (Table 7.9).

Table 7.9: Comparison of the TLD (II) and TLD (I) measuring techniques.

Slice width (mm)	10	3-7	< 3	All
No. of data sets	13	27	13	53
Average ratio	1.018	1.023	1.016	1.020
Standard deviation	0.008	0.015	0.030	0.019
2 × sem	0.004	0.006	0.017	0.005
Maximum	1.039	1.063	1.074	1.074
Minimum	1.008	0.985	0.967	0.967

Overall from the analysis made above it could be concluded that there was no significant difference between the estimated CTDI values due to two different dosimeters (IC and TLDs) used. This conclusion is obviously subject to the application of both dosimeters without any considerable time gap during which the

CT scanner characteristics could be changed. In addition there was no significant difference between the CTDI integrated from the TLDs over 30 mm with that of 100 mm length. Therefore it is concluded that the longer length of the IC (100 mm) than that of the stack of TLDs (30 mm) does not have a significant effect on CTDI. On the other hand there was no significant difference between the CTDI estimated from the gaussian curve fitted to the TLD values with that resulting from the common TLD measuring technique. Nevertheless, more analysis confirmed that the ratio between the gaussian and the TLD measuring technique depended on slice width and the use of a gaussian curve is therefore incorrect.

7.3.2.2 Variation of CTDI by Slice Width

The integrated dose profile should be proportional to slice width on the assumption that the output profile across the slice is homogeneous, output is independent of width because of minimum scatter, and penumbra shape is not a function of width. Because CTDI is the integrated profile normalised to nominal slice width, it should therefore be constant for all slice widths for a particular scanner. Deviation from constancy indicates that the nominal slice widths may be in error. Normalising the data to the CTDI for a 10 mm slice width shows consistency (within 10%) for all scanners in the survey for slice widths greater than 2 mm (Table 7.10). However, for narrow slice widths some errors were noted. For the GE 8800 scanner the CTDI ratios between the 1.5 mm and 10 mm slice widths were 1.10 (for the HEAD filter) and 1.11 (for the BODY filter), indicating that the true slice width should be about 10% more than the nominal slice width of 1.5 mm. For the GE HiSpeed Advantage scanner, the CTDI for a 1 mm slice width relative to that of 10 mm, increased from 1.048 at 80 kV to 1.124 at 140 kV (Table 7.10) indicating that this error is energy dependent. This is presumably due to collimator leakage or increased scatter. This effect was also noted for the Siemens scanner in which the ratio between the 1 mm and 10 mm slice widths was 1.436 and 1.745 for 120 kV and 137 kV respectively (Table 7.10). The high ratio suggests that the true slice width at this setting was approximately 1.4 mm. A big discrepancy was also found for the GE Sytec scanner for which the CTDI of a 1 mm slice width was 33% greater than that

for the 10 mm slice width, indicating that the true slice width was approximately 1.3 mm. As could be noted in the table the ratios have not been influenced by the choice of the HEAD or the BODY filter for the GE 8800 and GE 9000HP scanners. Similar variation was observed in the estimated CTDI values using the TLDs by the slice width (Table 7.11).

Table 7.10: Ratios of estimated CTDI values (with the IC) to that of 10 mm slice width for all the CT scanners.

Slice widths (mm)	7	5	3	2	1.5	1
GE 8800 (BODY)	-	0.996	-	-	1.104	-
GE 8800 (HEAD)	-	0.995	-	-	1.106	-
GE 9000HP (BODY)	-	0.993	-	0.971	-	-
GE 9000HP (HEAD)	-	1.000	-	0.977	-	-
GE Sytec 3000 Plus	-	0.997	1.058	-	-	1.329
GE HiSpeed Advantage (80 kV)	1.012	1.000	1.048	-	-	1.048
GE HiSpeed Advantage (100 kV)	1.000	1.000	1.044	-	-	1.074
GE HiSpeed Advantage (120 kV)	1.005	1.005	1.049	-	-	1.089
GE HiSpeed Advantage (140 kV)	1.007	1.007	1.058	-	-	1.124
Philips Tomoscan CX/S	-	0.995	-	1.081	-	-
Siemens Somatom Plus (120 kV)	1.068	1.051	1.094	-	-	1.436
Siemens Somatom Plus (137 kV)	1.051	1.038	1.089	-	-	1.745

Table 7.11: Ratios of estimated CTDI values (with the TLDs) to that of 10 mm slice width for all the CT scanners.

Slice widths (mm)	7	5	3	2	1.5	1
GE 8800 (BODY)	-	1.021	-	-	1.135	-
GE 8800 (HEAD)	-	0.979	-	-	1.094	-
GE 9000HP (BODY)	-	0.992	-	0.967	-	-
GE 9000HP (HEAD)	-	1.008	-	0.938	-	-
GE Sytec 3000 Plus	-	1.051	1.097	-	-	1.477
GE HiSpeed Advantage (80 kV)	1.026	1.052	1.065	-	-	1.078
GE HiSpeed Advantage (100 kV)	0.942	1.007	1.029	-	-	1.065
GE HiSpeed Advantage (120 kV)	1.016	1.000	1.042	-	-	1.115
GE HiSpeed Advantage (140 kV)	1.019	1.027	1.073	-	-	1.178
Philips Tomoscan CX/S	-	0.968	-	1.068	-	-
Siemens Somatom Plus (120 kV)	1.057	1.049	1.114	-	-	1.480
Siemens Somatom Plus (137 kV)	1.051	1.038	1.089	-	-	1.741

The TLDs provided dose profiles enabling us to investigate about the variation of the CTDI values by the slice widths and to validate the nominal slice widths of the scanners.

Figure 7.14 - Figure 7.17 show a few samples of the recorded dose profiles by the TLDs for the widest and the narrowest slice width settings for the Siemens Somatom Plus CT scanner.

This allowed the calculation of the full width at half maximum (FWHM) value for the CT scanners.

As can be noted, the Siemens dose profiles presented in Figure 7.16 and Figure 7.17 indicate a significantly bigger FWHM value than the nominal slice widths for the narrowest slice width for the Siemens scanner.

Table 7.12 compares the narrowest nominal slice widths with their estimated FWHM based on the TLD measurements. These are compared with values referred from the IC measurements of CTDI. The IC values were calculated by multiplying the CTDI value normalised to the 10 mm width (from Table 7.10) by the nominal slice width. The assumption in the calculation is that the true slice width for the nominal 10 mm slice is correct and that the penumbra shapes of the dose profiles are identical for the largest and smallest slice width. There are significant uncertainties in the FWHM measured from the profiles for narrow slice widths because of the very poor resolution given by 0.85 mm thick TLDs in the measurements.

Table 7.12: A comparison between the nominal slice width with the FWHM and the true values derived from the dose profiles and CTDI ratios for the narrowest slice widths of all the CT scanners.

CT scanner	Option	slice width (mm)		
		nominal value	FWHM	IC value *
GE 8800	HEAD	1.5	2.01	1.65
	BODY	1.5	2.01	1.66
GE 9000HP	HEAD	2	2.21	1.94
	BODY	2	2.21	1.96
GE Sytec 3000 Plus	-	1	1.61	1.05
GE HiSpeed Advantage	80 kV	1	1.20	1.05
	100 kV	1	1.80	1.07
	120 kV	1	2.01	1.09
	140 kV	1	1.81	1.12
Philips Tomoscan CX/S	-	2	2.51	2.16
Siemens Somatom Plus	120 kV	1	1.61	1.44
	137 kV	1	2.01	1.75

* These values were calculated by multiplying the nominal slice widths by the CTDI ratios of the slice widths to that of the 10 mm (Table 7.10).

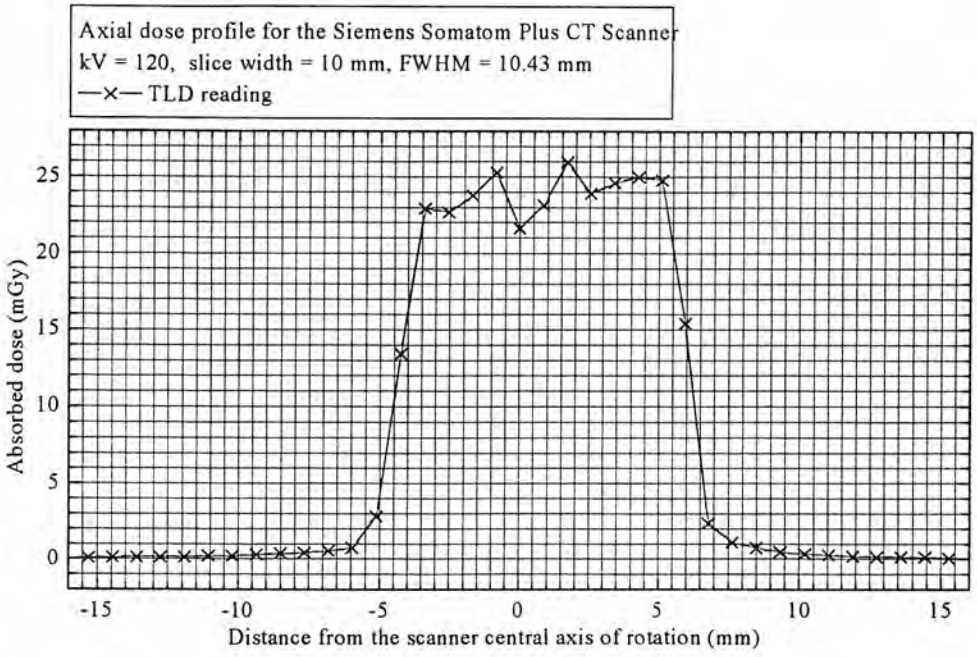

Figure 7.14: Free in air recorded dose profile for the Siemens Somatom Plus scanner (120 kV, 10 mm nominal slice width).

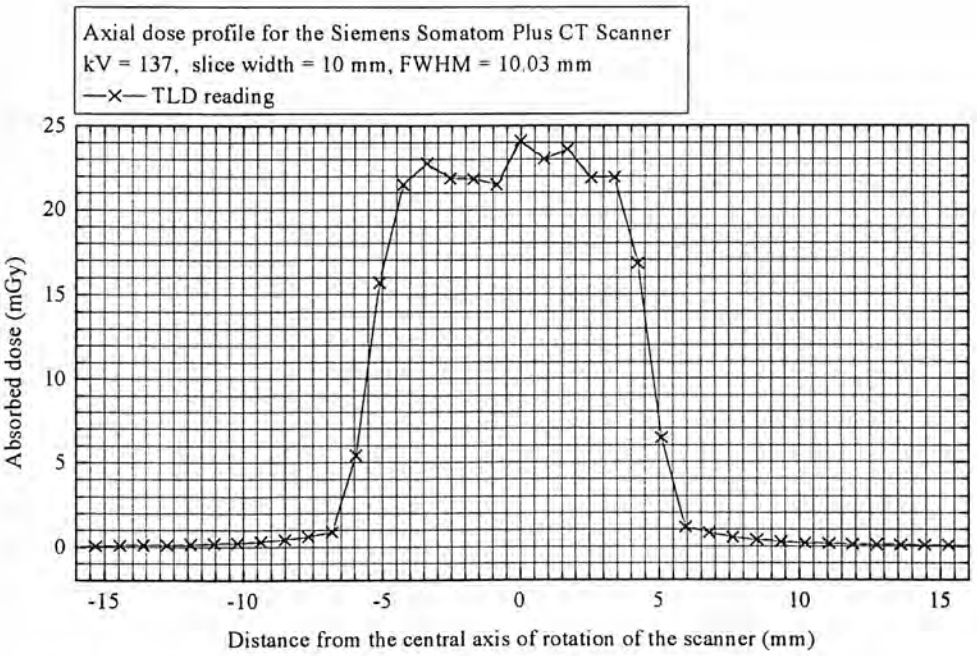

Figure 7.15: Free in air recorded dose profile for the Siemens Somatom Plus scanner (137 kV, 10 mm nominal slice width).

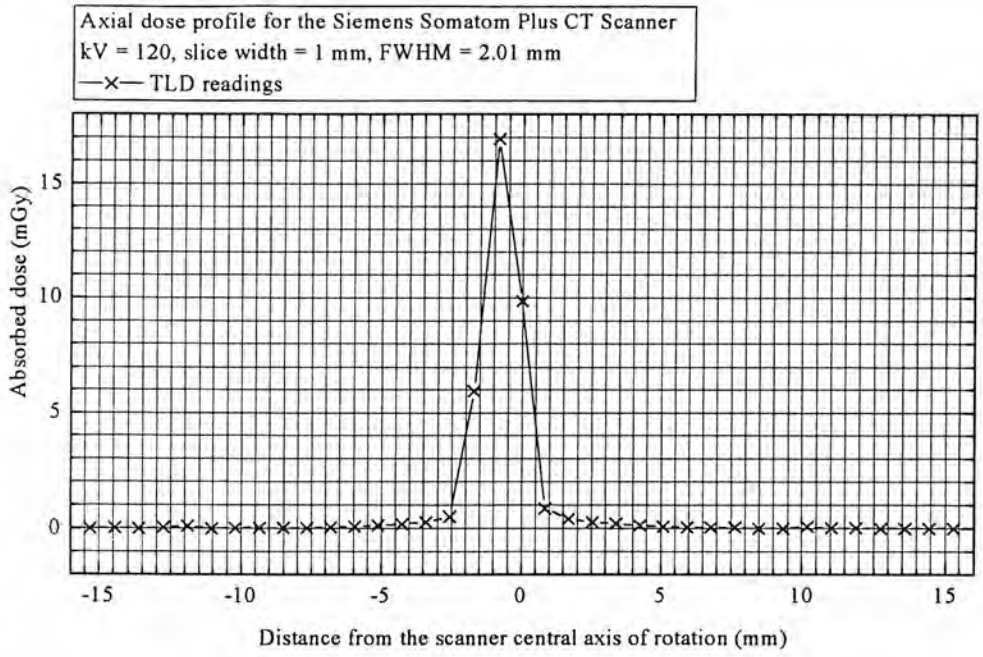

Figure 7.16: Free in air recorded dose profile for the Siemens Somatom Plus scanner (120 kV, 1 mm nominal slice width).

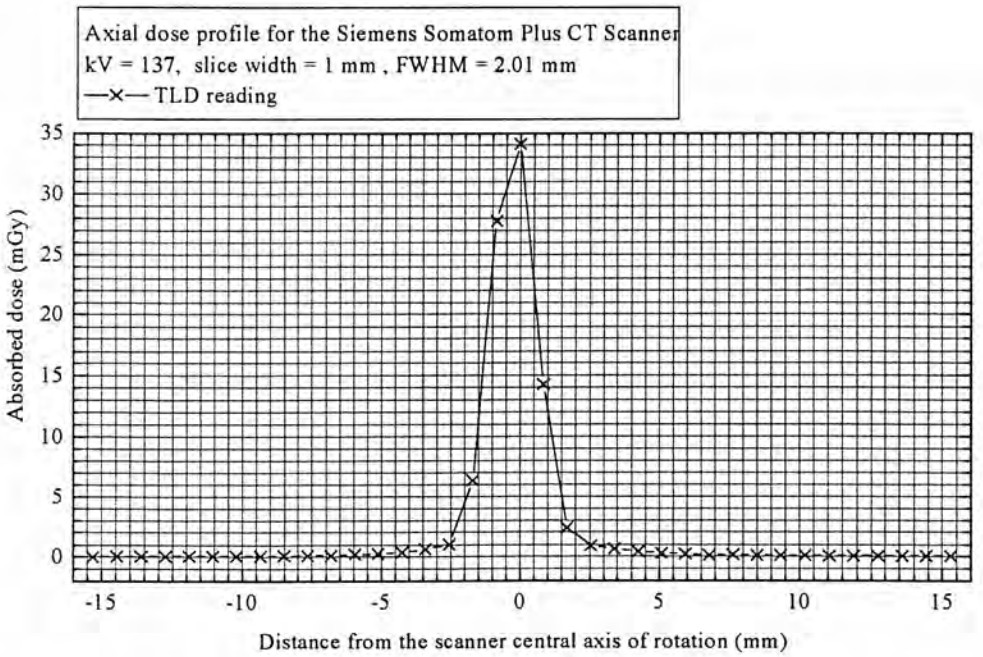

Figure 7.17: Free in air recorded dose profile for the Siemens Somatom Plus scanner (137 kV, 1 mm nominal slice width).

7.3.2.3 Variation of CTDI by Tube Potential

The GE HiSpeed Advantage and the Siemens Somatom Plus scanners had four and two tube potential settings available respectively. Variation of estimated CTDI values (with the IC) by the tube potential are summarised in Table 7.13 for these scanners. The data presented in this table were calculated from the CTDI values for five slice widths available with either of these scanners.

As could be seen in Table 7.13 the estimated CTDI value has significantly increased with the increase in the tube potential.

Table 7.7 and Figure 7.19 also demonstrate the variation of estimated CTDI values with the kV for the GE HiSpeed Advantage and the Siemens Somatom Plus scanner respectively.

Table 7.13: Variation of CTDI values (with the IC) by the kV.

CT scanner	GE HiSpeed Advantage			Siemens
kV ratio	100/80	120/80	140/80	137/120
No. of data sets	5	5	5	5
Average ratio	1.630	2.464	3.369	1.391
Standard deviation	0.022	0.044	0.104	0.135
2 × sem	0.020	0.039	0.093	0.120
Maximum	1.667	2.540	3.552	1.631
Minimum	1.607	2.429	3.298	1.320

Similar variation was observed in the estimated CTDI values with the TLDs by the tube potentials for these scanners (Table 7.14).

Table 7.14: Variation of CTDI values (with the TLDs) by the kV.

CT scanner	GE HiSpeed Advantage			Siemens
kV ratio	100/80	120/80	140/80	137/120
No. of data sets	5	5	5	5
Average ratio	1.744	2.457	3.411	1.346
Standard deviation	0.057	0.076	0.153	0.116
2 × sem	0.051	0.068	0.136	0.104
Maximum	1.805	2.566	3.675	1.549
Minimum	1.658	2.358	3.284	1.269

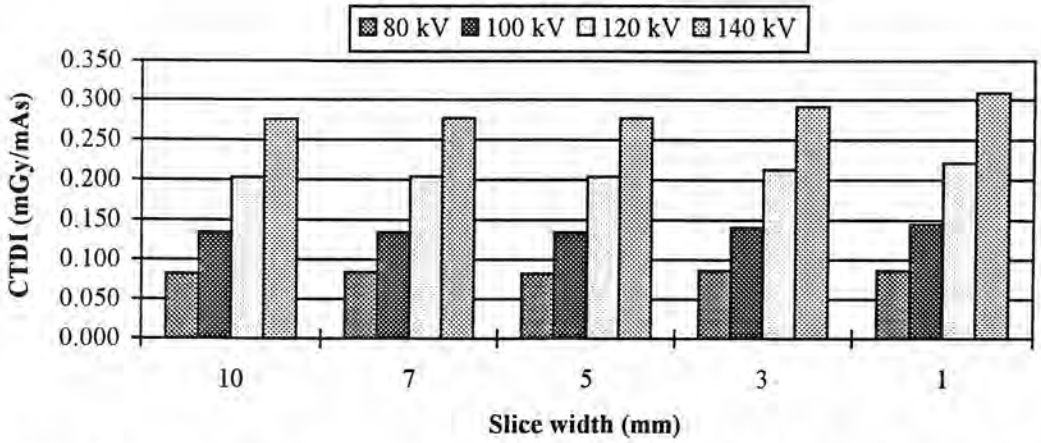

Figure 7.18: variation of estimated CTDI values (using IC) with the tube potential for the GE HiSpeed Advantage CT scanner.

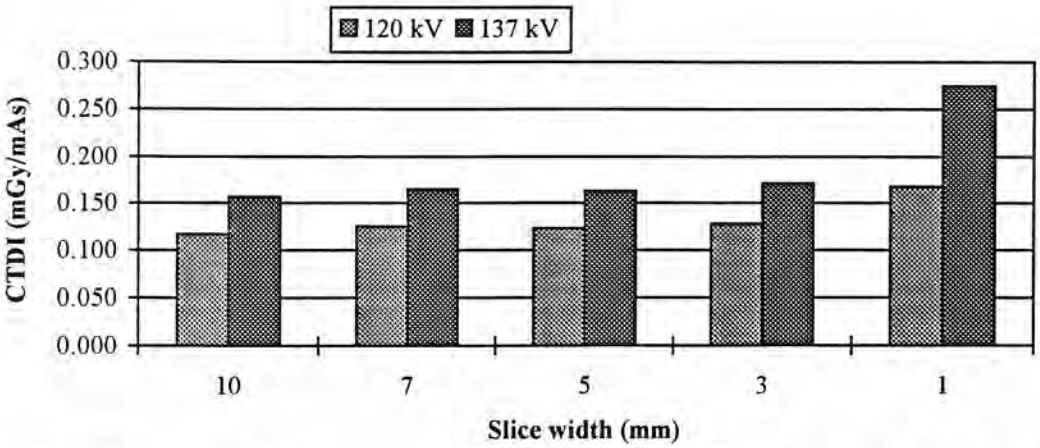

Figure 7.19: variation of estimated CTDI values (using IC) with the tube potential for the GE Siemens Somatom Plus CT Scanner.

7.3.2.4 Variation of CTDI by Scanner Model

Figure 7.20 and Figure 7.21 demonstrate variation of our measured CTDI values in air normalised to the exposure setting (mGy/mAs), using the TLDs, by scanner type and tube potential for the nominal slice width of 10 mm and 5 mm respectively. As can be seen in these figures the CTDI values vary considerably by the CT scanner make and model and also by the different kV settings used for a particular scanner.

Overall, for the nominal slice width of 10 mm (Figure 7.20) the modern model of GE HiSpeed Advantage (at 80 kV) shows the lowest CTDI value (0.077 mGy/mAs) and the GE Sytec 3000 model (at 120kV) shows the highest CTDI value (0.352 mGy/mAs). But if the CTDI values for the most common kV setting (120 kV) for all scanners are noted, although the GE Sytec again shows the highest value, the GE 9000HP model, with the head filter option, gives the lowest value (0.123 mGy/mAs). Similarly, for 5 mm nominal slice width (Figure 7.21), the GE HiSpeed Advantage (with 80 kV) shows the lowest (0.081 mGy/mAs) and the GE Sytec 3000 (with 120 kV) shows the highest (0.370 mGy/mAs) CTDI value. If the CTDI values for the most common kV setting (120kV) are compared with each other for 5 mm slice width, although again the GE Sytec 3000 demonstrates the highest value, the GE 9000HP scanner, with the head filter, shows the lowest value (0.122 mGy/mAs). It can be concluded that, the GE Sytec 3000 Plus gives the highest and the GE HiSpeed Advantage the lowest CTDI values for the same condition of exposures (120 kV and 5 or 10 mm slice width). In addition, it is noted that for both of these nominal slice width settings there is a significant variation up to a factor of 5 among our measured CTDI values for different types of CT scanners. This reflects differences in the scanners' beam geometry and radiation quality. Even for the same radiation quality a variation of up to a factor of 3 is noted between different types of the CT scanners.

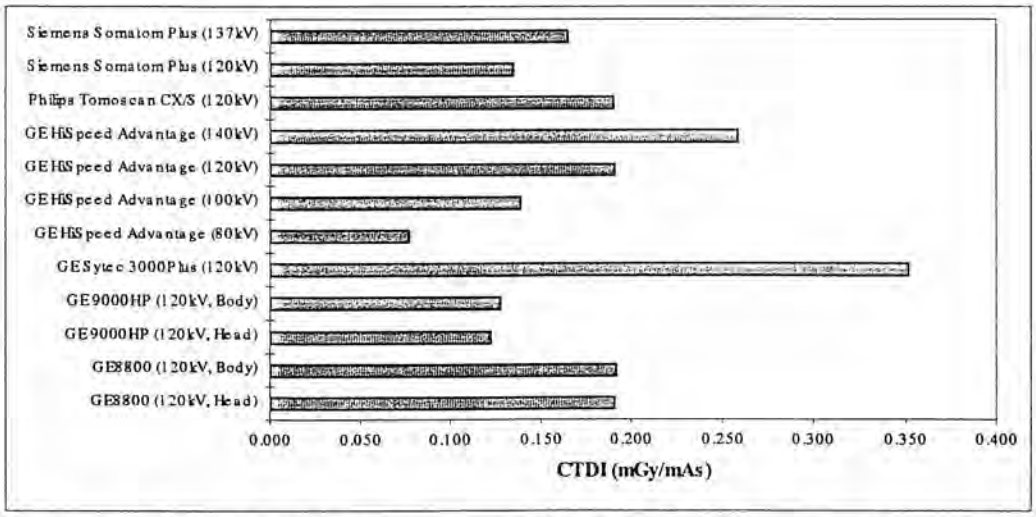

Figure 7.20: Variation of CTDI values by the type of CT scanner and kV (for 10 mm slice width).

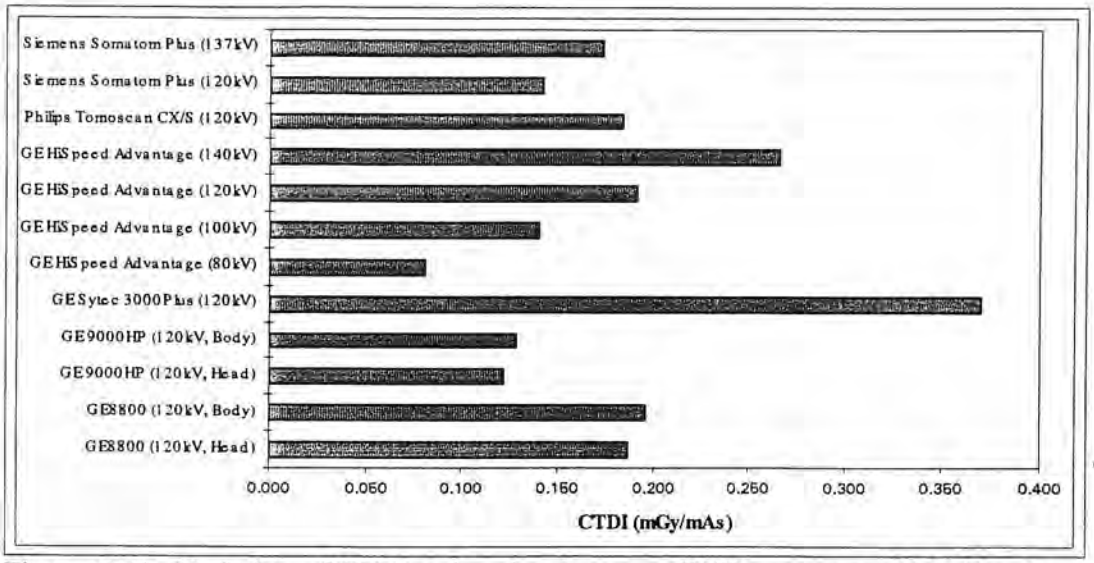

Figure 7.21: Variation of CTDI values by the type of CT scanner and kV (for 5 mm slice width).

As noted above there were discrepancies at smaller (< 2mm) slice widths. Therefore to demonstrate the variation of CTDI values among the CT scanners it is better to compare the estimated CTDI values for the 10 mm slice width and the most common tube potential (120 kV). In this regard the maximum, minimum, and maximum to minimum ratios of the CTDI values, measured with both types of the dosimeters, for these settings of the slice width and tube potential are summarised in Table 7.15.

Table 7.15: Variation of CTDI among the CT scanners (10 mm slice width, 120 kV)

CTDI measuring technique	(IC)	TLD (I)
Maximum	0.377	0.352
Minimum	0.117	0.123
Maximum/minimum ratio	3.2	2.9

As can be noted from the table, there was a significant variation in the estimated CTDI values, with both dosimetry devices (IC and TLD), among different makes and models of the CT scanners. This variation, being up to a factor of three, is due to differences in beam geometry, filtration, and radiation quality of the CT scanners. CTDI in air is principally a function of kV, filtration, and focus to central axis distance of the CT scanner.

7.3.2.5 Comparison of CTDI Values with the NRPB Mean Values

In this section our estimated CTDI values with the TLDs (for 10 mm slice width) have been compared with that of the NRPB from the national survey of CT practice in the UK (Shrimpton et al. 1991b). This has been done for the scanners included in the NRPB survey consisting of a GE 8800, a GE 9000HP, and a Philips Tomoscan CX/S scanner.

The ratios between our estimated CTDI values and the NRPB mean and maximum values for the same types and model of CT scanner have been calculated and presented in Table 7.16.

Table 7.16: Ratios between estimated CTDI values with the TLDs for all the CT scanners and the NRPB values (from the national survey of CT practice in the UK).

CT Scanner	Option	Mean	Max
GE 8800	HEAD	1.641	1.223
	BODY	1.579	1.282
GE 9000HP	HEAD	1.139	0.984
	BODY	1.133	0.992
Philips CX/S	-	0.995	0.913

Data presented in the above table show that our estimated CTDI values for the GE 8800 scanner has not only been more than the NRPB mean value but also significantly (22% HEAD and 28% BODY) higher than the NRPB maximum values. For the GE 9000HP scanner too, the above table shows that our estimated CTDI values have been significantly (14% HEAD, 13% BODY) higher than the NRPB mean values (Table 7.16). However, as may be noted in the table, the ratios show that our estimated CTDI values have been less than the NRPB maximum values (2% HEAD, 1% BODY) for this scanner. For the Philips Tomoscan CX/S scanner the table shows that our estimated CTDI value has been within 1% of the NRPB mean value.

7.4 Patient Doses

As mentioned earlier there is neither any data file nor the scanner specifications data required for calculating organ or tissue doses and effective dose values for those rather modern models of CT scanners included in this study. Therefore we were able to calculate organ or tissue doses and effective doses only for three CT scanners in our study for which data files were available from the NRPB national survey of CT practice (Jones and Shrimpton 1993). These were a GE 8800, a GE 9000 HP and a Philips Tomoscan CX/S CT scanner. As mentioned earlier both of the GE models are not anymore in clinical use and were replaced with a modern GE HiSpeed Advantage model.

In this section first calculated organ or tissue doses and effective doses based on our CTDI measurements free in air and the MC dosimetry approach will be presented. This will be done for all routine examinations performed by these CT scanners. Then the estimated patient doses by this dosimetry method, in terms of effective doses, from the three different scanner models in this study will be compared with each other. Finally our estimated effective dose values will be compared with the typical effective dose values reported recently by Wall and Hart (1997) from the NRPB national survey of CT practice in the UK (Shrimpton et al. 1991a, 1991b; Jones and Shrimpton 1991) for the most routine examinations.

7.4.1 Organs and Effective Doses

Patient doses were estimated in terms of organ or tissue doses, effective dose equivalent and effective dose values as recommended by the ICRP (1977, 1991). In order to derive organ or tissue doses and effective doses for CT examinations using the MC Dosimetry approach and the CTDI data, as described above it was necessary to determine details of the scan protocols used for all the routine examinations for all the CT scanners for which data files were available from the NRPB national survey of CT practice (Shrimpton et al. 1991a, 1991b; Jones and Shrimpton 1991). The required parameters of scan protocols were: applied potential (kV), exposure setting (mAs), number of slices (or scan volume), nominal slice width (mm), couch increment

(or slice spacing or table feed) (mm), physical filter setting (if variable), and starting position. These parameters were determined by matching clinical scanning conditions as closely as possible, through consulting with the radiologists and radiographers who used the CT scanners. These were the same parameters as applied for the dose assessment using our developed direct dosimetry approach. The typical scanning parameters listed in Table 7.17, Table 7.18, and Table 7.19 were used for these CT scanners.

Table 7.17: Typical clinical scanning parameters for the GE 8800 CT Scanner.

Examination	Physical filter	kV	mA	mAs	Slice width (mm)	Couch increment (mm)	No. of slices	Start Position*
Head	Head	120	320	737	10	10	4	801
			250	576	10	10	4	841
			160	369	10	10	2	881
Orbit	Head	120	320	737	5	3	9	850
			250	576	10	10	1	877
Posterior fossa	Head	120	400	922	5	5	7	801
			320	737	10	10	3	836
			250	576	10	10	3	866
			200	461	10	10	1	896

* Distance from the base of the mathematical phantom in mm (detailed information in section 7.2.2).

Table 7.18: Typical clinical scanning parameters for the GE 9000HP CT Scanner.

Examination	Physical filter	kV	mA	mAs	Slice width (mm)	Couch increment (mm)	No. of slices	Start Position*
Head	Head	120	250	888	10	10	5	801
			200	710	10	10	6	851
Chest	Body	120	250	533	10	15	18	400
Abdomen & pelvis	Body	120	250	533	10	15	28	000

*Distance from the base of the mathematical phantom in mm (detailed information in section 7.2.2).

Table 7.19: Typical clinical scanning parameters for the Philips Tomoscan CX/S CT Scanner.

Examination	kV	mA	mAs	Slice width	Couch increment (mm)	No. of slices	Start Position*
Head	120	220	356	10	10	11	801
Neck	120	220	356	10	10	10	700
Posterior fossa	120	270	437	5	5	6	801
		220	356	10	10	9	831
Chest	120	356	356	10	15	18	400
Abdomen & pelvis	120	270	437	10	15	28	000
Lumbar spine	120	270	437	5	5	10	220

* Distance from the base of the mathematical phantom in mm (detailed information in section 7.2.2).

Having determined the CT scanning parameters, the estimated CTDI values with the TLDs free in air were used in combination with the NRPB data files (Jones and Shrimpton 1993) and the available software (CTDOSE by Le Heron 1993), as explained earlier, to determine the radiation doses to organs and tissues of interest, effective dose equivalent, and effective dose values for all common CT examinations performed by these scanners.

The CTDI values resulting from our TLD measurements were used for calculating organ doses, effective dose (E) and effective dose equivalent (H_E) values by this dosimetry approach, although calculating CTDI values using the pencil IC was more convenient and had better precision and accuracy. The main reason for this was that when we implemented our developed direct CT dosimetry method we just had the TLD results available. It is quite obvious that in order to be able to compare our developed direct method with the MC method it was necessary to use both dosimetry methods simultaneously. Furthermore, this was decided not only in order to be consistent with the NRPB dosimetry procedure, but also because of the differences observed between the CTDI results from the two dosimetry devices for some of the CT scanners as explained above.

Table 7.20 shows the calculated organ doses, effective dose equivalent, and effective dose for three common examinations performed by the GE 8800 CT scanner. The routine scanning parameters for these examinations are mentioned above. This was one of the earliest and old RR CT scanner and had a very poor and slow scan and reconstruction time compared with the other models. Although this scanner had the potential capability for other examinations in the body region, it was

mainly used for the head region examinations. This was mainly because it was used in a clinical neuroscience unit dedicated mainly for "head" examinations. However as mentioned in previous chapters, this scanner was replaced in 1996 with a more advanced GE model.

Table 7.21 shows the calculated organ doses, effective dose equivalent, and effective dose values for three common examinations performed by the GE 9000 HP CT scanner. The routine scanning parameters for these examinations are mentioned above. Although this CT scanner was a more advanced RR model, compared with the GE 8800 model, with much better performance and was used for examinations covering all body regions, it was still quite old and slow compared with the modern CT scanners. As mentioned earlier, this scanner was also replaced in 1995 with another more advanced GE model.

Table 7.22 shows the calculated organ doses, effective dose equivalent, and effective dose values for three common examinations performed by the Philips Tomoscan CX/S CT scanner. The routine scanning parameters for these examinations and with this CT model, are mentioned above.

Table 7.20: Calculated organ doses and dose indices for different examinations using the GE 8800 CT scanner.

Organ/tissue	Calculated dose (mGy)		
	Head	Orbit	Posterior fossa
Gonads	0.00	0.00	0.00
Red Bone Marrow	1.73	0.97	2.18
Colon	0.00	0.00	0.00
Lungs	0.07	0.03	0.09
Stomach	0.00	0.00	0.00
Bladder	0.00	0.00	0.00
Breasts	0.02	0.01	0.02
Liver	0.00	0.00	0.01
Oesophagus	0.05	0.01	0.06
Thyroid	1.58	0.42	1.94
Skin	1.35	0.86	1.73
Bone Surface	7.86	4.61	9.93
Remainder (mSv, ICRP 26)	1.80	1.70	2.28
H_E (mSv)	2.31	1.97	2.19
Remainder (mSv, ICRP 60)	0.77	0.71	0.97
E (mSv)	1.15	0.91	1.46

Table 7.21: Calculated organ doses and dose indices for different examinations using the GE 9000 HP CT scanner.

Organ/tissue	Calculated dose (mGy)		
	Head	Chest	Abdomen & pelvis
Gonads	0.00	0.02	7.95
Red Bone Marrow	1.62	3.74	5.32
Colon	0.00	0.03	11.63
Lungs	0.06	13.92	0.99
Stomach	0.00	2.87	12.44
Bladder	0.00	0.01	16.60
Breasts	0.02	10.38	0.30
Liver	0.00	4.68	10.14
Oesophagus	0.04	18.71	0.22
Thyroid	1.33	1.42	0.02
Skin	1.30	2.46	3.77
Bone Surface	7.42	7.24	6.65
Remainder (mSv, ICRP 26)	1.85	0.92	4.58
H_E (mSv)	2.31	4.86	7.56
Remainder (mSv, ICRP 60)	0.78	0.53	0.29
E (mSv)	1.14	4.86	7.00

Table 7.22: Calculated organ doses and dose indices for different examinations using the Philips Tomoscan CX/S CT scanner.

Organ/tissue	Calculated dose (mGy)					
	Head	Neck	Posterior fossa	Chest	Abdomen & pelvis	Lumbar spine
Gonads	0.00	0.00	0.00	0.04	14.90	1.54
Red Bone Marrow	2.00	1.64	2.27	6.01	10.52	2.30
Colon	0.00	0.00	0.00	0.05	22.87	3.85
Lungs	0.07	0.62	0.08	23.03	2.05	0.24
Stomach	0.00	0.02	0.00	4.66	24.65	7.32
Bladder	0.00	0.00	0.00	0.02	28.42	0.68
Breasts	0.02	0.09	0.03	18.32	0.60	0.09
Liver	0.01	0.04	0.01	7.55	20.76	14.66
Oesophagus	0.06	0.58	0.06	26.25	0.46	0.05
Thyroid	1.40	44.75	1.57	2.41	0.05	0.00
Skin	1.95	2.03	2.25	4.05	7.58	2.14
Bone Surface	8.77	5.41	9.92	11.44	12.99	2.97
Remainder (mSv, ICRP 26)	1.96	0.13	2.11	1.51	8.17	4.76
H_E (mSv)	2.51	1.92	2.74	8.16	13.90	3.97
Remainder (mSv, ICRP 60)	0.83	0.09	0.89	0.76	1.00	0.58
E (mSv)	1.26	2.71	1.38	7.70	13.91	2.86

7.5 Summary and Conclusion

MC CT dosimetry method was implemented for three CT scanners in this study for which the required data files were available from the NRPB national survey of CT practice in the UK (Shrimpton et al. 1991a, 1991b; Jones and Shrimpton 1991). The estimation of patient doses with this dosimetry method, as used in this study, was quite simple and straightforward compare with the other common CT dosimetry approaches. Nevertheless, this dosimetry method is only applicable to rather older CT scanner models included in the NRPB survey. On the other hand developing this dosimetry method for newer and upcoming scanners requires both the expertise in the MC technique and the scanner configurations that are not normally readily available. However the implementation of this dosimetry approach in this study helped us to compare our developed dosimetry approach with another well established dosimetry method. This comparison is given in chapter eight. In addition, the measurements of the CTDI in air for all different CT scanners provided a good base for analysing different common CTDI measuring techniques and identifying the best technique for the estimation of CTDI in air. Furthermore, the comprehensive CTDI measurements carried out provided a good tool to study the variation of this index by slice width, kV and CT scanner models. Comparison of the estimated patient doses by this dosimetry approach with the NRPB typical values also provided a good base to evaluate the performance of the relevant CT scanners regarding the patient doses and the ALARA principle.

It was noted that the estimated CTDI values for all the scanners for slice widths greater than 2 mm were consistent, while there were discrepancies for smaller slice widths. This implied that the true slice widths may be different from the nominal value for smaller (< 2mm) slice widths for some of the scanners. Further analysing of these discrepancies, for the scanners with multiple kV options, indicated that this error was energy dependent. The strong dependence of CTDI on the kV was noted for the GE HiSpeed Advantage scanner operating at four tube potentials in the range of 80 to 140 kV. At 120 kV and 10 mm slice width, the lowest and highest value of CTDI estimated with the IC were 0.117 mGy/mAs (GE 9000HP with the HEAD filter) and 0.377 mGy/mAs (GE Sytec 3000) respectively. These values were 0.123

and 0.352 mGy/mAs when estimated with the TLDs. As explained the pencil IC has the advantages of being more precise than the TLDs and does not need any other extra work as required for the readout and calibration process of the TLDs. Therefore, if the only purpose would be estimating CTDI values, not acquiring the CT dose profile, it is recommended that the pencil IC will be used. Otherwise the TLDs can be used for CTDI estimation. Based on the discussion made above regarding the use of TLDs, it is concluded that measuring the dose profile over a length longer than what was adopted in this study does not influence the resultant CTDI value. In addition, the gaussian measuring technique leads to incorrect CTDI estimation. Therefore, if the TLDs are used for the estimation of CTDI, it is recommended that it will be used based on the simple measuring technique adopted in this study being based on the NRPB method (Shrimpton et al. 1991b).

It is also concluded that except for the GE 8800 scanner for which the estimated CTDI values were significantly higher than the maximum values reported by the NRPB, for the other two scanners the estimated CTDI values fell within the NRPB reported range. However, as mentioned earlier, the GE 8800 and the GE 9000HP scanners have been replaced with the newer models and are not used anymore. Furthermore it was noted that there were some uncertainties in the measurements carried out on the GE 8800 scanner. Unfortunately, because this scanner was not accessible enough and was later taken out of service, we were not able to do more investigation on it. Overall, the CTDI values estimated with the TLDs ranged from 0.077 to 0.520 (Table 7.4), with significant variations up to a factor of 6.8, reflecting differences in the CT scanners' characteristics and the kV settings used by different types and models of the CT scanners. This variation factor is nearly two times the factor (3.5) reported by the NRPB resulting from its survey on much more CT scanners (nearly 200) operating in the UK up until 1989 (Shrimpton et al. 1991a, 1991b; Jones and Shrimpton 1991). This confirms that there is now a greater diversity in the CT scanner characteristics than what existed about a decade ago.

8. Comparison of Different Dosimetry Approaches and Estimated Patient Doses

In this chapter the two dosimetry approaches employed in this study for the estimation of patient doses from CT examinations will be compared with each other. In addition the estimated patient doses for similar conventional and spiral examinations will be compared with each other. Finally, the variation of patient doses estimated with the developed direct dosimetry method among the CT scanners will be discussed. Furthermore, the estimated patient doses for the most common CT examinations will be compared with the NRPB typical doses.

Section one will compare the two dosimetry approaches. In this regard, the estimated patient doses in terms of the organ doses and the other dose indices resulting from the developed direct CT dosimetry method will be compared with that of the MC dosimetry method. In addition, the differences between the two dosimetry approaches will be highlighted, analysed and discussed. This will be done for those scanners for which we were able to implement the MC dosimetry approach. Furthermore, the level of errors involved in both of the dosimetry approaches will be discussed and compared with each other. Section two will analyse and discuss the variation of effective dose values resulting from the direct dosimetry approach among the different CT scanners for every common scanning technique. Patient doses resulting from the conventional and the spiral examinations, with the direct dosimetry method, will be compared with each other in section three. Section four discusses the differences between the estimated effective dose equivalent and effective dose values for the most common examinations resulting from the direct dosimetry approach. Finally section five will compare the estimated effective dose values, resulting from the developed direct dosimetry approach for every CT scanner, with the typical mean values (Wall and Hart 1977) resulting from the national survey of CT practice in the UK (Shrimpton et al. 1991a, Shrimpton et al. 1991b, Jones and Shrimpton 1991).

8.1 Comparison of Patient Doses Resulting from the Direct and the MC Dosimetry Approaches

As noted in the previous chapter, required data files were not available for all models of the CT scanners and we were able to implement the MC CT dosimetry approach only for the three CT scanners. These scanners were a GE 8800, a GE 9000HP, and a Philips Tomoscan CX/S model.

In this section estimated patient doses resulting from the implementation of both of the dosimetry approaches, i.e. the developed direct method and the MC method, are compared and their differences are analysed and discussed. The comparison is made in terms of doses to all organs and tissues of interest, effective dose equivalent (E) (ICRP 1977) and effective dose (H_E) (ICRP 1991) values for each scanner. This is done for all the most common scanning techniques performed by the three scanners being grouped under "head & neck", "chest", and "abdomen & pelvis".

8.1.1 Head & Neck

In the head and neck region, the tissues which principally contribute to effective dose are the brain (remainders), red bone marrow (RBM), and bone (and oesophagus and thyroid for scans of the neck). The relative contribution of these tissues to effective dose for the measured protocols are shown in Table 8.1 and Table 8.2 for the direct and the MC dosimetry methods respectively.

For all these examinations (except the neck) between 55%-61% (the direct method) and 66%-78% (the MC method) of the effective dose is due to the dose to remainder organs, which in turn is mainly due to the dose to the brain. This is because brain is the only organ included in the ICRP list (ICRP 1991) which is wholly or mainly included within the scan volume of these head scanning techniques. A smaller proportion of the total bone and RBM in the whole body (9-12%) is also included in the scan volume for these examinations. Hence the contribution of these organs to the effective dose from the direct method (12-14% bone, 23-26% RBM) (Table 8.1) and the MC method (5-7% bone, 13-18% RBM) (Table 8.2) was less. For the neck examinations it is mostly thyroid (direct method: 64% and MC method 83%) which

contribute to the resulting effective dose. The other main contributions are from oesophagus and RBM.

Table 8.1: Contribution of organ/tissue doses to effective dose from the direct dosimetry method for the head and neck examinations.

Organ/tissue	GE 8800			GE 9000HP	Philips Tomoscan CX/S		
	Head	Orbit	PF*	Head	Head	PF*	Neck
RBM	23.1%	25.9%	24.2%	23.4%	23.8%	20.2%	11.7%
Oesophagus	0.4%	0.4%	0.5%	0.4%	0.4%	0.2%	11.6%
Thyroid	1.9%	2.0%	2.7%	2.0%	2.1%	6.3%	64.0%
Bone sarface	12.6%	14.2%	13.2%	12.8%	12.1%	7.3%	4.6%
Remainder (ICRP 60)	60.3%	55.4%	58.2%	60.1%	60.1%	63.1%	1.0%

* Posterior fossa

Table 8.2: Contribution of organ/tissue doses to effective dose from the MC dosimetry method for the head and neck examinations.

Organ/tissue	GE 8800			GE 9000HP	Philips Tomoscan CX/S		
	Head	Orbit	PF*	Head	Head	PF*	Neck
RBM	18.1%	12.8%	17.9%	17.1%	19.0%	19.7	7.3%
Oesophagus	0.2%	0.1%	0.2%	0.2%	0.2%	0.2	1.1%
Thyroid	6.9%	2.3%	6.6%	5.8%	5.6%	5.7	82.6%
Bone sarface	6.8%	5.1%	6.8%	6.5%	7.0%	7.2	2.0%
Remainder (ICRP 60)	67.0%	78.0%	66.4%	68.4%	65.9%	64.5	3.3%

* Posterior fossa

The ratio of doses derived from the direct and MC dosimetry methods are shown in Table 8.3. The table includes the ratios of doses to the five most significant organs/tissues and the ratios of doses to remainder organs and E. It can be seen that the differences in effective dose values calculated by two methods can be attributed to the differences in doses to the brain for the examinations of the head because of the dominant influence of this tissue on the calculation.

The results presented in this table are not consistent. The GE 9000HP and the Philips CX/S scanners have higher effective doses calculated by the direct method (8%-47%), whereas for the GE 8800 the measured doses were consistently lower than those calculated (by between 33% and 38%) for these protocols. It was reported previously that the CTDI measurements for the GE 8800 scanner were high in comparison with data published by the NRPB. It is possible that measurement error or mis-calibration of the scanner may have influenced these results, which unfortunately

could not be repeated. For the other scanners, CTDI measurements were made in the scan day as the direct dose measurements providing a greater certainty in the ratios presented here.

Table 8.3: Ratios of organ/tissue, remainder, brain and effective doses between the direct and the MC dosimetry methods for the head and neck examinations.

Organ/tissue	GE 8800			GE 9000HP	Philips Tomoscan CX/S		
	Head	Orbit	PF*	Head	Head	PF*	Neck
RBM	0.87	1.25	0.91	2.02	1.67	1.47	2.37
Oesophagus	1.20	4.00	1.67	3.25	2.33	3.17	15.91
Thyroid	0.19	0.52	0.27	0.50	0.51	0.58	1.14
Bone sarface	1.25	1.73	1.30	2.90	2.31	2.04	3.37
Remainder (mSv, ICRP 60)	0.61	0.44	0.59	1.29	1.22	1.15	0.44
(Brain	***0.62***	***0.44***	***0.60***	***1.31***	***1.24***	***1.08***	***1.07)***
E (mSv)	0.68	0.62	0.67	1.47	1.33	1.23	1.47

* Posterior fossa

Table 8.4 shows the contribution to effective dose from the different body organs/tissues for chest examinations from both dosimetry methods. We have excluded from the table gonads, colon, bladder, skin, thyroid, and bone which have a negligible contribution. Most of the dose is due to six organs, three of which are totally included within the chest scan volume (lungs, breasts, and oesophagus), and three which are partially included (liver, stomach, and RBM). From these organs/tissues lung, stomach, and RBM have a higher tissue weighting factor (0.12) than the other three (0.05). The contribution of remainder dose to effective dose is also high because of the inclusion of the thymus and adrenals in the chest scan volume.

Table 8.4: Contribution of organ/tissue doses to effective dose from the direct and MC dosimetry methods for the chest examination.

Organ/tissue	GE 9000HP		Philips CX/S	
	Direct	MC	Direct	MC
RBM	8.1%	9.2%	8.4%	9.4%
Lungs	30.5%	33.6%	31.6%	35.9%
Stomach	13.5%	7.1%	13.4%	7.3%
Breasts	14.9%	10.7%	14.3%	11.9%
Liver	5.7%	4.8%	5.9%	4.9%
Oesophagus	11.0%	19.2%	10.4%	17.0%
Remainder (mSv, ICRP 60)	8.6%	10.9%	7.9%	9.9%

8.1.2 Chest

The ratios of doses between the two dosimetry methods for chest examinations are shown in Table 8.5 for the GE 9000HP and Philips Tomoscan CX/S scanners. The ratios between measured and calculated doses are mentioned in the table for the effective dose and for the above six organs/tissues plus the remainder having a significant contribution to the effective dose. The direct dosimetry method indicated an increased effective dose of 38% and 27% for the GE 9000HP and the Philips scanner respectively. This increase is due to the higher contribution of stomach, breast and liver to effective dose from which the stomach has a high tissue weighting factor causing the biggest discrepancy for this organ. The measured doses to RBM and lung were also higher than the calculated values. But the increase in the measured effective dose was less affected by these two organs than the other three organs because the contributions of these organs to effective dose from both dosimetry methods were very close to each other (Table 8.4). On the other hand the measured dose to the oesophagus was 11% and 12% less than the MC calculations for the GE 9000HP and the Philips scanners respectively. This was due to higher contribution of this organ to effective dose from the MC method than that of the direct method. However, since the tissue weighting factor for oesophagus is much less than that of the other five organs and tissues, the much lower dose from the direct method to this organ is offset by increased doses to other organs/tissues (RBM, lungs, stomach, breasts, and liver).

Overall, the differences observed in estimated organ doses between the two dosimetry methods are due to differences in the shape, size and location or distribution of these organs in the physical and the mathematical phantoms. In other words, differences in organ/tissue doses and effective doses reflect differences in the size, shape and location of the organs/tissues in the physical (Rando) and computational (mathematical) phantoms. This again reflects the difference between the defined anatomy of the Rando phantom (Figure 4.1, 4.2, 4.4 and Appendix A) and the mathematical phantom (Figure 6.7), for which there is a sharp division between the locations of the thoracic and abdominal organs. The reader is referred to chapter four and seven for a full description of the physical and mathematical phantoms respectively.

Table 8.5: Ratios of organ/tissue, remainder, and effective doses between the direct and the MC dosimetry methods for the chest examinations.

Organ/tissue	GE 9000 HP	Philips CX/S
RBM	1.22	1.14
Lungs	1.25	1.12
Stomach	2.63	2.34
Breasts	1.93	1.52
Liver	1.65	1.52
Oesophagus	0.79	0.78
Remainder (mSv, ICRP 60)	1.09	1.01
E (mSv)	1.38	1.27

8.1.3 Abdomen & Pelvis

For the abdomen and pelvis CT protocols seven organs/tissues contribute significantly to effective dose. These are gonads, stomach, colon, RBM, bladder, liver, and remainder organs (including kidneys, lower large intestine (LLI), small intestine (SI), and pancreas). The contribution of each of these organs to measured and calculated effective dose is shown in Table 8.6 for the GE 9000HP and the Philips Tomoscan CX/S scanners.

Table 8.6: Contribution of organ/tissue doses to effective dose from the direct and MC dosimetry methods for the abdomen and pelvis examinations.

CT scanner	GE 9000HP		Philips Tomoscan CX/S			
CT examination	Abdomen & pelvis		Abdomen & pelvis		Lumbar Spine	
Dosimetry method	Direct	MC	Direct	MC	Direct	MC
Gonads	24.3%	22.7%	24.4%	21.4%	22.5%	10.8%
RBM	7.4%	9.1%	8.7%	9.1%	18.3%	9.7%
Colon	16.6%	19.9%	18.2%	19.7%	21.4%	16.2%
Stomach	22.1%	21.3%	20.0%	21.3%	4.7%	30.7%
Bladder	6.9%	11.9%	7.2%	10.2%	4.2%	1.2%
Liver	5.3%	7.2%	7.8%	7.5%	2.5%	8.1%
Remainder (mSv, ICRP 60)	6.8%	4.1%	7.0%	7.2%	19.8%	20.3%

Table 8.7: Ratios of organ/tissue doses and effective dose between the direct and the MC dosimetry methods for CT abdomen & pelvis examinations.

CT scanner	GE 9000HP	Philips CX/S	Philips CX/S
CT examination	Abdomen & pelvis	Abdomen & pelvis	Lumbar Spine
Gonads	1.46	1.38	2.40
RBM	1.11	1.15	2.18
Colon	1.13	1.11	1.52
Stomach	1.41	1.13	0.18
Bladder	0.79	0.85	4.01
Liver	1.00	1.26	0.36
Remainder(mSv, ICRP 60)	2.24	1.17	1.12
E (mSv)	1.36	1.21	1.15

It can be seen in Table 8.7 that the direct dosimetry method led to 36% and 21% higher estimates of effective dose for the full scans of "abdomen & pelvis" for the GE 9000HP and the Philips Tomoscan CX/S scanners respectively. The measured effective dose for the lumbar spine scan was also 15% more than the calculated value. Similar to "head & neck" and "chest" scans, a general explanation for the increases in measured doses for these abdomen and pelvis scans could be the different physical (Rando) and computational (mathematical) phantoms used by the dosimetry methods and different assumptions made for the shape, size and location of the radiosensitive organs in these phantoms.

For those organs which are completely or nearly completely included in the scan volume, namely gonads, colon, stomach, bladder, and liver, the dose ratio between dosimetry techniques varies from 0.79 to 1.49 and from 0.85 to 1.38 for "abdomen & pelvis" scans for the two scanners respectively. These tissues contribute to approximately 75% of the total dose. The lower values of the mentioned ranges

arise from the higher contribution of bladder dose to calculated effective dose. However, the much lower dose from the direct method to this organ is offset by increased doses to the other organs (gonads, colon, stomach, and liver) for this scanning protocol.

For the Philips scanner comparison of dose estimations were made for two protocols. These were "abdomen & pelvis" covering 14 sections of the Rando phantom, and "lumbar spine" over three sections. For the direct dosimetry method, the most significant contributions to effective dose arise from the gonads (ovaries and testes), RBM, colon, and remainder tissues (upper large intestine (ULI), SI, and kidneys) for "lumbar spine" examinations. These account for 82% of the dose derived by this dosimetry method for these examinations. However, for the MC calculations there is a significant contribution from stomach and liver (30.7% and 8.1% respectively) for "lumbar spine" scan indicating the differences in the anatomy of the two phantoms. However, the much lower doses from the direct method to these tissues are offset by increased doses to gonads, RBM and colon.

8.1.4 Comparison of Measurements Errors in the Dosimetry Approaches

The NRPB (Shrimpton et al. 1991b) has reported an estimate of about 12% as the overall uncertainty at the 95% confidence level in their measurements of CTDI normalised to exposure setting when they have combined all random and systematic components in the manner described by the International Atomic Energy Agency (IAEA 1985).

In chapter five it was noted that there were 35 TLD calibration data sets in this study from which the level of uncertainties in the TLD measurements were determined. An intermittent measurement error caused by the poor contact between either the TLDs and the trays or the trays and the heater compartment of the TLD reader was identified. The highest observed level of uncertainties was estimated to be about 10.8% at the 95% confidence level for an individual TLD calibration measurement if this error was included. However if the obvious faulty readings were excluded, the highest uncertainty was about 5.4% in an individual TLD calibration measurement. The root mean square of the coefficient variation (CV) of all the

calibration data sets indicated an overall 4.1% uncertainty (standard deviation) in a single TLD reading (Table 8.8).

Apart from 20 TLDs (10 irradiated and 10 unirradiated) used for the TLD calibration measurements, 37 TLDs were used for every CTDI measurement. The level of uncertainties for the CTDI measurements depends on the nominal slice width. For narrower slice widths only a few TLDs contribute to the CTDI value, so that the level of uncertainty will depend on the actual number which contribute to the integral. For the narrowest (1 mm) and the widest (10 mm) slice widths about 5 and 13 TLDs contribute to 90% or more of the CTDI values. Therefore, with some simplification the level of uncertainties in the sum of the TLD readings ranges from 2.2% to 3.6% at the 95% level of confidence for the widest and the narrowest slice widths respectively. By taking into account the uncertainties involved in the TLD calibration measurement (caused by the dosed TLDs), the overall uncertainty in our CTDI measurements is estimated to range from 4.0% to 5.3% at the 95% confidence level (Table 8.8) based on the IAEA (1994) recommendations for the calculation of combined uncertainties. The contribution of the 10 unirradiated TLDs used for the calibration process was less than 0.3%. Therefore the uncertainty due to these TLDs was ignored when the overall uncertainties were calculated.

For every patient dose estimate using the developed direct dosimetry method, apart from 20 TLDs used for the TLD calibration measurements, a pair of TLDs was used for central axis dose measurements in every section of the Rando phantom inside the scanned volume and two more sections outside the scan volume. If it is assumed that each section contributes equally to the effective dose, then the overall uncertainty depends on the number of phantom central axis dose measurements. This ranges from 6 to 16 for the "head" and "abdomen & pelvis" examinations respectively. The overall uncertainty for the central phantom TLD measurements ranges from 2.6 to 1.4% at the 95% level of confidence for the "head" and "abdomen & pelvis" examinations respectively. By taking into account the uncertainties involved in the TLD calibration measurement (from the dosed TLDs), the overall experimental uncertainty at the 95% confidence level in our measurements of measured effective doses is estimated to

range from 3.6 to 2.9% based on the IAEA (1994) recommendations for the calculation of combined uncertainties (Table 8.8).

Table 8.8: Percentage of the individual (the calibration and the phantom central doses) and the overall uncertainties (the CTDI and the "head" and "abdomen & pelvis" examinations) resulting from the TLD measurements.

Measurement	Uncertainty * (%)
single TLD	4.1
calibration (10 TLDs)	2.6
central doses (2 TLDs)	5.7
CTDI (1 mm slice width)	4.4
CTDI (10 mm slice width)	3.4
Head examination	3.6
Abdomen & pelvis examination	2.9

* This value is derived from the root mean square of the CVs of all the TLDs calibration data sets for the single TLD measurement. The values are calculated at the 95% level of confidence for the other measurements.

There are other sources of measurement errors in the MC and developed direct dosimetry approaches. As the NRPB indicated (Shrimpton et al. 1991b) there is also about 10% overall uncertainties in calculations of CTDI to tissue dose factors due to interaction cross section data used and the effect of modelling the body tissues in terms of only five materials in the MC calculations. Furthermore, the MC technique takes no account of couch attenuation and ignores any slight over-rotation of the x-ray beam that may occur in practice.

Another source of measurement errors in the developed direct dosimetry method was highlighted in chapter six when some of the assumptions were validated. This uncertainty arises from the assumptions made regarding the similarity of the dose distribution in parallel sections to the representative sections and the uniformity of the dose distributions in the phantom sections outside the scan volume for this dosimetry method. The most significant discrepancy noted was for the "abdomen & pelvis" examinations for which an overestimation of 10 to 20% in the calculated doses was noted due to the assumption of the similarity of the dose distribution in parallel sections to the representative section of the "abdomen & pelvis" area. Therefore, if this source of uncertainty is also taken into account, the overall uncertainty in the

developed direct dosimetry method is estimated to range from about 4% in head and neck to 20% for the abdomen and pelvis.

In addition there are other systematic errors in the two dosimetry techniques. The phantoms used for the studies are not necessarily representative of a true patient. In particular the mathematical phantom for the MC calculations is an idealised model of the human body (Shrimpton et al. 1991b). As was noted in earlier chapters, the location and shape of the organs in the NRPB mathematical phantom have been simplified and designed based on simple geometrical shapes, while a more realistic approach has been followed for the physical phantom used for the developed direct method. This probably accounts for most of the observed differences between the two measurements techniques (section 8.1.5). It should also be noted that neither phantom takes any account of variation in body size and shape.

8.1.5 Summary of Dose Comparison

Overall the developed direct dosimetry method has estimated higher effective dose values for all routine scanning techniques practised by the GE 9000HP and Philips Tomoscan CX/S CT scanners. Other researchers (Shrimpton et al. 1991b, Geleijns et al. 1994, Calzado et al. 1995) have also reported higher patient dose estimates from the common direct dosimetry method compare with that of the MC dosimetry method for CT practices. Geleijns et al. (1995) have reported that using the Rando phantom and the direct dosimetry method has yielded up to 40% higher effective dose values compared with that of the mathematical phantom and the MC dosimetry method using the NRPB data files on a Philips CT scanner. Shrimpton et al. (1991b) have also compared reported organ and effective dose equivalent values resulting from the common direct CT dosimetry method (Nishizawa et al. 1991) for four complete examinations for selected types of scanners for similar condition of exposure with their results from the MC method. They have reported higher effective dose values from the direct dosimetry method of up to 50%, 60%, and 50% for head, chest and upper abdomen examinations, respectively.

As noted above the estimates of effective dose values determined by the direct dosimetry method for two scanners were also higher than that of the MC dosimetry

method. The estimated effective dose values with the direct dosimetry method for the Philips Tomoscan CX/S and the GE 9000HP scanners were up to a maximum of 47% higher than that estimated with the MC dosimetry method. Contrary to the results on these scanners and what has long been known, the estimated effective dose values from the developed direct dosimetry method were lower than that of the MC method for all the scanning techniques used with the GE 8800 scanner. As was noted at the beginning of this chapter, our estimates of the CTDI values for this scanner were considerably higher (22-24% more than the maximum values) than the NRPB mean values reported for this scanner. This made us suspicious about the consistency of the GE 8800 scanner performance and the accuracy of the measured CTDI values. However during the course of this study this scanner was replaced with a newer model and we were not able to carry out more measurements to investigate the large discrepancies which existed between our measured CTDI values and the NRPB reported mean values (Shrimpton et al. 1991b). Even when this CT scanner model was operating, it was difficult to get access. The higher estimates of dose indices for this scanner with the MC approach could be attributed to overestimated CTDI values. Hence the patient doses estimated from the MC dosimetry approach for this CT scanner should be treated with great caution.

While it was not possible to investigate more about the contradictory results on the GE 8800 scanner, it can be concluded that systematic differences occur when organ and effective doses are determined with the developed direct dosimetry method compared with that of the MC dosimetry method. The degree of the differences yielded in our study are in good agreement with other reports (Shrimpton et al. 1991b, Geleijns et al. 1994). These systematic differences can however be explained. They are mainly due to differences between the two different phantoms used to simulate an average human body in the direct and MC dosimetry approaches. The physical phantom used in the developed direct approach (Rando Alderson) is different from the mathematical phantom used in the MC approach. The overall shape and size of the Rando phantom is different from the mathematical phantom. In addition, the location, shape, and size of the organs of interest in both phantoms are different. The location and shape of the organs in the mathematical phantom, as used by the NRPB

(Shrimpton et al. 1991b), have been simplified and designed based on simple geometrical shapes (Figure 6.7). But, as explained in detail in chapter four and appendix A, the location and shape of the organs in the Rando phantom were determined more realistically for the developed direct dosimetry method (Figure 4.5). For example in the mathematical phantom there is a sharp boundary between thoracic organs such as lungs and abdominal organs such as liver, stomach and intestines. However these organs are normally extended over both of these areas of the body. As another example, the head and neck size of the computational mathematical phantom is much smaller than that of the physical Rando phantom.

8.2 Variation of Effective Doses among the CT Scanners and the Normalised Effective Dose

As mentioned in detail in chapter six, several factors affect the patient doses resulting from CT practices. These factors must be noted if a comparison is going to be made between different scanner models for a particular CT examination. It was noted that some of these factors like x-ray inherent filtration, collimation, detector efficiency, scan field diameter (source to isocentre distance), and so on could not be controlled. These factors are normally either fixed or pre-set by the manufacturers for every CT model. It was also noted that there is another category of factors affecting the patient doses such as the kV, the mAs, the slice width, the couch increment or the pitch, and the scan length which are controlled by the operator. But, as was noted for most of these parameters, too, there are either a limited number of options or different pre-set values recommended by the manufacturers for every particular examination. These parameters affect image quality and users generally accept protocols recommended by manufacturers even if the patient dose may be greater than what is necessary for an adequate image quality.

Therefore due to the constraints imposed by the lack of control over most of the parameters affecting the patient doses, and in an attempt to compare the CT scanners in a more similar condition of scanning techniques, the normalised effective dose value was introduced in chapter six. In this regard the measured effective dose

values were normalised to 100 mAs, 10 mm scan volume, the packing factor of one, and the CTDI for all CT examinations and were presented in chapter six.

It is recognised that in practice some of the older scanner models, examined in this study, do not allow the users to change their exposure setting for a particular CT examination. In addition, it is recognised that even if a unique mAs setting is virtually employed by all the CT scanners, the quality of the image produced by different scanner models will not necessarily be the same. In this respect it is also recognised that employing a higher mAs setting does not guarantee a better image quality for different scanner models. For instance we witnessed that even though some of the CT scanners in this study employ a higher mAs setting than other ones for similar examinations, they produce a poorer image quality. It is also known that in normalising effective dose values to 10 mm scan volume, the total scan length for every particular CT examination should be exactly the same. That was not always achievable for some of special examinations. On the other hand, while the above arguments are fully acknowledged, it would be very crude to compare patient doses resulting from different scanners without regard to this important category of factors (mAs, slice width and spacing, scan volume, and packing factor) that significantly affect the resultant patient doses from CT practices.

When the measured data was summarised in chapter six, comparison of the normalised effective dose values to mAs, scan volume, and CTDI among different CT scanner revealed that there was not a very significant variation for this value among different CT scanners for similar scanning protocols. Therefore in this section we will present the average values of the normalised effective dose values for each of the three distinct areas of the body, i.e. the head, chest and abdomen & pelvis areas. These values could provide a reliable tool for rapid estimations of effective dose values for any specific CT examination performed on the same body region.

Table 8.9 shows the average effective dose values normalised to 100mAs, 10 mm scan volume, and CTDI for three areas of the "head", "chest" and "abdomen & pelvis" of the body. These values have been provided by averaging the normalised effective dose values derived from the measured effective dose values from the examinations carried out over these areas of body by all the CT scanners excluding

the GE 8800 scanner. Because there were some uncertainties in the measured CTDI values for the GE 8800 scanner, as explained earlier in this chapter, this scanner was excluded from this procedure. For the head area both the routine "head" and "posterior fossa" examinations have been included. For the chest area both the conventional and spiral examinations were included. Similar to the "chest" for the "abdomen & pelvis" area both the spiral and conventional "abdomen & pelvis" examinations were included.

Table 8.9: Averaged normalise effective dose values to 100mAs, 10 mm scan volume, and CTDI over the measured effective dose values from all the CT scanners for three areas of the body.

Body area	Head (120 kV)	Chest (120kV)	Chest (137 kV)	Abdomen & pelvis (120 kV)
No of data sets	11	5	3	10
Mean	0.193	0.652	0.969	0.688
Standard deviation	0.020	0.090	0.046	0.082
Maximum	0.226	0.801	1.027	0.797
Minimum	0.157	0.548	0.916	0.499

Therefore the above average values could be used to estimate patient doses in terms of effective doses from CT examinations carried out by any scanner operating at the above tube potentials. If these values are multiplied by the applied mAs (to 100 mAs), scan volume (to 10 mm), and packing factor for the examination, and the value of CTDI in air for the scanner a good estimation of the patient dose in terms of the effective dose could be made for any CT examination carried out.

We believe that these normalised effective dose values could provide a very good approach to estimate patient dose for most of the scanning techniques used in CT practices. It is also very likely that if more dose measurements are carried out, the level of errors involved in the normalised effective dose values will be decreased.

8.3 Comparison of Patient Doses Resulting from Conventional and Spiral Examinations

Two CT scanners in this study, Siemens Somatom Plus and GE HiSpeed Advantage, were capable of performing both the conventional and spiral scanning techniques. Comparison of patient doses estimated for most of the conventional examinations with that of the spiral examinations indicated that, there was not a significant difference between these scanning techniques if similar condition of exposure and slice width and couch increment (or pitch for spiral examinations) are selected. In this regard the reader is referred to chapter six for the details of the results. There is, therefore, a potential for decreasing patient doses with the spiral examinations by increasing the pitch setting without losing so much imaging information that will inevitably happen if an equivalent conventional scanning technique is performed.

8.4 Comparison of Effective Dose and Effective Dose Equivalent Values

As noted in chapter two, effective dose equivalent and effective dose are both the sum of the doubly weighted absorbed dose in all the tissues and organs of the body recommended in 1977 and 1990 respectively by the ICRP (ICRP 1977, ICRP 1991). The double weighting factors are the radiation and the tissue weighting factors. The value of radiation weighting factor has been selected to be representative of the relative biological effectiveness of the radiation in inducing stochastic effects at low doses. A value of unity for this factor has been chosen for all radiations of low linear energy transfer (LET) including X-rays of all energies in both the 1977 and 1990 ICRP recommendations. The tissue weighting factor represents the relative contribution of the organ/tissue to the total detriment resulting from uniform irradiation of the whole body. E superseded H_E in 1990 ICRP recommendations. The introduction of the name effective dose was associated with the change to equivalent dose. However, the ICRP emphasised that this change was not connected with changes in the number or magnitude of the tissue weighting factors. In the 1990 recommendations the ICRP took into account new biological information and trends

for all organs and tissues and recommended different values of tissue weighting factors compared with that recommended in 1977 for effective dose equivalent. The only difference between H_E and E is differences in tissue weighting factors. E has weighting factors for a larger number of specified organs and tissues and is likely to be a better indicator of the radiation risk than H_E (Table 2-2).

We measured and presented H_E along with E values throughout this study because E was not widely used. Furthermore this was done to provide an opportunity for comparing our results with previous reports on patient doses from CT and other X-ray practices reporting patient doses in terms of H_E. It is useful therefore to consider the differences that would arise from the differences between the tissue weighting factors of E and H_E for the two dosimetry methods used in this study.

The ratios between H_E and E for the most common routine examinations for both the direct and the MC dosimetry methods are summarised in Table 8.10.

Table 8.10: Ratios of H_E to E for the most common CT examinations.

CT examination	Dosimetry method	No. of data sets	Mean	Standard deviation	Maximum	Minimum
Head and posterior fossa	direct	13	2.40	0.04	2.44	2.29
	MC	5	1.90	0.23	2.03	1.50
Chest	direct	8	1.50	0.03	1.53	1.44
	MC	2	1.03	0.04	1.06	1.00
Abdomen & pelvis	direct	10	1.15	0.04	1.26	1.12
	MC	2	1.04	0.06	1.08	1.00

As could be seen in the table, measured H_E values (with the direct method) were greater than the E values by a factor of 2.40, 1.50, and 1.15 for the "head" & "posterior fossa", "chest" and "abdomen & pelvis" examinations respectively. The bigger discrepancy in the head is principally through the treatment of remainder organs. The brain is the main contributor to H_E and E in the "head" examinations (see section 8.3). In ICRP 26, as a remainder organ, the dose equivalent for this organ is weighted by a factor of 0.06. However, since the dose to the brain is greater than other main organs, ICRP 60 requires that it is weighted by a factor of 0.025.

On the other hand, there was no significant difference between calculated E and H_E values.(from the MC method) except for the head examination for which the E

and H_E ratio was 1.90. This indicated a disagreement between the two dosimetry methods. Therefore, the output data resulting from the computer program, CTDOSE (Le Heron 1993) used to calculate organ dose, effective dose, and effective dose equivalent values from the NRPB normalised data files (Jones and Shrimpton 1993) were thoroughly examined. An inconsistency was found in the CTDOSE program with the 1977 ICRP recommendations (ICRP 1977) regarding the remainder organs.

Based on the 1977 ICRP recommendations five organs or tissues receiving the highest dose equivalents should be regarded as the remainder organs. Nevertheless, it was noted that for some examinations calculated dose values for some other organs were higher than those taken as remainder organs by the CTDOSE program.

For the chest examination instead of thymus, oesophagus, and adrenals, other organs (spleen, stomach, and gall bladder) receiving lower doses were taken as the remainder organs by the CTDOSE. If doses are recalculated on this basis the H_E to E ratio will be 1.46, in good agreement with the direct method. For "abdomen & pelvis" there is an agreement in the tissues to be used as remainder by the CTDOSE. Therefore the ratios for the two dosimetry methods are in reasonable agreement. For examinations of the head area (including "head" and "posterior fossa") part of the reason for the greater ratios for the direct method is that skin was included as a remainder tissue. This was not done by the CTDOSE. Including the skin as a remainder organ would change the H_E to E ratio to 2.15 in a better agreement with the direct method. Overall this meant that thymus, oesophagus, adrenals and skin have not been regarded as remainder organs for H_E calculation by the CTDOSE program. It must also be noted here that, in the absence of an oesophagus from the NRPB mathematical phantom, the dose to this organ had been assumed to be the same as the dose to the thymus (Shrimpton et al. 1991b).

NRPB reported ratios of E to H_E (Shrimpton et al. 1991b). Taking the average of "head" and "posterior fossa" and of "abdomen" and "pelvis" examinations indicates that the H_E to E ratios for "head" & "posterior fossa", "chest", and "abdomen & pelvis" examinations were 1.82, 1.10, and 1.27 respectively. However, it must be noted that the remainder doses for E have been calculated in a different way by the NRPB. They have been done by splitting the relevant remainder tissues

weighting factors (0.05) equally between mean body dose (as averaged over the entire mathematical phantom including head and legs) and one other organ receiving the highest dose among the nine others that comprise the remainder tissues. The NRPB concluded that the approximations inherent in this approach were likely to have a minor effect on the estimation of effective dose (Shrimpton et al. 1991b). However the corrected ratios found between H_E and E for the MC method contradict the NRPB conclusion in this regard.

8.5 Comparison of Measured Patient Doses with the NRPB Typical Doses

As mentioned earlier several factors affect the patient doses even if a comparison of patient doses in terms of organ and effective doses based on the ICRP recommendations (1991) is going to be made between two identical scanners for a similar examination protocol. Unfortunately a wide range of examination protocols are practised at different places for the same examination even when identical CT scanners are used and there is not an internationally accepted standard for CT practices.

Furthermore as raised in this study different dosimetry approaches are followed for the estimation of patient doses. In addition these different dosimetry approaches have not yet been established and standardised.

For example, two national bodies in the UK (Jones and Shrimpton 1991) and in Germany (Zankl et al. 1991) have used the MC based CT dosimetry approach and provided normalised organ doses for a wide range of CT scanners. But these two widely used MC based CT dosimetry approaches have used different models of computational phantoms to simulate the human body. Therefore if they are implemented for estimation of patient doses for the same condition of exposure and scanning protocol for a particular CT scanner, they will consequently lead to different results (Geleijns et al. 1994).

There is the same story with the direct CT dosimetry approach using physical humanoid phantoms. Different physical phantoms have been used for the direct dosimetry method. In addition, even if the same physical phantom is used, different techniques are followed for determining the location of organs of interest. On the

other hand not all the published reports in the literature on the patient doses resulting from the CT practices have reported details of examination protocols or dosimetry techniques.

Therefore it is not very sensible to compare our results with others reporting patient doses for either different scanner models, or different scanning techniques, or with different dosimetry techniques. The NRPB carried out a national survey of CT practice in the UK in 1989. The results of this survey were published separately in three comprehensive parts including: aspects of examination frequency and quality assurance (Shrimpton et al. 1991a), dosimetric aspects (Shrimpton et al. 1991b) , and finally normalised organ doses (Jones and Shrimpton 1991). Later on an additional software report was provided by the NRPB including tables of dose conversion factors for 23 different models of CT scanners normalised to the CTDI measured free in the air (Jones and Shrimpton 1993). The latter report has been used extensively by several other individuals and national bodies (Crawley and Rogers 1994, Calzado et al. 1995, Geleijns et al. 1995, Naik et al. 1996, Adams et al. 1997, Van Unnik et al. 1997, Wall and Hart 1997) for estimation of patient doses from the same or similar type of CT scanners.

The typical doses for CT examinations have been extracted and presented in Table 8.11 from a revision (Wall and Hart 1997) on a recent review of doses to patients from medical X-ray examinations in the UK by the NRPB (Hart et al. 1996b). These doses are based on the mean values of the distributions seen in the national survey of CT practice in the UK (Shrimpton et al. 1991a, Shrimpton et al. 1991b, Jones and Shrimpton 1991). These typical doses are often taken as guideline CT doses by researchers in the UK and other countries. Therefore, we compare the patient doses resulting from the developed direct dosimetry method with these typical doses for CT examinations. The comparison will be made for the most common CT examinations performed by all the CT scanners to evaluate the performance of these scanners against these typical CT doses resulting from the NRPB national survey of CT practice.

Table 8.11: Typical effective doses to standard adult patients in the 1990s (From Wall and Hart 1997).

CT examination	Typical effective dose (mSv)	5^{th}-95^{th} percentile range (mSv)
Head	2	0.9-3.0
Chest	8	2.4-16
Abdomen	10	4.0-18
Pelvis	10	4.0-18

The results for routine head examinations were lower than the typical value reported by the NRPB. The exception was the GE Sytec 3000 scanner for which the effective dose was 2.6 which is still within the reported range of values.

All the estimated effective doses for the routine "posterior fossa" examinations carried out by four different models of the CT scanners were also less than the typical CT "head" dose.

For "chest" scans, three out of five scanners gave doses which were below the NRPB value (8 mSv). Higher doses were noted for the Philips Tomoscan CX/S (9.8 mSv) and the GE Sytec 3000 Plus (13.5 mSv), the latter value is at the upper end of the range

The NRPB reported doses for "abdomen" and "pelvis" examinations separately whereas the clinical protocols studied here combined these two regions. The measured effective doses were all less than the summed typical doses for abdomen and pelvis apart from the GE Sytec 3000 Plus. For this scanner the dose was 32.8 mSv.

Another point that must be regarded in the above comparisons is that the doses presented in the above table are based on the MC dosimetry approach employed by the NRPB in the survey, while our results are based on the direct dosimetry method. As mentioned earlier in this chapter, our study and other researchers indicate that the patient doses estimated with the direct CT dosimetry approach could be up to 60% higher than that estimate by the MC approach. Therefore it could be concluded that the patient doses resulting from almost all typical CT examinations from all the CT scanners fall either below or around the NRPB reported doses.

8.6 Summary

In this chapter, it has been shown that the direct dosimetry method overestimates effective dose by between 15% and 47% when compared with the MC method. Normalisation of effective dose to mAs, scan volume and CTDI has produced dose factors for each region of the body which can be used to estimate effective dose for any scan protocol provided that the in air CTDI is known.

The comparison of dose measurements for conventional and spiral scanning is given which shows the expected change of the dose with pitch.

A comparison is given of the quantities effective dose equivalent and effective dose. The biggest differences occur for scans in the head and neck in which H_E is more than double of E due to the weight accorded to remainder tissues.

The doses measured in this study are compared with those from the UK national survey of CT practice (Wall and Hart 1997). Other than for one of the scanners tested, the doses were in the same range as for the national survey.

9. DISCUSSION AND CONCLUSION

9.1 Discussion

This thesis described the underlying principles and assumptions of the direct CT dosimetry method developed and implemented in this study. The developed direct dosimetry method is a simple and practical method enabling the assessment of patient doses resulting from any examination using any CT scanner model independently. All dosimetry related concepts for the developed dosimetry technique were considered. Comprehensive dose measurements carried out enabled us to estimate and report the level of error involved in the approach. In addition, the review of CT dosimetry methods provided a comprehensive and critical analysis of the methods developed to date. Furthermore the MC dosimetry approach employed for some of the CT scanners enabled us to compare the patient doses estimated with the developed dosimetry method with that of the MC method.

Both the MC and the direct dosimetry approaches used commonly for the assessment of patient doses from CT examinations have inevitable constraints.

If the common direct CT dosimetry approach is selected, there are 23 organs and tissues of interest distributed all over the 35 sections of the Rando physical phantom for which the absorbed dose must be determined. Therefore, to estimate effective dose value for every particular CT examination more than 200 TLD measurements are required. Obviously this is a laborious, time consuming, and impractical way for the routine assessment of patient doses from the fast growing varieties of scanning techniques.

The constraint with the MC dosimetry approach is that the available conversion factors do not include all available CT scanners, in particular the newer models. This becomes important when the older CT scanners are either taken out of service or replaced with the newer models for which the conversion factors are not available.

As mentioned in chapter three, the UK Medical Device Agency has set up a dedicated CT evaluation facility called the ImPACT. This facility has recently (1997)

decided to carry out a survey to determine the radiation dose characteristics of CT scanners in current clinical use. This is going to be done by matching newer scanners to scanners which are represented in the NRPB Monte Carlo data sets, in order that these data sets might be used for the calculation of patient doses for these scanners.

In another attempt by the National Radiation Laboratory of New Zealand, a method has been used for measurement of patient dose applicable to all types of CT scanners in this country, not just those included in the NRPB data sets (Poletti 1996). They have done this by determining a set of factors to determine the effective dose from the CTDI measured at 1 cm depth in standard Perspex head and body phantoms, and the effective length of the scan. These factors have been determined from comparison of the phantom CTDI measurements with the effective dose determined for those scanners included in the NRPB data sets.

Apart from the uncertainties involved in these efforts, these surveys will enable us to find a solution for current newer CT scanners and the problem will exist for future models that are going to be introduced into clinical practice. Therefore this dosimetry approach will not easily be applicable for the future models that will come into clinical practice afterwards.

An attempt has also been made to make the representation of the human body and its organs in computational phantoms more accurate and realistic by Caon et al. (1997). They have introduced voxel-based computational models of human anatomy. They have said that their models represent internal human anatomy more faithfully than mathematical phantoms such as those of Cristy (1982) that have been used with some modifications in the MC CT dosimetry approaches. In these computational models anatomy is represented as voxels being constructed from CT data. They have claimed that using the MC calculation to determine dose to voxel based phantoms has given acceptably accurate results when compared to the actual measured values, as long as the X-ray spectrum is calculated for the scanner and the details of the beam shaping filter are known. This method may improve the accuracy of currently available organ doses derived from the unrealistic anatomy of mathematical phantoms and reduces significant differences observed in this and other studies between the direct and the MC dosimetry methods.

To overcome the above constraints in CT dosimetry the direct dosimetry method was developed by assessing the CT axial and longitudinal dose distributions in an anthropomorphic physical phantom. Measurement of these dose distributions for any scanner enables us to quickly measure organ doses and effective dose, and hence patient doses for any examination protocol with a limited number of TLDs (10-32 apart from the TLDs used for the calibration process).

The reduction of the extensive measurements required by the common direct dosimetry method was achieved mainly by the assumptions made for these dose distributions. Further measurements carried out for the validation of the accuracy of these assumptions revealed the degree of errors caused by them. However the overall degree of the uncertainties in the developed dosimetry method was not more than the degree reported for the NRPB MC method. The dosimeters chosen for the dose measurements (LiF TLDs) showed a good degree of consistency and a low degree of uncertainty. A systematic error due to the poor contact between the TLD tray and the heater compartment of the TLD reader was detected and avoided in this study by using a pair of TLDs for point dose measurements. If this technical problem is sorted out the number of TLDs required for the patient dose estimates with this dosimetry method will be halved.

The customised computer spreadsheet developed in this study also provided a very simple and user friendly tool for further simplification of the developed CT dosimetry method. The spreadsheet does all the required calculations and reports the patient doses by executing the macro programs.

The average normalised effective dose values to 100 mAs, 10 mm scan volume, and CTDI were presented for three areas of the "head", "chest", and "abdomen & pelvis" of the body in chapter seven. These values could be used to estimate approximate patient doses for most of the CT examinations carried out in CT practice with the 120 kV tube potential. This only requires the CT examination parameter and the scanner CTDI value. If the normalised effective dose values are multiplied by the CT applied mAs (to 100 mAs), scan volume (to 10 mm), packing factor, and the CTDI value in air, a good estimation of the effective dose could be made for the examination.

The MC dosimetry approach was also implemented in this study for some of the older scanners for which the conversion factors were available (Jones and Shrimpton 1993). The results of our proposed direct method were compared with this commonly used dosimetry method for the most routine examinations performed by these scanners. The differences observed between the patient doses resulting form the developed direct dosimetry approach and the MC approach were in a good agreement with other reports. The free in air CTDI measurements were carried out for all the CT scanners for all possible combinations of the kVs and slice widths. CTDI values were estimated using all the common measuring techniques using both of the dosimetry devices (the TLDs and the pencil IC) used for this purpose. The comprehensive measurements of the CTDI values provided a good tool to identify the best measuring technique. This also enabled us to investigate the variation of the CTDI by slice width, kV, and the scanner model and compare them with values reported by the NRPB from the national survey of CT practice in the UK (Shrimpton et al 1991a, 1991b; Jones and Shrimpton 1991).

9.2 Conclusion

The main purpose of the work presented in this thesis was to contribute to the improvement of the CT dosimetry methods by reviewing the available methods and proposing a practical and simple method with an acceptable degree of accuracy and consistency.

The main outcomes of this study were:

1. A detailed review of the importance of CT dosimetry, basic dosimetric quantities required to be considered, and the CT scanner developments and characteristics.
2. A detailed and critical review of the common approaches used in CT dosimetry.
3. Development of a practical direct CT dosimetry method by identifying and overcoming most of the constraints and limitations imposed by the common direct and the MC CT dosimetry methods.

4. Implementation of the developed CT dosimetry method and validating the assumptions made for it.
5. Implementation of the MC dosimetry method.
6. Assessment and analysis of patient doses using the developed dosimetry method for all the routine CT practices performed by all the CT scanners in the NHS hospitals in Lothian and Fife areas of Scotland.
7. Assessment of patient doses using the MC dosimetry method for all the routine CT practices performed by some of the CT scanners in the NHS hospitals in Lothian and Fife areas of Scotland.
8. Comparison of patient doses resulting from the developed dosimetry method with that of the MC method and identifying and explaining their differences.
9. Introduction of a quick method for the estimation of patient doses for similar scanning protocols with a good degree of approximation (normalised effective dose).

The direct dosimetry method developed and proposed in this study provides an easy, practical, and independent way for estimation of patient doses resulting from CT practices. This dosimetry method has now been used for several scanner models. The developed dosimetry method has been successfully implemented to assess the radiation doses resulting from various examination protocols using the recent modern CT modalities, that could not easily be investigated by other dosimetry approaches. For the implementation of this approach for any scanning technique performed by the CT models included in this study, not more than 30 TLD measurements are required at 15 central locations of the Rando phantom. To be able to implement this dosimetry approach for any other CT model a considerable number of TLD measurements are required to determine the dose distributions in three representative sections of the Rando physical phantom. But, afterward further patient dose assessment for any particular scanning technique will not require more than the number of TLD measurements mentioned above.

We believe that the developed direct CT dosimetry approach overcomes many limitations imposed by other common approaches. It also provides a reliable and

practical method for the assessment of patient doses from CT practices for a wide range of scan protocols. Estimation of measurement errors in the developed dosimetry method showed an error in methodology leading to an underestimate of dose by about 8% for chest scan and overestimate by 14% for abdomen & pelvis. This is in addition to a random error of about 2% due to the TLD. This may be compared with the overall uncertainties reported (Calzado et al. 1995) for the common MC and direct dosimetry approaches (18-23% and 10-20% respectively). In addition this level can be decreased if further work is carried out as outlined in the following section. The major advantage of the developed direct dosimetry method is that, it could easily and independently be adapted and implemented for any upcoming new model of CT scanner to be introduced into clinical practice.

9.3 Future Work

We assumed that the dose distribution in parallel sections of the phantom inside the CT scanned volume are identical. We also assumed that the dose distribution in the phantom sections outside the CT scanned volume is uniform. A limited number of measurements was carried out on one of the CT scanners (Siemens Somatom Plus). This enabled us to validate the accuracy of these assumptions and to reveal the level of errors caused by these assumptions in the developed dosimetry method. It may also be needed to do further investigation for the validation of these assumptions on other CT scanner models used in this study.

Other assumptions made for our developed direct CT dosimetry method including the degree of rotation and the use of packing factors to determine doses from contiguous scanning techniques are exactly the same as those made for the MC approach by the NRPB.

More improvements in the developed direct CT dosimetry method could be achieved by choosing extra representative sections in the physical phantom to decrease the degree of error caused by the significant inhomogeneity existed especially in the overlap regions between the "chest" and the "abdomen" areas of the phantom.

The developed dosimetry method was implemented for six models of the CT scanners. The implementation of this dosimetry method for other scanners requires a relatively extensive initial measurements to determine the axial and longitudinal dose distributions. Consequently the spreadsheet computer program must also be adapted and the required changes are carried out in the stored data to use it for other scanners. However when this initial work is carried out, the estimation of patient doses for any examination protocol can be done with a very limited number of TLD measurements.

The averaged normalised effective dose values presented in chapter seven were calculated when we reached the end of this study by analysing and comparing the patient doses resulted from both of the dosimetry methods implemented. These values could provide a very good approach to estimate patient doses for most of the common scanning techniques in CT practices. It is very likely that, if further dose measurements were carried out on other scanners and the values were normalised to CTDI in a Perspex phantom (instead of free in air), the level of errors observed in the normalised effective dose values in this study would be decreased.

8. REFERENCES

Adams E. J., Brettle D. S., Jones A. P., Hounsell A. R. and Mott D. J. (1997). Estimation of fetal and effective dose for CT examinations. Br. J. Radiology, 70, pp: 272-278.

Agarwal S. K., Friesen E. J., Bhaduri D., and Courlas G. (1979). Dose distribution from a Delta-25 head scanner. Med. Phys., 6 (4), pp: 302-304.

Alderson S. W., Lanzl L. H., Rollins M., and Spira J. (1962). An instrumented phantom system for analog computation of treatment plans. Am. J. Roentgenol., 87, pp: 185.

Ambrose J. (1973). Computerized transverse axial scanning (tomography): Part 2. Clinical Applications. Br. J. Radiology, 46, pp: 1023-1047.

Ambrose J. , Hounsfield G. N. (1972). Computerized transverse axial tomography. Proceedings of the British Institute of Radiology: Abstracts of papers read at the Thirty-second Annual Congress, April 20-21, 1972 (Br. J. Radiology, 46, pp: 148-149 (1973)).

Andreo P. (1991). Monte Carlo techniques in medical radiation physics. Phys. Med. Biol., 36 (7), pp: 861-920.

Atherton J. V. (1993). A Monte Carlo study of dose distributions and energy imparted in computed tomography dosimetry phantoms. Ph.D. Thesis, University of Florida (Gainseville, Florida).

Atherton J. V. and Huda W. (1995). CT doses in cylindrical phantoms. Phys. Med. Biol., 40, pp: 891-911.

Atherton J. V. and Huda W. (1996). Energy Imparted and effective doses in computed tomography. Med. Phys. 23 (5), pp: 735-741.

Babbel R., Harnsberger H. R., Nelson B., Sonkens J, and Hunt S. (1991) Optimization of techniques in screening CT of the sinuses. Am. J. Roentgenol., 157, pp: 1093-1098.

Bassano D. A., Chamberlin C. C., Mozely J. M., and Kieeffer S. A. (1977). Physical, performance and dosimetric characteristics of the -Scan 50 whole-body/brain scanner. Radiology, 123, pp: 455-462.

Bengtsson G., Blomgren P. G., Bergman K., and Aberg L. (1978). Patient exposures and radiation risks in Swedish diagnostic radiology. Acta Radiologica Oncology 17, pp: 81-105, Fasc. 2.

Boyd D. P., Margulis A. R., and Korobkin M. (1977). Comparison of translate-rotate and pure rotary computed tomography (CT) body scanners. SPIE Proceedings: Optical Instrumentation in Medicine VI, pp: 280-285.

Bracewell G. L. (1956). Australas J. Phys., 9, pp: 198-217.

Brasch R. C. and Cann C. E. (1982). Computed Tomographic Scanning in children: II an update comparison of radiation dose and resolving power of commercial scanners. Am. J. Roentgenol., 138, pp: 127-133.

Brasch R. C. Douglas P., Gooding C. A. (1978). Computed tomographic scanning in children: Comparison of radiation dose and resolving power of commercial CT scanners. Am. J. Roentgenol., 131, pp: 95-101.

Brooks R. A. and Di Chiro G. (1976). Principles of computer assisted tomography (CAT) in radiographic and radioisotopic imaging. Phys. Med. Biol., 21 (5), pp: 689-732.

Brunnett C. J. et al. (1990). Design considerations and specifications. Piker International, CT Engineering Department, OH.

Budinger T. F. and Gullberg G. T. (1974). IEEE Trans. Nucl. Sci., NS-21 (2), pp: 2-20.

Bunge R. E. and Herman C. L. (1987). Usage of diagnostic imaging procedures: a nationwide hospital study. Radiology, 163, 2, pp: 569-573.

Cack R. K. and Hendee W. R. (1979). Performance evaluation of a fourth-generation computed tomography (CT) scanner. Proceeding of the society of Photo-Optical Instrumentation Engineers, 173, pp: 199-207.

Calzado A., Ruiz Sanz S., Melchor M., and Vañó E. (1995). A comparison of measured and calculated organ doses from CT examinations. Radiation Protection Dosimetry, Vol. 57, Nos. 1-4, pp: 381-385 (Nuclear Technology Publishing).

Caon M. Bibbo G. and Pattison J. (1997). A comparison of radiation dose measured in CT dosimetry phantoms with calculations using EGS4 and voxel based computational models. Phys. Med. Biol., 42, pp: 219-229.

Cashwell E. D. and Everett C. (1959). A practical manual on the Monte Carlo method for random walk problems. (New York: Pergamon Press).

Christensen J. J., Jensen L. C., Jessn K. L., Jøgensn J., Petersen J., and Sorensen E. W. (1992). Dosimetric investigations in computed tomography. Radiation Protection Dosimetry, Vol. 43, pp: 233-236 (Nuclear Technology Publishing).

Cohen G. j. (1979). Contrast-defarl-dose analysis od six different computed tomography scanners. Am. J. Comput. Assist. Tomography, 3 (2), pp: 197-203.

Collie D. A., Wright A. R., Williams J. R., Hashemi-Malayeri B., Stevenson A. J. M., and Turnball C. M. (1994a). Comparison of spiral-acquisition computed tomography and conventional computed tomography in the assessment of pulmonary metastatic diseases. Br. J. Radiology, 67, pp: 436-444.

Collie, D.A., Wright, A.R., Williams, J.R., Hashemi-Malayeri, B., Stevenson, A.J.M., and Turnbull, C.M. (1994b). The effect of spiral CT pitch on the delectability of lung metastases. Br. J. Radiology, Congress Supplement 67, pp: 103. (Abstract)

Conway B. L., McCrohan J. L., Antonsen R. G. Rueter F. G., Stayton R. J. and Suleiman O. H. (1992). Average radiation dose in standard CTR examination of the head : Results of the 1990 NEXT survey. Radiology, 184, pp: 135-140.

Cormack A. M. (1963). Representation of a function by its line integrals with some radiological applications. J. Appl. Phys., 34, pp: 2722-2727.

Cormack A. M. (1964). Representation of a function by its line integrals with some radiological applications II. J. Appl. Phys., 35, pp: 2908-2913.

Cormack A. M. (1980). Early two dimensional reconstruction and recent topic stemming from it (Nobel Prize Lecture). Science 209, pp: 1482-1486.

Cranley K., Gilmore B. J., Fogarty G. W. A., and Desponds L. (1997). Catalogue of Diagnostic X-ray Spectra and Other Data. Produced for the Diagnostic Radiology and Magnetic Resonance Special Interest Group of the Institute of Physics and Engineering in Medicine. IPEM Report 78: Electronic version prepared by D. Sutton.

Crawley M. T. and Rogers A. T. (1994). A Comparison of computed tomography practice in 1989 an 1991. Br. J. Radiology, 67, pp: 872-876.

Cristy M. (1980). Mathematical phantoms representing children of various ages for use in estimates of internal dose. Oak Ridge National Laboratory, NUREG/CR-11159 (Oak Ridge, TN).

Cristy M. (1981). Active bone marrow distribution as a function of age in human. Phys. Med. Biol., 26, pp: 389-400.

Cristy M. and Eckerman K. F. (1987). Specific absorbed fractions of energy at various ages from internal photon sources, part1: methods. Oak Ridge National Laboratory, Report No. ORNL/TM-8381/V1 (Oak Ridge, TN).

Curry T. S. Dowdey J. E. Murry R. C. (1990). Christensen's Physics of Diagnostic Radiology. 4th edition. (Malven, Pennsylvania: Lea & Febiger).

Dixon R. L. and Ekstrand K. E. (1978). A film dosimetry system for use in computed tomography. Radiology, 127: 1, pp: 255-258.

Drexler G., Panzer W., Widenmann L., Williams G., and Zankl M. (1984). The calculation of dose from external photon exposures using reference human phantoms and Monte Carlo methods: Part 3: Organ doses in X-ray diagnosis. Gesellshaft fuuer Strahlen- und Umwelforschung, GSF Report S-1026 (Munich: GSF-Bericht).

Edholm P. (1975). Image construction in transversal computer tomography. Acta Radiol. Suppl. (Stockh.), 346, pp:21-38 .

Edyvean S., Lewis L., Britten A., and Collaborates (May 1997). ImPACT, Department of Medical Physics, St. George Hospital (London, England).

Ekestubbe A., Thilander A., Gröndahl K., Gröndahl H. G. (1993). Absorbed doses

from computed tomography for dental implant surgery: comparison with conventional tomography. Dentomaxillofac. Radiol., 22: 1, pp: 13-17.

Ellis H., Logan B. M., and Dixon A. (1991). Human cross-sectional anatomy: atlas of body section and CT images. (London: Butterworth-Heinemann Ltd).

Ellis R. E. (1961). The distribution of active bone marrow in the adult. Phys. Med. Biol., 5, pp: 255-258.

Evans S. H., Davis R. Cook J., and Anderson W. A. (1989). A comparison of radiation dose to the breast in computed tomography chest examination for two scanning protocols. Clin. Radiol. 40, pp: 45-46.

Faulkner K. and Moores B. M. (1987). Radiation dose and somatic risk from computed tomography. Acta Radiol., 28, pp: 483-488.

FDA (1980a). 21 CFR Part 1020: Diagnostic X-ray systems and their major components; amendments to performance standard: Computed tomography equipment –1020.33. Food and Drug Administration Agency, Bureau of Radiological Health (USA), Federal Register/Vol. 45, No. 213/Friday, October 31, 1980/Proposed Rules.

FDA (1980b). Standard computed tomography dosimetry phantoms as required by 21 CFR 1020.33 (c)(2). Food and Drug Administration, Bureau of Radiological Health, Draft, May 30, 1980 (USA).

FDA (1985). Food and Drug Administration, 21 CFR Ch. 1 (4-1-85) Edition, FDA, NHS (USA) 1020.33.

FDA (1997). Performance standards for ionising radiation emitting products. Sec. 1020.33. Computed Tomography (CT) equipment. Food and Drug Administration, Bureau of Radiological Health (USA).

Fearon T. and Vucich J. (1985). Pediatric patient doses from CT examinations: GE CT/T 9800 scanner. Am. J. Roentgenol. , 144, pp: 805-809.

Fearon T. and Vucich J. (1987). Normalized pediatric organ-absorbed doses from CT-examinations. Am. J. Roentgenol., 148, pp: 171-174.

Felmlee J. P., Gray J. E., Leetzow M. L., And Price J. C. (1990). Estimated fetal radiation dose from multislice CT studies. Am. J. Radiology, No. 154, pp: 185-190.

Fisher H. L. JR. and Snyder W. S. (1967). Distribution of dose in the body from a source of gamma rays distributed uniformly in an organ. Heath physics division annual report for period ending July 1, 1967, pp: 245-257. Oak Ridge National Laboratory, Report No. ORNL-4168. (Oak Ridge, TN).

Fisher H. L. JR. and Snyder W. S. (1968). "Distribution of dose in the body from a source of gamma rays distributed uniformly in an organ". pp: 1473-1486 in Proceedings of the First International Congress on Radiation Protection, (Oxford: Pergamon Press).

Geleijns J., Broerse J. J., Zoetelief J., Zweers D., and Van Unnik J.G. (1995). Patient

dose and image quality for computed tomography in several Dutch hospitals. Radiation Protection Dosimetry, Vol. 57, Nos. 1-4, pp: 129-133 (Nuclear Technology Publishing).

Geleijns J., Van Unnick J. G., Zoetelief J., Zweers J., and Broerse J. J. (1994). Comparison of two methods for assessing patient dose from computed tomography. Br. J. Radiology, 67, pp: 360-365.

Gordon R. and Herman G. T. (1974). Three-dimensional reconstruction from projection. Int. Rev. Cytol., 38, pp: 111-123.

Guidozzi F., Anderson J., and Moore R. (1987). Experimental estimation of intrauterine fetal irradiation dosage in computed tomography using a Rando phantom. Br. J. Obs. Gyn., 94, pp: 35-37.

Hart D., Hillier M. C., Wall B. F. Shrimpton P. C., and Bungay D. (1996b). Doses to patients from medical x-ray examinations in the UK -- 1995 review. National Radiological Protection Board, NRPB-R289. (London: HMSO).

Hart D., Jones D. G., and Wall B. F. (1994). Normalised organ doses for medical X-ray examinations calculated using Monte Carlo techniques. National Radiological Protection Board, NRPB-SR262 (Oxon, England).

Hart D., Jones D. G., and Wall B. F. (1996a). Normalised organ doses for paediatric X-ray examinations calculated using Monte Carlo techniques. National Radiological Protection Board, NRPB-SR279 (Oxon, England).

Hashemi-Malayeri B. and Williams J. R. (1996a). A Practical Approach for the Assessment of Patient Doses from CT Examinations. IPEMB Second Annual National Conference 10-12 September 1996.

Hashemi-Malayeri B. and Williams J. R. (1996c). Patient Doses from Computed Tomography Examinations. The Third Iranian Medical Science Seminar at Manchester, December 1996.

Hashemi-Malayeri B. and Williams J. R. (1996b). A Practical Method for the Assessment of Effective Dose in an Anthropomorphic Phantom. QA and dose assessment of CT Scanners Meeting at the Royal Marsden Hospital, London, on 17 October 1996 (Organised by the IPEMB Diagnostic Radiology & Magnetic Resonance Special Interest Group).

Hayes R. L. and Brucer M. (1960). "Compartimentalized phantoms for the standard man, adolescent and child". Int. J. Appl. Radiat. Isot. 9, pp: 113.

Hobday P. and Parker R. P. (1978). Radiation exposure to the patient in computerized tomography (letter). Br. J. Radiology, 51, pp: 925-926.

Horsely R. J. and Peters V. G. (1976). Short Communication: Radiation exposure from EMI scanner-multiple scans. Br. J. Radiology, 49, 810-811.

Hounsfield G. N. (1973). Computerized transverse axial scanning (tomography): part 1: description of system. Br. J. Radiology, 46, pp: 1016-1022.

Hounsfield G. N. (1980). Computed medical imaging (Nobel Prize Lecture). Science 210, pp: 22-28.

Hubbell J. H. (1977). Photon mass attenuation and energy-absorption coefficients for H, C, N, O, Ar, and seven mixture from 0.1 keV to 20 MeV. Radiat. Res., 70, pp: 58.

Hubbell J. H. (1982). Photon mass attenuation and energy-absorption coefficients from 1 keV to 20 MeV. Int. J. Appl. Rad. Isot. 33, pp: 1269-1290.

Hubbell J. H., Veigele W. J., Briggs E. A., Brown R. T. Cromer D. T. and Howerton R. J. (1975). Atomic from factor, incoherent scattering functions and photon scattering cross sections. J. Phys. Chem. Ref. Data, 4, pp: 471.

Huda W. and Atherton J. V. (1994). Energy imparted in computed tomography. Med. Phys., 22 (8), pp: 1263-1269.

Huda W. and Sandison G. A. (1984). Estimation of mean organ doses in diagnostic radiology from Rando phantom measurements. Health Phys., 47, pp: 463-467.

Huda W. and Sandison G. A. (1985). CT dosimetry and risk estimates. Radiation Protection Dosimetry, Vol. 12, No. 3, pp: 241-249.

Huda W., Sandison G. A., and Lee T. Y. (1989). Patient doses from computed tomography in Manitoba from 1977 to 1987, Br. J. Radiology, 62, pp: 138-144.

Hughes J. S. and O'Riordan M. C. (1993). Radiation exposure of the UK population -- 1993 Review. National Radiological Protection Board, NRPB-R263 (London: HMSO).

IAEA (1979). The Calibration of dosemeters used in radiotherapy. Vienna, International Atomic Energy Agency, Report series No. 185.

IAEA (1994). Calibration of dosemeters used in radiotherapy. Vienna, International Atomic Energy Agency, Technical Reports Series No. 374.

ICRP[1] (1975). Report of the task group on reference man. ICRP Publication 23 (Oxford: Pergamon Press).

ICRP (1977). Recommendations of the International Commission on Radiological Protection. ICRP Publication 26, Ann. ICRP, Vol. 1, No. 3 (Oxford: Pergamon Press).

ICRP (1987). Data for use in protection against external radiation. ICRP publication 51, Ann. ICRP, Vol. 17, No. 2/3, (Oxford: Pergamon Press).

ICRP (1991). 1990 Recommendations of the International Commission on Radiological Protection. ICRP Publication 60, Ann. ICRP, Vol. 21, No. 1-3 (Oxford: Pergamon Press).

ICRU[2] (1979). Average Energy Required to Produce An Ion Pair. ICRU Report 31

[1] **International Commission on Radiological Protection.**
[2] **International Commission on Radiation Units and Measurements.**

(Washington, DC: ICRU).

ICRU (1980). Radiation quantities and units. ICRU Report 33 (Washington, DC: ICRU).

ICRU (1989). Tissue substitutes in radiation dosimetry and measurement. ICRU Report 44 (Bethesda, Maryland: ICRU).

ICRU (1992). Phantoms and computational models in therapy, diagnosis and protection. ICRU Report 48 (Bethesda, Maryland: ICRU).

IEC 1223-2-6 (1993). Evaluation and routine testing in medical imaging departments. Part 2-6: Constancy tests of equipment for computed tomography. Draft IEC SC 62B (Central Office) 107.

Jones D. E. A. and Raine H. C. (1949). Letter, Br. J. Radiology, 22, 549.

Jones D. G. and Shrimpton P. C. (1991). Survey of CT practice in the UK: part 3: normalised organ doses calculated using Monte Carlo techniques. National Radiological Protection Board, NRPB-R250 (London: HMSO).

Jones D. G. and Shrimpton P. C. (1993). Normalised organ doses for X-ray computed tomography calculated using Monte Carlo techniques. National Radiological Protection Board, NRPB-SR250 (London: HMSO).

Jones D. G. and Wall B. F. (1985). Organ doses from medical X-ray examinations calculated using Monte Carlo techniques. National Radiological Protection Board, NRPB-R186 (London: MSO).

Jones K. P. and Garett J. H. (1985). Patient absorbed dose for Philips Tomoscan 300 CT scanner. Br. J. Radiology. 58, pp: 365-367.

Jucius R. A. and Kambic G. X. (1977). Radiation dosimetry in computed tomography. Proceedings of the Society of Photo-Optical Instrumentation Engineers, 127, pp: 286-295.

Kienböck R. (1906). On the quantimetric method. Arch. Roentgen Ray 11,17.

Knight J. N. Roussin R. W. (1983). Photon interaction data DLC-99/HUGO. Radiation Shielding Information Center. Oak Ridge National Laboratory (Oak Ridge, TN).

Kramer R., Zankl M., and Williams G. (1982). The calculation of dose from external photon exposure using reference human phantoms and Monte-Carlo methods. Part 1: The male (Adam) and female (Eva) adult mathematical phantoms. Gesellshaft fuuer Strahlen - und Umwelforschung m.b.H, Muenchen, GSF-S-885 (Neuherberg, Germany: GSF-Bericht).

Krauss O. and Shumacher H. (1977). Absorbed dose to the patient by computerized whole body X-ray tomography. Proceedings of the 4th International Radiation Protection Association Meeting, Paris, April 24-30, 1977. Vol. 4, pp: 1095-1098.

Kron T. (1995).Thermoluminescence dosimetry and its applications in medicine - Part 2: History and applications. Australas. Phys. Eng. Sci. Med., 18: 1, pp: 1-25.

Le Heron J. C. (1992). Estimation of effective dose to the patient during medical x-ray examinations from measurements of the dose-area product. Phys. Med. Biol., 37, pp: 2117-2126.

Le Heron J. C. (1993). CTDOSE: a user's guide. National Radiation Laboratory (Christchurch, New Zealand: Ministry of Health).

Lund E. and Halaburt H. (1982) Irradiation dose to the lens of the eye during CT of the head. Neuroradiology, 22, pp: 181-181.

Maclennan A. C. and Hadley D. M. (1995). Radiation dose to the lens from compute tomography scanning in a neuroradiology department. Br. J. Radiology, 68, pp: 19-22.

Markus B. (1956). Über den begriff der gewebe äquivalenz und enige 'vasserähnliche' phantom-substanzen für quanten von 10 keV bis 100 MeV sowie schnelle elektronen, Strahentherapie,101, 111. (Cited in ICRU 1992).

Marmolya G., Wiesen E. J., Yagan R., Haria C. D. and Shah A. C. (1991). Paranasal sinuses: low dose CT. Radiology, 181, pp: 689-691.

Mayo J. R., Jackson S. A., and Muller N. L. (1993). High resolution CT of the chest. Am. J. Roentgenol., 160, pp: 479-481.

Mayo J. R., Webb W. R., Gould R., Stein M. G., Bass I., Gamsu G., and Goldberg H. I. (1987). High resolution CT of the lungs: An optimal approach. Radiology, 163, pp: 507-510.

McCrohan J. L., Patterson J. F., Gagne R. M., and Goldstein H. A. (1987). Average dose in a standard head examination for 250 CT systems. Radiology, 163, pp: 263-268.

McCullough E. C. and Payne J. T. (1978). Patient dosage in computed tomography. Radiology, 129, 457-463.

McCullough E. C., Baker H. L., Houser O. W., and Reese D. F., (1974). An evaluation of the quantitative and radiation features of a scanning X-ray transverse axial tomography: the EMI scanner. Radiology, 111, pp: 709-715.

McCullough E., C., Payne J. T., Baker H. L., Hatterly R. R., Sheedy P. F., Stephens D. H., and Gedgaudus E. (1976). Performance evaluation and quality assurance of computed tomography scanners, with illustration from EMI, ACTA, and Delta scanners. Radiology, 120, pp: 173-188.

McKinlay A. F. (1981). Thermoluminescence dosimetry. (Bristol: Adam Hilger Ltd).

MDA (1994). An assessment of the imaging performance of the Siemens Somatom Plus-S CT scanner. (Crown: HMSO).

MDA (1995). An assessment of the imaging performance of the IGE HiSpeed Advantage CT scanner. (Crown: HMSO).

MDD (1991). Single product CT report on the imaging performance of the IGE Sytec

3000 Scanner. (Crown: HMSO).

Moore M. M., Cacak R. K., and Hendee W. R. (1981). Multisegmented ion chamber for CT scanner dosimetry. Med. Phys. 8 (5), pp: 640-645.

Moss A. A. and Goldberg, H. I. (1980). Computed tomography, ultrasound and X-ray: an integrated approach. (Academic Press).

Mossman K. L. (1982). Analysis of risk in computerized tomography and other diagnostic radiology procedures. Comput. Radiol., 6 (5), pp:251-256.

Murphy F. and Heaton B. (1985). Patient doses received during whole body scanning using a Elscint 905 CT scanner. Br. J. Radiology. 58, pp: 1197-1201.

Naidich D. P. (1994). Helical computed tomography of the thorax. Clinical application. Radiologic Clinics of North America, 32 (4), pp: 759-774.

Naidich D. P., Marshal C. H., Gribbin C., Arams R. S., and McCauley D. I. (1990). Low dose CT of the lung: preliminary observation. Radiology, 175, pp:729-731.

Naik K. S., Ness L. M., Bowker A. M., and Robinson P. J. A. (1996). Is computed tomography of the body overused? An Audit of 2068 attendances in a large acute hospital. Br. J. Radiology, 69, pp: 126-131.

NCRP[3] (1989). Exposure of the US population from diagnostic medical radiation. NCRP Report No. 100 (Bethesda, MD, USA: NCRP).

NCRP (1990). The relative biological effectiveness of radiations of different quality. NCRP Report No. 104. (Bethesda, MD, USA: NCRP).

New Scientists (1972). X-ray diagnosis peers inside the brain. New Scientist, 27 April, pp: 207.

Nishizawa K., Maruyama T., Takayama M., Okada M., Hachyia J., and Furuya Y. (1991). Determination of organ doses and effective dose equivalent from computed tomographic examinations. Br. J. Radiology, 64, pp: 20-28.

NRC[4] (1990). 1990 Health effects of exposure to low levels of ionizing radiation - BEIR V (Washington, DC: National Academy Press).

NRPB (1990). Patient dose reduction in diagnostic radiology. Document of the National Radiological Protection Board, Vol. 1, No. 3 (London: HMSO).

NRPB (1992). Protection of the patient in X-ray computed tomography and further statement on radon affected areas. Documents of the National Radiological Protection Board, Vol. 3, No. 4, (London: HMSO).

Olson A. and High M. (1979). Performance characteristics of a translate-rotate head scanner with xenon detectors. Proceedings of the Society of Photo-Optical Instrumentation Engineers, 173, pp: 208-215.

---

[3] **(USA) National Council on Radiation Protection and Measurements.**
[4] **(USA) National Research Council.**

Panzer E., Scheurer C., and Zankl M. (1989). Doses to patients in CT examinations. Results and consequences from a field study in the Federal Republic of Germany. BIR Report 20: optimization of image quality and patient exposure in diagnostic radiology (Eds. B. M. Moores, B. F. Wall, H. Eriskat, and H. Schibilla) pp: 185-188 (London: British institute of Radiology).

Panzer W. and Zankl M. (1989). A method of estimating embryo doses resulting from computed tomographic examinations. Br. J. Radiology, 62, 936-939.

Perry B. J. and Bridges C. (1973). Computerized transverse axial scanning (tomography): part 3: radiation dose considerations. Br. J. Radiology, 46, pp: 1048-1051.

Peters T. M. (1975). Principles of computerised tomography. Australas Radiol.,19(2), pp:118-126.

Poletti J. L. (1984) An ionisation chamber based CT dosimetry system. Phys. Med. Biol., 29, pp: 725-731.

Poletti J. L. (1992). Doses to patients from CT scanning in New Zealand. National Radiation Laboratory (Christchurch, New Zealand).

Poletti J. L. (1996). Patient doses from CT in New Zealand and a simple method for estimating effective dose. Br. J. radiology, 69, pp: 4332-436.

Redpath T. A. (1992). Private communication.

Romans L. E. (1995). Introduction to computed tomography. (London: Williams and Wilkins).

Rosenstein M. (1976). Organ doses in diagnostic radiology. US Department of Health, Education and Welfare Bureau of Radiological Health Technical Publication FDA 76-8030.

Rosenstein M. (1989). Handbook of selected tissue doses for projections common in diagnostic radiology. HHS Publication, 89-8031, December 1989 (FDA, USA).

Sager E. M., Skretting A., and LindskÖld L. (1989). Absorbed dose resulting from a specially designed computer tomography technique for examination of the urinary bladder. Acta Radiol., 30, pp: 57-60.

Schofield K. A., McNeil E. A., Turner S., and Pryce R. (1996). Computed Tomography dose variation in the west midland region in Final programme. In abstracts of: QA and Dose Assessment of CT scanners Meeting at the Royal Marsden Hospital, London. Organised by the Institute of Physics and Engineering in Medicine and Biology (York, England).

Seeram E. (1994). Computed tomography. Physical principles clinical applications & quality control. (W.B. Saunders Company).

Shope T. B., Gange R. M., and Johnson G. C. (1981). A method for describing the dose delivered by transmission X-ray compute tomography. Med. Phys. 8, pp:488-495.

Shope T. B., Morgan T. J., Showalter C. K., Pentlow K. S., Rothenberg L. N., White D. R., and Speller R. D. (1982). Radiation dosimetry of computed tomography systems from ten manufacturers. Br. J. Radiology, 55, pp: 60-69.

Shrimpton P. C. (1985). Energy imparted as a measure of radiological hazards to patients from X-ray examinations. J. Int. Fed. Med. Biol. Eng. 23, Suppl. Part 2, pp: 1135-1136.

Shrimpton P. C. and Wall B. F. (1986). Dose to patients from medical examinations in Great Britain. Radiol. Prot. Bull., No. 77, pp: 10-14.

Shrimpton P. C. and Wall B. F. (1992). Assessment of patient doses from computed tomography. Radiation Protection Dosimetry, Vol. 43 Nos. 1-4, pp: 205-208 (Brussels-Luxembourg: Nuclear Technology Publishing).

Shrimpton P. C. and Wall B. F. (1993). CT -- An increasingly important slice of the medical exposure of patients. Br. J. Radiology, 66, 1067-1068 (1993).

Shrimpton P. C., Hart D., Hillier M. C., Wall B. F., and Faulkner K. (1991a). Survey of CT Practice in the UK. Part 1: aspects of examination frequency and quality assurance. NRPB-R248, National Radiological Protection Board (London: HMSO).

Shrimpton P. C., Jones D. G., Hillier M. C., Wall B. F., Le Heron J. C., and Faulkner K. (1991b). Survey of CT practice in the UK. Part 2: dosimetric aspects. National Radiological Protection Board, NRPB-R249 (London: HMSO).

Shrimpton P. C., Wall B. F., and Fisher E. S. (1981). The Tissue equivalence of the Alderson Rando anthropomorphic phantom for X-ray of diagnostic qualities. Phys. Med. Biol., Vol. 26, No. 1, pp: 133-139.

Shrivastava P. N., Lynn S. L., and Ting J. Y. (1977). Exposures to patients and personnel in computed axial tomography. Radiology, 125, pp: 411-415.

Snyder W. S., Fisher H. L., Ford M. R., and Warner G. G. (1969). Estimates of absorbed fractions for monoenergetic photon sources uniformly distributed in various organs of a heterogeneous phantom. J. Nucl. Med., 10, Suppl. 3, Pamphlet No. 5.

Snyder W. S., Ford M. R., and Warner G. G. (1974). Revision of MIRD pamphlet No. 5 entitled "Estimates of absorbed fractions for monoenergetic photon sources uniformly distributed in various organs of a heterogeneous phantom". Health Phys. Div., Annual Prog. Rep., 5 ORNL-4979.

Southon F. C. (1981). CT scanner comparison. Med. Phys. 8(1), pp: 62-75.

Speller R. D. , White D. R., Veerappan R., Coleman A. J., and Waller P. E. (1981b). A Survey of 29 EMI CT machines in Britain. Br. J. Radiol., 54, pp: 232-240.

Speller R. D., White D. R., Showalter C. K., Rothenberg L. N., Pentlow K. S., Morgan T. J., and Shope T. B. (1981a). An evaluation of CT systems from ten manufacturers. Br. J. Radiology, 54, pp: 1053-1061.

Stacy A. J., Bevan A. R., and Dickens C. W. (1961). A new phantom material employing depolymerised natural rubber. Br. J. Radiology, 34, 510.

Storm E. and Israel H. I. (1970). Photon cross section from 1 keV to 100 MeV. Nucl. Data sect. Vol. No. 6, A7, pp: 565-681.

Storrs B. B. and Byrd S. E. (1988). Radiation exposure to the ocular lens during CT scanning. Pediatr. Neurosci., 14, pp: 254-257.

Strong A. B. et al. (1990). Application of three-dimensional display techniques in medical imaging. J. Biomedical Eng., 12, pp: 237-238

Suzuki A. and Suzuki M. N. (1978). Use of a pencil-shaped ionisation chamber for measurement of exposure resulting from a computed tomography scan. Med. Phys., 5(6), pp: 536-539.

Thomas S. R., Schneider A. J., Kereiakes J. G., Lukin R. R., Chambers A. A., and Tomsik T. A. (1978). An evaluation of the performance characteristics of different types of collimators used with the EMI brain scanner (MKI) and their significance in specific clinical applications. Med. Phys., 5(2), pp: 124-132.

Udapa J. K. and Odhner D. (1991). Fast visualization manipulation and analysis of binary volumetric object. IEEE Comput. Graph. Appl., 11, pp:53-62.

UNSCEAR[5] (1988). 1988 report to the General Assembly: sources, effects, and risks of ionising radiation. (New York: United Nations).

Vañó E., Gonzàles L., Galzado A., Moràn P., and Delgado V. (1989). Some indicative parameters on diagnostic radiology in Spain: First dose estimators. Br. J. Radiology, 62, pp: 20-26.

Van Unnik J.G., Broerse J. J., Geleijns J., Jansen J. Th. M., Zoetelief J., and Zweers D. (1997). Survey of CT techniques and absorbed dose in various Dutch hospitals. Br. J. Radiology, 70, pp: 367-371.

Villafana T. (1987). CT and MRI, in computed tomography: cranial (by Lee S. H. and Rao K. C. V. G. eds.). pp: 1-43 (New York: McGraw-Hill).

Villafana T., Scouras J., and Kirkland L. (1978). Health physics aspects of the EMI computerized tomography brain scanner. Health Physics, Vol. 34, pp: 71-82.

Wagner L. K., Archer B. R., and Zeck O. F. (1986). Conceptus dose from two state-of-the-art CT scanners. Radiology, 159, pp: 787-792.

Wall B. F. and Hart D. (1997). Revised radiation doses for typical X-ray examinations: report on a recent review of doses to patients from medical X-ray examinations in the UK by the NRPB. Br. J. Radiology, 70, pp: 437-439.

Wall B. F., Green D. A. C., and Veerappan R. (1979). The radiation dose from EMI brain and body scanners. Phys. Med. Biol., 53, 615, pp: 189-196.

Wall B. F., Harrison R. M., and Spiers F. W. (1988). Patient dosimetry techniques in diagnostic radiology. Report No. 53, the Institute of Physical Sciences in Medicine

---

[5] United Nations Scientific Committee on the Effect of Atomic Radiation

(Oxford: Bocardo Press).

Webb S. (1990). From watching of shadows the origins of radiological tomography. (Adam Hilger).

Webb S. (ed.) (1988). The physics of medical imaging.(Bristol: IOP Publishing Ltd).

Weinstein M. A., Berlin A. J., and Duchesneau P. M. (1976). High resolution compute tomography of the orbit with the Ohio Nuclear Delta head scanner. Am. J. Roentgenol., 127, pp: 175-177.

White D. R., Speller R. D., and Taylor B. A. (1981). Evaluation performance characteristics in computerized tomography. Br. J. Radiology, 54, pp: 221-231.

Wright A. R., Collie D. A., Williams J. R., Hashemi-Malayeri, B., Stevenson A. J. M., and Turnbull C. M. (1996). Pulmonary Nodules: Effect on Detection of Spiral CT Pitch. Radiology, 199, pp: 837-841.

Zankl M., Panzer W., and Drexler G. (1991). The calculation of dose from external photon exposures using reference human phantom and Monte Carlo methods. Part VI: Organ doses from computed tomographic examinations. Gesellshaft fuuer Strahlen - und Umwelforschung, GSF Report 30/91 (Neuherberg, Germany: GSF-Bericht).

Zankl M., Panzer W., and Drexler G. (1992). The calculation of organ doses from computed tomography examinations. Radiation Protection Dosimetry, Vol. 43, No. 1/4, pp: 237-239 (Nuclear Technology Publishing).

Zankl M., Panzer W., Petoussi-Henβ N., and Drexler G. (1995). Organ doses for children from computed tomographic examinations. Radiation Prot. Dosimet., Vol. 57, Nos.: 1-4, pp: 393-396 (Nuclear Technology Publishing).

Zwirewich C. V., Mayo J. R., and MÜller N. L. (1991) Low dose high resolution CT of lung parenchyma. Radiology, 180, pp: 413-417.

RANDO PHANTOM DESIGN

(Location of Organs and Tissues of Interest)

In this appendix the location of organs and tissues of interest are shown for every slice (section) of the phantom. The design of the Rando phantom for determining the location of organs and tissues of the interest has been carried out based on the principles mentioned earlier in chapter four.

There is now a world wide agreement over the orientation of sections and cross sectional images. Following an extensive effort over the last few years, the axial cross-sectional images of the body are now viewed in a standard conventional manner that has been adopted almost in all recent anatomy books and atlases of body sections and CT images. All cross-sectional images in routine clinical practice are now viewed from "below" and "looking up" (Figure A.1).

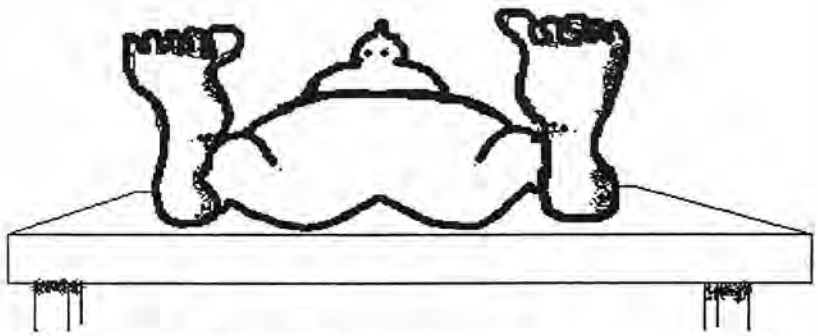

Figure A.1: View from below looking up.

This is the logical method in which a doctor approaches for the examination of a supine patient that is from the right hand, foot end of the coach. The image is thus in the correct orientation for doctor's palpating right hand. Based on this standard all axial sections should be displayed with an orientation logo shown in Figure A.2. Here the right of the patient is on the viewer's left.

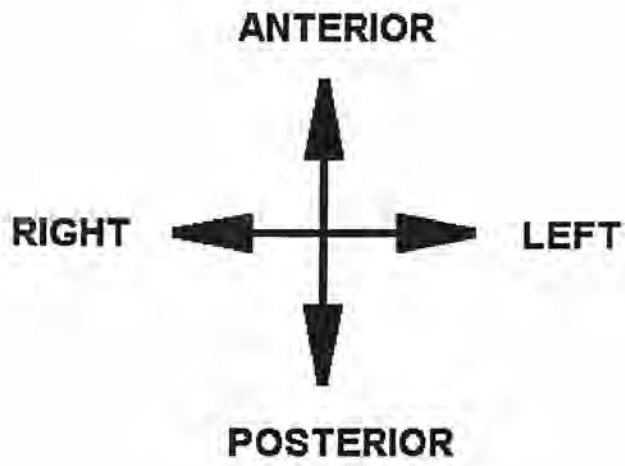

Figure A.2: The standard orientation used for displaying (viewing) CT cross sectional images.

Therefore to keep our diagrams consistent with this standard, this approach has been employed for each diagram in this appendix showing the position of organs or tissues of interest in a single slice (2.5 cm thick cross-sectional portion) of the Rando phantom.

Notes on the diagrams

It has been tried to keep a consistent approach for demarcation of organs on every slice of the phantom. The diagrams are presented in sequence for transverse slices of the Rando physical phantom showing the corresponding location of organs and tissues of interest. Every diagram represents one slice of the Rando phantom starting from the slice number one at the top of the head and finishing at the slice number thirty four at the base of the trunk of the phantom. Based on the atlas of body sections and CT images (Ellis et al. 1991) used as a reference for determining the location of organs and tissues of interest in the phantom, It was assumed that there is no organ or tissue of interest to be demarcated in slice number of zero, eight, and thirty five. Therefore no diagram has been presented for these three slices. The shape and location of organs and tissues of interest were demarcated by taking the relevant

vertebra of the phantom skeleton as the reference point and then defining the position of organs and tissues from the relevant sections to the vertebra from the atlas of body sections and CT images (Ellis et al. 1991). Table A.1 shows the corresponding vertebra (thoracic, lumbar or cervical) taken as the reference point for each slice of the phantom. Table A.2 shows the list of organs and tissues of interest in each slice of the phantom excluding bone, red bone marrow and skin found in all slices.

Table A.1: The position of the corresponding vertebra in the Rando Phantom.

Phantom slice no.	Vertebra* no.
5	C_1
6	C_1, C_{1-2}
7	C_2, C_3, C_{3-4}
8	C_{3-4}, C_5
9	C_5, C_6, C_7
10	C_7, T_{1-2}
11	T_{1-2}, T_3
12	T_3, T_{4-5}
13	T_{4-5}, T_{5-6}
14	T_{5-6}, T6-7
15	T_{6-7}, T_{7-8}
16	T_{7-8}
17	T_{7-8}, T_{8-9}
18	T_{8-9}, T_{9-10}
19	T_{9-10}, T_{10}
20	T_{10}, T_{11}
21	T_{11}, T_{12}
22	T_{12}, T_{12}-L_1
23	T_{12}-L_1, L_{1-2}
24	L_{1-2}, L_2
25	L_2, L_{2-3}
26	L_{2-3}, L_3
27	L_3, L_4
28	L_4, L_{4-5}
29	L_{4-5}, L_5, S_1
30	L_5, S_1, S_2
31	$S_{2(male)}$, $S_{3(female)}$)
32	$S_{3(male)}$, $S_{4(male)}$, $S_{5(male)}$
33	$S_{5(male)}$, $Coccyx_{(male\ and\ female)}$

*** C: Cervical Vertebra, T: Thoracic Vertebra, L: Lumbar Vertebra, S: Sacrum Segments.**

Table A.2: The list of organs and tissues of interest in every slice of the Rando phantom.

Slice no.	Organs and tissues of interest
0	Brain
1	Brain
2	Brain
3	Brain
4	Parotid
5	Parotid
6	Parotid
7	Parotid
9	Thyroid, Oesophagus
10	Thyroid, Oesophagus, Lung
11	Thyroid, Oesophagus, Lung
12	Thymus, Oesophagus, Lung
13	Thymus, Oesophagus, Lung
14	Oesophagus, Lung, Breasts
15	Oesophagus, Lung, Breasts
16	Oesophagus, Lung, Breasts
17	Oesophagus, Lung, Breasts
18	Oesophagus, Lung, Liver, Breasts
19	Lung, Liver, Spleen, Stomach, Breasts
20	Liver, Spleen, Stomach, Adrenal
21	Liver, Spleen, Stomach, Adrenal, Kidney, Pancreas, SI*, ULI*
22	Liver, Spleen, Stomach, Kidney, Pancreas, SI, ULI, LLI*
23	Liver, Kidney, Pancreas, SI, ULI, LLI
24	Liver, Kidney, Pancreas, SI, ULI, LLI
25	Liver, Kidney, SI, ULI, LLI
26	SI, ULI, LLI
27	SI, ULI, LLI
28	SI, ULI, LLI
29	SI, ULI, LLI
30	SI, ULI, LLI, Uterus
31	SI, ULI, LLI, Uterus, Ovaries
32	SI, ULI, LLI, Uterus, Bladder
33	LLI, Bladder, Prostate
34	LLI, Bladder, Testis

* SI: small intestine; ULI: upper large intestine; LLI: lower large intestine

In each diagram two perpendicular axes represent the anterior-posterior and right-left orientations of the slice based on the standard manner of displaying CT images. In each diagram the outer lines shows the layout of the relevant slice of the phantom. The position of two pegs (plastic rods) which hold parallel slices of the phantom together are shown with two grey shaded circles in every slice.

Diagram 1: Location of organs and tissues of interest in slice #1 of the Rando phantom.

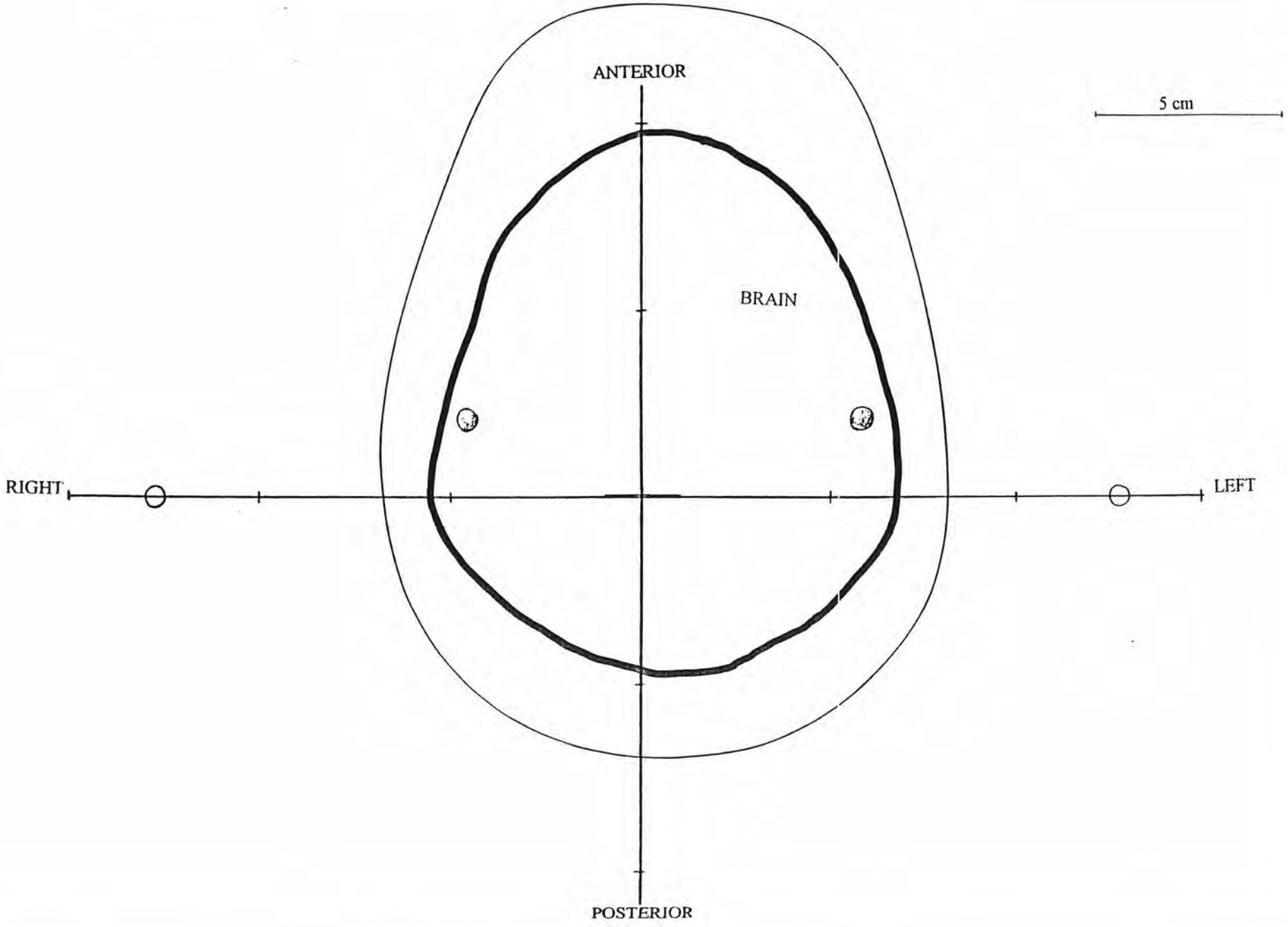

Diagram 2: Location of organs and tissues of interest in slice #2 of the Rando phantom.

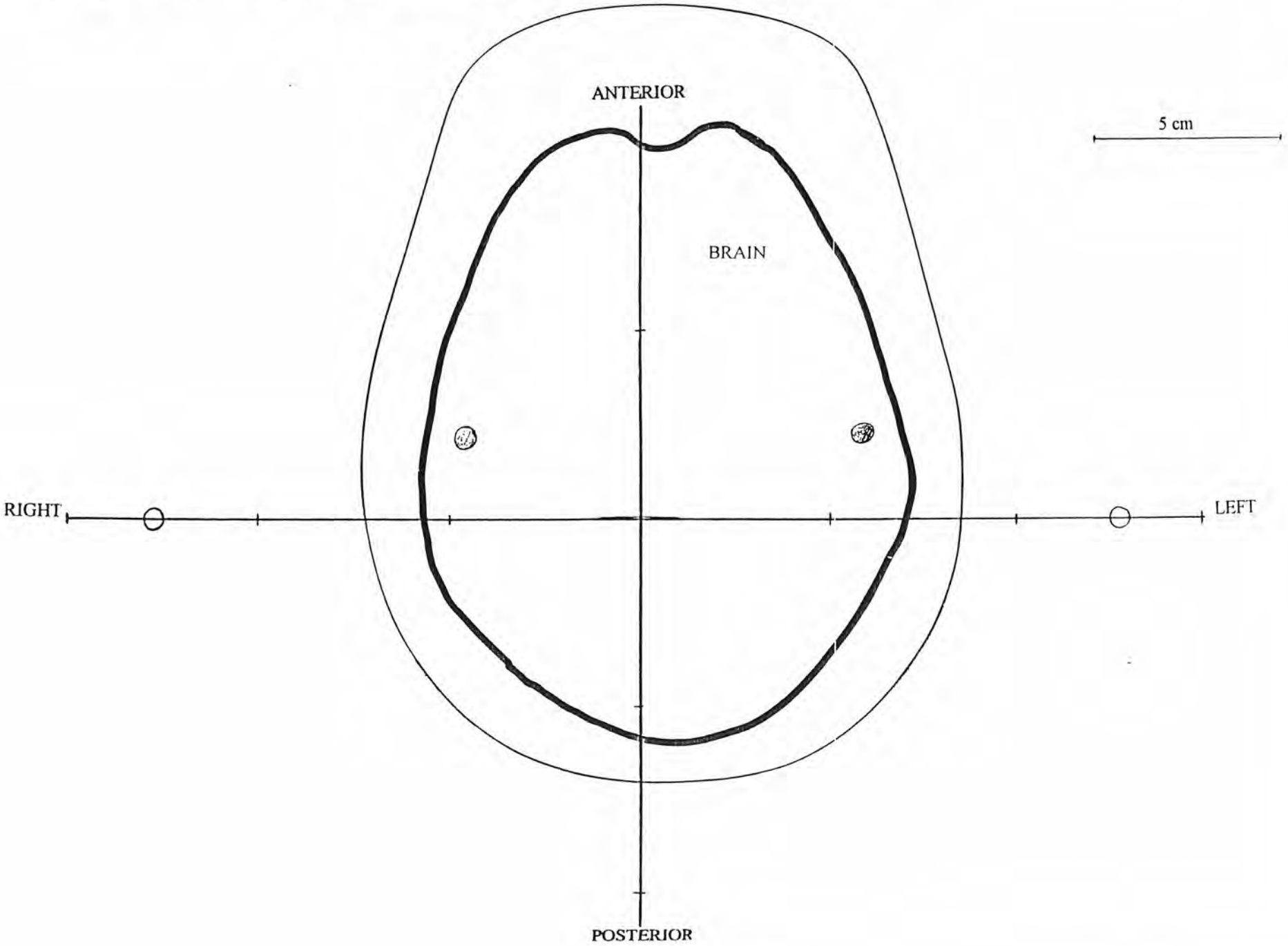

Diagram 3: Location of organs and tissues of interest in slice #3 of the Rando phantom.

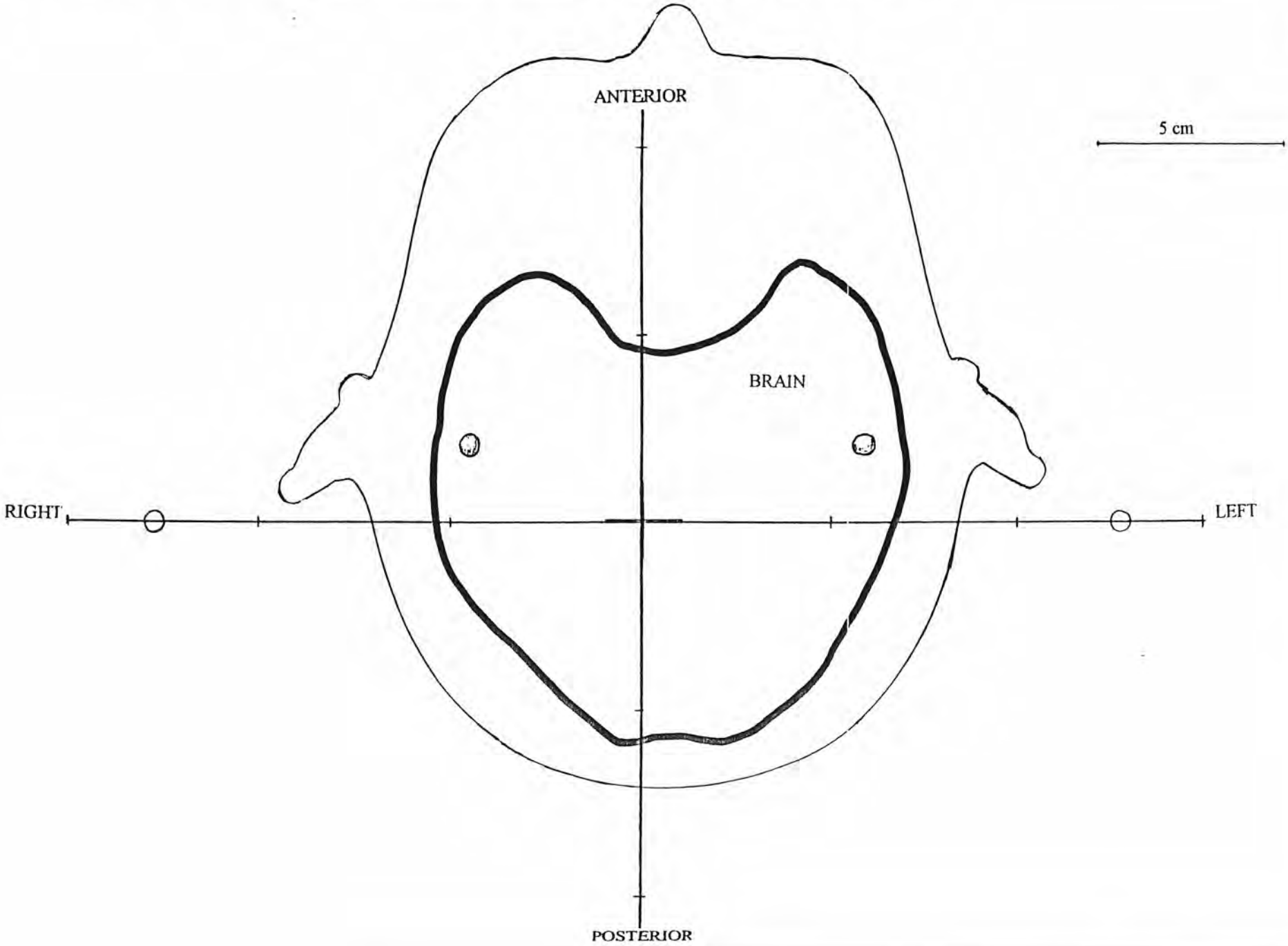

Diagram 4: Location of organs and tissues of interest in slice #4 of the Rando phantom.

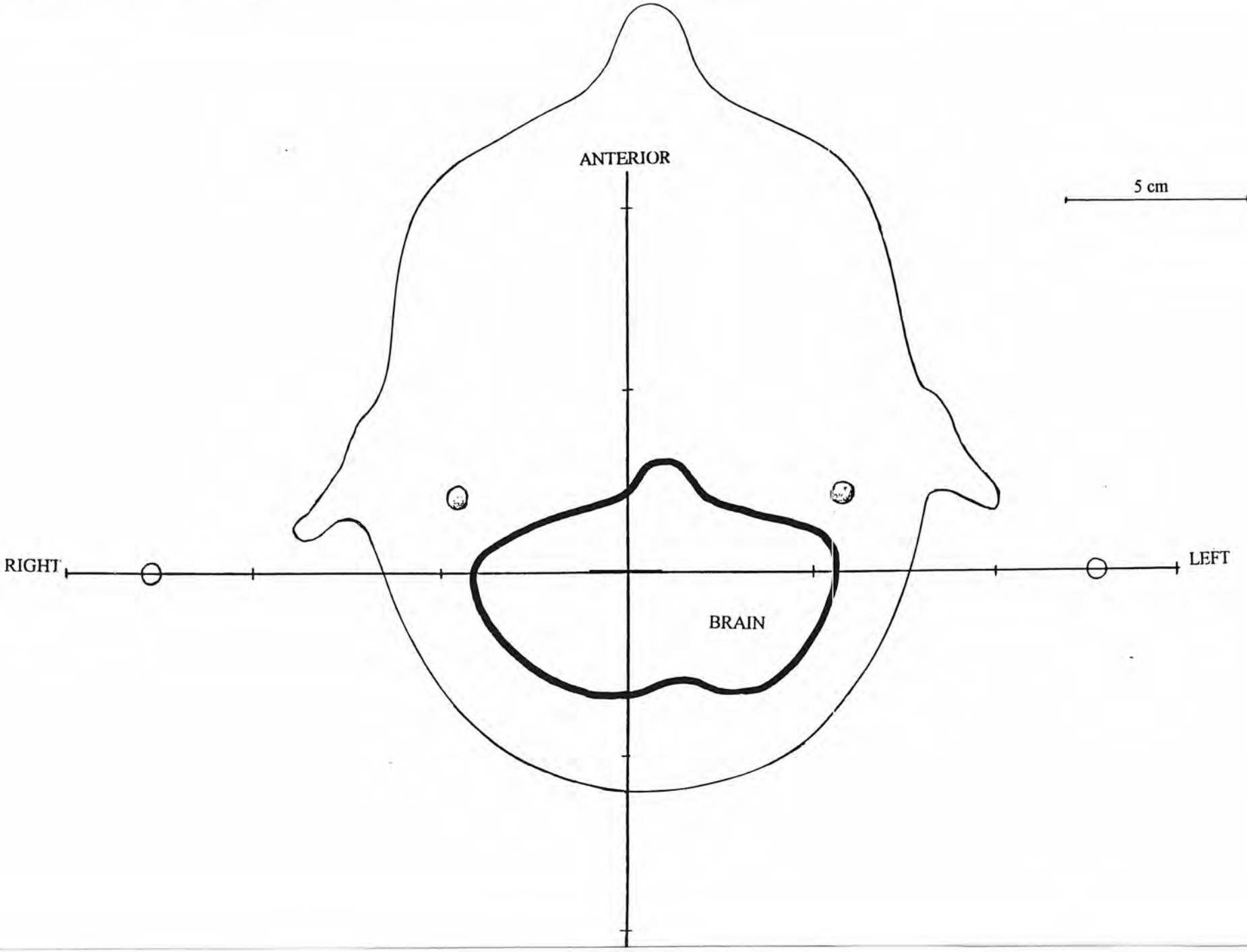

Diagram 5: Location of organs and tissues of interest in slice #5 of the Rando phantom.

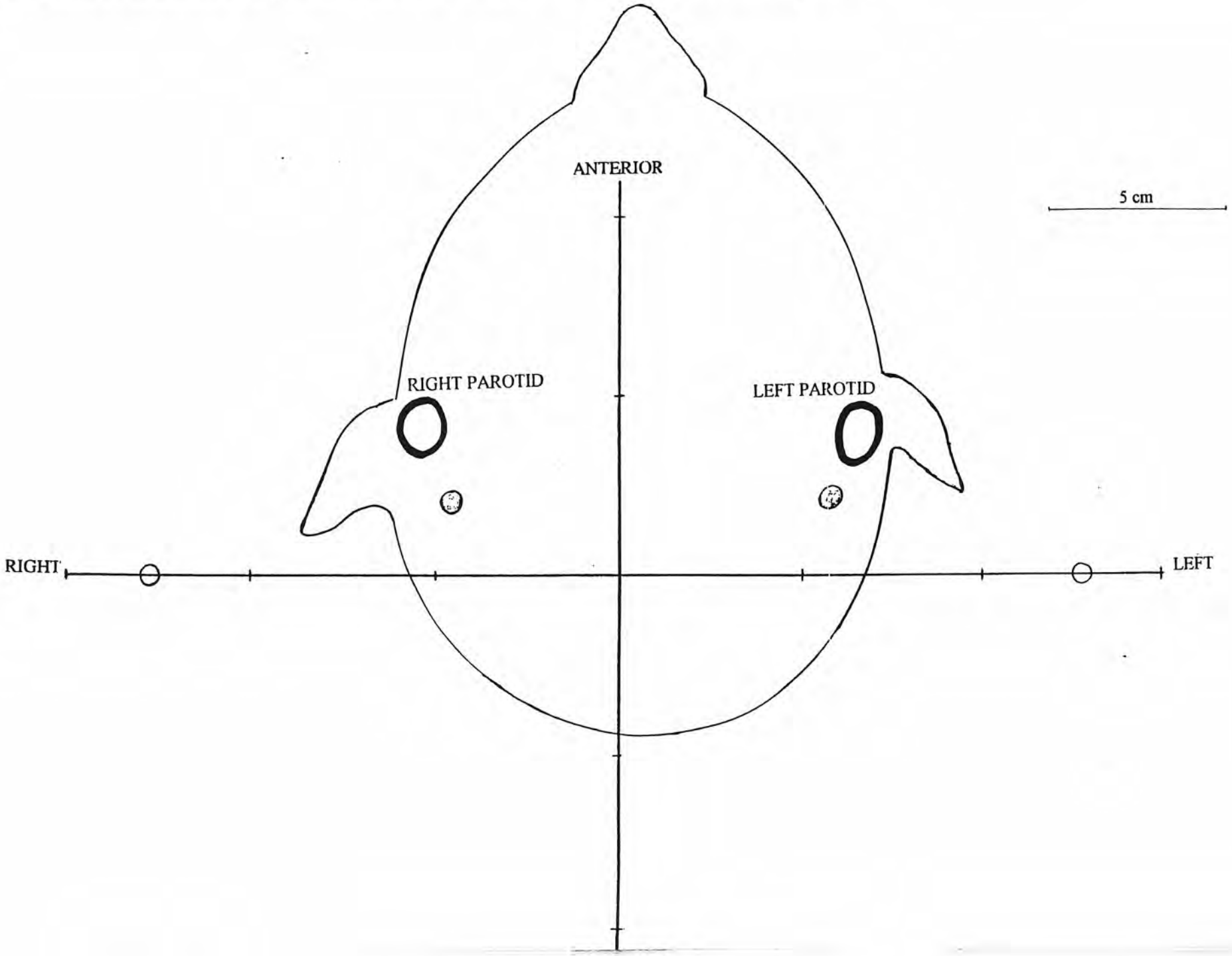

Diagram 6: Location of organs and tissues of interest in slice #6 of the Rando phantom.

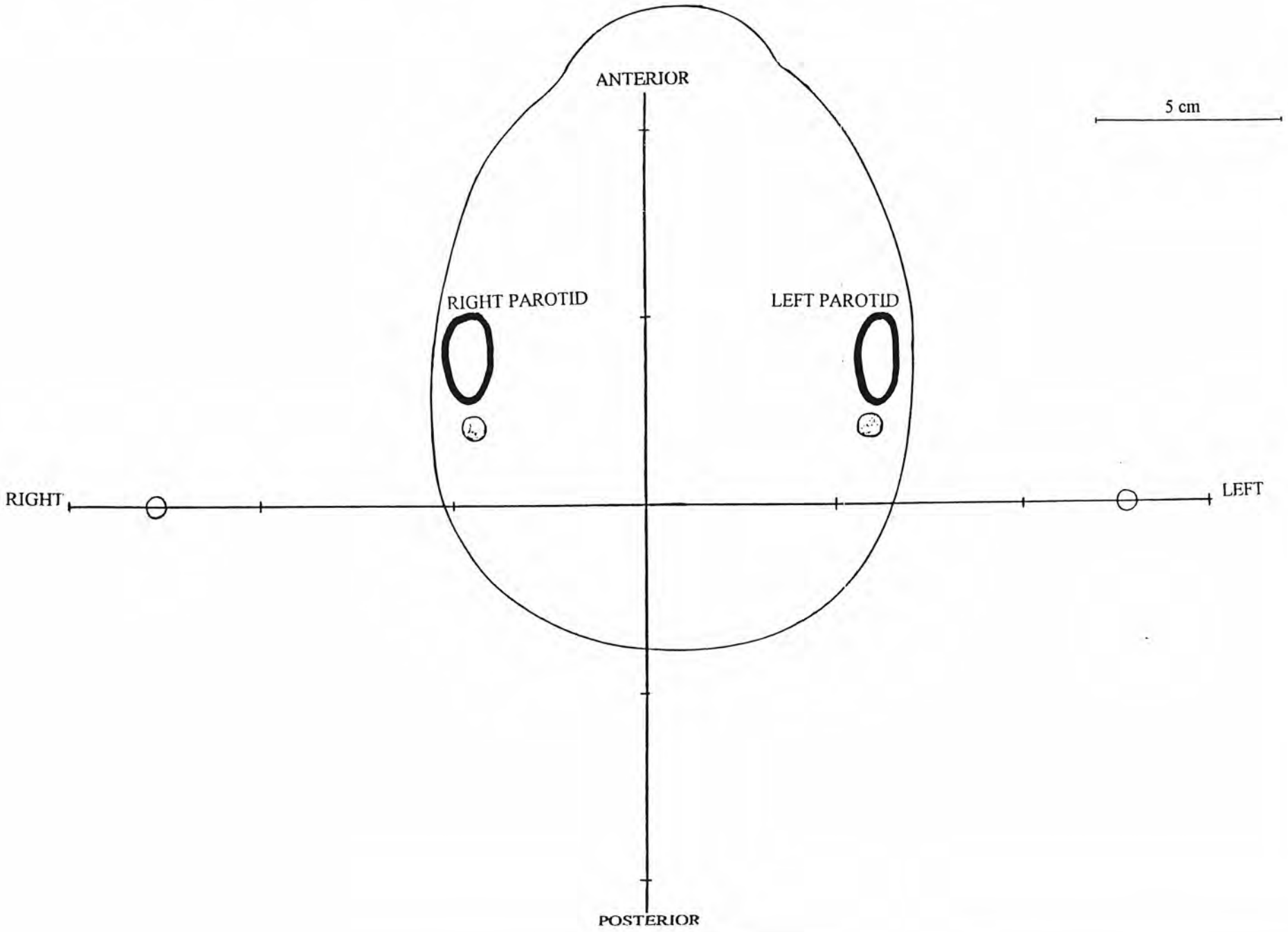

Diagram 7: Location of organs and tissues of interest in slice #7 of the Rando phantom.

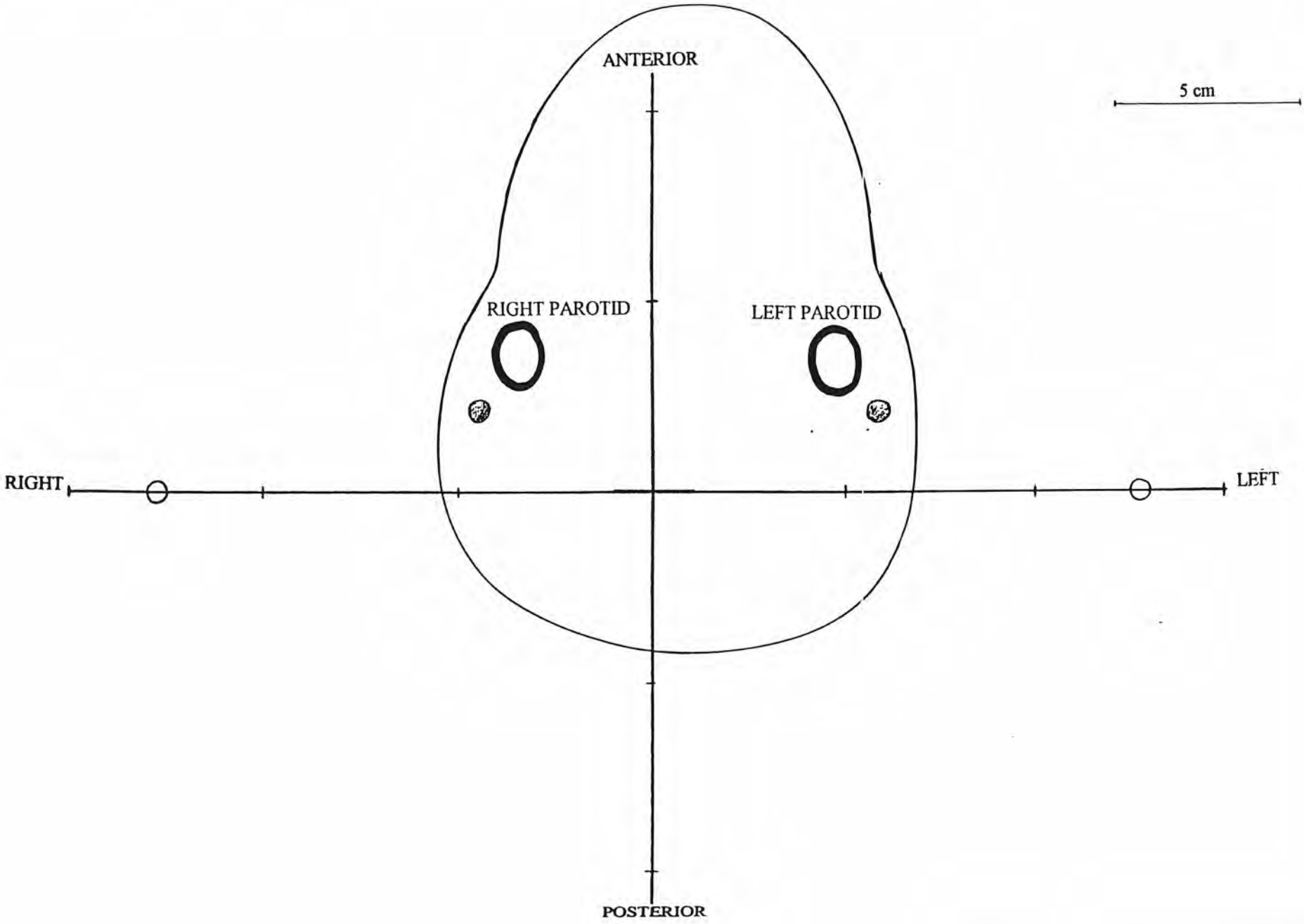

Diagram 8: Location of organs and tissues of interest in slice #9 of the Rando phantom.

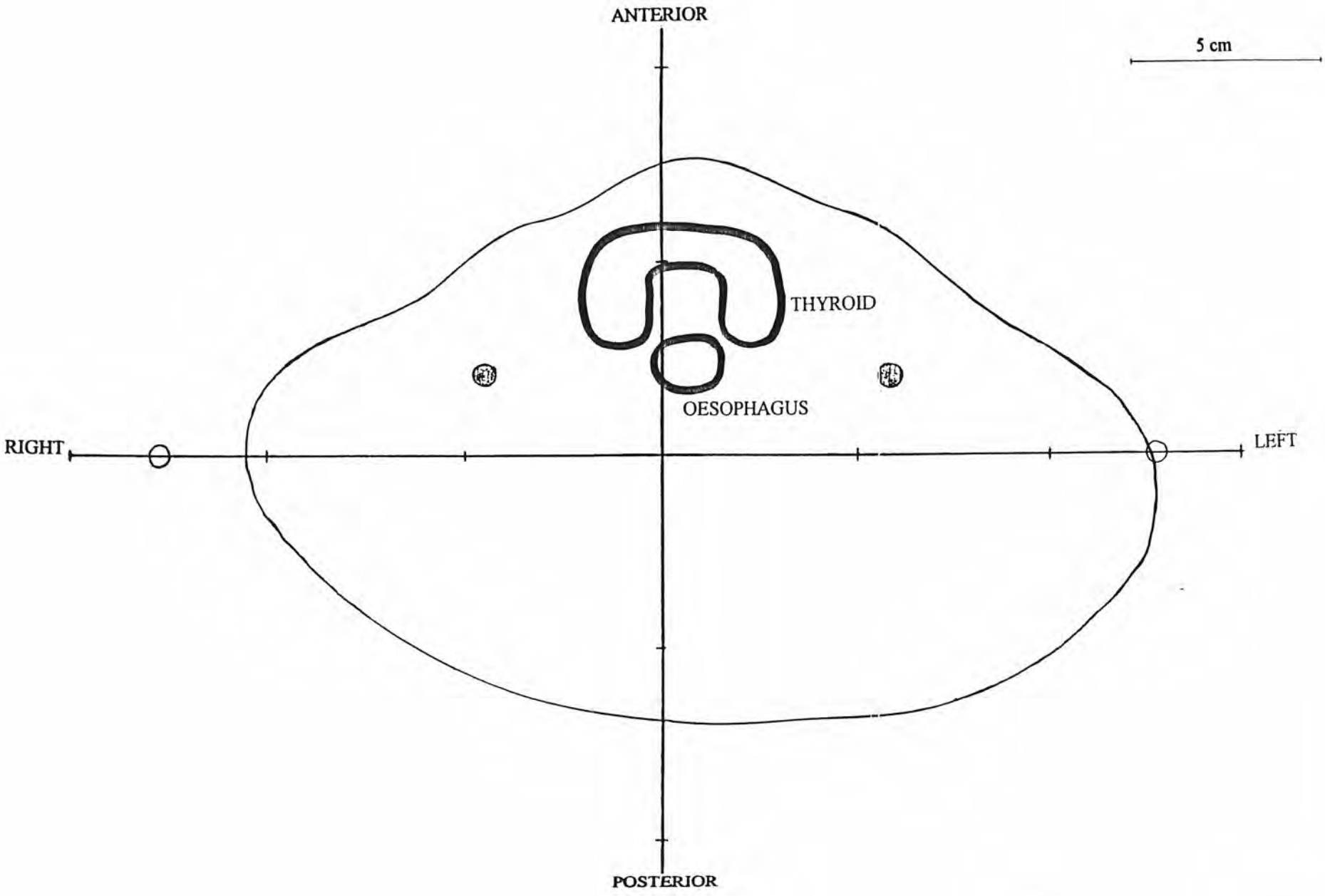

Diagram 9: Location of organs and tissues of interest in slice #10 of the Rando phantom.

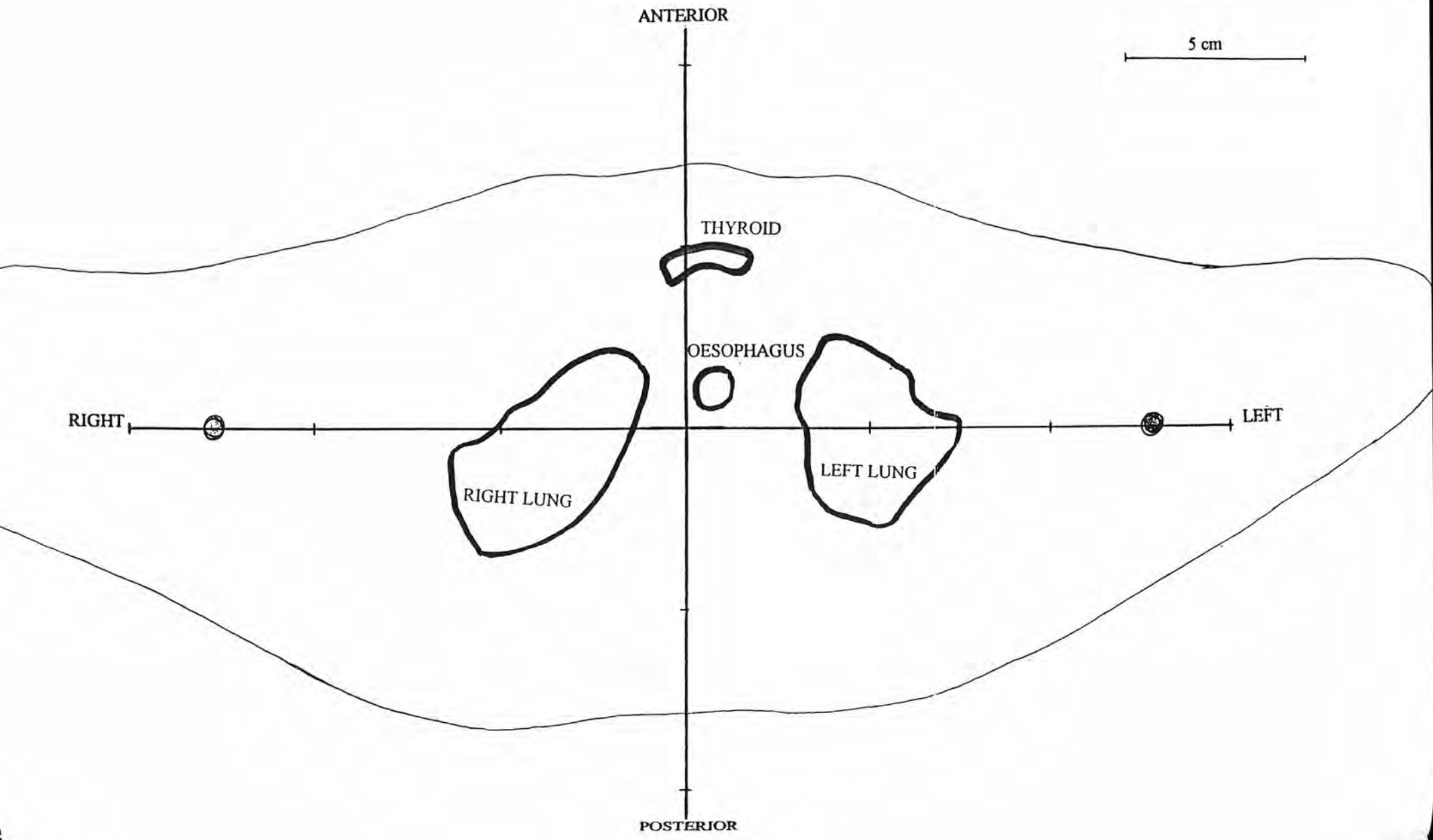

Diagram 10: Location of organs and tissues of interest in slice #11 of the Rando phantom.

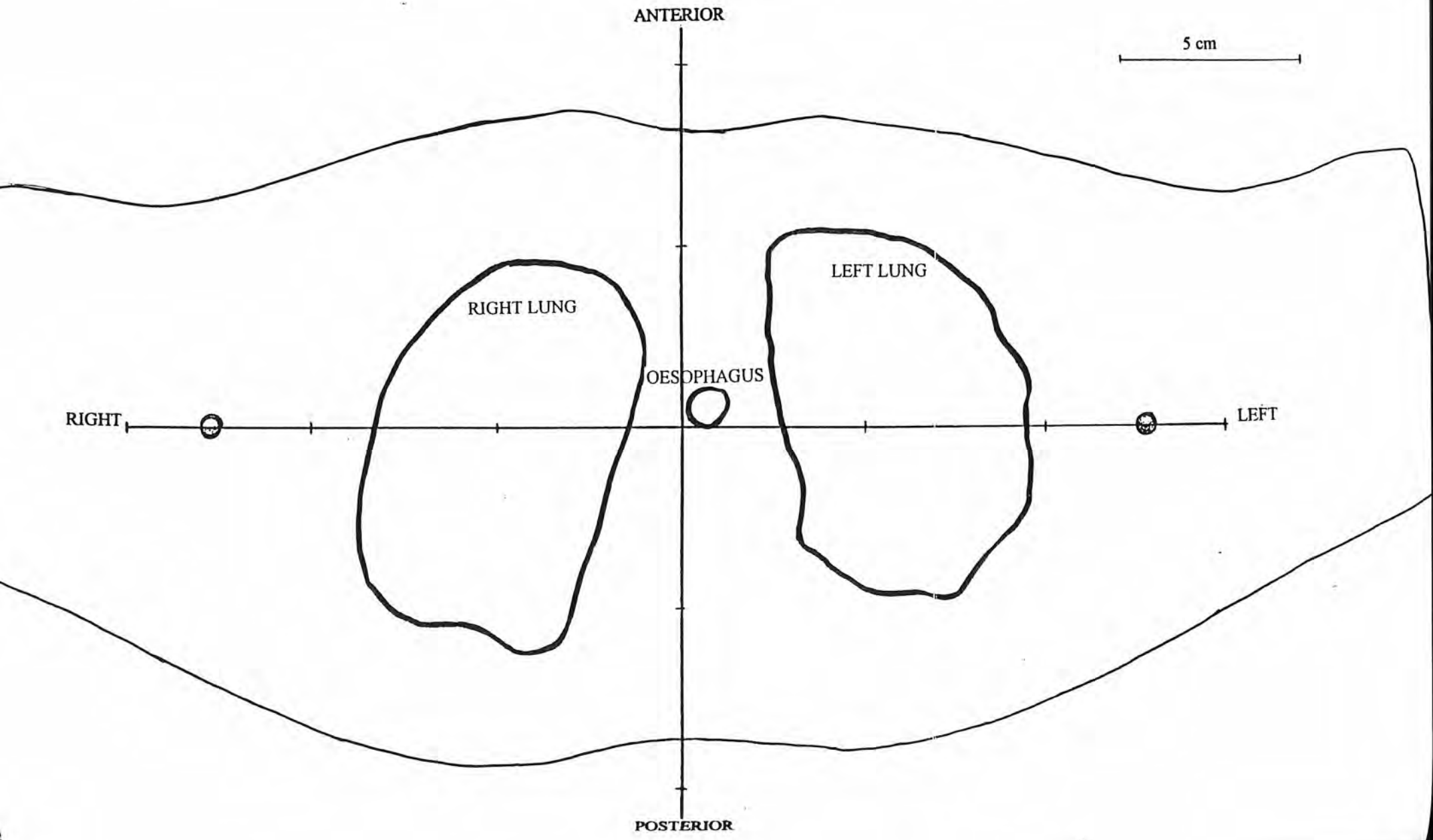

Diagram 11: Location of organs and tissues of interest in slice #12 of the Rando phantom.

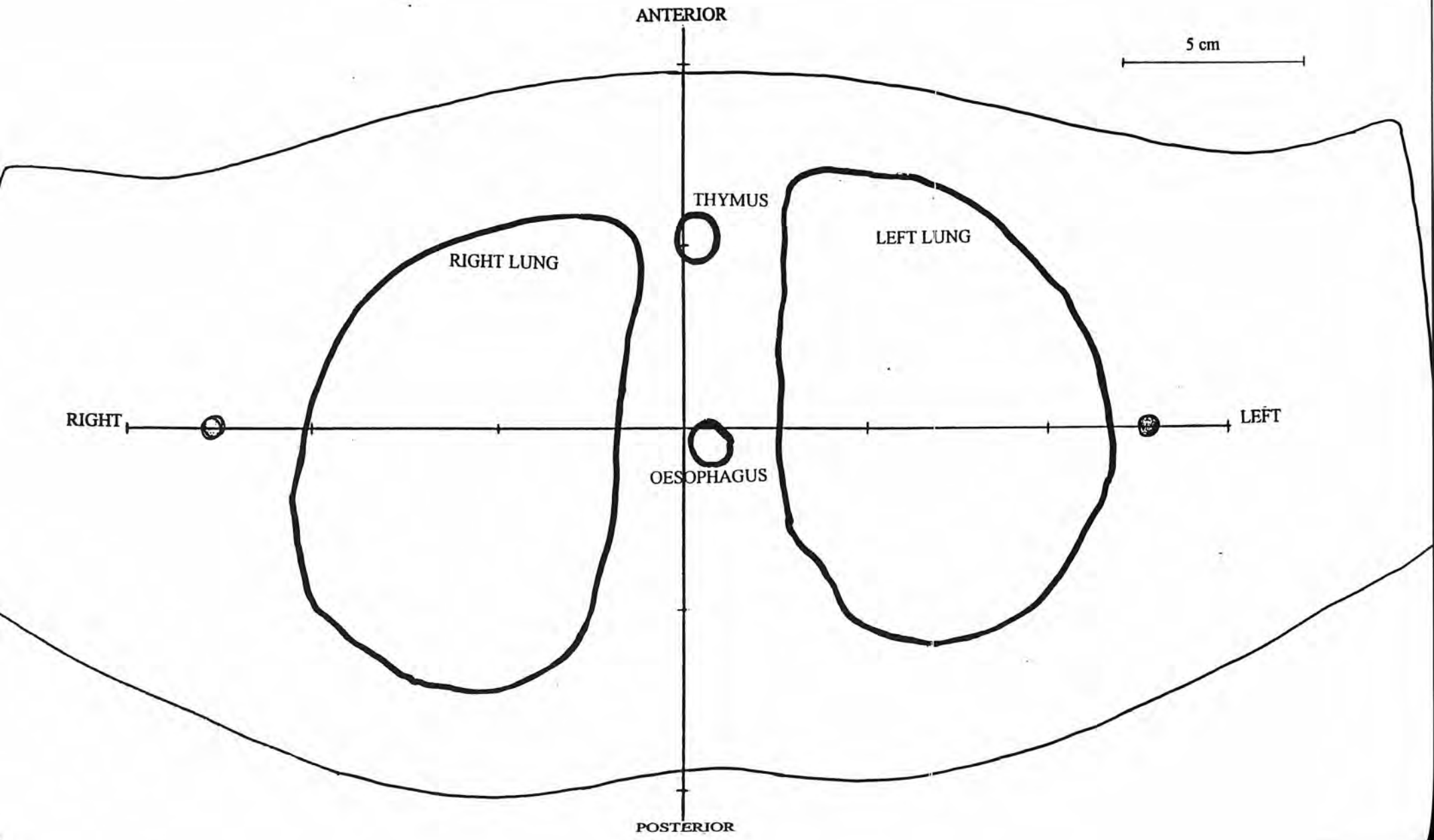

Diagram 12: Location of organs and tissues of interest in slice #13 of the Rando phantom.

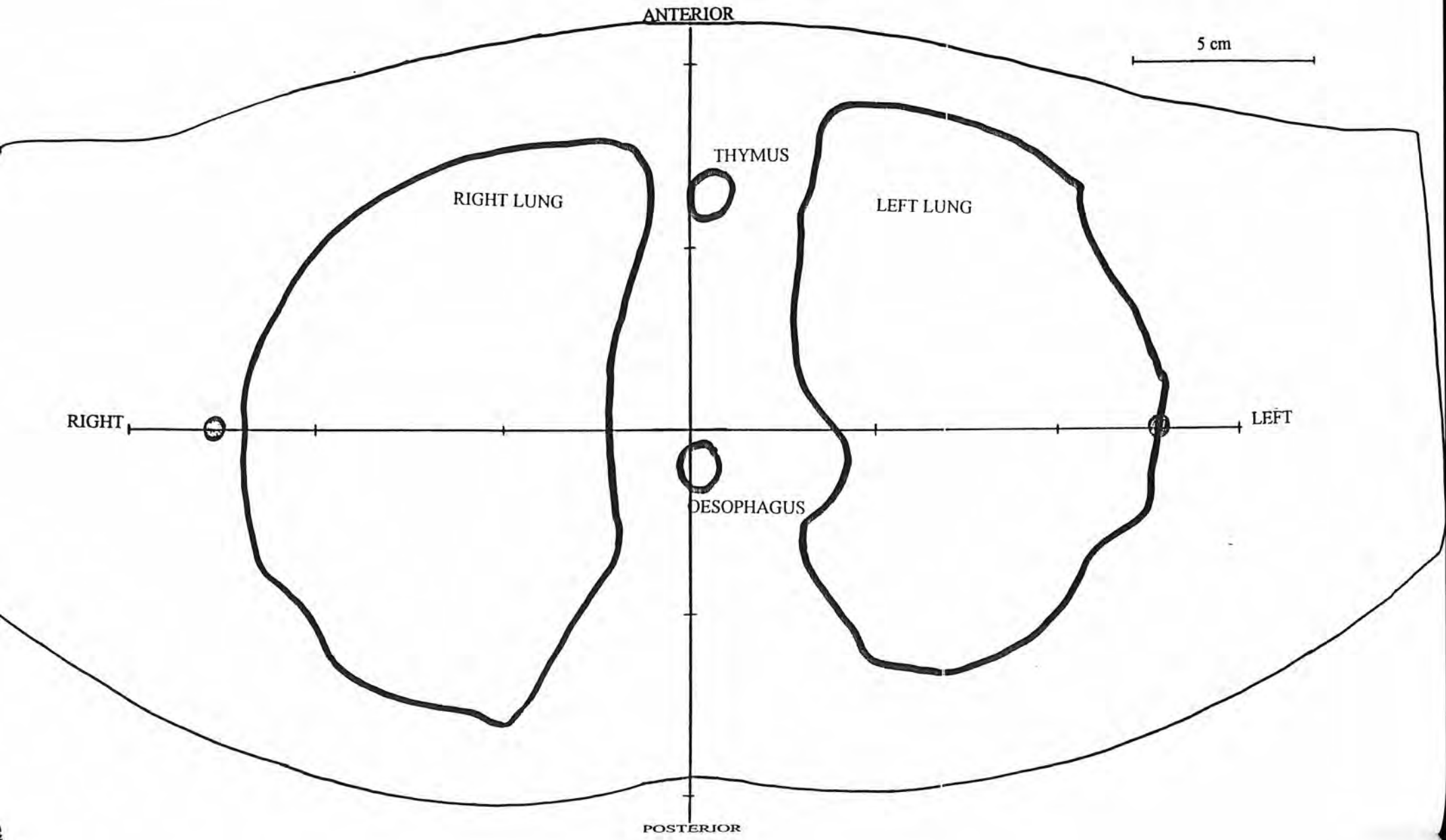

Diagram 13: Location of organs and tissues of interest in slice #14 of the Rando phantom.

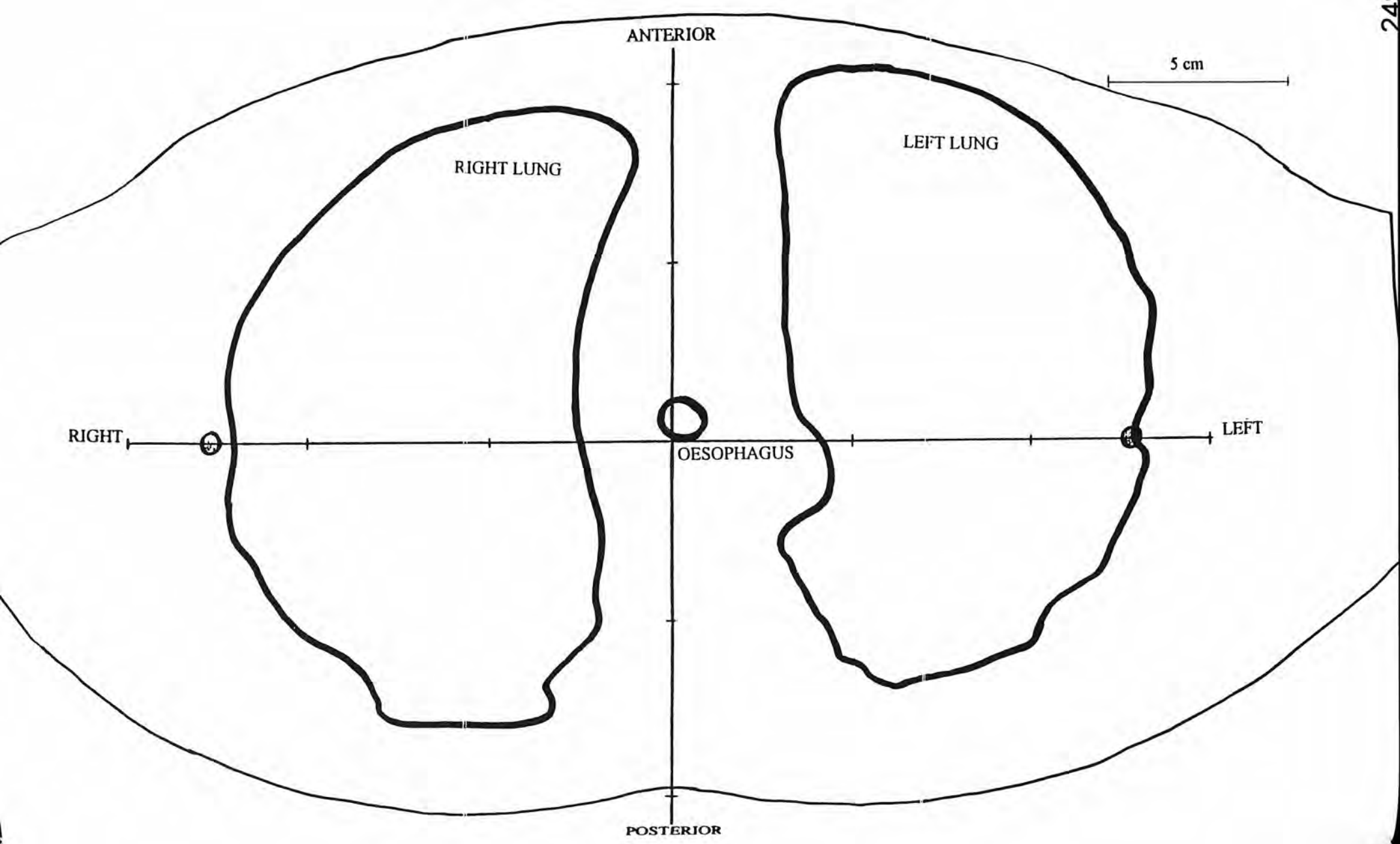

Diagram 14: Location of organs and tissues of interest in slice #15 of the Rando phantom.

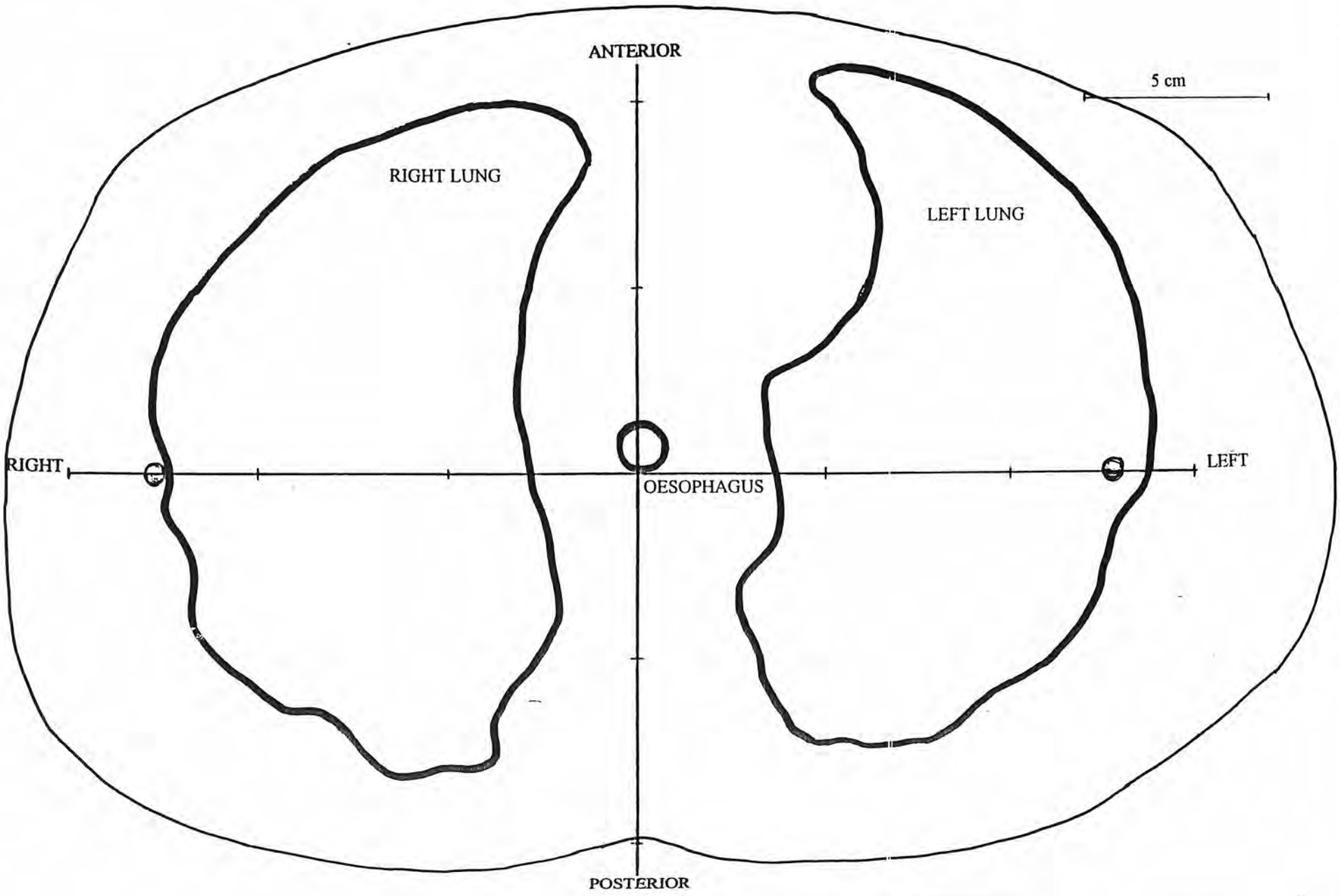

Diagram 15: Location of organs and tissues of interest in slice #16 of the Rando phantom.

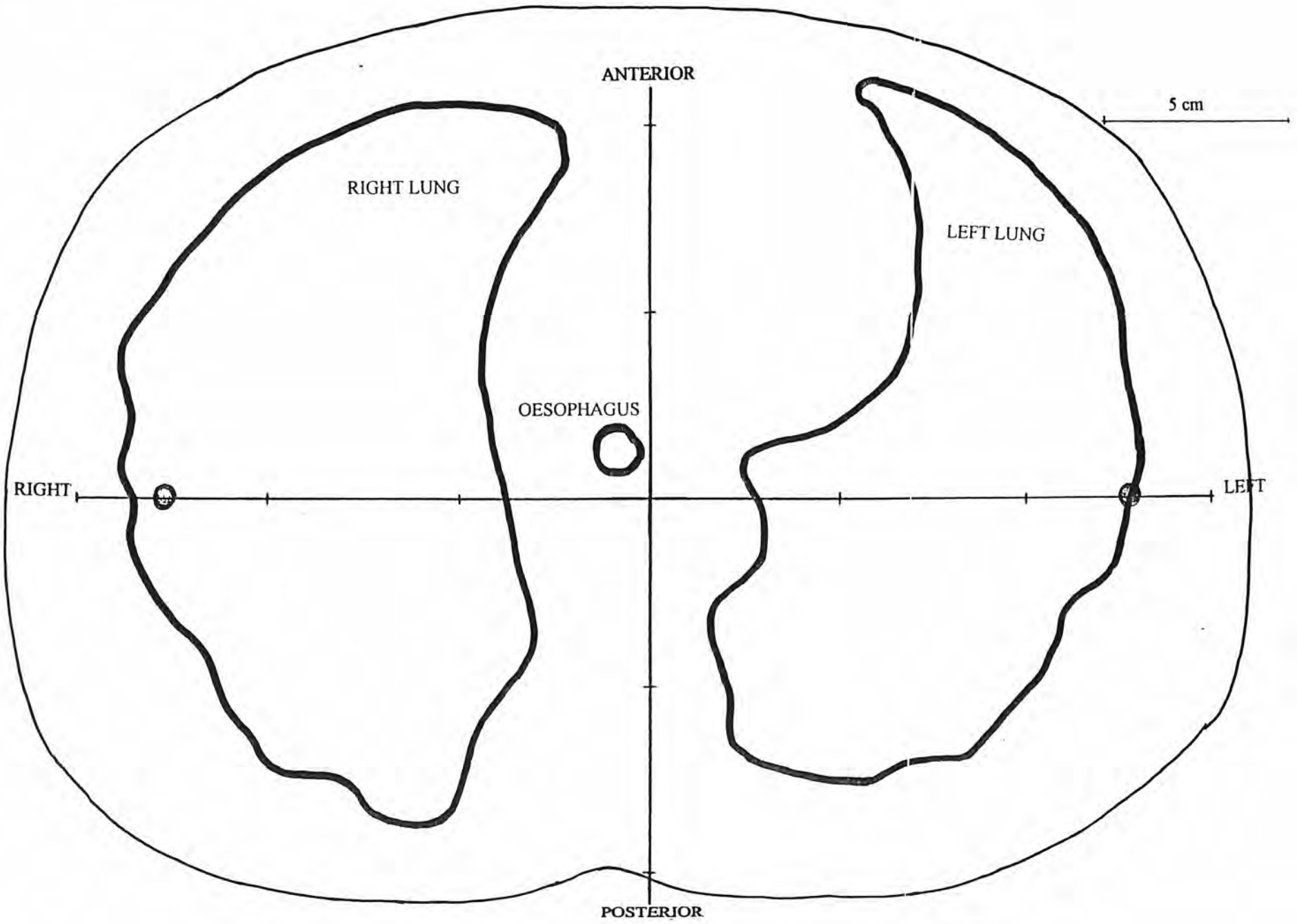

Diagram 16: Location of organs and tissues of interest in slice #17 of the Rando phantom.

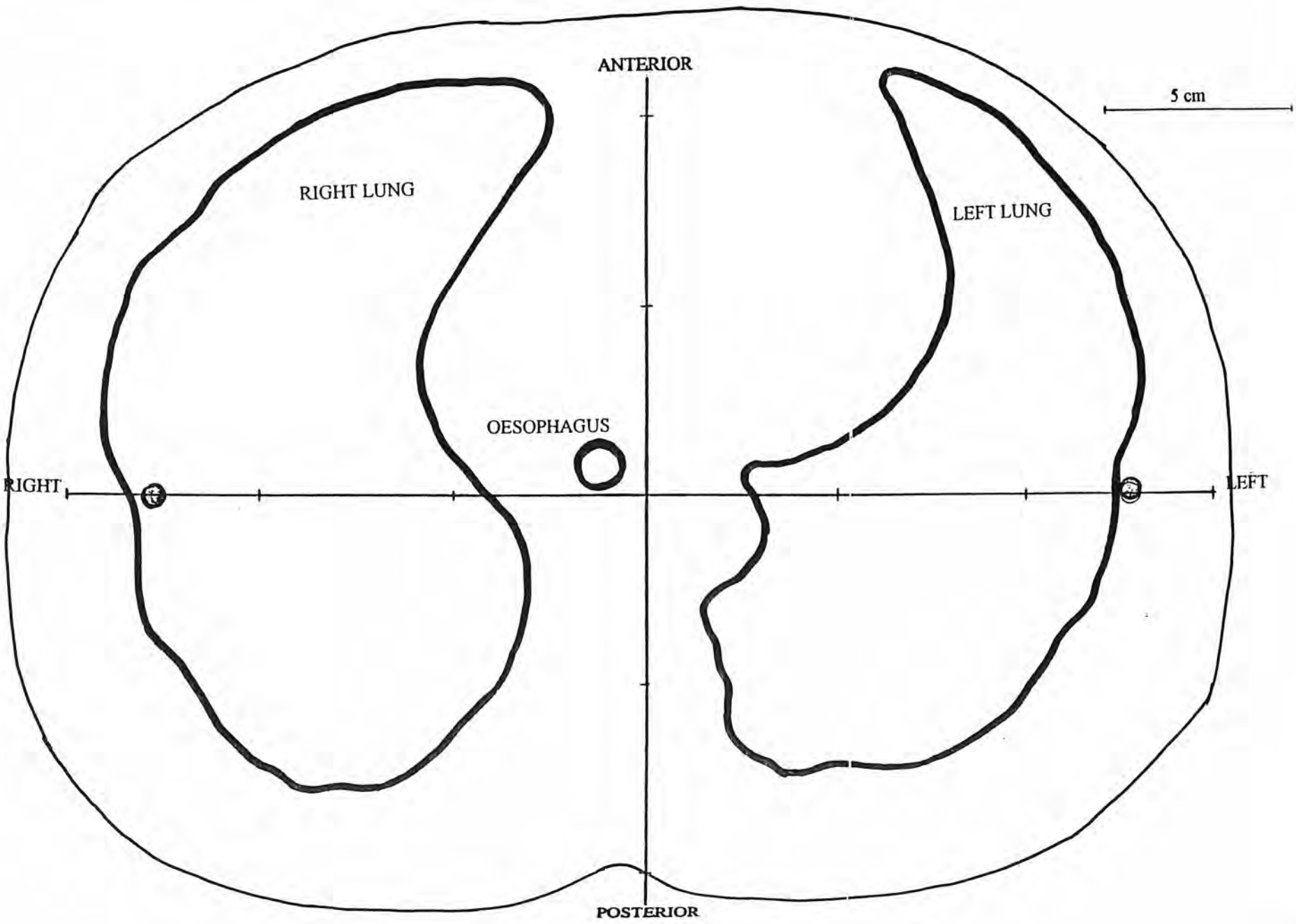

Diagram 17: Location of organs and tissues of interest in slice #18 of the Rando phantom.

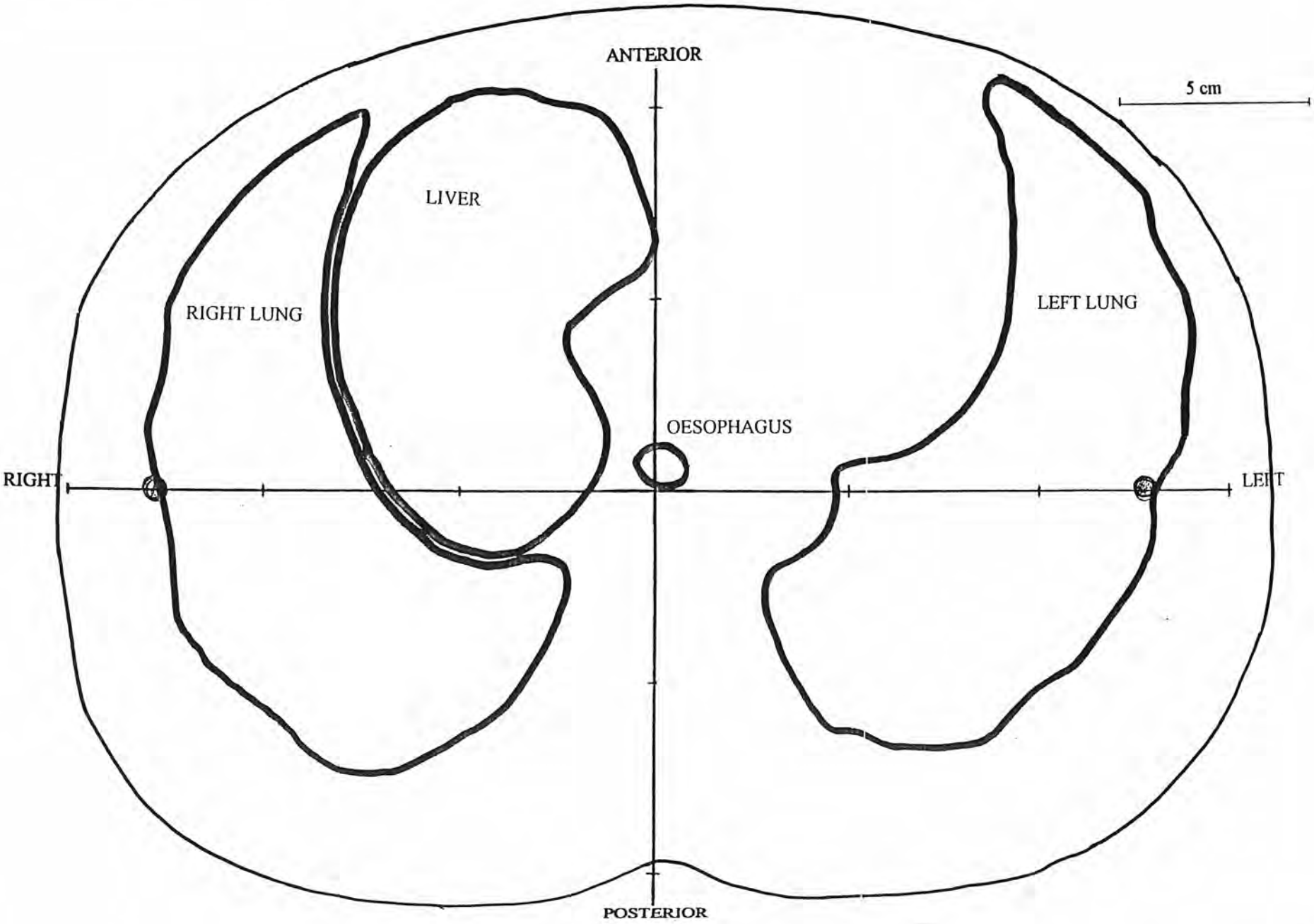

Diagram 18: Location of organs and tissues of interest in slice #19 of the Rando phantom.

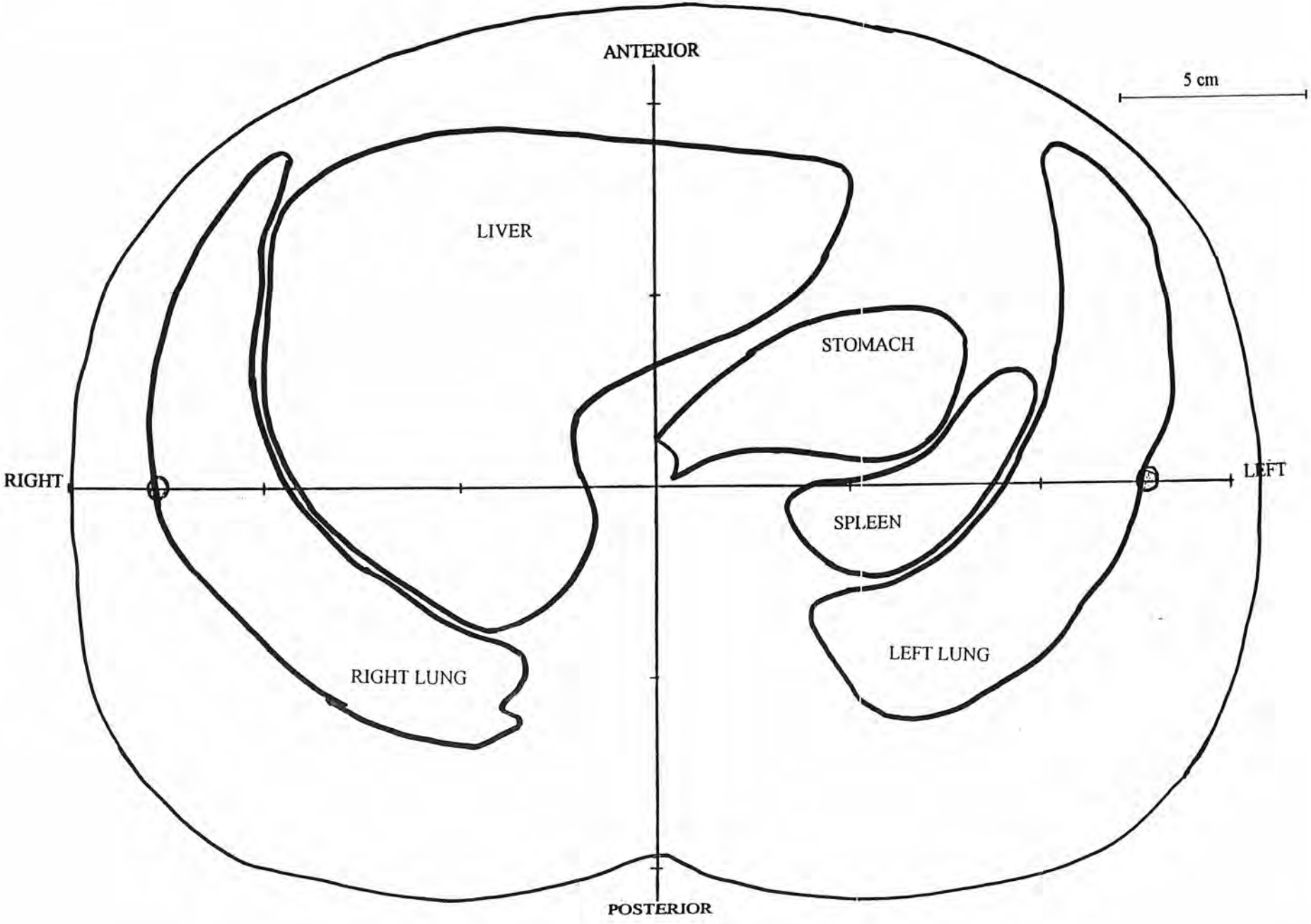

Diagram 19: Location of organs and tissues of interest in slice #20 of the Rando phantom.

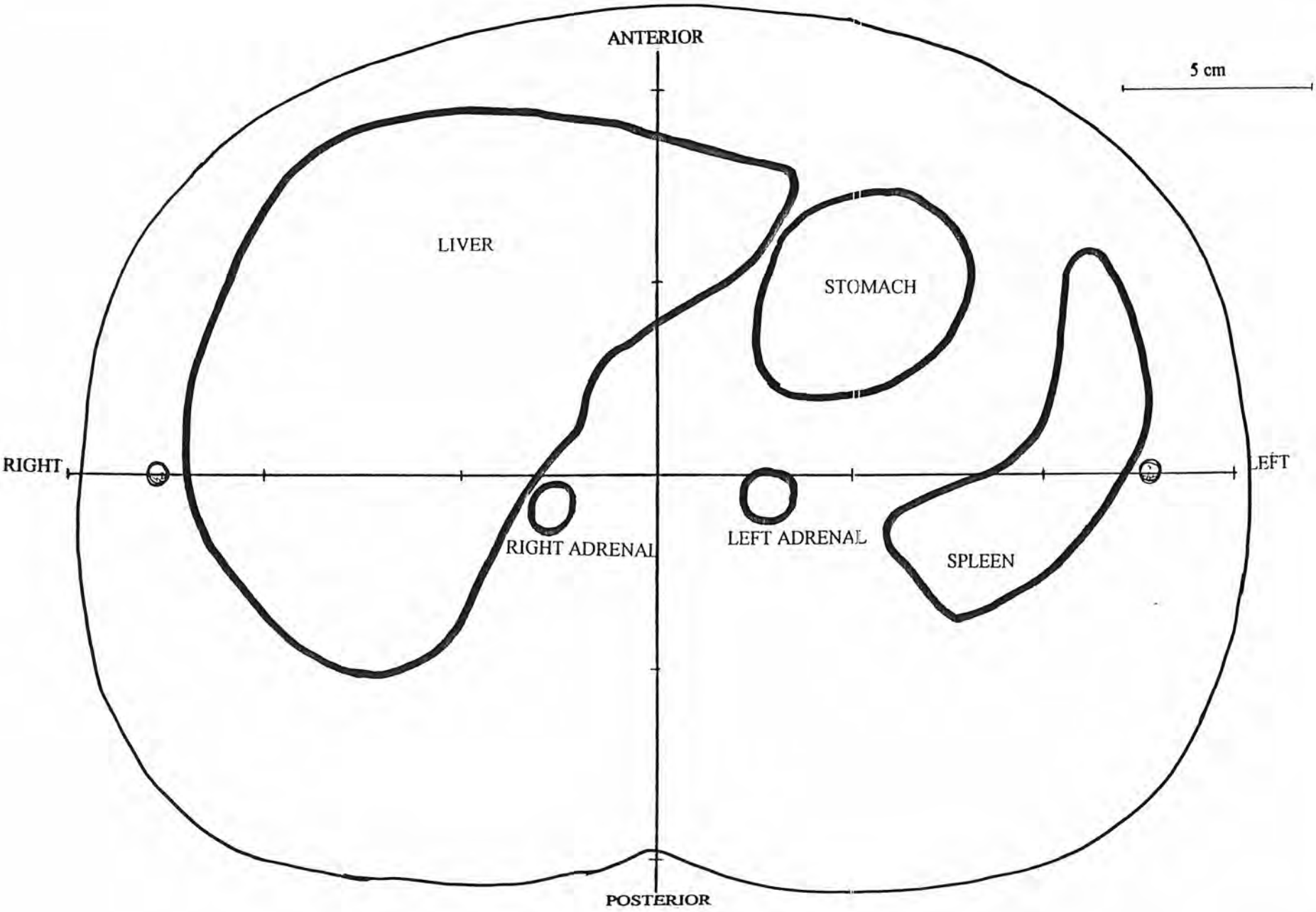

Diagram 20: Location of organs and tissues of interest in slice #21 of the Rando phantom.

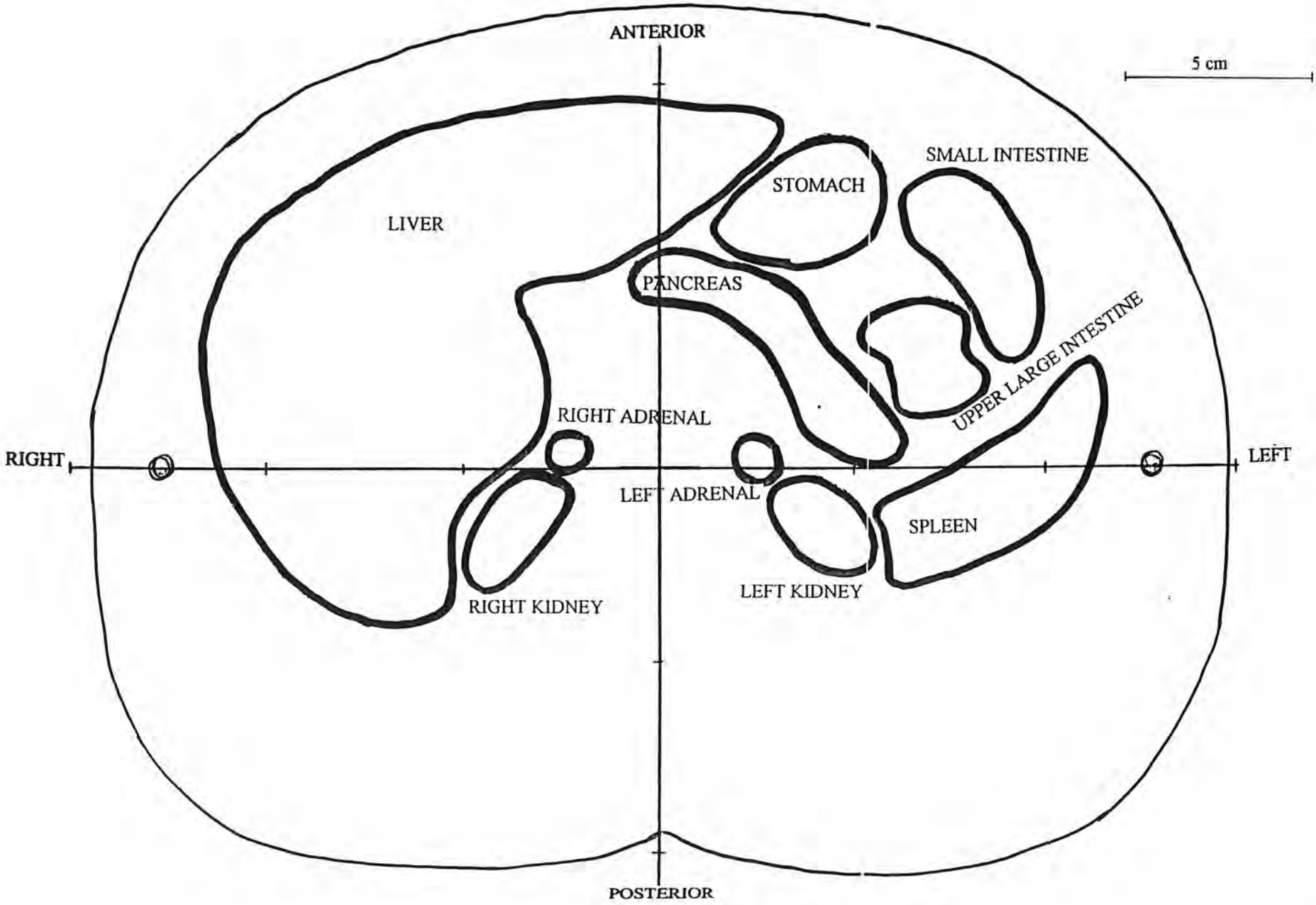

Diagram 21: Location of organs and tissues of interest in slice #22 of the Rando phantom.

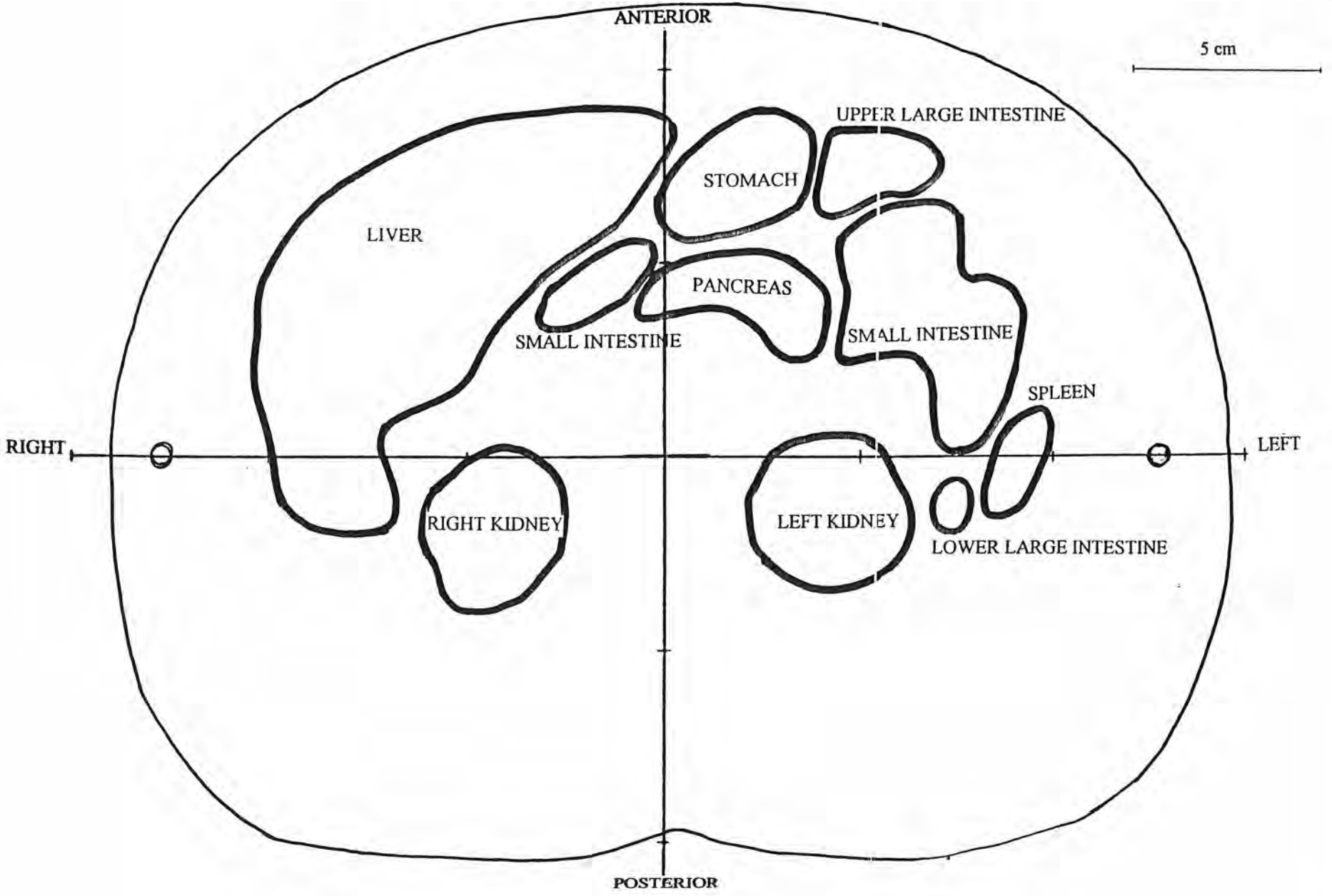

Diagram 22: Location of organs and tissues of interest in slice #23 of the Rando phantom.

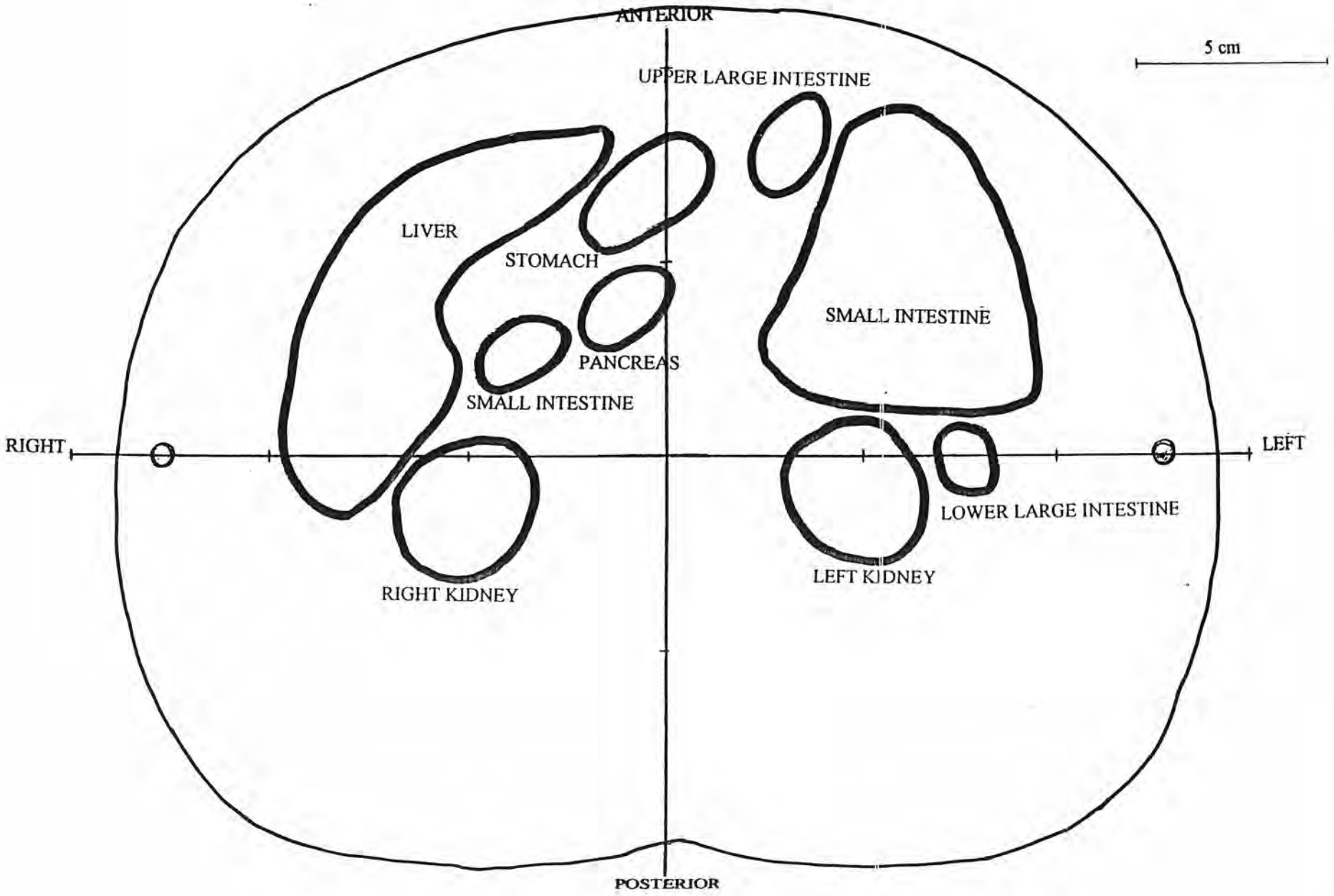

Diagram 23: Location of organs and tissues of interest in slice #24 of the Rando phantom.

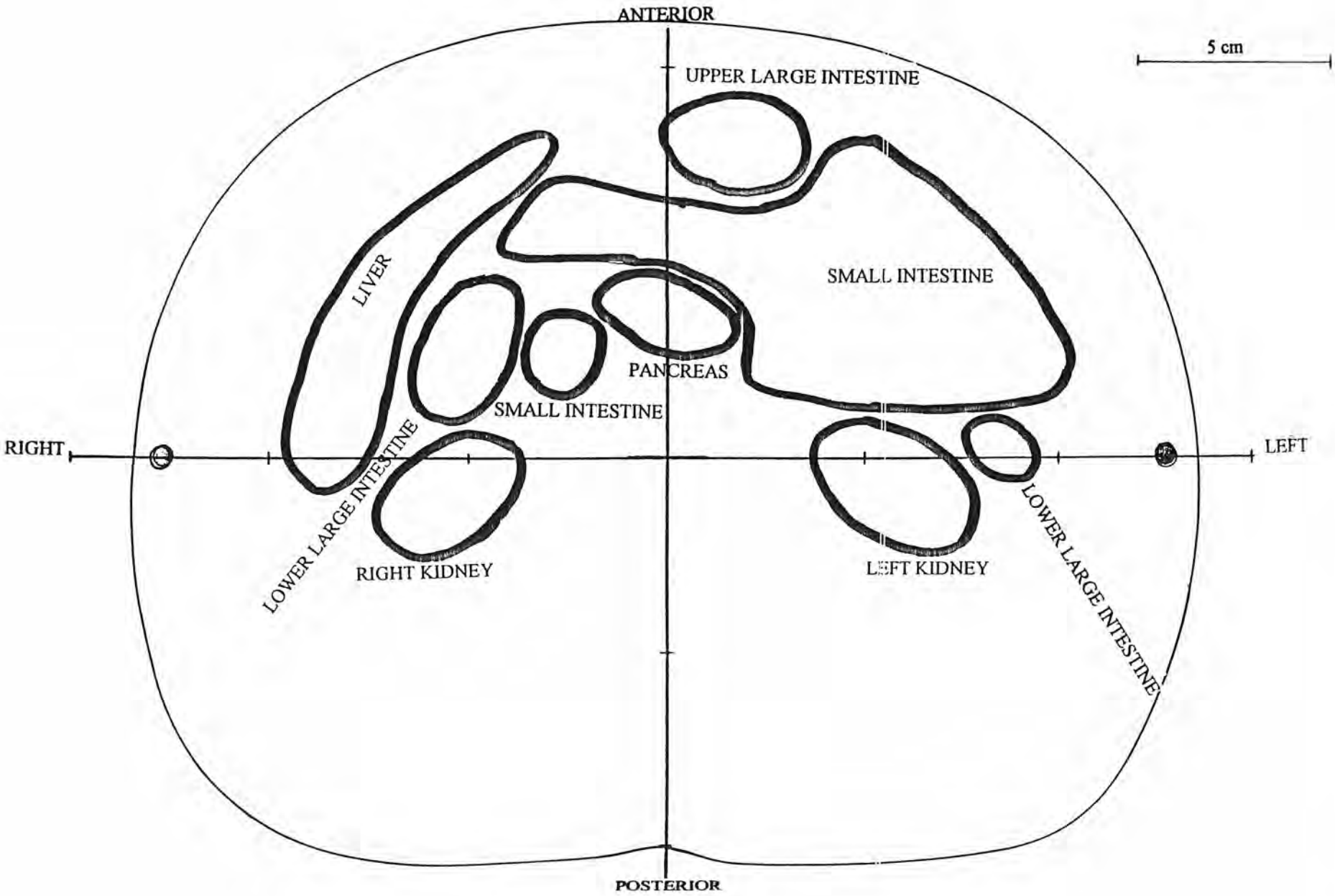

Diagram 24: Location of organs and tissues of interest in slice #25 of the Rando phantom.

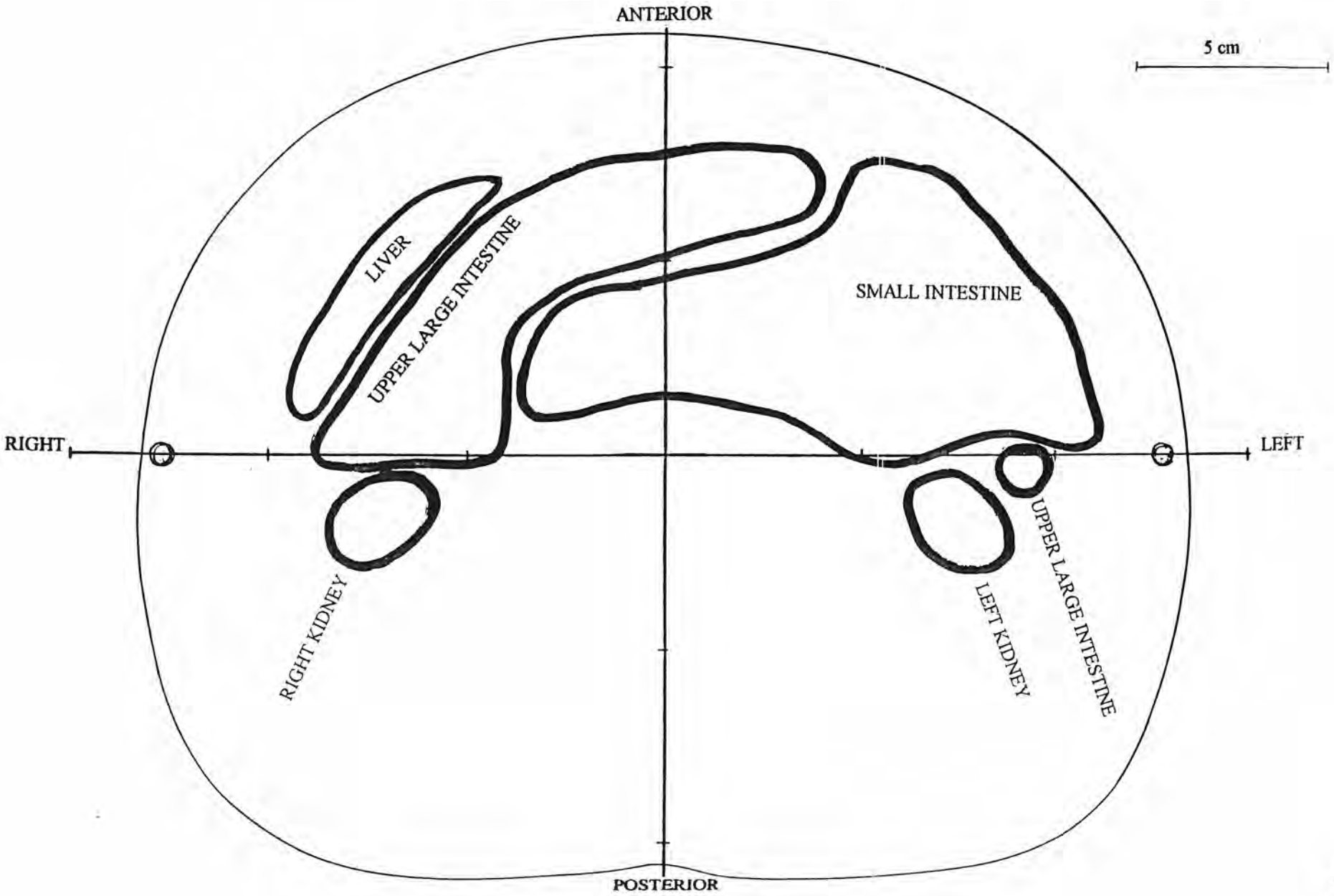

Diagram 25: Location of organs and tissues of interest in slice #26 of the Rando phantom.

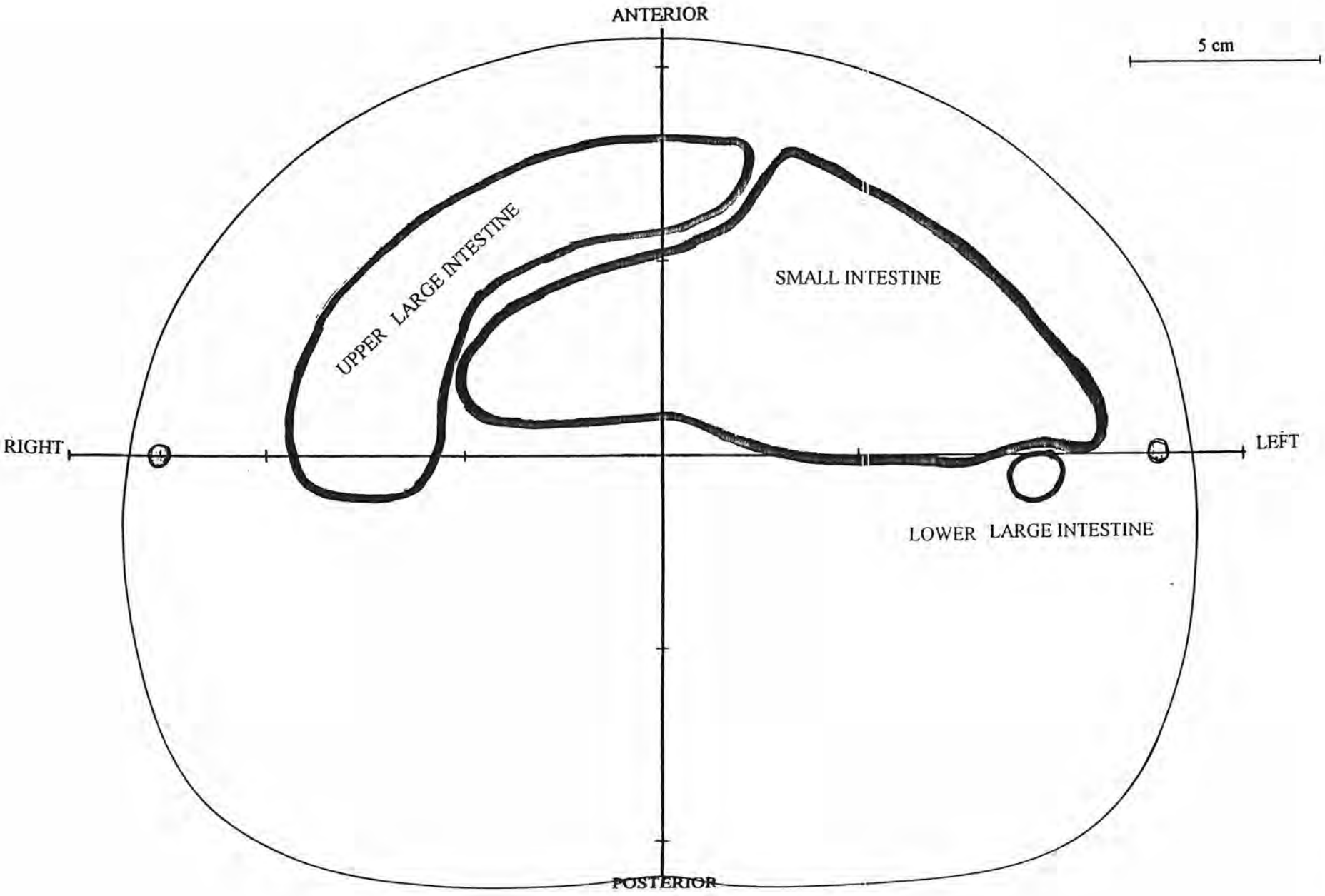

Diagram 26: Location of organs and tissues of interest in slice #27 of the Rando phantom.

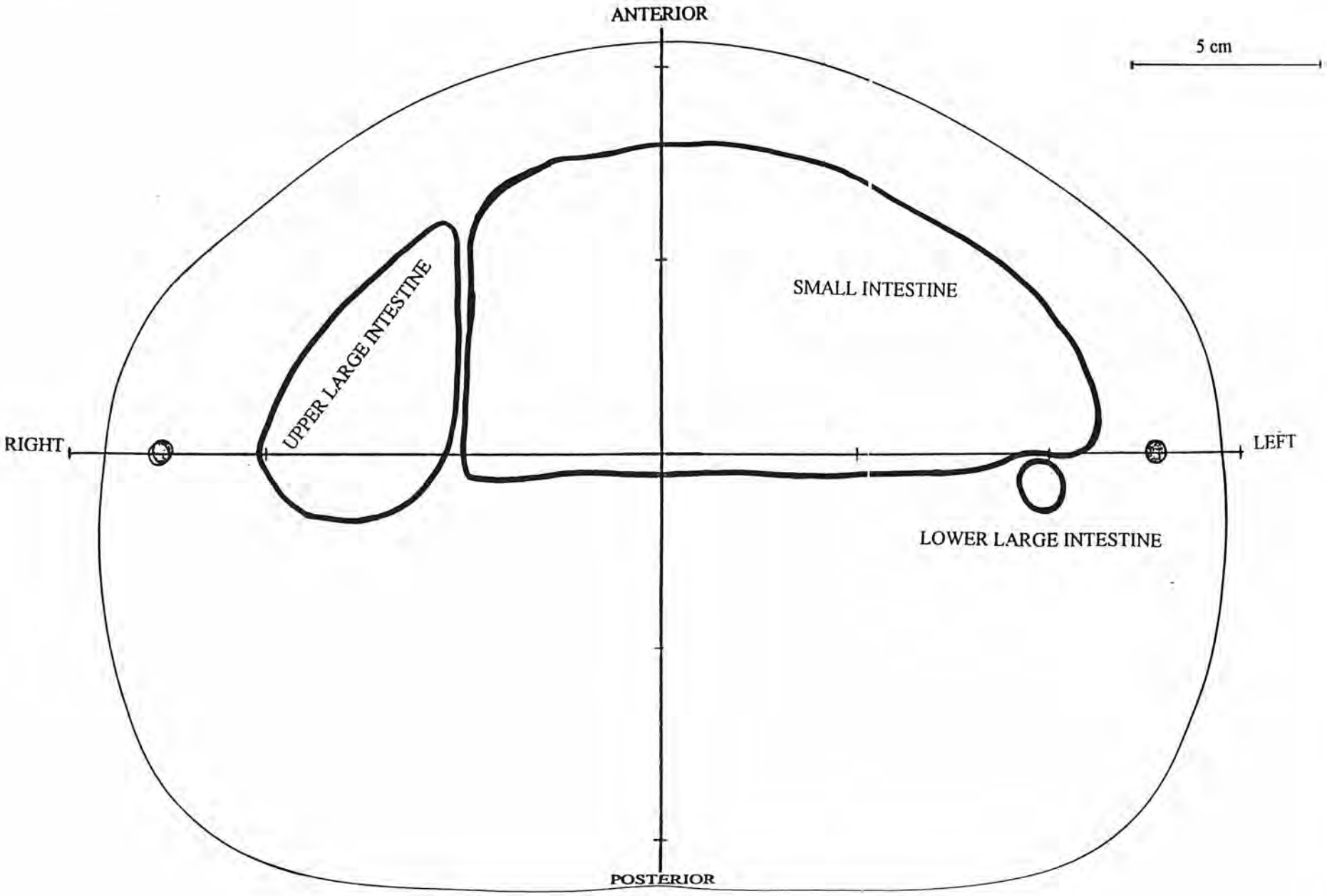

Diagram 27: Location of organs and tissues of interest in slice #28 of the Rando phantom.

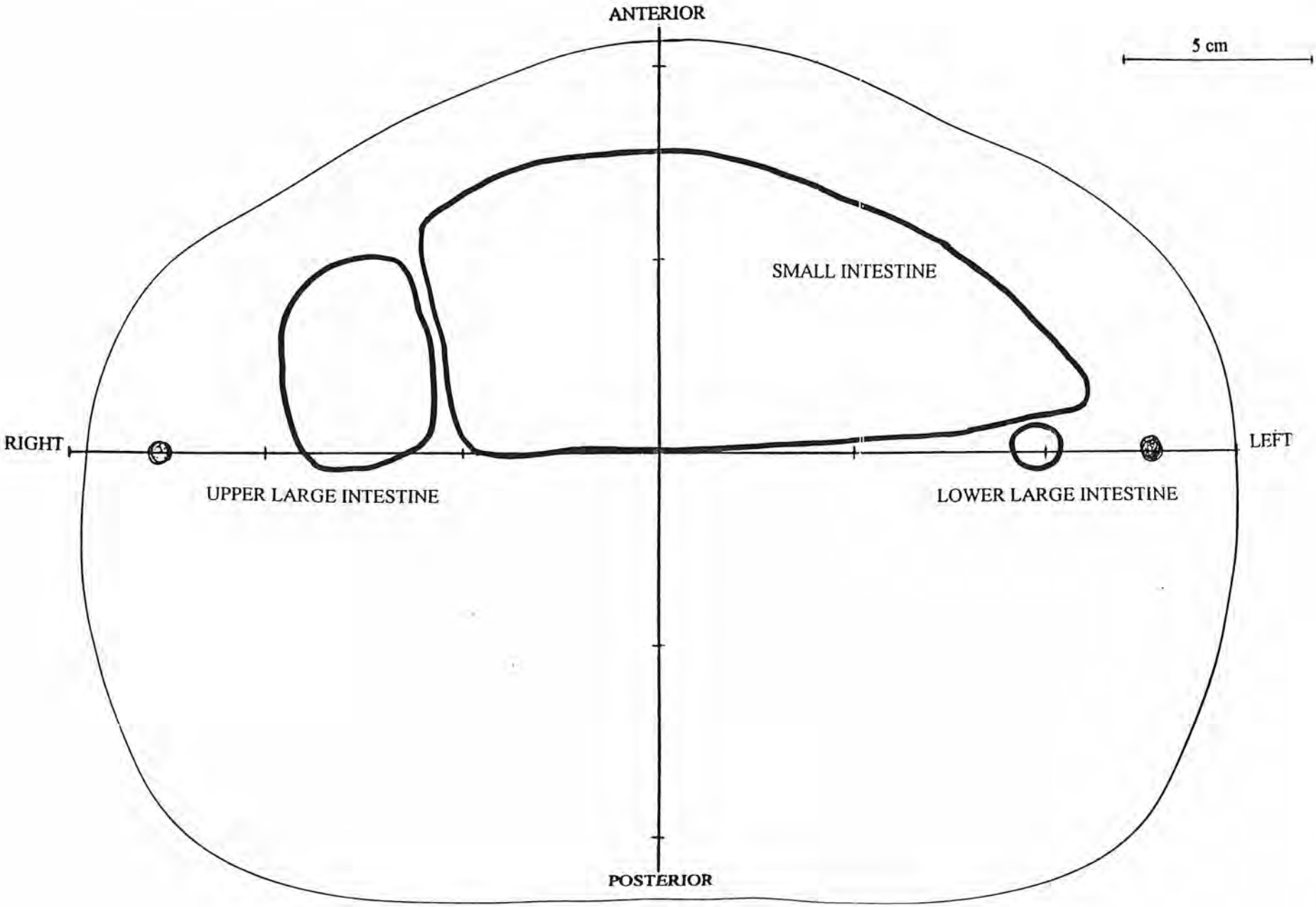

Diagram 28: Location of organs and tissues of interest in slice #29 of the Rando phantom.

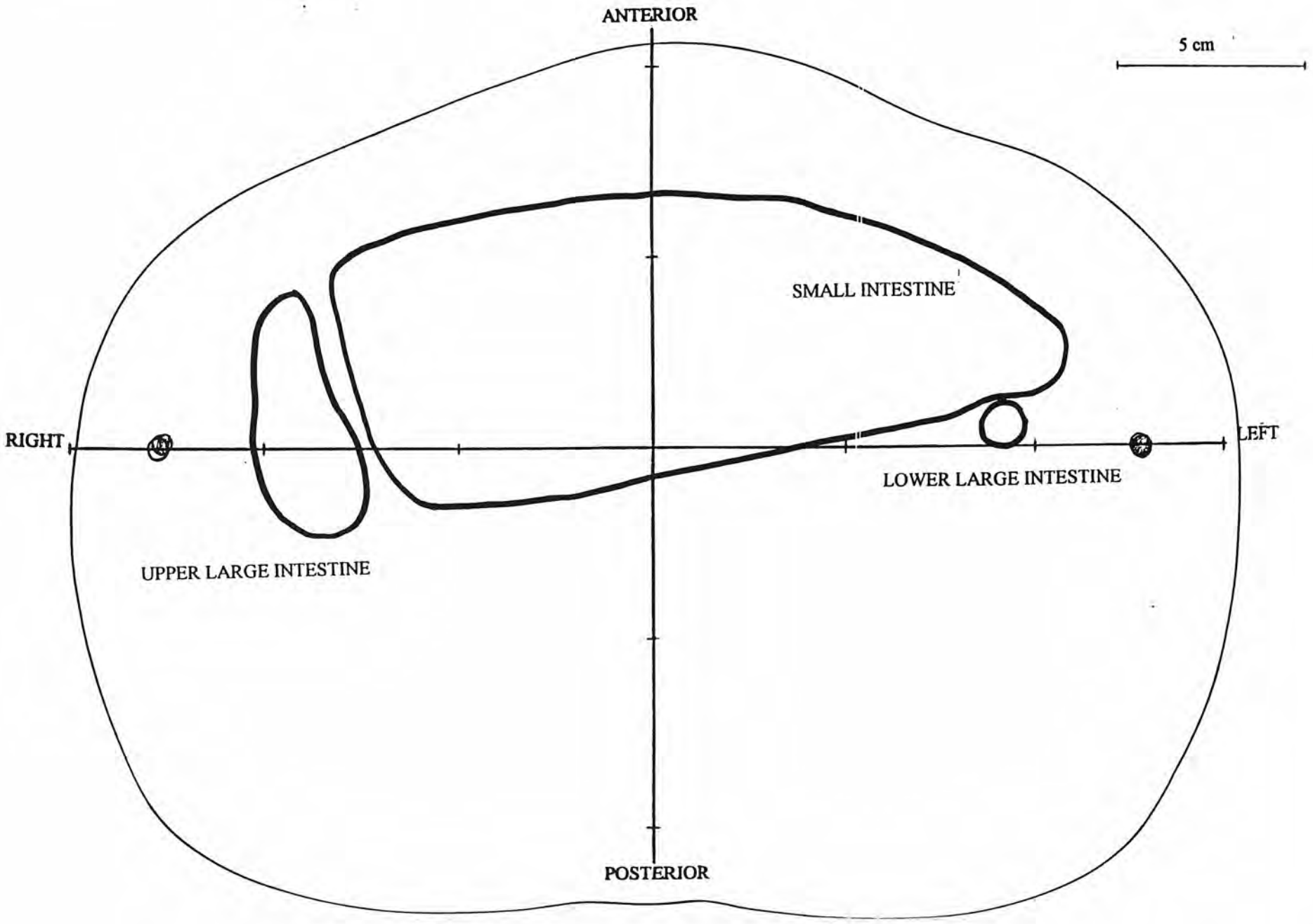

Diagram 29: Location of organs and tissues of interest in slice #30 of the Rando phantom.

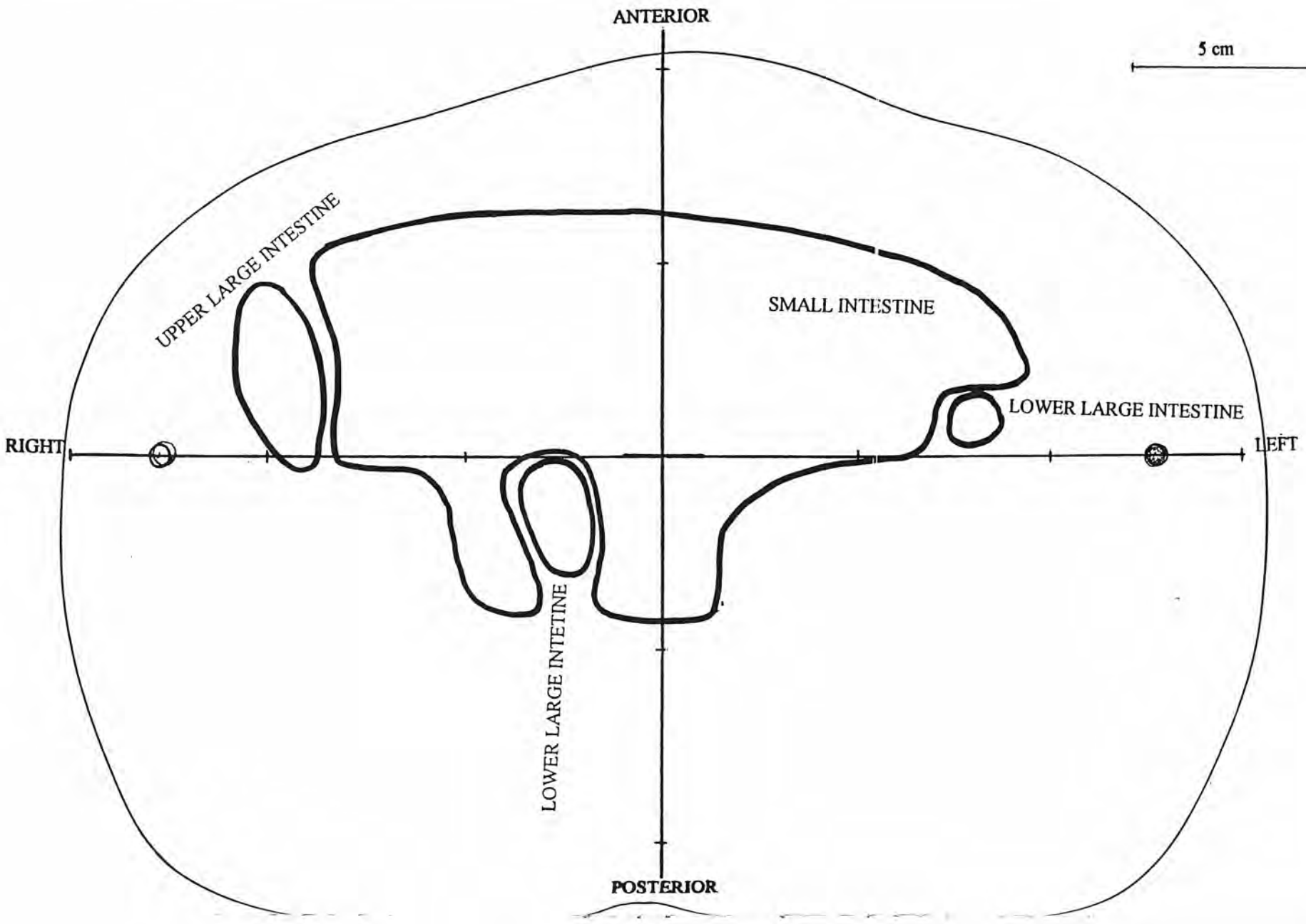

Diagram 30: Location of organs and tissues of interest in slice #31 of the Rando phantom.

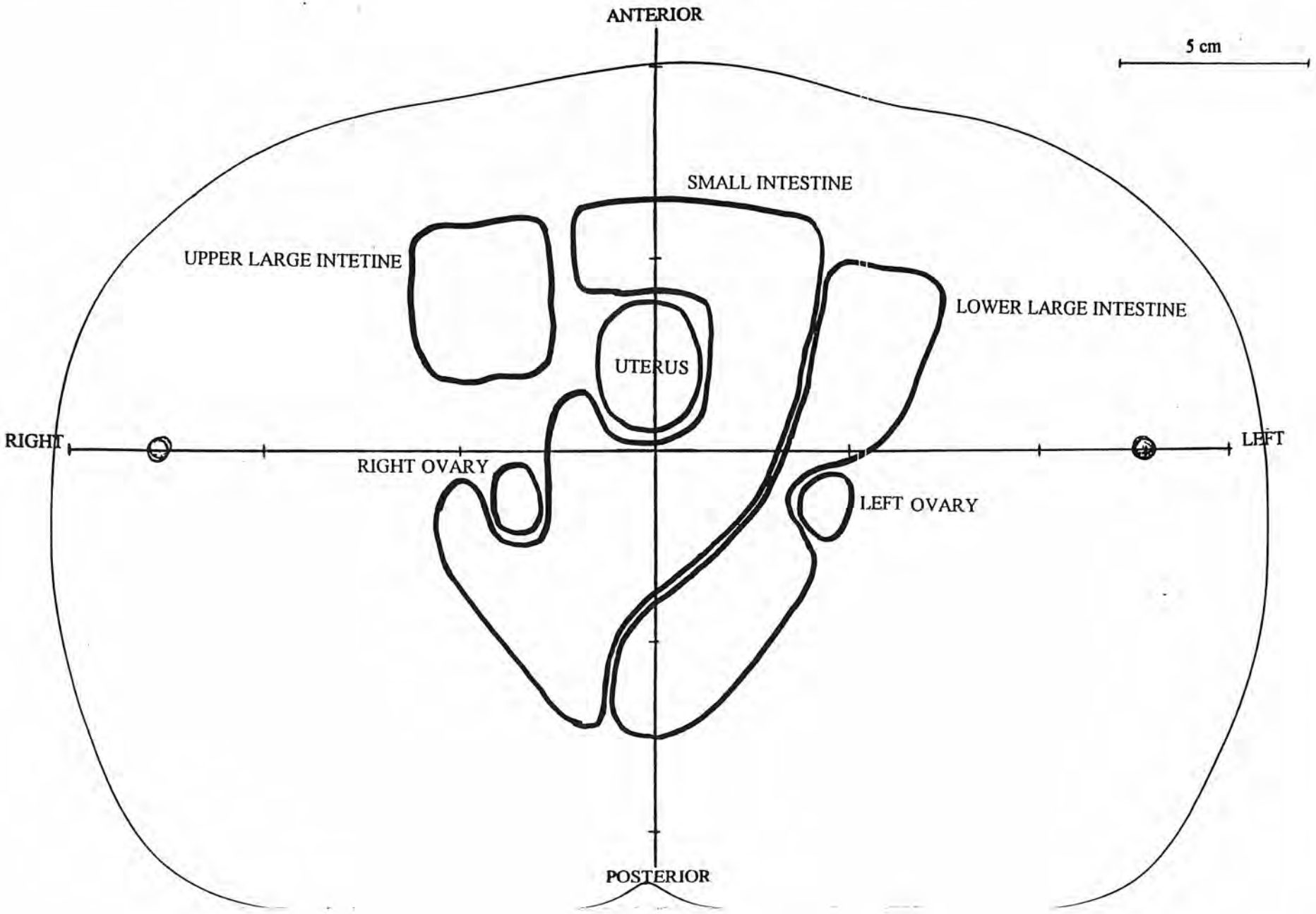

Diagram 31: Location of organs and tissues of interest in slice #32 of the Rando phantom.

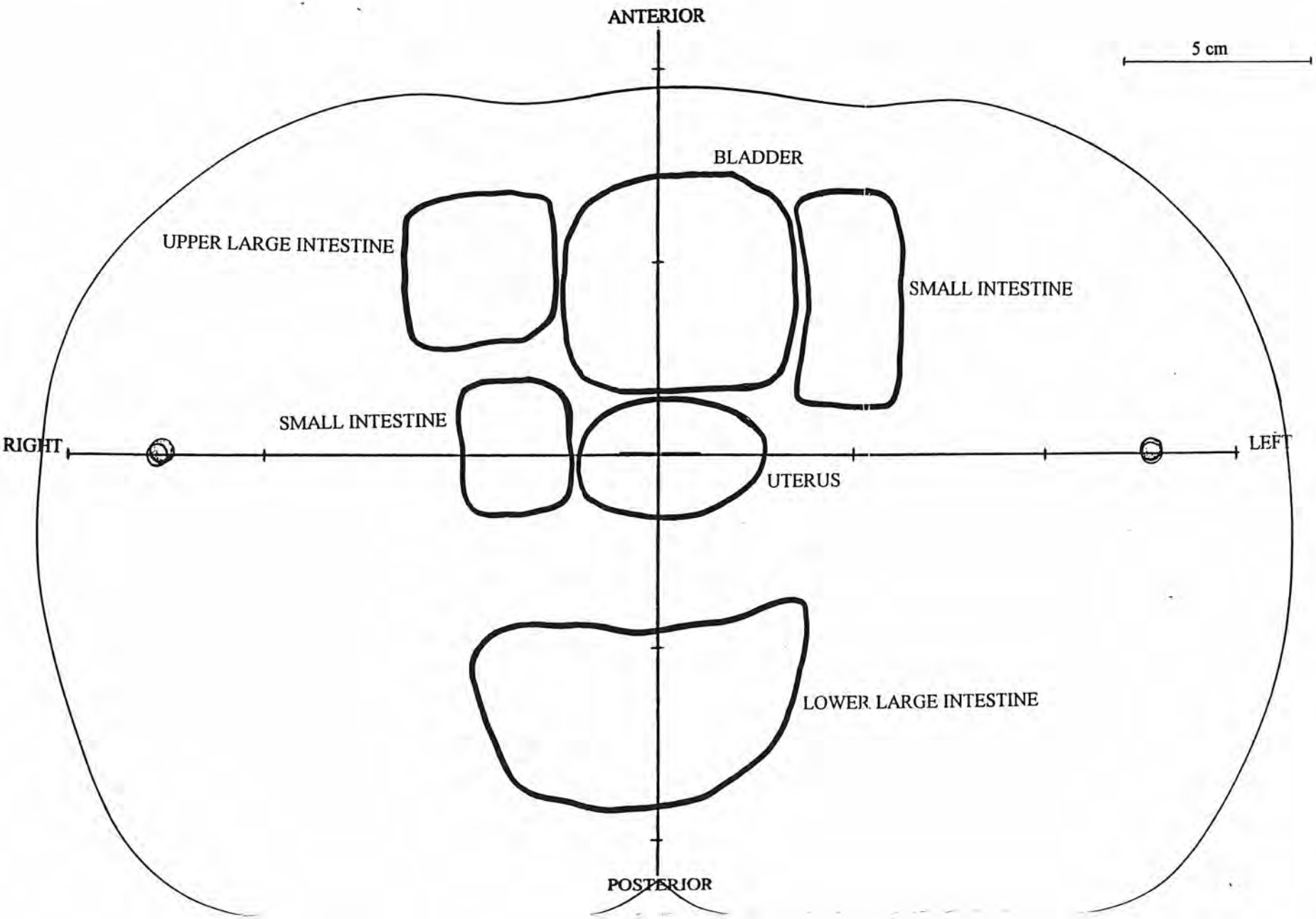

Diagram 32: Location of organs and tissues of interest in slice #33 of the Rando phantom.

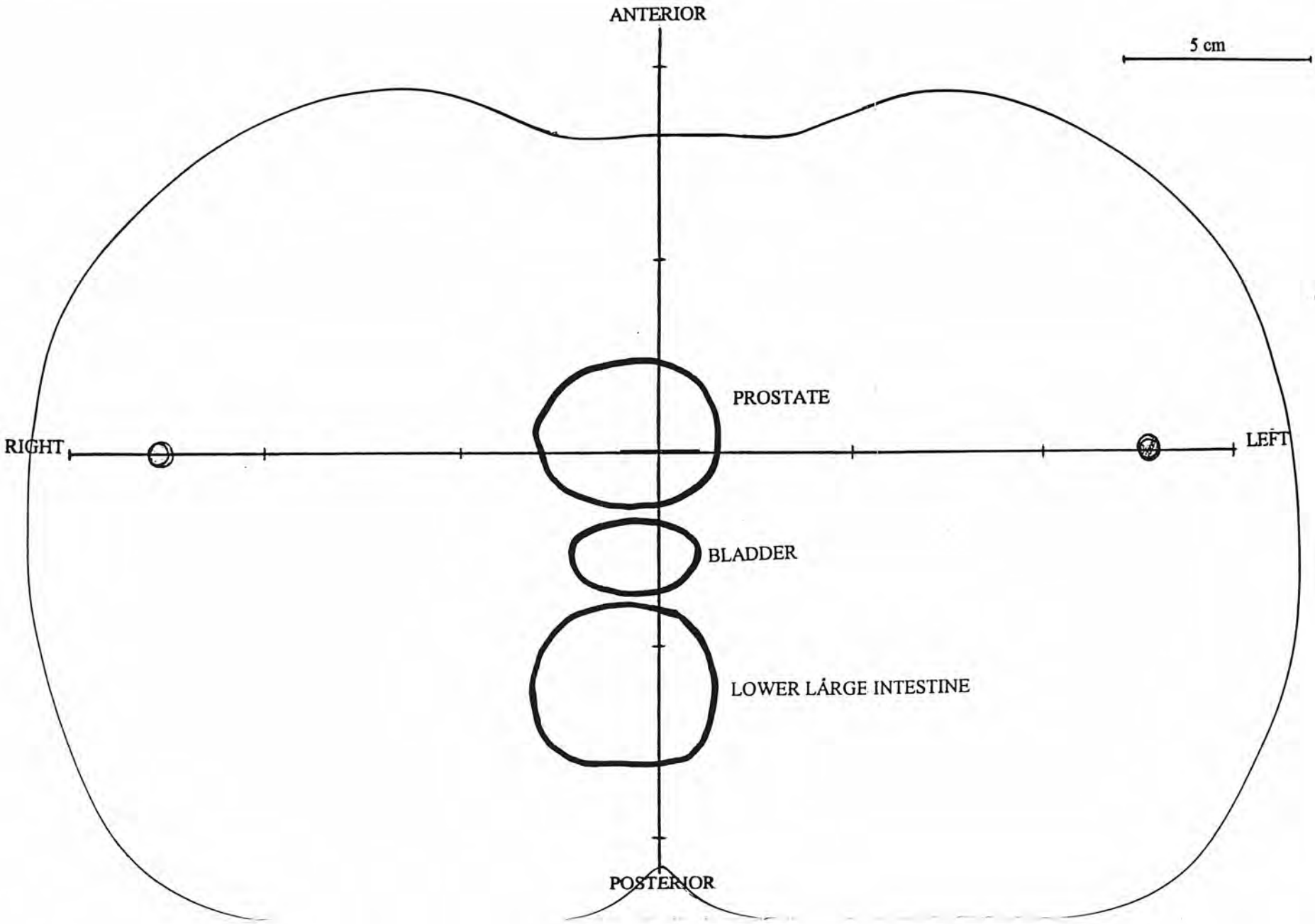

Diagram 33: Location of organs and tissues of interest in slice #34 of the Rando phantom.

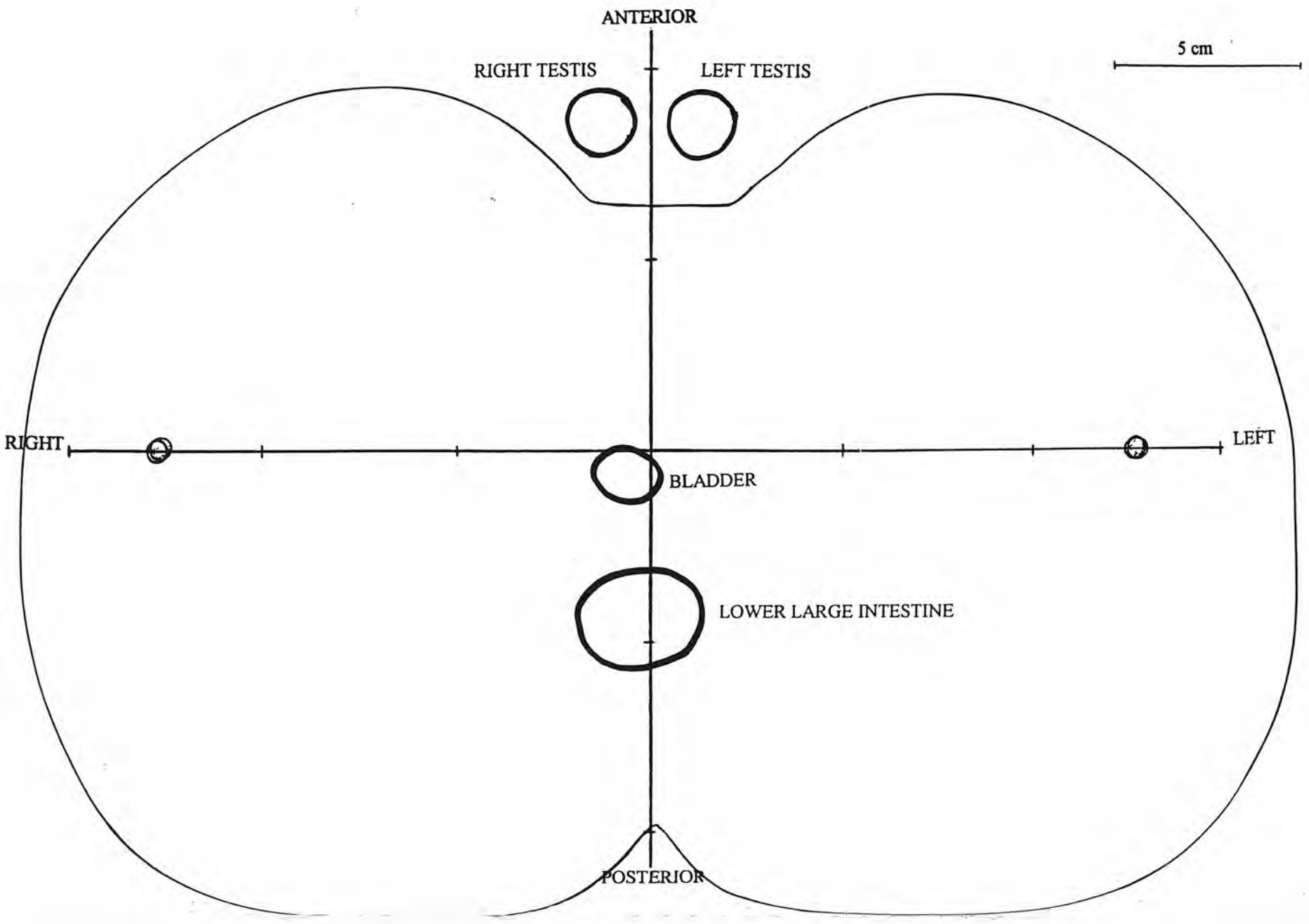

Appendix B. CT Scanners Dose Conversion Factors

(The GE 8800 scanner was only used for "head" examinations; R: Right, L: Left; RBM: red bone marrow; SI: Small Intestine; ULI: Upper Large Interstine; LLI: Lower Large Intestine)

Phantom	Position		Organ or	Siemens Somatom		GE 8800 *		GE 9000HP		GE HiSpeed Advantage		Philips (CX/S)		GE Sytec 3000	
section no.	X axis	Y axis	Tissue	Point factor	Mean factor	Point factor	Mean factor	Point factor	Mean factor	Point factor	Mean factor	Point factor	Mean factor	Point factor	Mean factor
0	-	-	Bone Surface	1.08	1.08	1.00	1.00	1.00	1.00	1.00	1.00	1.01	1.01	0.94	0.94
	-	-	RBM	1.08	1.08	1.00	1.00	1.00	1.00	1.00	1.00	1.01	1.01	0.94	0.94
	-	-	Skin	1.08	1.08	1.00	1.00	1.00	1.00	1.00	1.00	1.01	1.01	0.94	0.94
	-	-	Brain	1.08	1.08	1.00	1.00	1.00	1.00	1.00	1.00	1.01	1.01	0.94	0.94
1	-	-	Bone Surface	1.08	1.08	1.00	1.00	1.00	1.00	1.00	1.00	1.01	1.01	0.94	0.94
	-	-	RBM	1.08	1.08	1.00	1.00	1.00	1.00	1.00	1.00	1.01	1.01	0.94	0.94
	-	-	Skin	1.08	1.08	1.00	1.00	1.00	1.00	1.00	1.00	1.01	1.01	0.94	0.94
	-	-	Brain	1.08	1.08	1.00	1.00	1.00	1.00	1.00	1.00	1.01	1.01	0.94	0.94
2	-	-	Bone Surface	1.08	1.08	1.00	1.00	1.00	1.00	1.00	1.00	1.01	1.01	0.94	0.94
	-	-	RBM	1.08	1.08	1.00	1.00	1.00	1.00	1.00	1.00	1.01	1.01	0.94	0.94
	-	-	Skin	1.08	1.08	1.00	1.00	1.00	1.00	1.00	1.00	1.01	1.01	0.94	0.94
	-	-	Brain	1.08	1.08	1.00	1.00	1.00	1.00	1.00	1.00	1.01	1.01	0.94	0.94
3	-	-	Bone Surface	1.08	1.08	1.00	1.00	1.00	1.00	1.00	1.00	1.01	1.01	0.94	0.94
	-	-	RBM	1.08	1.08	1.00	1.00	1.00	1.00	1.00	1.00	1.01	1.01	0.94	0.94
	-	-	Skin	1.08	1.08	1.00	1.00	1.00	1.00	1.00	1.00	1.01	1.01	0.94	0.94
	-	-	Brain	1.08	1.08	1.00	1.00	1.00	1.00	1.00	1.00	1.01	1.01	0.94	0.94
4	-	-	Bone Surface	1.08	1.08	1.00	1.00	1.00	1.00	1.00	1.00	1.01	1.01	1.00	1.00
	-	-	RBM	1.08	1.08	1.00	1.00	1.00	1.00	1.00	1.00	1.01	1.01	1.00	1.00
	-	-	Skin	1.08	1.08	1.00	1.00	1.00	1.00	1.00	1.00	1.01	1.01	1.00	1.00
5	-6	2	R-Parotid	1.10	1.10	1.02	1.04	1.05	1.05	1.02	1.02	1.08	1.09	1.00	1.01
	6	2	L-Parotid	1.10		1.06		1.05		1.02		1.10		1.02	
	-	-	Bone Surface	1.08	1.08	1.00	1.00	1.00	1.00	1.00	1.00	1.01	1.01	1.00	1.00
	-	-	RBM	1.08	1.08	1.00	1.00	1.00	1.00	1.00	1.00	1.01	1.01	1.00	1.00
	-	-	Skin	1.08	1.08	1.00	1.00	1.00	1.00	1.00	1.00	1.01	1.01	1.00	1.00

Phantom section no.	Position		Organ or Tissue	Siemens Somatom		GE 8800 *		GE 9000HP		GE HiSpeed Advantage		Philips (CX/S)		GE Sytec 3000	
	X axis	Y axis		Point factor	Mean factor	Point factor	Mean factor	Point factor	Mean factor	Point factor	Mean factor	Point factor	Mean factor	Point factor	Mean factor
6	-6	2	R-Parotid	1.10	1.10	1.02	1.04	1.05	1.05	1.02	1.02	1.08	1.09	1.00	1.01
	6	2	L-Parotid	1.10		1.06		1.05		1.02		1.10		1.02	
	-	-	Bone Surface	1.08	1.08	1.00	1.00	1.00	1.00	1.00	1.00	1.01	1.01	1.00	1.00
	-	-	RBM	1.08	1.08	1.00	1.00	1.00	1.00	1.00	1.00	1.01	1.01	1.00	1.00
	-	-	Skin	1.08	1.08	1.00	1.00	1.00	1.00	1.00	1.00	1.00	1.00	1.00	1.00
7	-5	2	R-Parotid	1.10	1.10	1.02	1.04	1.05	1.05	1.02	1.02	1.08	1.09	1.00	1.01
	5	2	L-Parotid	1.10		1.06		1.05		1.02		1.10		1.02	
	-	-	Bone Surface	1.08	1.08	1.00	1.00	1.00	1.00	1.00	1.00	1.01	1.01	1.00	1.00
	-	-	RBM	1.08	1.08	1.00	1.00	1.00	1.00	1.00	1.00	1.01	1.01	1.00	1.00
	-	-	Skin	1.08	1.08	1.00	1.00	1.00	1.00	1.00	1.00	1.01	1.01	1.00	1.00
8	-	-	Bone Surface	1.08	1.08	1.00	1.00	1.00	1.00	1.00	1.00	1.01	1.01	1.00	1.00
	-	-	RBM	1.08	1.08	1.00	1.00	1.00	1.00	1.00	1.00	1.01	1.01	1.00	1.00
	-	-	Skin	1.08	1.08	1.00	1.00	1.00	1.00	1.00	1.00	1.01	1.01	1.00	1.00
9	-2	2	Thryroid	1.05	1.09	-	-	1.10	1.17	1.10	1.12	1.17	1.19	1.08	1.08
	0	4	Thryroid	1.12		-		1.21		1.15		1.22		1.08	
	2	2	Thryroid	1.09		-		1.21		1.10		1.17		1.08	
	0	0	Oesophagus	1.00	1.00	-	-	1.00	1.00	1.00	1.00	1.00	1.00		0.00
	-	-	Bone Surface	1.08	1.08	-	-	1.00	1.00	0.95	0.95	1.01	1.01	1.00	1.00
	-	-	RBM	1.08	1.08	-	-	1.00	1.00	0.95	0.95	1.01	1.01	1.00	1.00
	-	-	Skin	1.08	1.08	-	-	1.00	1.00	0.95	0.95	1.01	1.01	1.00	1.00
10	0	4	Thryroid	1.09	1.09	-	-	1.16	1.16	1.10	1.10	1.17	1.17	1.08	1.08
	0	0	Oesophagus	1.00	1.00	-	-	1.00	1.00	1.00	1.00	1.00	1.00	1.00	1.00
	-4	0	R-Lung	0.98	0.98	-	-	0.99	1.02	0.95	0.95	1.07	1.07	1.08	1.06
	4	0	L-Lung	0.98		-		1.04		0.95		1.07		1.04	
	-	-	Bone Surface	1.04	1.04	-	-	1.00	1.00	0.95	0.95	1.08	1.08	1.00	1.00
	-	-	RBM	1.04	1.04	-	-	1.00	1.00	0.95	0.95	1.08	1.08	1.00	1.00
	-	-	Skin	1.04	1.04	-	-	1.00	1.00	0.95	0.95	1.08	1.08	1.00	1.00
11	0	1	Oesophagus	1.00	1.00	-	-	1.00	1.00	1.00	1.00	1.00	1.00	1.00	1.00

Phantom section no.	Position		Organ or Tissue	Siemens Somatom		GE 8800 *		GE 9000HP		GE HiSpeed Advantage		Philips (CX/S)		GE Sytec 3000	
	X axis	Y axis		Point factor	Mean factor	Point factor	Mean factor	Point factor	Mean factor	Point factor	Mean factor	Point factor	Mean factor	Point factor	Mean factor
	-4	2	R-Lung	1.02	1.00	-	-	0.99	1.02	1.05	0.96	1.17	1.12	1.08	1.06
	-4	-2	R-Lung	1.02		-		0.88		0.90		1.05		1.08	
	6	2	L-Lung	0.98		-		1.15		1.00		1.15		1.08	
	6	-2	L-Lung	0.98		-		1.04		0.90		1.10		1.00	
	-	-	Bone Surface	1.04	1.04	-	-	1.00	1.00	0.95	0.95	1.08	1.08	1.00	1.00
	-	-	RBM	1.04	1.04	-	-	1.00	1.00	0.95	0.95	1.08	1.08	1.00	1.00
	-	-	Skin	1.04	1.04	-	-	1.00	1.00	0.95	0.95	1.08	1.08	1.00	1.00
12	0	0	Oesophagus	1.00	1.00	-	-	1.00	1.00	1.00	1.00	1.00	1.00	1.00	1.00
	0	5	Thymus	1.12	1.12	-	-	1.21	1.21	1.15	1.15	1.20	1.20	1.08	1.08
	-4	2	R-Lung	0.98	0.96	-	-	0.99	1.00	1.05	0.94	1.12	1.10	1.08	1.00
	-4	-4	R-Lung	0.91		-		0.82		0.85		1.02		0.92	
	6	4	L-Lung	1.05		-		1.21		1.05		1.20		1.08	
	8	-4	L-Lung	0.91		-		0.99		0.80		1.07		0.92	
	-	-	Bone Surface	1.04	1.04	-	-	1.00	1.00	0.95	0.95	1.08	1.08	1.00	1.00
	-	-	RBM	1.04	1.04	-	-	1.00	1.00	0.95	0.95	1.08	1.08	1.00	1.00
	-	-	Skin	1.04	1.04	-	-	1.00	1.00	0.95	0.95	1.08	1.08	1.00	1.00
13	0	0	Oesophagus	1.00	1.00	-	-	1.00	1.00	1.00	1.00	1.00	1.00	1.00	1.00
	0	6	Thymus	1.15	1.15	-	-	1.21	1.21	1.15	1.15	1.22	1.22	1.08	1.08
	-4	2	R-Lung	1.04	0.99	-	-	0.99	0.99	1.05	0.93	1.12	1.11	1.08	0.98
	-6	-4	R-Lung	0.95		-		0.77		0.80		1.05		0.88	
	6	4	L-Lung	1.05		-		1.21		1.05		1.20		1.08	
	8	-4	L-Lung	0.91		-		0.99		0.80		1.07		0.88	
	-	-	Bone Surface	1.04	1.04	-	-	1.00	1.00	0.95	0.95	1.08	1.08	1.00	1.00
	-	-	RBM	1.04	1.04	-	-	1.00	1.00	0.95	0.95	1.08	1.08	1.00	1.00
	-	-	Skin	1.04	1.04	-	-	1.00	1.00	0.95	0.95	1.08	1.08	1.00	1.00
14	0	0	Oesophagus	1.00	1.00	-	-	1.00	1.00	1.00	1.00	1.00	1.00	1.00	1.00
	-6	4	R-Lung	1.02	1.00	-	-	1.04	1.00	1.05	0.93	1.20	1.13	1.04	0.96
	-6	-6	R-Lung	0.95		-		0.71		0.75		1.02		0.84	

Phantom section no.	Position		Organ or Tissue	Siemens Somatom		GE 8800 *		GE 9000HP		GE HiSpeed Advantage		Philips (CX/S)		GE Sytec 3000	
	X axis	Y axis		Point factor	Mean factor	Point factor	Mean factor	Point factor	Mean factor	Point factor	Mean factor	Point factor	Mean factor	Point factor	Mean factor
	6	6	L-Lung	1.12		-		1.25		1.10		1.22		1.08	
	8	-4	L-Lung	0.91		-		0.99		0.80		1.07		0.88	
	-	-	Bone Surface	1.04	1.04	-	-	1.00	1.00	0.95	0.95	1.08	1.08	1.00	1.00
	-	-	RBM	1.04	1.04	-	-	1.00	1.00	0.95	0.95	1.08	1.08	1.00	1.00
	-	-	Skin	1.04	1.04	-	-	1.00	1.00	0.95	0.95	1.08	1.08	1.00	1.00
15	0	0	Oesophagus	1.00	1.00	-	-	1.00	1.00	1.00	1.00	1.00	1.00	1.00	1.00
	(-3)-(-10)	11-10	R-Breast	1.12	1.14	-	-	1.21	1.21	1.05	1.05	1.22	1.22	1.08	1.08
	3-10	11-10	L-Breast	1.16		-		1.21		1.05		1.22		1.08	
	-6	6	R-Lung	1.05	1.00	-	-	1.10	1.01	1.05	0.91	1.22	1.13	1.04	0.96
	-6	-6	R-Lung	0.95		-		0.71		0.75		1.02		0.84	
	8	6	L-Lung	1.09		-		1.25		1.05		1.22		1.08	
	8	-4	L-Lung	0.91		-		0.99		0.80		1.07		0.88	
	-	-	Bone Surface	1.04	1.04	-	-	1.00	1.00	0.95	0.95	1.08	1.08	1.00	1.00
	-	-	RBM	1.04	1.04	-	-	1.00	1.00	0.95	0.95	1.08	1.08	1.00	1.00
	-	-	Skin	1.04	1.04	-	-	1.00	1.00	0.95	0.95	1.08	1.08	1.00	1.00
16	0	0	Oesophagus	1.00	1.00	-		1.00		1.00		1.00		1.00	
	(-2.5)-(-10)	12-9	R-Breast	1.11	1.13	-	-	1.21	1.21	1.05	1.05	1.22	1.22	1.08	1.08
	2.5-10	12-9	L-Breast	1.16		-		1.21		1.05		1.22		1.08	
	-8	6	R-Lung	1.05	1.00	-	-	1.04	0.99	1.00	0.88	1.22	1.13	1.00	0.92
	-8	-6	R-Lung	0.95		-		0.71		0.70		1.02		0.76	
	6	-4	L-Lung	0.91		-		0.94		0.80		1.05		0.92	
	10	6	L-Lung	1.09		-		1.25		1.00		1.22		1.00	
	-	-	Bone Surface	1.04	1.04	-	-	1.00	1.00	0.95	0.95	1.08	1.08	1.00	1.00
	-	-	RBM	1.04	1.04	-	-	1.00	1.00	0.95	0.95	1.08	1.08	1.00	1.00
	-	-	Skin	1.04	1.04	-	-	1.00	1.00	0.95	0.95	1.08	1.08	1.00	1.00
17	0	0	Oesophagus	1.00	1.00	-	-	1.00	1.00	1.00	1.00	1.00	1.00	1.00	1.00
	(-1)-(-12)	12.5-8	R-Breast	1.12	1.13	-	-	1.21	1.21	1.05	1.07	1.22	1.22	1.08	1.08
	1-12	12.5-8	L-Breast	1.14		-		1.21		1.08		1.22		1.08	

Phantom section no.	Position		Organ or Tissue	Siemens Somatom		GE 8800 *		GE 9000HP		GE HiSpeed Advantage		Philips (CX/S)		GE Sytec 3000	
	X axis	Y axis		Point factor	Mean factor	Point factor	Mean factor	Point factor	Mean factor	Point factor	Mean factor	Point factor	Mean factor	Point factor	Mean factor
	-8	6	R-Lung	1.05	1.00	-	-	1.04	0.99	1.00	0.90	1.22	1.13	1.00	0.96
	-8	-4	R-Lung	0.95		-		0.71		0.75		1.05		0.88	
	4	-4	L-Lung	0.91		-		0.94		0.85		1.02		0.96	
	10	6	L-Lung	1.09		-		1.25		1.00		1.22		1.00	
	-	-	Bone Surface	1.04	1.04	-	-	1.00	1.00	0.95	0.95	1.08	1.08	1.00	1.00
	-	-	RBM	1.04	1.04	-	-	1.00	1.00	0.95	0.95	1.08	1.08	1.00	1.00
	-	-	Skin	1.04	1.04	-	-	1.00	1.00	0.95	0.95	1.08	1.08	1.00	1.00
18	0	0	Oesophagus	1.00	1.00	-	-	1.00	1.00	1.00	1.00	1.00	1.00	1.00	1.00
	(-1)-(-12)	12-8	R-Breast	1.12	1.13	-	-	1.21	1.21	1.08	1.08	1.22	1.22	1.08	1.08
	1-12	12-8	L-Breast	1.14		-		1.21		1.08		1.22		1.08	
	-10	4	R-Lung	0.95	0.96	-	-	0.99	1.00	0.90	0.84	1.22	1.16	0.92	0.89
	-8	-4	R-Lung	0.95		-		0.71		0.75		1.05		0.84	
	10	-2	L-Lung	0.91		-		1.04		0.80		1.15		0.88	
	12	4	L-Lung	1.02		-		1.25		0.90		1.22		0.92	
	-4	4	Liver	1.02	1.05	-	-	1.10	1.10	1.10	1.08	1.17	1.15	0.92	1.03
	-3	0	Liver	0.98		-		0.99		1.00		1.05		1.08	
	-2	8	Liver	1.15		-		1.21		1.15		1.22		1.08	
	-	-	Bone Surface	1.04	1.04	-	-	1.00	1.00	0.95	0.95	1.08	1.08	1.00	1.00
	-	-	RBM	1.04	1.04	-	-	1.00	1.00	0.95	0.95	1.08	1.08	1.00	1.00
	-	-	Skin	1.04	1.04	-	-	1.00	1.00	0.95	0.95	1.08	1.08	1.00	1.00
19	(-3)-(-10)	12-9	R-Breast	1.12	1.14	-	-	1.21	1.21	1.05	1.05	1.22	1.22	1.08	1.08
	3-10	12-9	L-Breast	1.16		-		1.21		1.05		1.22		1.08	
	-12	4	R-Lung	0.95	0.98	-	-	0.99	1.00	0.90	0.88	1.22	1.14	0.92	0.92
	-6	-4	R-Lung	0.95		-		0.77		0.80		1.05		0.88	
	8	-4	L-Lung	0.91		-		0.99		0.80		1.07		0.88	
	10	6	L-Lung	1.09		-		1.25		1.00		1.22		1.00	
	-6	2	Liver	0.98	1.04	-	-	0.99	1.03	1.00	1.02	1.15	1.14	1.04	1.05
	-4	-1	Liver	0.98		-		0.88		0.95		1.05		1.04	

Phantom section no.	Position		Organ or Tissue	Siemens Somatom		GE 8800 *		GE 9000HP		GE HiSpeed Advantage		Philips (CX/S)		GE Sytec 3000	
	X axis	Y axis		Point factor	Mean factor	Point factor	Mean factor	Point factor	Mean factor	Point factor	Mean factor	Point factor	Mean factor	Point factor	Mean factor
	-2	6	Liver	1.15		-		1.21		1.10		1.22		1.08	
	0	0	Stomach	0.98	1.03	-	-	1.00	1.10	1.00	1.03	1.00	1.10	1.00	1.05
	2	2	Stomach	1.05		-		1.10		1.05		1.10		1.08	
	6	4	Stomach	1.05		-		1.21		1.05		1.20		1.08	
	4	-1	Spleen	0.98	0.98	-	-	1.04	1.10	0.95	0.95	1.07	1.10	1.00	1.02
	7	1	Spleen	0.98		-		1.15		0.95		1.12		1.04	
	-	-	Bone Surface	1.04	1.04	-	-	1.00	1.00	0.95	0.95	1.08	1.08	1.00	1.00
	-	-	RBM	1.04	1.04	-	-	1.00	1.00	0.95	0.95	1.08	1.08	1.00	1.00
	-	-	Skin	1.04	1.04	-	-	1.00	1.00	0.95	0.95	1.08	1.08	1.00	1.00
20	-6	2	Liver	1.43	1.41	-	-	1.36	1.36	1.37	1.33	1.38	1.31	1.43	1.40
	-6	-2	Liver	1.26		-		1.20		1.26		1.17		1.24	
	0	6	Liver	1.54		-		1.52		1.37		1.38		1.52	
	4	4	Stomach	1.43	1.46	-	-	1.44	1.52	1.37	1.40	1.38	1.38	1.43	1.48
	6	6	Stomach	1.48		-		1.60		1.43		1.38		1.52	
	7	-2	Spleen	1.37	1.40	-	-	1.12	1.24	1.32	1.38	1.17	1.25	1.24	1.24
	10	2	Spleen	1.43		-		1.36		1.43		1.32		1.24	
	-3	-1	R-Adrenal	1.21	1.21	-	-	1.04	1.00	1.21	1.21	1.08	1.08	1.14	1.14
	3	-1	L-Adrenal	1.21		-		0.96		1.21		1.08		1.14	
	-	-	Bone Surface	1.34	1.34	-	-	1.56	1.56	1.30	1.30	1.09	1.09	1.32	1.32
	-	-	RBM	1.34	1.34	-	-	1.56	1.56	1.30	1.30	1.09	1.09	1.32	1.32
	-	-	Skin	1.34	1.34	-	-	1.56	1.56	1.30	1.30	1.09	1.09	1.32	1.32
21	-8	2	Liver	1.48	1.46	-	-	1.44	1.44	1.37	1.39	1.38	1.32	1.43	1.46
	-8	-2	Liver	1.37		-		1.28		1.37		1.21		1.33	
	-4	6	Liver	1.54		-		1.60		1.43		1.38		1.62	
	4	6	Stomach	1.54	1.54	-	-	1.52	1.52	1.43	1.43	1.38	1.38	1.62	1.62
	8	-2	Spleen	1.43	1.43	-	-	1.28	1.36	1.32	1.38	1.21	1.24	1.24	1.24
	10	0	Spleen	1.43		-		1.44		1.43		1.26		1.24	
	-3	0	R-Adrenal	1.21	1.24	-	-	1.12	1.12	1.21	1.21	1.17	1.17	1.14	1.14

Phantom	Position		Organ or	Siemens Somatom		GE 8800 *		GE 9000HP		GE HiSpeed Advantage		Philips (CX/S)		GE Sytec 3000	
section no.	X axis	Y axis	Tissue	Point factor	Mean factor	Point factor	Mean factor	Point factor	Mean factor	Point factor	Mean factor	Point factor	Mean factor	Point factor	Mean factor
	3	0	L-Adrenal	1.26		-		1.12		1.21		1.17		1.14	
	-4	-2	R-Kidney	1.21	1.21	-	-	1.12	1.12	1.21	1.21	1.08	1.08	1.14	1.14
	4	-2	L-Kidney	1.21		-		1.12		1.21		1.08		1.14	
	2	4	Pancreas	1.43	1.40	-	-	1.44	1.36	1.37	1.37	1.30	1.28	1.43	1.38
	4	2	Pancreas	1.37		-		1.28		1.37		1.26		1.33	
	8	6	SI	1.48	1.46	-	-	1.60	1.56	1.43	1.43	1.32	1.32	1.43	1.38
	9	4	SI	1.43		-		1.52		1.43		1.32		1.33	
	7	3	ULI	1.43	1.43	-	-	1.44	1.44	1.37	1.37	1.32	1.32	1.43	1.43
	-	-	Bone Surface	1.34	1.34	-	-	1.56	1.56	1.30	1.30	1.09	1.09	1.32	1.32
	-	-	RBM	1.34	1.34	-	-	1.56	1.56	1.30	1.30	1.09	1.09	1.32	1.32
	-	-	Skin	1.34	1.34	-	-	1.56	1.56	1.30	1.30	1.09	1.09	1.32	1.32
22	-8	0	Liver	1.43	1.49	-	-	1.36	1.48	1.37	1.40	1.30	1.34	1.33	1.48
	-6	6	Liver	1.54		-		1.60		1.43		1.38		1.62	
	2	7	Stomach	1.54	1.54	-	-	1.60	1.60	1.43	1.43	1.38	1.38	1.71	1.71
	9	0	Spleen	1.43	1.43	-	-	1.36	1.36	1.37	1.37	1.26	1.26	1.33	1.33
	-4	-2	R-Kidney	1.21	1.21	-	-	1.12	1.12	1.21	1.21	1.08	1.08	1.14	1.14
	4	-2	L-Kidney	1.21		-		1.12		1.21		1.08		1.14	
	2	5	Pancreas	1.48	1.48	-	-	1.52	1.52	1.37	1.37	1.38	1.38	1.43	1.43
	-2	4	SI	1.43	1.45	-	-	1.44	1.47	1.37	1.41	1.38	1.36	1.43	1.43
	7	5	SI	1.48		-		1.52		1.43		1.38		1.43	
	8	3	SI	1.43		-		1.44		1.43		1.32		1.43	
	6	-1	LLI	1.32	1.32	-	-	1.20	1.20	1.32	1.32	1.17	1.17	1.24	1.24
	5	7	ULI	1.54	1.54	-	-	1.60	1.60	1.43	1.43	1.38	1.38	1.62	1.62
	-	-	Bone Surface	1.34	1.34	-	-	1.56	1.56	1.30	1.30	1.09	1.09	1.32	1.32
	-	-	RBM	1.34	1.34	-	-	1.56	1.56	1.30	1.30	1.09	1.09	1.32	1.32
	-	-	Skin	1.34	1.34	-	-	1.56	1.56	1.30	1.30	1.09	1.09	1.32	1.32
23	-8	0	Liver	1.37	1.46	-	-	1.36	1.48	1.37	1.40	1.30	1.34	1.33	1.48
	-6	6	Liver	1.54		-		1.60		1.43		1.38		1.62	

Phantom section no.	Position		Organ or Tissue	Siemens Somatom		GE 8800 *		GE 9000HP		GE HiSpeed Advantage		Philips (CX/S)		GE Sytec 3000	
	X axis	Y axis		Point factor	Mean factor	Point factor	Mean factor	Point factor	Mean factor	Point factor	Mean factor	Point factor	Mean factor	Point factor	Mean factor
	1	7	Stomach	1.54	1.54	-	-	1.60	1.60	1.43	1.43	1.38	1.38	1.71	1.71
	-5	-1	R-Kidney	1.26	1.29	-	-	1.12	1.12	1.26	1.26	1.21	1.21	1.24	1.24
	5	-1	L-Kidney	1.32		-		1.12		1.26		1.21		1.24	
	-1	4	Pancreas	1.43	1.43	-	-	1.44	1.44	1.37	1.37	1.30	1.30	1.43	1.43
	6	6	SI	1.48	1.46	-	-	1.60	1.52	1.43	1.40	1.38	1.34	1.52	1.43
	8	2	SI	1.43		-		1.44		1.37		1.30		1.33	
	8	0	LLI	1.43	1.43	-	-	1.36	1.36	1.37	1.37	1.26	1.26	1.33	1.33
	3	8	ULI	1.54	1.54	-	-	1.60	1.60	1.43	1.43	1.38	1.38	1.71	1.71
	-	-	Bone Surface	1.34	1.34	-	-	1.56	1.56	1.30	1.30	1.09	1.09	1.32	1.32
	-	-	RBM	1.34	1.34	-	-	1.56	1.56	1.30	1.30	1.09	1.09	1.32	1.32
	-	-	Skin	1.34	1.34	-	-	1.56	1.56	1.30	1.30	1.09	1.09	1.32	1.32
24	-8	2	Liver	1.48	1.51	-	-	1.44	1.52	1.37	1.40	1.38	1.38	1.43	1.53
	-6	6	Liver	1.54		-		1.60		1.43		1.38		1.62	
	-5	-1	R-Kidney	1.26	1.29	-	-	1.12	1.12	1.26	1.26	1.21	1.21	1.24	1.24
	5	-1	L-Kidney	1.32		-		1.12		1.26		1.21		1.24	
	0	4	Pancreas	1.43	1.43	-	-	1.44	1.44	1.37	1.37	1.30	1.30	1.43	1.43
	6	6	SI	1.48	1.43	-	-	1.52	1.40	1.43	1.40	1.38	1.34	1.52	1.43
	6	2	SI	1.37		-		1.28		1.37		1.30		1.33	
	8	0	LLI	1.43	1.43	-	-	1.36	1.36	1.37	1.37	1.26	1.26	1.33	1.33
	-5	3	ULI	1.43	1.49	-	-	1.44	1.52	1.37	1.40	1.38	1.38	1.43	1.57
	2	8	ULI	1.54		-		1.60		1.43		1.38		1.71	
	-	-	Bone Surface	1.34	1.34	-	-	1.56	1.56	1.30	1.30	1.09	1.09	1.32	1.32
	-	-	RBM	1.34	1.34	-	-	1.56	1.56	1.30	1.30	1.09	1.09	1.32	1.32
	-	-	Skin	1.34	1.34	-	-	1.56	1.56	1.30	1.30	1.09	1.09	1.32	1.32
25	-8	4	Liver	1.48	1.48	-	-	1.52	1.52	1.43	1.43	1.38	1.38	1.52	1.52
	-7	-2	R-Kidney	1.32	1.35	-	-	1.20	1.20	1.32	1.32	1.26	1.26	1.33	1.29
	7	-2	L-Kidney	1.37		-		1.20		1.32		1.26		1.24	
	4	2	SI	1.37	1.43	-	-	1.28	1.44	1.37	1.40	1.26	1.32	1.33	1.43

Phantom section no.	Position		Organ or Tissue	Siemens Somatom		GE 8800 *		GE 9000HP		GE HiSpeed Advantage		Philips (CX/S)		GE Sytec 3000	
	X axis	Y axis		Point factor	Mean factor	Point factor	Mean factor	Point factor	Mean factor	Point factor	Mean factor	Point factor	Mean factor	Point factor	Mean factor
	6	6	SI	1.48		-		1.60		1.43		1.38		1.52	
	9	0	LLI	1.43	1.43	-	-	1.36	1.36	1.37	1.37	1.38	1.38	1.33	1.33
	-6	1	ULI	1.37	1.45	-	-	1.36	1.44	1.32	1.35	1.30	1.35	1.43	1.49
	-4	4	ULI	1.43		-		1.44		1.37		1.38		1.43	
	1	6	ULI	1.54		-		1.52		1.37		1.38		1.62	
	-	-	Bone Surface	1.34	1.34	-	-	1.56	1.56	1.30	1.30	1.09	1.09	1.32	1.32
	-	-	RBM	1.34	1.34	-	-	1.56	1.56	1.30	1.30	1.09	1.09	1.32	1.32
	-	-	Skin	1.34	1.34	-	-	1.56	1.56	1.30	1.30	1.09	1.09	1.32	1.32
26	-2	2	SI	1.26	1.35	-	-	1.28	1.36	1.32	1.35	1.03	1.21	1.24	1.34
	4	4	SI	1.43		-		1.44		1.37		1.38		1.43	
	9	0	LLI	1.43	1.43	-	-	1.36	1.36	1.37	1.37	1.38	1.38	1.33	1.33
	-6	2	ULI	1.43	1.49	-	-	1.44	1.52	1.37	1.37	1.38	1.38	1.43	1.53
	-2	6	ULI	1.54		-		1.60		1.37		1.38		1.62	
	-	-	Bone Surface	1.34	1.34	-	-	1.56	1.56	1.30	1.30	1.09	1.09	1.32	1.32
	-	-	RBM	1.34	1.34	-	-	1.56	1.56	1.30	1.30	1.09	1.09	1.32	1.32
	-	-	Skin	1.34	1.34	-	-	1.56	1.56	1.30	1.30	1.09	1.09	1.32	1.32
27	-4	2	SI	1.26	1.35	-	-	1.36	1.44	1.32	1.35	1.30	1.33	1.33	1.40
	2	4	SI	1.37		-		1.52		1.37		1.30		1.43	
	6	4	SI	1.43		-		1.44		1.37		1.38		1.43	
	10	-1	LLI	1.43	1.43	-	-	1.36	1.36	1.43	1.43	1.26	1.26	1.24	1.24
	-8	0	ULI	1.43	1.46	-	-	1.36	1.44	1.37	1.40	1.30	1.34	1.33	1.43
	-6	4	ULI	1.48		-		1.52		1.43		1.38		1.52	
	-	-	Bone Surface	1.34	1.34	-	-	1.56	1.56	1.30	1.30	1.09	1.09	1.32	1.32
	-	-	RBM	1.34	1.34	-	-	1.56	1.56	1.30	1.30	1.09	1.09	1.32	1.32
	-	-	Skin	1.34	1.34	-	-	1.56	1.56	1.30	1.30	1.09	1.09	1.32	1.32
28	-3	2	SI	1.32	1.43	-	-	1.36	1.44	1.32	1.35	1.26	1.34	1.33	1.43
	0	6	SI	1.54		-		1.52		1.37		1.38		1.52	
	4	4	SI	1.43		-		1.44		1.37		1.38		1.43	

Phantom section no.	Position		Organ or Tissue	Siemens Somatom		GE 8800 *		GE 9000HP		GE HiSpeed Advantage		Philips (CX/S)		GE Sytec 3000	
	X axis	Y axis		Point factor	Mean factor	Point factor	Mean factor	Point factor	Mean factor	Point factor	Mean factor	Point factor	Mean factor	Point factor	Mean factor
	10	0	LLI	1.43	1.43	-	-	1.36	1.36	1.43	1.43	1.30	1.30	1.24	1.24
	-8	2	ULI	1.48	1.48	-	-	1.44	1.44	1.37	1.37	1.38	1.38	1.43	1.43
	-	-	Bone Surface	1.34	1.34	-	-	1.56	1.56	1.30	1.30	1.09	1.09	1.32	1.32
	-	-	RBM	1.34	1.34	-	-	1.56	1.56	1.30	1.30	1.09	1.09	1.32	1.32
	-	-	Skin	1.34	1.34	-	-	1.56	1.56	1.30	1.30	1.09	1.09	1.32	1.32
29	-4	3	SI	1.37	1.35	-	-	1.44	1.36	1.37	1.33	1.38	1.30	1.43	1.37
	0	2	SI	1.26		-		1.28		1.26		1.21		1.24	
	5	3	SI	1.43		-		1.36		1.37		1.30		1.43	
	9	1	LLI	1.43	1.43	-	-	1.44	1.44	1.43	1.43	1.38	1.38	1.33	1.33
	-9	0	ULI	1.43	1.43	-	-	1.36	1.36	1.37	1.37	1.38	1.38	1.43	1.43
	-	-	Bone Surface	1.34	1.34	-	-	1.56	1.56	1.30	1.30	1.09	1.09	1.32	1.32
	-	-	RBM	1.34	1.34	-	-	1.56	1.56	1.30	1.30	1.09	1.09	1.32	1.32
	-	-	Skin	1.34	1.34	-	-	1.56	1.56	1.30	1.30	1.09	1.09	1.32	1.32
30	-4	4	SI	1.43	1.30	-	-	1.44	1.25	1.37	1.24	1.38	1.23	1.43	1.37
	0	-2	SI	1.04		-		0.88		0.99		0.94		1.24	
	4	4	SI	1.43		-		1.44		1.37		1.38		1.43	
	-2	-2	LLI	1.04	1.24	-	-	0.96	1.16	1.10	1.24	1.03	1.15	0.95	1.14
	8	1	LLI	1.43		-		1.36		1.37		1.26		1.33	
	-10	2	ULI	1.48	1.48	-	-	1.44	1.44	1.43	1.43	1.38	1.38	1.43	1.43
	-	-	Bone Surface	1.34	1.34	-	-	1.56	1.56	1.30	1.30	1.09	1.09	1.32	1.32
	-	-	RBM	1.34	1.34	-	-	1.56	1.56	1.30	1.30	1.09	1.09	1.32	1.32
	-	-	Skin	1.34	1.34	-	-	1.56	1.56	1.30	1.30	1.09	1.09	1.32	1.32
31	-2	-3	SI	1.04	1.26	-	-	0.96	1.23	1.04	1.21	0.94	1.15	0.95	1.17
	0	5	SI	1.48		-		1.52		1.37		1.38		1.43	
	2	1	SI	1.26		-		1.20		1.21		1.12		1.14	
	2	-4	LLI	1.43	1.40	-	-	0.88	1.08	1.04	1.21	0.90	1.10	1.04	1.19
	6	2	LLI	1.37		-		1.28		1.37		1.30		1.33	
	-4	4	ULI	1.43	1.46	-	-	1.44	1.48	1.37	1.40	1.38	1.38	1.43	1.48

Phantom	Position		Organ or	Siemens Somatom		GE 8800 *		GE 9000HP		GE HiSpeed Advantage		Philips (CX/S)		GE Sytec 3000	
section no.	X axis	Y axis	Tissue	Point factor	Mean factor	Point factor	Mean factor	Point factor	Mean factor	Point factor	Mean factor	Point factor	Mean factor	Point factor	Mean factor
	-5	5	ULI	1.48		-		1.52		1.43		1.38		1.52	
	-4	-1	R-Ovary	1.21	1.27	-	-	1.20	1.16	1.21	1.21	1.12	1.12	1.14	1.14
	4	-1	L-Ovary	1.32		-		1.12		1.21		1.12		1.14	
	0	2	Uterus	1.26	1.26	-	-	1.28	1.28	1.26	1.26	0.94	0.94	1.24	1.24
	-	-	Bone Surface	1.34	1.34	-	-	1.56	1.56	1.30	1.30	1.09	1.09	1.32	1.32
	-	-	RBM	1.34	1.34	-	-	1.56	1.56	1.30	1.30	1.09	1.09	1.32	1.32
	-	-	Skin	1.34	1.34	-	-	1.56	1.56	1.30	1.30	1.09	1.09	1.32	1.32
32	-4	0	SI	1.26	1.37	-	-	1.28	1.39	1.26	1.35	1.21	1.30	1.24	1.33
	5	5	SI	1.48		-		1.52		1.43		1.38		1.43	
	5	2	SI	1.37		-		1.36		1.37		1.30		1.33	
	0	-6	LLI	1.10	1.10	-	-	0.96	0.96	1.15	1.15	0.94	0.94	1.14	1.14
	-5	5	ULI	1.48	1.48	-		1.52	1.52	1.43	1.43	1.38	1.38	1.52	1.52
	0	0	Uterus	1.10	1.10	-	-	1.00	1.00	1.04	1.04	1.00	1.00	1.04	1.04
	0	4	Bladder	1.43	1.43	-	-	1.44	1.44	1.37	1.37	1.32	1.32	1.43	1.43
	-	-	Bone Surface	1.34	1.34	-	-	1.56	1.56	1.30	1.30	1.09	1.09	1.32	1.32
	-	-	RBM	1.34	1.34	-	-	1.56	1.56	1.30	1.30	1.09	1.09	1.32	1.32
	-	-	Skin	1.34	1.34	-	-	1.56	1.56	1.30	1.30	1.09	1.09	1.32	1.32
33	-1	-6	LLI	1.10	1.10	-	-	0.96	0.96	1.15	1.15	0.94	0.94	1.14	1.14
	0	0	Bladder	1.10	1.10	-	-	1.00	1.00	1.04	1.04	1.00	1.00	1.04	1.04
	-1	-3	Prostat	1.04	1.04	-	-	1.00	1.00	1.21	1.21	0.94	0.94	0.95	0.95
	-	-	Bone Surface	1.34	1.34	-	-	1.56	1.56	1.30	1.30	1.09	1.09	1.32	1.32
	-	-	RBM	1.34	1.34	-	-	1.56	1.56	1.30	1.30	1.09	1.09	1.32	1.32
	-	-	Skin	1.34	1.34	-	-	1.56	1.56	1.30	1.30	1.09	1.09	1.32	1.32
34	0	-5	LLI	1.04	1.04	-	-	0.88	0.88	1.10	1.10	1.00	1.00	1.04	1.04
	-1	-1	Bladder	1.00	1.00	-	-	1.00	1.00	1.00	1.00	1.00	1.00	1.04	1.04
	0	9	Testis	1.54	1.54	-	-	1.60	1.60	1.43	1.43	1.38	1.38	1.81	1.81
	-	-	Bone Surface	1.34	1.34	-	-	1.56	1.56	1.30	1.30	1.09	1.09	1.32	1.32
	-	-	RBM	1.34	1.34	-	-	1.56	1.56	1.30	1.30	1.09	1.09	1.32	1.32

Phantom section no.	Position		Organ or Tissue	Siemens Somatom		GE 8800 *		GE 9000HP		GE HiSpeed Advantage		Philips (CX/S)		GE Sytec 3000	
	X axis	Y axis		Point factor	Mean factor	Point factor	Mean factor	Point factor	Mean factor	Point factor	Mean factor	Point factor	Mean factor	Point factor	Mean factor
	-	-	Skin	1.34	1.34	-	-	1.56	1.56	1.30	1.30	1.09	1.09	1.32	1.32

Appendix C. MACRO PROGRAMS

This appendix includes some of the macro computer programs used for sorting the organ absorbed doses and calculating the effective dose equivalent and effective dose values. These macros have been created in the spreadsheets designed with the Microsoft Excel ™ program and are in visual basic computer language.

```
'**********************************************************
'
' EDE_Macro Macro
' Effective Dose Equivalent Macro
' Sorting data to calculate the effective dose equivalent based on ICRP Publication No. 26 (1977).
'
'
Sub EDE_Macro()
    Sheets("EDE").Select
    Range("C8").Select
    ActiveWindow.LargeScroll Down:=1
    ActiveWindow.SmallScroll Down:=-11
    Range("C8:D24").Select
    Selection.ClearContents
    Range("A8:B24").Select
    Selection.Copy
    Range("C8").Select
    Selection.PasteSpecial Paste:=xlValues, Operation:=xlNone, _
        SkipBlanks:=False, Transpose:=False
    Application.CutCopyMode = False
    Selection.Sort Key1:=Range("D8"), Order1:=xlDescending, Header:= _
        xlGuess, OrderCustom:=1, MatchCase:=False, Orientation:= _
```

```
        xlTopToBottom
    ActiveWindow.LargeScroll Down:=-1
    Range("A1").Select
    Application.MaxChange = 0.001
    ActiveWorkbook.PrecisionAsDisplayed = False
    Calculate
End Sub
'
' ED_Macro Macro
' Effective Dose Macro
' Sorting data to calculate the effective dose based on ICRP Publication No.
60 (1990).
'
'
Sub ED_Macro()
    Sheets("ED").Select
    Range("C8:D15").Select
    Selection.ClearContents
    Range("A8:B15").Select
    Selection.Copy
    Range("C8").Select
    Selection.PasteSpecial Paste:=xlValues, Operation:=xlNone, _
        SkipBlanks:=False, Transpose:=False
    Application.CutCopyMode = False
    Selection.Sort Key1:=Range("D8"), Order1:=xlDescending, Header:= _
        xlGuess, OrderCustom:=1, MatchCase:=False, Orientation:= _
        xlTopToBottom
    Range("G8").Select
    ActiveWindow.SmallScroll ToRight:=1
    ActiveWindow.SmallScroll Down:=2
    Range("G8:H19").Select
```

```
    Selection.ClearContents
    Range("E8:F19").Select
    Selection.Copy
    Range("G8").Select
    Selection.PasteSpecial Paste:=xlValues, Operation:=xlNone, _
      SkipBlanks:=False, Transpose:=False
    Application.CutCopyMode = False
    Selection.Sort Key1:=Range("H8"), Order1:=xlDescending, Header:= _
      xlGuess, OrderCustom:=1, MatchCase:=False, Orientation:= _
      xlTopToBottom
    ActiveWindow.SmallScroll ToRight:=-1
    ActiveWindow.SmallScroll Down:=-2
    Range("A1").Select
    Application.MaxChange = 0.001
    ActiveWorkbook.PrecisionAsDisplayed = False
    Calculate
End Sub
**************************************************************
```